Université de Sherbrooke
Faculté de génie
Département de génie chimique et de génie biotechnologique

Méthode inverse pour estimer les paramètres électrochimiques et thermophysiques des batteries aux ions lithium composées de différents matériaux pour l'électrode positive

An inverse method for estimating the electrochemical and the thermophysical parameters of lithium-ion batteries with different positive electrode materials

Thèse de doctorat
Spécialité : génie chimique

Ali Jokar

Jury : Martin Désilets (directeur)
Marcel Lacroix
Bernard Marcos
Jocelyn Veilleux
Mark Pritzker

Sherbrooke (Québec) Canada Dec. 2017

À ma famille et mon adorable épouse,

Farzaneh

Résumé

La sécurité de plusieurs systèmes électriques est fortement dépendante de la fiabilité de leur bloc-batterie à base de piles aux ions lithium (Li-ion). Par conséquent, ces batteries doivent être suivis et contrôlés par un système de gestion des batteries (BMS). Le BMS interagit avec toutes les composantes du bloc-batterie de façon à maintenir leur intégrité. La principale composante d'un BMS est un modèle représentant le comportement des piles Li-ion et capable de prédire ses différents points d'opération. Dans les industries de l'électronique et de l'automobile, le BMS repose habituellement sur des modèles empiriques simples. Ceux-ci ne sont cependant pas capables de prédire les paramètres de la batterie lorsqu'elle vieillit. De plus, ils ne sont applicables que pour des piles spécifiques. D'un autre côté, les modèles électrochimiques sont plus sophistiqués et plus précis puisqu'ils sont basés sur la résolution des équations de transport et de cinétique électrochimique. Ils peuvent être utilisés pour simuler les caractéristiques et les réactions à l'intérieur des piles aux ions lithium.

Pour résoudre les équations des modèles électrochimiques, il faut connaître les différents paramètres électrochimiques et thermo-physiques de la pile. Les variables les plus significatives des piles Li-ion peuvent être divisées en 3 catégories : les paramètres géométriques, ceux définissant les matériaux et les paramètres d'opération. Les paramètres géométriques et de matériaux peuvent être facilement obtenus à partir de mesures directes ou à partir des spécifications du manufacturier. Par contre, les paramètres d'opération ne sont pas faciles à identifier. De plus, certains d'entre eux peuvent dépendre de la technique de mesure utilisée et de l'âge. Finalement, la mesure de certains paramètres requiert le démantèlement de la pile, une procédure risquée et destructive.

Plusieurs recherches ont été réalisées afin d'identifier les paramètres opérationnels des piles aux ions lithium. Toutefois, la plupart de ces études ont porté sur l'estimation d'un nombre limité de paramètres et se sont attardées sur un seul type de matériau pour l'électrode positive utilisé dans la fabrication des piles Li-ion. De plus, le couplage qui existe entre les paramètres électrochimiques et thermo-physiques est complètement ignoré. Le but principal de cette thèse est de développer une méthode générale pour identifier simultanément différents paramètres électrochimiques et thermo-physiques et de prédire la performance des piles Li-ion à base de différents matériaux d'électrodes positives. Pour atteindre ce but, une méthode inverse efficace a été introduite. Des modèles directs représentatifs des piles Li-ion à base de différents matériaux d'électrodes positives ont également été développés. Un

modèle rapide et précis simulant la performance de piles Li-ion avec des électrodes positives à base de $LiMn_2O_4$ ou de $LiCoO_2$ est présenté. Également, deux modèles ont été développés pour prédire la performance des piles Li-ion avec une électrode positive de $LiFePO_4$. Le premier, appelé modèle mosaïque modifié (MM), est basé sur une approche macroscopique alors que le deuxième, appelé le modèle mésoscopique, est plutôt basé sur une approche microscopique. Des études d'estimation de paramètres ont été conduites en utilisant les modèles développés et des données expérimentales fournies par Hydro-Québec. Tous les paramètres électrochimiques et thermo-physiques des piles Li-ions ont été simultanément identifiés et appliqués à la prédiction de la performance des piles. Finalement, une technique en temps réel reposant sur des réseaux de neurones est introduite dans la méthode d'estimation des paramètres intrinsèques au piles Li-ion.

Mots clés: Piles Li-ion, Modèle pseudo-2D (P2D), Estimation de paramètres, Méthode inverse, Analyse de sensibilité, Algorithme génétique, Matériau d'électrode positive à base de LiFePO4 (LFP), Modèle mosaïque modifié, Optimisation multi-objectif, Piles Li-ion cylindriques, Modèle mésoscopique, Estimation de paramètres en ligne, Réseaux neuronaux, Système de gestion de batteries.

Abstract

The safety of many electrical systems is strongly dependent on the reliable operation of their lithium-ion (Li-ion) battery packs. As a result, the battery packs must be monitored by a battery management system (BMS). The BMS interacts with all the components of the system so as to maintain the integrity of the batteries. The main part of a BMS is a Li-ion battery model that simulates and predicts its different operating points. In the electronics and in the automobile industries, the BMS usually rests on simple empirical models. They are however unable to predict the battery parameters as it ages. Furthermore, they are only applicable to a specific cell. Electrochemical-based models are, on the other hand, more sophisticated and more precise. These models are based on chemical/electrochemical kinetics and transport equations. They may be used to simulate the Li-ion battery characteristics and reactions.

In order to run the electrochemical-based mathematical models, it is imperative to know the different electrochemical and thermophysical parameters of the battery. The significant variables of the Li-ion battery can be classified into three groups: geometric, material and operational parameters. The geometric and material parameters can be easily obtained from direct measurements or from the datasheets provided by the manufacturer. The operational properties are, on the other hand, not easily available. Furthermore, some of them may vary according to the measurement techniques or the battery age. Sometimes, the measurement of these parameters requires the dismantling of the battery itself, which is a risky and destructive procedure.

Many investigations have been conducted to identify the operational parameters of Li-ion batteries. However, most of these studies focused on the estimation of limited parameters, or considered only one type of the positive electrode materials used in Li-ion batteries. Moreover, the coupling of the thermophysical parameters to the electrochemical variables is ignored in all of them. The main goal of this thesis is to develop a general method to simultaneously identify different electrochemical and thermophysical parameters and to predict the performance of Li-ion batteries with different positive electrode materials. To achieve this goal, an effective inverse method is introduced. Also, direct models representative of Li-ion batteries are developed, applicable for all of the positive electrode materials. A fast and accurate model is presented for simulating the performance of the Li-ion batteries with the $LiMn_2O_4$ and $LiCoO_2$ positive electrodes. Moreover, two macro- and micro-based models are developed for predicting the performance of Li-ion battery with the $LiFePO_4$ positive electrode, namely the Modified Mosaic (MM) and the mesoscopic-based models. The parameter estimation studies are then implemented by means of the developed direct models and experimental data provided by Hydro-Québec. All electrochemical and thermophysical parameters of the Li-ion batteries are simultaneously identified and applied for the prediction of the battery performance. Finally, a real-time technique resting on neural networks is used for the estimation of the Li-ion batteries intrinsic parameters.

Keywords: Li-ion battery, P2D model, Parameter estimation, Inverse method, Sensitivity analysis, Genetic Algorithm, LiFePO4 (LFP) positive electrode material, Modified Mosaic model, Multi-objective parameter estimation, Cylindrical Li-ion battery, Mesoscopic model, On-line parameter estimation, Neural Networks, Battery management system.

Acknowledgments

I would like to express my deep appreciation to my supervisor Martin Désilets, and my co-supervisor Marcel Lacroix for their continued support, valuable guidance, and the academic environment they provided during the course of research.

I would like to thank my committee members, Dr. Mark Pritzker, Dr. Jocelyn Veilleux and Dr. Bernard Marcos for their time to review and approve my thesis.

I am grateful to my friends and colleagues at the Université de Sherbrooke (Mohsen Ariana, Barzin Rajabloo, Giuliana Litrico, Elaheh Oliaii, and Gabriel St-Pierre Lemieux) for providing a friendly and dynamic environment in the office. I have had a great time working with you guys and have enjoyed each and every one of you.

I would like to acknowledge my parents and my brother for the unlimited love and support you provided me throughout all these years. Without your support, I would not have made it so far.

Last, but not least, my most sincere thanks go to my lovely wife, Farzaneh, for all her love, encouragement and support.

Table of contents

List of figures

List of tables

1. Introduction

1.1. Lithium-ion batteries

The prime characteristics of lithium-ion (Li-ion) batteries compared to the other kinds of batteries, have made it the preferred candidate for many electrical storage applications. Not only do Li-ion batteries have a high energy density (20-240 Wh/kg), but they also provide a higher power density (200-2000 W/kg) in comparison with other rechargeable batteries. Beside these mentioned points, long cycle life, wide temperature range, low self-discharge rate, rapid charging-discharging capability, and no maintenance have been reported in the literature as the other advantages of the Li-ion batteries [1-3]. Li-ion batteries have been manufactured in four different shapes, namely coin, cylindrical, prismatic, and flat, as depicted in Figure 1.1 [4].

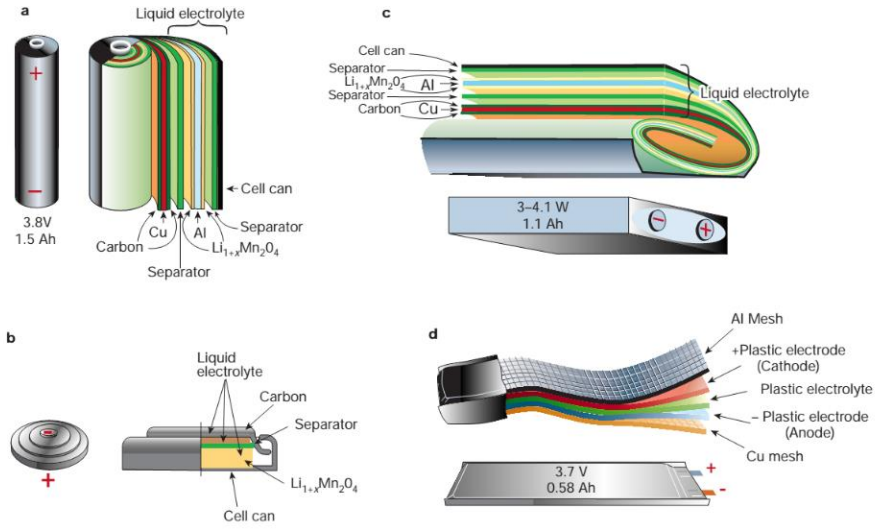

Figure 1.1: Schematics of all kinds of Li-ion battery a: Cylindrical; b: coin; c: prismatic; and d: thin and flat [4]

The Li-ion battery internal structure comprises four main sections including positive and negative electrodes, an electrolyte, and a separator as shown in Figure 1.2 [5]. The common materials used in these different parts have been gradually changed to improve the efficiency, safety, performance, and to decrease its initial costs. Today, the typical materials of positive electrode are $LiMn_2O_4$ (LMO), $LiCoO_2$ (LCO) and $LiFePO_4$ (LFP), and graphite for negative electrode [1-3, 6]. The separator also consists of an ionic conductor material. It prevents short-circuiting of the cell while permitting the mass flow of ions. During the discharge, due to a spontaneous electrochemical reaction, electrons (e^-) are released from the negative electrode to the positive electrode through an external circuit. As a result, an

electrical potential difference is developed between the two electrodes. In order to satisfy the electroneutrality condition, the lithium-ions (Li^+) transfer from the negative to the positive electrode through electrolyte. This process occurs in reverse during the battery charge process by applying an external electrical power source to the cell. It is noted that, the mass flux of Li-ions is based on three transport phenomena including migration, diffusion, and convection. These phenomena are triggered by an electric potential, concentration difference and pressure gradient respectively [2, 7].

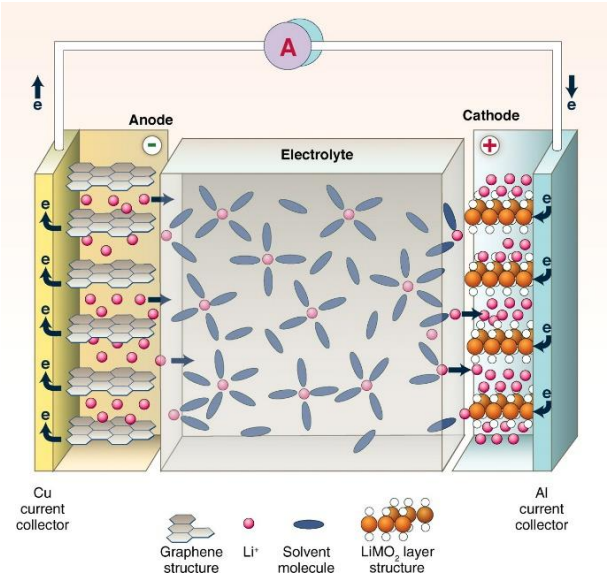

Figure 1.2: The inside structure and phenomena during the discharge of a Li-ion battery [5]

1.2. Li-ion battery models

Nowadays, Li-ion batteries serve as the core energy storage for many important electrical systems, such as electronics industry, hybrid electric vehicles (HEVs), plug-in hybrid electric vehicles (PHEVs), etc. In order to control and monitor these systems, it is imperative to rely on a fast and accurate model to be applied to Battery Management Systems (BMS). Therefore, considerable researches have been carried out to develop the Li-ion battery models for applications in control, on-line monitoring, optimization, parameter estimation, and age prediction [8-10]. In general, Li-ion battery models can be divided into two classes: empirical models and electrochemical-based models [9, 10]. The aim of all these models is to determine the battery State of Charge (SoC) and State of Health (SoH) [8].

Empirical models such as equivalent circuit-based models and neural network models are widely used in the BMSs of electronics and vehicle industries [15,16]. These models rest on battery past experimental data to predict its future states. Electrochemical-based models are, on the other hand, more sophisticated and precise. These models are based on

chemical/electrochemical kinetics and transport equations. They may be used to simulate the Li-ion battery characteristics and reactions [12]. The Pseudo-two-Dimensional (P2D) model and the Single Particle Model (SPM) are among the most popular electrochemical-based models. A detailed description of the empirical and the electrochemical-based models can be found in Chapter 2.

1.3. Inverse method and parameter estimation

The success of the Li-ion battery models depends, among other things, on the precise knowledge of the electrochemical and thermophysical properties of the battery [11-13]. Direct measurement of these properties is, however, a tedious task. It typically requires the dismantling of the battery. Moreover, the measured properties are dependent on the battery age and may vary according to the measurement technique. In this thesis, to overcome the difficulties of measuring the battery properties, parameter estimation techniques coupled to inverse methods have been proposed.

Inverse methods are used for the parameter estimation of a system or for its functional identification. In the former, the unknown parameters can be estimated by means of some experimental data. In the latter, the unknown functions can be determined in a finite or an infinite dimensional space [14]. The solution methods used to solve inverse problems are usually more complicated than for direct problems. Direct problems are well-posed problems. The conditions that define a well-posed problem are that (1) the solution must exist; (2) it is unique and (3) it must be a continuous function. Inverse problems are, on the other hand, ill-posed problems. The solution of most inverse problems is highly dependent on the initial condition and on the boundary conditions as well as on the measured signals. There have been numerous attempts to tackle these difficulties and to convert inverse problems into well-posed problems [14-16].

1.3.1. Inverse method formulation

In parameter estimation problems, the experimental signals play a key role in finding the expected parameters. These parameters must be measurable and accurate when compared with the direct model. In the identification of the Li-ion battery parameters, the time-varying cell potential, surface temperature, and current values can be measured during the charge/discharge process. Figure 1.3 illustrates the relationship between the different elements of a parameter estimation study based on an inverse method. The objective function is defined here as the difference between the experimental data and the predictions of the

direct model. A mathematical optimizer is employed to minimize the objective function so as to find the best values of the expected parameters.

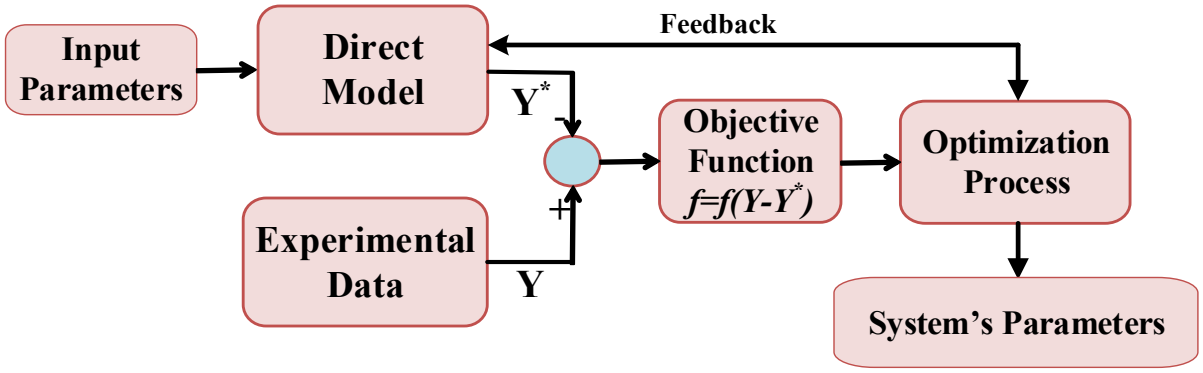

Figure 1.3: Different elements of a parameter estimation study based on an inverse method [13]

The experimental data of the Li-ion battery charge/discharge process are measured in small time intervals between zero and cut-off time ($0 < t < t_c$). Therefore, the inverse problem of the Li-ion battery should be defined as a "whole time domain" approach. It is assumed that the measurement error of experimental data is a random variable. The experimental data vector ($\mathbf{Y}^*$) consists of one charge/discharge process at N time intervals as shown in Eq. 1.1:

$$Y^* = \begin{bmatrix} Y_1^* \\ Y_2^* \\ \vdots \\ Y_N^* \end{bmatrix}_{N\times 1} ; t = t_1, t_2, ..., t_N \qquad (1.1)$$

The measurement of random errors is always a concern in the solution of inverse problems. The stability of the inverse method is sensitive to these errors. The solution technique for the inverse problem should be stable with the measurement errors and for small time intervals [14, 15]. Beck proposed eight statistical standard assumptions for dealing with this concern as follows [16]:

1) The definition of the random error (e) of i^{th} experimental data is:

$$e_i = (Y_m^*)_i - (Y_a^*)_i \qquad (1.2)$$

where subscripts m and a represent the measurement and actual variables, respectively.

2) The measurement errors are unbiased. Therefore, it has a zero expected value ($E(.)$):

$$E(e_i) = 0 \qquad (1.3)$$

3) The random errors have a constant variance. It means that the variance of Y_i is independent of the measurement, that is:

$$\sigma_i^2 = E\left\{\left[Y_m^* - E(Y_m^*)\right]^2\right\} = \sigma^2 = constant \quad (1.4)$$

4) The different errors are uncorrelated, which means the covariance of e_i and e_j is zero:

$$\mathrm{cov}\left(e_i, e_j\right) = 0 \ for i \neq j \quad (1.5)$$

5) The measurement random errors have a normal (Gaussian) distribution, that is:

$$f\left(e_i\right) = \frac{1}{\sigma\sqrt{2\pi}} \exp\left(\frac{-e_i^2}{2\sigma^2}\right) \quad (1.6)$$

6) The statistical parameters such as errors and variance are known.

7) Only the measured data are assumed to have random errors; the values of the other variables such as time and position are assumed to be accurately known.

8) If some prior information regarding the estimated parameters is known, it can be incorporated into the solution process to achieve more accuracy.

Generally, the objective function (S) is defined as the ordinary least-squares function of measured data (**Y***) and calculated values (**Y**) as follows [14, 15].

$$S = \left(\mathbf{Y}^* - \mathbf{Y}\right)^T \left(\mathbf{Y}^* - \mathbf{Y}\right) = \sum_{i=1}^{N} \left(Y_i^* - Y_i\right)^2 \quad (1.7)$$

where the superscript T indicates the transpose. When the experimental data are collected from M charge/discharge processes, Eq. 1.7 should be written as [14, 15]:

$$S = \left(\mathbf{Y}^* - \mathbf{Y}\right)^T \left(\mathbf{Y}^* - \mathbf{Y}\right) = \sum_{m=1}^{M} \sum_{i=1}^{N} \left(Y_{im}^* - Y_{im}\right)^2 \quad (1.8)$$

It is noted that the calculated vector (**Y**) should be derived as a function of the unknown parameters (**P**). In order to estimate only few unknown parameters, the objective function based on the Eq. 1.8 can be stable. However, oscillation about the solution may occur for the inverse problems with a large number of unknown parameters. This instability will be reduced by adding some regularization terms to the least-squares objective function using other techniques such as a Tikhonov's regularization and Alifanov's iteration regularization methods [14, 17]. The solution techniques should minimize the objective function (S) in order to determine the unknown vector **P**. They are chosen depending on how complex the direct model and how many parameters are to be identified. This process must be implemented by an optimizer by considering the system constraints and conditions.

1.3.2. Optimization

Due to the numerous parameters used in the objective function of the present parameter estimation study, there may be several local minima in the vicinity of the global minimum.

As a result, the optimization process for the inverse problem is mathematically challenging, slow to converge and computationally expensive [14-16]. Colaço et al. presented detailed descriptions and comparisons between different solution methods for inverse problems using the steepest descent method, the conjugate gradient method, the Newton-Raphson method, the quasi-Newton method, the Levenberg-Marquardt method (LM), Genetic Algorithms (GA), differential evolutions, the particle swarm method and the simulated annealing method [17]. In general, these optimization tools can be divided into two categories: deterministic techniques and stochastic methods. Although deterministic methods are usually faster than the stochastic methods, they easily fall into system local extrema and have complex structures. Stochastic-based optimization methods employ, on the other hand, random-based operation functions ideally suited for reaching the system global extremum [17, 18].

In this thesis, a stochastic technique called the genetic algorithm (GA) will be applied to all of the inverse problems for estimating the large number of electrochemical and thermophysical parameters of Li-ion batteries. The detailed description of this stochastic method is presented in Chapters 3, 4, and 6.

1.4. Thesis objectives and motivation

Many investigations have been conducted to identify the operational parameters of Li-ion batteries. However, most of these studies focused on the estimation of limited parameters, or considered only one type of positive electrode materials of the Li-ion battery. The detailed literature review of these works is presented in Chapter 3, 4, and 6. Moreover, the coupling of the thermophysical parameters to the electrochemical variables is ignored in all of them. The main goal of this thesis is to develop a general method to simultaneously identify different electrochemical and thermophysical parameters and to predict the performance of Li-ion batteries.

To achieve this goal, it is vital to develop an effective inverse method. Also, it is necessary to have a fast and accurate direct model for all positive electrode materials. As discussed before, the P2D model is the most popular and accurate electrochemical-based model for the Li-ion batteries. Three important drawbacks can however be enumerated for this model: (1) It is too complex to be used for a typical parameter identification process; (2) Its simplest version, SPM, is not accurate enough to be applied at high battery charge/discharge rates; (3) The P2D and SPM models cannot adequately simulate the behavior of batteries with LFP positive electrodes [19]. The main reason is that these models rely on Fick's law which does

not take into account the two-phase behavior of the LFP particles. Based on the aforementioned points, the main objectives of this thesis are presented as follows:

- Developing a simplified version of the P2D model for simulating the performance of the Li-ion batteries with the LMO and LCO positive electrodes. This model should be able to predict the battery polarization function for both low and high charge/discharge battery rates.
- Developing an accurate model to capture the two-phase behavior of the LFP particles. The model should be able to predict the plateau and the finial capacity of the LFP electrode.
- Developing a heat transfer model to be coupled to the developed electrochemical Li-ion battery models. This model should be able to simulate the surface temperature or the average temperature of the battery.
- Parameter estimation of the properties of the Li-ion batteries with different positive electrode materials. The process should be implemented in three separate steps for different applications: (1) Electrochemical parameter estimation; (2) Thermophysical properties identification; and (3) Simultaneous electrochemical and thermophysical parameter estimation. The first case is helpful in isothermal conditions to investigate different changes in the battery as it ages. The second case is useful for its application in the thermal management battery systems to predict the battery behavior independent of the electrochemical parameters. The third case covers the general condition and is helpful for all real applications.
- Developing a real-time technique to estimate the Li-ion batteries properties. This method can be helpful for all on-line applications such as the battery control and monitoring in the BMSs.

1.5. Thesis outline

This thesis includes nine chapters. Chapter 1 is an introduction to the study. In chapter 2, a review of all simplified versions of the P2D model is presented. Different physical and mathematical simplification techniques are investigated to be used for the Li-ion battery model development in other chapters. The electrochemical parameter estimation process is discussed in Chapter 3. A simplified version of the P2D model is developed in this chapter for the parameter estimation process. Moreover, a novel parameter estimation method is presented by virtue of the sensitivity analysis. The technique is validated for the Li-ion

batteries with the LMO, LCO, and LFP positive electrodes. Chapter 4 deals with the identification of the thermophysical properties of a Li-ion batteries independent of the electrochemical parameters. A heat transfer model is developed to be used as the direct model. A new model for the Li-ion batteries with the LFP positive electrode is introduced in Chapter 5, namely the Modified Mosaic (MM) model. This model is not based on the microscopic behavior of the LFP particles; instead it is developed by means of a macroscopic approach to estimate the battery performance at low and high charge/discharge rates. By using the MM model, a simultaneous electrochemical and thermophysical parameter estimation is carried out in Chapter 6. This process is a multi-objective inverse problem which can successfully capture all electro-thermal behaviors of the battery. In Chapter 7, a mesoscopic model is developed for the Li-ion battery with the LFP positive electrode. The results demonstrate a good agreement between the experimental data and the MM modeling results. However, it is very expensive as it should be solved for many particles, at the same time. In Chapter 8, a novel approach for the on-line parameter estimation is presented. This technique is suitable for real-time applications and employs a Neural Network (NN) to estimate some properties of the Li-ion battery. Finally, the thesis conclusions and the future work suggestions are presented in Chapter 9.

CHAPITRE 2 : AVANT-PROPOS

Auteurs et affiliation:

- Ali Jokar: étudiant au doctorat, Université de Sherbrooke, Faculté de génie, Département de génie chimique et de génie biotechnologique.
- Barzin Rajabloo: étudiant au doctorat, Université de Sherbrooke, Faculté de génie, Département de génie chimique et de génie biotechnologique.
- Martin Désilets: professeur, Université de Sherbrooke, Faculté de génie, Département de génie chimique et de génie biotechnologique.
- Marcel Lacroix: professeur, Université de Sherbrooke, Faculté de génie, Département de génie mécanique.

Date d'acceptation: 10 juillet 2016

État de l'acceptation: version finale publiée

Revue: Journal of Power Sources

Référence: [10]

Titre français: Revue des modèles pseudo-2D simplifiés pour les piles aux ions lithium

Contribution au document: Cet article présente une revue des travaux scientifiques portant sur le développement de versions simplifiées du modèle P2D. Ces modèles sont essentiels aux travaux de cette thèse puisque les méthodes inverses développées plus tard dans la thèse doivent s'appuyer sur un modèle direct de pile aux ions lithium rapide et représentatif. En outre, cet article de revue est utile car il permet de connaître les meilleures approches de simplification.

Résumé français:

Durant les dix dernières années, plusieurs efforts ont été consacrés au développement de modèles pour la prédiction, le contrôle, l'optimisation et l'estimation de paramètres de piles aux ions lithium (Li-ion). Selon toute vraisemblance, le modèle électrochimique le plus performant pour représenter le comportement des piles Li-ion est le modèle pseudo-2D (P2D). Cependant, les équations inhérentes à ce modèle étant complexes, il ne peut pas être utilisé pour les applications en temps réel telles que les systèmes de gestion des batteries (BMS). Plusieurs travaux de recherche ont été menés pour simplifier le modèle P2D et combler cette lacune. Des méthodes mathématiques et physiques ont été employées pour réduire l'ordre des équations du modèle P2D. Cet article présente une revue des études portant sur la modélisation des piles Li-ion utilisant des modèles P2D simplifiés. Les

hypothèses ayant servi au développement de ces modèles sont indiquées, les méthodes de calcul examinées, les avantages et les inconvénients des différents modèles sont discutées et les applications sont présentées. Des suggestions pour palliers aux inconvénients de ces modèles sont proposées. Les défis et les futures orientations des prochains travaux portant sur la modélisation des piles Li-ion sont également discutées.

2. Review of simplified Pseudo-Two-Dimensional models of lithium-ion batteries

2.1. Abstract

Over the last decade, many efforts have been deployed to develop models for prediction, control, optimization and parameter estimation of lithium-ion (Li-ion) batteries. It appears that the most successful electrochemical-based model for Li-ion battery is the pseudo-two-dimensional model (P2D). Due to the fact that the governing equations are complex, this model cannot be used in real-time applications such as Battery Management Systems (BMSs). To remedy the situation, several investigations have been carried out to simplify the P2D model. Mathematical and physical techniques are employed to reduce the order of magnitude of the P2D governing equations. The present paper is a review of the studies on the modeling of Li-ion batteries with simplified P2D models. The assumptions on which these models rest are stated, the calculation methods are examined, the advantages and the drawbacks of the models are discussed and their applications are presented. Suggestions for overcoming the shortcomings of the models are made. Challenges and future directions in the modeling of Li-ion batteries are also discussed.

Keywords: Review, Li-ion battery, P2D model, Simplified model, Battery management system

Nomenclature:

a_k	Specific surface area of electrode k $(k = p,n)$, m^2/m^3
a,b,c,d	Time-dependent constants
A,B,C,D	Time-dependent constants
$c_{e,k}$	Electrolyte concentration in region k $(k = p,s,n)$, mol/m^3
$c_{e,k}^{ini}$	Initial condition of electrolyte concentration in region k $(k = p,s,n)$, mol/m^3
$c_{s,k}$	Solid-state concentration of electrode k $(k = p,n)$, mol/m^3
$c_{s,k}^{ini}$	Initial condition of solid-state concentration of electrode k $(k = p,n)$, mol/m^3
$c_{s,k}^{max}$	Maximum concentration of Li^+ in the particle of electrode k $(k = p,n)$, mol/m^3
$c_{s,k}^{surf}$	Concentration of Li^+ on the surface of the particles of the electrode k $(k = p,n)$, mol/m^3
$c_{s,k}^{ave}$	Average Concentration of Li^+ on the particles of the electrode k $(k = p,n)$, mol/m^3
$D_{eff,k}$	Effective diffusion coefficient of Li+ in electrolyte for region k $(k = p,s,n)$, m^2/s
$D_{s,k}$	Li^+ diffusion coefficient in the particle of electrode k $(k = p,n)$, m^2/s
F	Faraday's constant, C/mol
I	Applied current density, A/m^2
i_0	Exchange current density for the solvent reduction reaction, A/m^2
J_k	Wall flux of Li^+ on the particle of electrode k $(k = p,n)$, mol/m^2s
K_k	Reaction rate constant of electrode k $(k = p,n)$, $m^{2.5}/mol^{0.5}$ s

L	Total thickness, m
L_k	Thickness of region k $(k = p, s, n)$, m
n	Negative electrode
p	Positive electrode
r	Radial coordinate, m
R	Universal gas constant , J/(mol K)
$R_{s,k}$	Radius of the particle of electrode k $(k = p, n)$, m
s	Separator
SOC_k	state of charge of electrode k
t	Time, s
T	Absolute temperature, K
t_+	Li^+ transference number in the electrolyte
U_k	Open-circuit potential of electrode k $(k = p, n)$, V
x	Spatial coordinate, m
V_{cell}	Voltage of cell, V

Greek

$\alpha, \beta, \zeta, \psi$	Time-dependent constants
ε_k	Porosity of region k $(k = p, s, n)$
$\kappa_{eff,k}$	Effective ionic conductivity of the electrolyte in region k $(k = p, s, n)$, S/m
$\mu_{s,k}$	Overpotential of electrode k $(k = p, n)$, V
$\sigma_{eff,k}$	Effective electronic conductivity of the solid phase of electrode k $(k = p, n)$, S/m
$\phi_{e,k}$	Electrolyte potential in region k $(k=p,s,n)$, V
$\phi_{s,k}$	Solid-phase potential of electrode k $(k = p, n)$, V

2.2. Introduction

The distinctive intrinsic characteristics of the lithium-ion (Li-ion) battery have made it the preferred device for many electrical storage applications [1, 2]. The main reason for this success is its prime position in the Ragone plot (Fig. 2.1). Not only do Li-ion batteries have attractive energy density, but they also provide a higher power density in comparison with other rechargeable batteries [3, 20-23]. Li-ion batteries also exhibit good electrochemical and thermal stability, long battery life [24, 25], low self-discharge rate [26], rapid charging-discharging capability, memory effect, and no maintenance [1, 27].

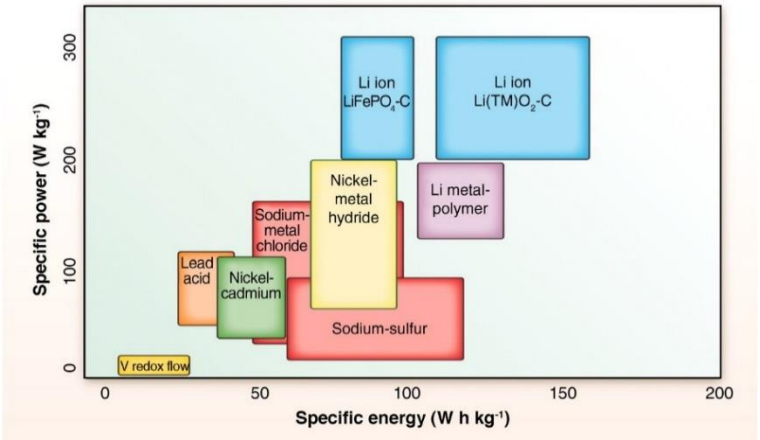

Figure 2.1: Ragone plot for different secondary batteries [3]

Li-ion batteries are manufactured in four different shapes, namely coin, cylindrical, prismatic, and flat. Their internal structure comprises four main sections including positive and negative electrodes, an electrolyte, and a separator [2]. The common materials used in these different sections have been modified gradually in order to improve their efficiency, safety, performance, and initial costs. During the discharge process, electrons (e^-) are released from the negative electrode to the positive electrode through an external circuit. This phenomenon is due to a spontaneous electrochemical reaction. As a result, an electrical potential difference is developed between the two electrodes. In order to satisfy the electro neutrality condition, the Li-ions (Li^+) move from the anode to the cathode through an electrolyte. The electrolyte usually consists of a single Li salt in an organic solvent. The transfer process is reversed when the battery is charging. This process is carried out by providing an external power source to the cell.

The mass flux of Li-ions is based on three transport phenomena, i.e., migration, diffusion, and convection. These phenomena are triggered by an electric potential, a concentration difference and a pressure gradient respectively. It should be noted that the last phenomenon is negligible in Li-ion batteries [1, 2].

One of the research challenges in the development of Li-ion batteries is to predict their behavior under different operating modes. In general, Li-ion battery models can be divided into two classes: empirical models and electrochemical models [9, 28]. The aim of all these models is to determine the battery state of charge (SoC) and state of health (SoH) [8].

Empirical models such as equivalent circuit-based models and neural network models are widely used in the Battery Management Systems (BMS) of electronics and vehicle industries [29, 30]. These models rest on the battery past experimental data to predict its future states. The main elements of the models are determined from the history of electric charge/discharge signals such as the cell potential and current. The main advantages of empirical models are that they are computationally fast and simple. But they also present some drawbacks. For instance, the physics-based parameters cannot be determined. The battery characteristics are never updated as the battery ages and the battery's empirical model cannot be transposed to other types of batteries. Therefore, the BMSs based on empirical models are unable to work properly after a certain number of charge/discharge cycles [28, 31, 32].

Electrochemical models are, on the other hand, more sophisticated. These models are based on chemical/electrochemical kinetics and transport equations. They may be used to simulate

the Li-ion battery characteristics and reactions [9]. The Pseudo-two-Dimensional (P2D) model and the Single Particle Model (SPM) are among the most popular electrochemical-based models. The P2D model rests on porous electrode theory, concentrated solution theory and kinetics equations [33, 34]. The P2D model has been extensively used in Li-ion battery investigations [32]. Its predictions are relatively accurate and have shown, in general, good agreement with experimental data [35, 36].

In order to reduce the computational times, a simplified version of the P2D model, called the SPM, has been developed. In the SPM, the properties of the electrolyte are ignored and the transport phenomena are treated in a simple manner [37]. The effects of the thermal conditions on the Li-ion battery's performance are however considered [38, 39].

Nowadays, Li-ion batteries serve as the core energy storage for many important electrical systems (electronics industry, HEVs, PHEVs, etc). In order to control and to monitor these systems on-line, it is imperative to rely on a fast and accurate real-time simulation BMS. The P2D model is unquestionably rigorous and accurate. But it is too complicated and too slow to be applied to the BMSs. The SPM, on the other hand, provides quick responses but it is unsuitable for simulating high discharge rates and thick electrodes. The shortcomings of the SPM and the complexity of the P2D model have motivated the development of simplified versions of the P2D model to be used in the BMSs in different applications. These simplified P2D models have been designed mainly for applications in control, on-line monitoring, optimization, parameter estimation, and age prediction. Figure 2.2 depicts the general classification of Li-ion battery models. The BMSs with the simplified P2D models have significant advantages over those based on the empirical models. Due to their use of physical based equations, they are more accurate. They can be used for the parameter estimation and age prediction investigation of the Li-ion cells. Moreover, they can be updated as the battery ages to avoid the considerable errors of the empirical based models.

The present paper is a review of the studies on the modeling of Li-ion batteries with simplified P2D models. The assumptions on which these models rest are stated, the calculation methods are examined, the advantages and the drawbacks of the models are discussed and their applications are presented. Suggestions for overcoming the shortcomings of the models are made. Challenges and future directions in the modeling of Li-ion batteries are also discussed.

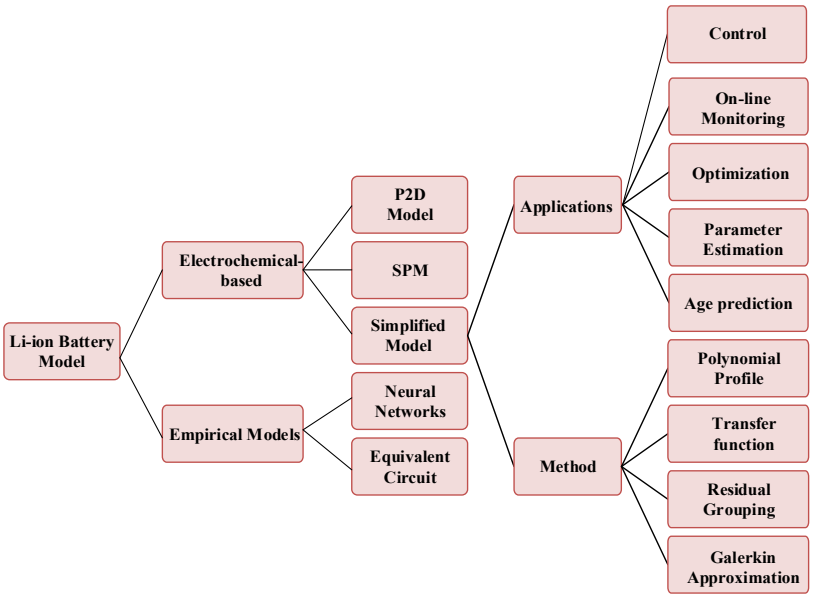

Figure 2.2: The general classification of Li-ion battery forward models

2.3. Pseudo-Two-Dimensional model (P2D)

One of the interesting aspects of the Li-ion battery is the porous structure of its electrodes. This feature increases the interfacial area between the solid and the electrolyte solution and, as a result, it dampens the negative effects of the slow electrochemical reactions [40]. Due to the complex geometry of the porous media, there have been practical difficulties in developing a reliable model of the battery. In 1975, Newman and Tiedemann developed the porous-electrode theory for battery applications using a macroscopic approach. To circumvent the difficulties associated with the geometry, the governing equations were derived based on the average quantities and continuous functions. In 1993, Doyle et al. introduced the Pseudo-Two-Dimensional (P2D) model for Li-ion batteries using a combination of the porous electrode theory and the concentrated solution theory. To this day, this model remains the most popular Li-ion battery model. It has been thoroughly tested and validated [33]. Figure 2.3 is a schematic of the Li-ion battery. The electrodes are considered as a porous matrix. Their behavior is modeled with spherical particles surrounded by the electrolyte. The intercalation and the de-intercalation processes of the Li-ions are performed through the surface area of these particles. Also, the transfer processes are predominantly unidirectional. Consequently, a 1-D mathematical model (x axis) may be applied [1, 34, 41].

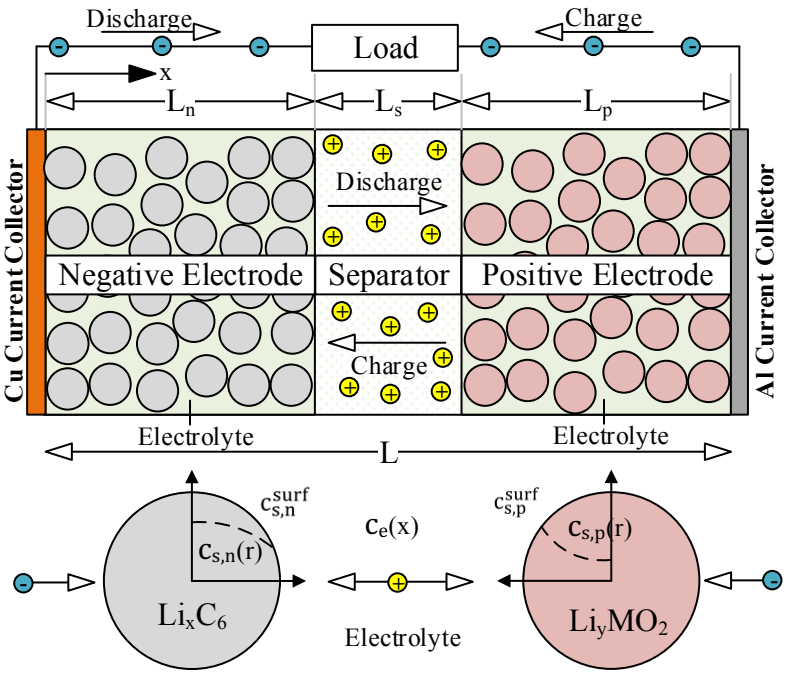

Figure 2.3: The Li-ion battery P2D model

The governing equations of the P2D model are reported in Table 2.1. The main features of these equations are: 1) solid-state Li^+ ion concentration (c_s) in the electrodes is derived from Fick's law of diffusion for spherical particles; 2) liquid-phase Li^+ ion concentration (c_e) in the electrolyte and in the separator is based on the conservation of Li^+ ions; 3) solid-state potential (Φ_s) in the electrodes is derived from Ohm's law; 4) The liquid-phase potential (Φ_e) in the electrolyte and in the separator is calculated using Kirchhoff's and Ohm's laws; 5) The pore wall flux of Li^+ ions (J) in the electrodes is described by the Butler-Volmer kinetics equation [34, 42].

In 1996, Doyle and Newman compared the predictions of the P2D model with their experimental data. Further investigations have confirmed the exactness of the P2D approach for modeling Li-ion batteries [9, 35, 36]. Indeed, in the absence of reliable experimental data, the P2D model predictions are often used as benchmarks [43-45].

Unfortunately, a full analytical solution of the governing P2D model equations is unavailable [46, 47]. Therefore, different numerical methods such as Finite-Difference Method (FDM), Finite-Element Method (FEM), the Finite-Volume Method (FVM), orthogonal projections [48] and, recently, the Chebyshev orthogonal collocation [32] have been employed to estimate the model parameters [49]. The FDM and the FEM have been extensively used with in-house codes and commercial software. Commercial software are practical tools for simulating complex geometries and battery stacks (COMSOL, Battery Design Studio (BDS) and AutoLion [50, 51]).

Table 2.1: The governing equations of P2D Model [44]

Region	Eq. no.	Governing equations
Electrodes (k=n,p)	(2.1)	$\frac{\partial c_{s,k}(x,r,t)}{\partial t} = \frac{D_{s,k}}{r^2}\frac{\partial}{\partial r}\left(r^2 \frac{\partial c_{s,k}(x,r,t)}{\partial r}\right)$
	(2.2)	$\varepsilon_k \frac{\partial c_{e,k}(x,t)}{\partial t} = \frac{\partial}{\partial x}\left(D_{eff,k}\frac{\partial c_{e,k}(x,t)}{\partial x}\right) + a_k(1-t_+)J_k(x,t)$
	(2.3)	$\sigma_{eff,k}\frac{\partial^2 \Phi_{s,k}(x,t)}{\partial x^2} = a_k F J_k(x,t)$
	(2.4)	$-\sigma_{eff,k}\frac{\partial \Phi_{s,k}(x,t)}{\partial x} - \kappa_{eff,k}\frac{\partial \Phi_{e,k}(x,t)}{\partial x} + \frac{2\kappa_{eff,k}RT}{F}(1-t_+)\frac{\partial \ln c_{e,k}}{\partial x} = I$
	(2.5)	$J_k(x,t) = K_k\left(c_{s,k}^{\max} - c_{s,k}^{surf}\right)^{0.5}\left(c_{s,k}^{surf}\right)^{0.5} c_{e,k}^{0.5}\left[\exp\left(\frac{0.5F\mu_{s,k}(x,t)}{RT}\right) - \exp\left(-\frac{0.5F\mu_{s,k}(x,t)}{RT}\right)\right]$ $\mu_{s,k}(x,t) = \Phi_{s,k}(x,t) - \Phi_{e,k}(x,t) - U_k;\ V_{cell}(t) = \Phi_{s,k}(0,t) - \Phi_{s,k}(L,t)$
Separator (k=s)	(2.6)	$\varepsilon_k \frac{\partial c_{e,k}(x,t)}{\partial t} = \frac{\partial}{\partial x}\left(D_{eff,k}\frac{\partial c_{e,k}(x,t)}{\partial x}\right)$
	(2.7)	$-\kappa_{eff,k}\frac{\partial \Phi_{e,k}(x,t)}{\partial x} + \frac{2\kappa_{eff,k}RT}{F}(1-t_+)\frac{\partial \ln c_{e,k}}{\partial x} = I$

2.4. Single Particle Model (SPM)

Atlung et al. have proposed three different approaches for simulating the motion of ions in and out of the electrodes. These approaches simulate an infinite plane, an infinitely long cylinder, and a number of spherical particles [52]. The spherical approach has been retained for modeling the electrochemical processes of porous electrodes [34, 53]. It has also been employed in the P2D model in conjunction with other governing equations for the x direction. In 2000, Zhang et al. proposed a simplified version of the P2D model known as the Single Particle Model (SPM). The SPM rests on two main assumptions. First, each electrode is modeled as two spherical particles in which intercalation and de-intercalation phenomena occur. Second, the variations in the electrolyte concentration and in the potential are ignored [54]. Figure 2.4 illustrates a schematic of the SPM. Equations (2.1) and (2.5) from Table 2.1 are the governing equations of the SPM. These equations comprise the solid-state concentration and the Butler-Volmer kinetics equations at both negative and positive electrodes.

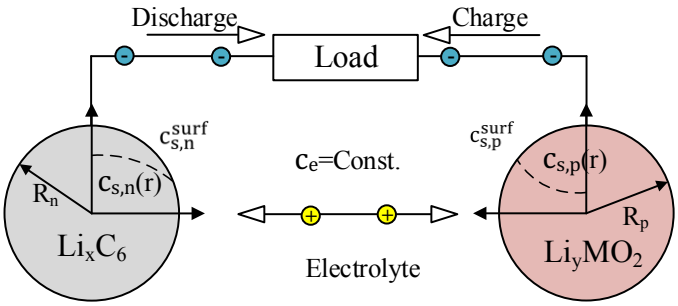

Figure 2.4: Schematic of Single Particle Model (SPM)

The main features of the SPM are: (1) its simplicity; (2) its solution requires minimum computational effort and (3) it can serve many purposes such as online estimation [37] and life modeling [55, 56] of Li-ion batteries. Its main drawback is that it must be fine-tuned according to the electrolyte properties for thick electrodes and at high discharge rates [9]. Improved versions of the SPM that alleviate these problems are however available [42, 50]. Multiple Particle (MP) models have also been proposed for dealing with particles of varying radii, different properties and a range of contact resistance (R_c) for Li-ion batteries equipped with $LiFePO_4$ electrodes (Figure 2.5) [56-58].

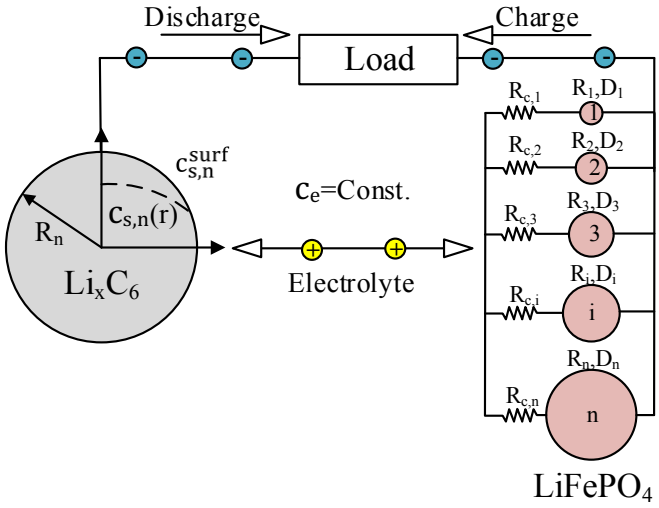

Figure 2.5: Schematic of Multiple Particle (MP) model

2.5. Thermal models

The effect of the operating temperature on the performance of Li-ion batteries has also been investigated [59-67]. It was found that the operating temperature plays a key role in the aging phenomenon. In general, low operating temperatures decrease the battery capacity and high temperatures degrade it [39, 59].

In 1985, Bernardi et al. developed an energy balance model for battery systems [38]. Pals and Newman used a P2D model coupled with this energy balance in order to compute the heat generation rate of single cell from a Li-ion battery [60]. Next, they modeled a cell stack based on the calculated characteristics of a single one [61]. Other solutions have also been obtained for thermal and electrochemical equations under uniform temperature conditions [9, 36]. 2-D and 3-D models have been developed to elucidate the behavior of Li-ion batteries under harsh operating conditions [62, 63]. In order to simplify the complex thermal models, Guo et al. coupled the SPM with the heat equations. Their numerical predictions showed good agreement with experimental data for low discharge rates [64]. Empirical-based simulations have also been carried out to quantify the Li-ion battery heat generation rate [59, 65] and to update the battery parameters [66, 67]. Bandhauer et al. (2011) have produced an extensive review of the thermal models for Li-ion batteries [39].

The conclusion that emerges from all these studies is that the combination of thermal and electrochemical models mimics more faithfully the behavior of Li-ion batteries. The information that it provides about the battery performance, its safety, and its maintenance is more reliable. As expected, these models are, however, computationally more expensive and require additional input data such as the specific heat capacity (C_p), the thermal diffusivity (α) and the thermal conductivity (k) of the materials.

2.6. Simplified models

2.6.1. Necessities

Figure 2.6 shows the variation in the electrolyte functions at the end of the discharge process. Calculations were performed with a Li-ion battery P2D model for different discharge rates [9]. It is seen that for low discharge rates (lower than 1C), the electrolyte properties can be assumed constant. In this case, a simple model like the SPM is the preferred option for the Li-ion battery. At higher discharge rates however, the story is different. The concentration and potential profiles vary significantly. In these cases, simple battery models are no longer suitable. More accurate and computationally intensive models must be sought. It is shown, in next section, that most of these models are based on one-dimension polynomial profiles for the electrolyte properties.

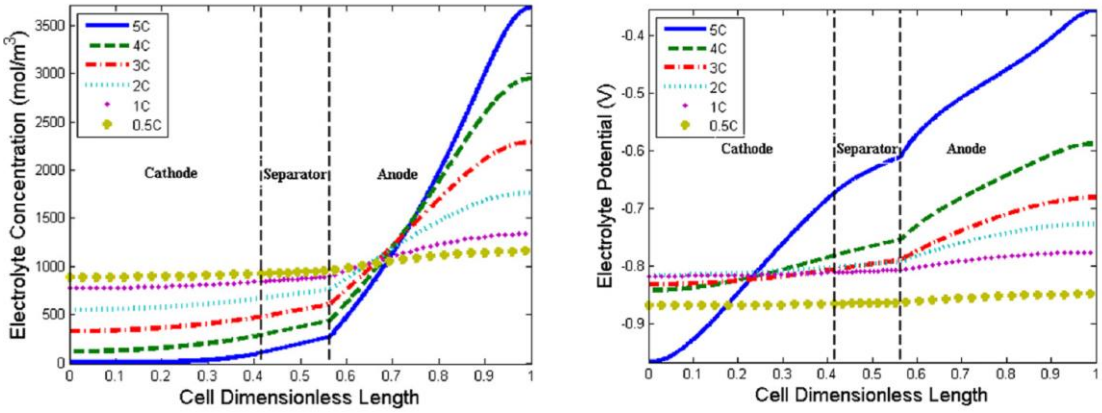

Figure 2.6: Change in the electrolyte properties at the end of discharge for different discharge rates [9]

2.6.2. Applications

The safety of many electrical systems is strongly dependent on the reliable operation of their Li-ion battery packs. As a result, the battery packs must be monitored by a Battery Management System (BMS). The BMS interacts with all the components of the system so as to maintain the integrity of the batteries [68-73]. The main part of a BMS is a Li-ion battery model that simulates and predicts its different operating points. In the electronics and in the automobile industries, the BMS usually rests on simple empirical models [74]. These models are simple and provide quick responses. They are however unable to predict the battery parameters as it ages. Furthermore, they are only applicable to a specific cell [28, 31, 32].

Due to these drawbacks, many efforts have been made to adapt electrochemical-based models to BMSs. The shortcomings of the SPM and the complexity of the P2D model have motivated the development of simplified versions of the P2D model. These simplified P2D models have been designed mainly for applications in control, on-line monitoring, optimization, parameter estimation, and age prediction. Figure 2.7 summarizes the applications, inputs and outputs of a BMS system.

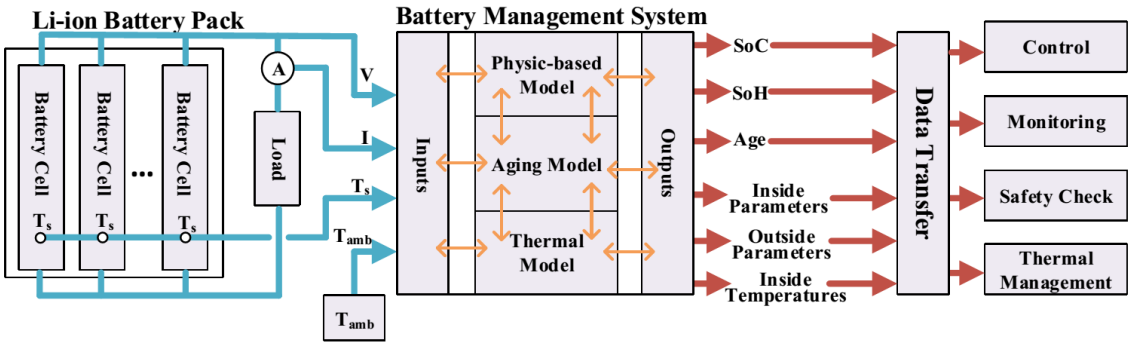

Figure 2.7: Schematic of BMS with different applications, inputs and outputs

2.6.3. Methodologies

Table 2.2 reports the main features of the P2D reduced models.

Table 2.2: Main features of the P2D simplified models

Author	Battery Material	Cycle Rate	Thermal model	Applications	Description and Methodology
Subramanian et al. (2001) [75]	-	1C	No	-	Parabolic Profile (PP) approximation in r direction Volume Averaging
Subramanian et al. (2005) [76]	$LiCoO_2$	2C	No	-	Combination of PP model and P2D model
Subramanian et al. (2007) [77]	$LiCoO_2$	C/2,1C	No	C	Initial concepts of the reformulation model
Smith et al. (2007) [43]	-	1C-5C	No	C	Combination of an analytical transfer function & a numerical transfer matrix to develop a State Variable Model (SVM)
Domenico et al. [78]	-	-	No	C	Electrode Averaged Model developed by using an average value for all cell variables and a Kalman filter
Smith et al. (2008) [79]	-	1C	No	C	Residue grouping technique
Cai et al. (2009) [80]	$LiMnO_2$	C/10-20C	No	-	Proper Orthogonal Decomposition (POD)
Subramanian et al. (2009) [81]	$LiCoO_2$	C/2,1C	No	C, PE	Mathematical model reformulation
Smith et al. (2010) [82]	-	-	No	C, M	Model using a residue grouping and a SVM and Kalman filter
Ramadesigan et al. (2010) [83]	-	5C, 10C	No	-	Solid-state concentration equation simplified: A polynomial eigenfunction, a finite difference method with Unequal Node Spacing
Guo et al., (2011) [64]	$LiCoO_2$	C/33, C/2, 1C	Yes	-	Thermal behaviour of SPM considered
Forman et al. (2011) [84]	-	C/10, C/2, 2.5C	No	C, PE	Linearized Butler-Volmer equation and Padé approximation method for solid concentration PDEs
Dao, et al. (2012) [44]	$LiCoO_2$	1C	No	C, PE	Combination of PP model & Galerkin's approximation
Lee et al. (2012) [85]	$LiMnO_2$	2C	No	C	Modify Smith models by using a linear BV equation and a discrete-time realization algorithm approach
Klein et al. (2013) [45, 86]	-	5C	Yes	M	Observer developed by using a PP model and a constant electrolyte concentration function
Luo et al. (2013) [86, 87]	$LiMnO_2$	4C	No	C	Extended single particle model by considering a non-uniform profile for pore wall fluxes and electrolyte properties distributions on SPM.
Marcicki et al. (2013) [88]	$LiFePO_4$	1C	No	C, PE	Padé approximation used to simplify all PDEs
Rahimian et al. (2013) [9]	$LiCoO_2$	1C-5C	No	C	Extended SPM by assuming a polynomial profile for electrolyte properties
Tanim et al. (2015) [42]	$LiNiCoMnO_2$	1C-5C	Yes	C,A	ESPM and ESPM-T developed by considering a polynomial function for the electrolyte concentration
Majdabadi et al. (2015) [89]	$LiFePO_4$	C/25-5C	No	C	Polynomial profiles for the electrolyte properties in the Multiple Particle (MP) model

* A: Age prediction, C=Control, M: Monitoring, PE: Parameter Estimation

Wang and Gu (1998) employed a polynomial profile to simulate the solid-state concentration function. Their model predicts both the battery and the fuel cell behavior [90]. Using a similar approach, Subramanian et al. introduced a simplified model, known as the Parabolic Profile approximation (PP), for Li-ion batteries [75, 76]. In the PP model, the solid concentration equation of the P2D model (Eq. 2.1) is simplified by assuming one of the solid-concentration polynomial profiles as shown in Eq. 2.8(a-c). This assumption allows the reduction of Partial Differential Equations (PDEs) to simpler Differential Algebraic

Equations (DAEs). The accuracy of the PP model is of course dependent on the order of the polynomial approximation. By using the volume-averaged method for computing the polynomial coefficients of Eq. 2.8(a), the PP model's governing equations (Eq. 2.9 and 2.10) are determined [76]:

$$c_{s,k}(r,t) = a(t) + b(t)(r/R_k)^2 \; ; k = n, p \tag{2.8a}$$

$$c_{s,k}(r,t) = a(t) + b(t)(r/R_k)^2 + c(t)(r/R_k)^4 \; ; k = n, p \tag{2.8b}$$

$$c_{s,k}(r,t) = a(t) + b(t)(r/R_k)^2 + c(t)(r/R_k)^4 + d(t)(r/R_k)^6 \; ; k = n, p \tag{2.8c}$$

$$\frac{d}{dt} c_{s,k,ave} + 3\frac{J_k}{R_k} = 0 \; ; k = n, p \tag{2.9}$$

$$\frac{D_{s,k}}{R_k}\left(c_{s,k}^{surf} - c_{s,k}^{ave}\right) = -\frac{J_k}{5} \; ; k = n, p \tag{2.10}$$

Santhanagopalan et al. (2006) compared the predictions of the P2D, of the SPM and of the PP models. They showed that: (1) For low discharge rates (up to 1C), the second-order PP model (Eq. 2.8(a)) and the SPM are in good agreement with the P2D predictions; (2) For medium and high discharge rates (more than 1C), the second-order PP model is more accurate than the SPM. One must, however, propose a higher order PP model (Eq. 2.8(b-c)) in order to successfully reproduce the P2D results; and (3) The CPU time for the PP model is 100 times smaller than that for the P2D model [37].

The solid concentration along the r-direction (Eq. 2.1) requires the solution of many different parameters [64]. As a result, in dynamic tests such as electric vehicle pulse loading, the PP model predictions would not show good agreement with real data. This problem results from the use of simple functions in the polynomial profiles. It may however be alleviated by using a combination of different functions to reduce the solid concentration equations.

Smith et al. used a residue grouping technique to reduce the full order of the Li-ion battery model. Their method is based on the transcendental transfer function approach presented in the frequency domain for control applications. The authors applied this method to the solid and electrolyte concentration equations [79]. The results show good agreement for the solution concentration, but the error related to the solid concentration function is higher than that obtained with the PP method.

Smith et al. also developed a reduced order Li-ion battery model for control applications. This model is known as the state variable model (SVM). The SVM comprises analytical transfer functions and a numerical transfer matrix [43, 79]. The comparison between the SVM and a full CFD simulation shows that the SVM model is only accurate at low discharge

rates (up to 1C). Moreover, the calculation process of the system eigenvalues is tedious and it depends on the numerical estimations.

An electrode averaged model (EAM) was proposed by Domenico et al. in 2008. By neglecting the solid concentration distribution along the electrode, they coupled the average solid material concentration with the average values of the chemical potentials, the electrolyte concentration and the current density. They also designed a Kalman Filter for on-line SOC estimation based on their electrochemical model [78]. Although their model can be useful for control and for rough estimation applications, its strong non-linearity is problematic for on-line parameter monitoring and identification [91]. Later, Smith et al. developed a combination between their previous model and the linear Kalman filter [82]. It improves the accuracy of the empirical-based models which use an equivalent circuit or a Kalman filter. It does not however account for the battery age and temperature dependent properties.

In 2009, Cai et al. presented a simplified Li-ion battery model using a proper orthogonal decomposition (POD). In this model, the number of equations is considerably reduced and so is the computational time. The predictions of the POD model show excellent agreement with that of the P2D model up to 20C discharge rates [80]. However, it is necessary to rely on experimental data to run the POD model. Also, the POD model does not work well for real time applications.

Subramanian et al. introduced a simplified Li-ion battery model based on a full order P2D model. Their main target is for control and optimization applications. At first, they presented a method to solve the P2D model assuming polynomial profiles for key parameters in the x direction. Different forms are suggested for x-dependent functions and simple polynomial functions are chosen for the model. As shown from Equations 2.11 to 2.14, these profiles are applied to four dependent variables, namely the pore wall flux (J), effective ionic conductivity of the electrolyte (k_{eff}), solid-phase average concentration ($c_{s,ave}$), and the electrolyte concentration (c_e) [77, 81].

$$J_k = \sum_{i=0}^{N} \alpha_{i,k} x^i \tag{2.11}$$

$$\frac{1}{\kappa_{eff,k}} = \sum_{i=0}^{N} \zeta_{i,k} x^i \tag{2.12}$$

$$c_{s,k}^{ave} = \sum_{i=0}^{N} \beta_{i,k}(t) x^i \tag{2.13}$$

$$c_{e,k} = \sum_{i=0}^{N} \psi_{i,k}(t)\, x^i \qquad (2.14)$$

$\alpha_{i,k}$, $\zeta_{i,k}$, $\beta_{i,k}$ and $\psi_{i,k}$ are coefficients which are calculated by applying the P2D equations and their boundary and initial conditions. Based on these profiles and using the P2D model equations, other parameters such as the electrolyte and the solid potential ($\Phi_{s,k}$, $\Phi_{e,k}$) are computed in the following manner:

$$\Phi_{s,k}(x) = \Phi_{s,k}\big|_{x=0} + \frac{a_p F}{s_{eff,p}} \sum_{i=0}^{N} \frac{a_{pi}}{i+1} \left\{ \frac{x^{i+2}}{i+2} - L_p^{i+2} \right\} \qquad (2.15)$$

$$\Phi_{e,p} = k_1 - 1 \sum_{i=0}^{N} \zeta_{pi} \frac{x^{i+1}}{i+1} - \sigma_{eff,p} \Gamma + \frac{2RT}{F}(1 - t_+) \ln c_e \qquad (2.16)$$

The Subramanian model is computationally faster than the finite-difference P2D model. The main drawback of this model is that no time-dependent variable is employed in the pore wall flux profile (J_k). This may cause significant errors in dynamic analyses, high-rate discharge estimations and battery aging studies [77, 81]. Later, a parameter estimation investigation for predicting the capacity fade of a Li-ion battery was conducted using the Subramanian model [92].

Ramadesigan et al. adopted two simplified approaches for solving the solid-state concentration equation that overcome the PP model limitations. Their methods were developed so as to decrease the computational time. The first Ramadesigan method approximates the solid-state concentration as a polynomial eigenfunction based on the Galerkin approximation. This method is in good agreement with the exact solution. It cannot however be applied to cases in which the diffusion coefficient varies with concentration as in the $LiFePO_4$ cathode. The second Ramadesigan method includes a finite difference approach with different node spacing. The number, size, and distribution of the nodes are optimized. This method has two main advantages: 1) a variable diffusion function can be modeled to simulate the $LiFePO_4$ cathode; and 2) it is adapted for modeling the cathode materials with moving boundaries [83]. The second Ramadesigan method is however too complex for on-line applications. Also, it does not account for the temperature and the age of the battery.

The first simplified thermal model of Li-ion batteries was developed by Guo et al. using the SPM coupled with thermal equations. The authors used ten eigenfunctions for the closed form solution of the solid concentration equations. The results show good agreement with experimental data down to low discharge rates [64].

In 2011, Forman et al. proposed another reduced version of the P2D model for optimization and control applications. The Forman model was developed using two simplification techniques. First, the linearized form of the Butler-Volmer equation about Φ_s and Φ_e is derived so as to yield simpler equations for solid and electrolyte potential functions:

$$J_k = 2i_{0,k}\left(\sinh\left(\frac{0.5F}{RT}m_{s,k}\right)+\cosh\left(\frac{0.5F}{RT}m_{s,k}\right)\frac{0.5F}{RT}\left(\left(F_{s,k}-F'_{s,k}\right)-\left(F_{e,k}-F'_{e,k}\right)\right)\right) \quad (2.17)$$

Second, an analytical method known as Padé approximation is used to reduce the order of the solid-state surface concentration equation. A comparison between the Forman model and other reduced models (PP model, residue grouping method and POD approximation) was performed [84, 93]. The Forman model is in excellent agreement with the other reduced models. Unfortunately, the Forman model does not reduce the CPU time and as a result, it is inadequate for real-time applications.

In 2012, Dao et al. employed a combination of the PP model and the Galerkin approximation to develop another simplified version of the P2D model. The Galerkin approximation is applied to convert electrolyte PDE equations to differential algebraic equations (DAEs). The simulation results show that the CPU time of the Dao model is significantly reduced. This Li-ion battery model is available in commercial software (Maplesim) [44, 94]. The main drawback of the Dao model is that the values of the Li^+ wall-flux on the particles (J_n, J_p) are assumed constant. Also, the model is valid for low discharge rates only.

In 2012, Lee et al. modified previously reported models [43, 79]. The transfer functions are applied to convert the full physics-based model to a computationally simple model. The linearized form of Butler-Volmer equation which keeps only the two first terms of its Taylor-series expansion is employed and the value of the reaction flux (J_k) is assumed to be independent of the electrolyte concentration. The film resistance parameter is added to the overpotential function so as to account for the effect of the battery age on the model equations. The discrete-time realization algorithm (DRA) approach is applied to the final transfer functions in order to decrease the model run-time and complexity. The comparison of Lee's estimates with that of the P2D is favorable up to a 2C discharge rate. The main drawback of Lee's model is the complexity of the mathematical equations [85].

In 2013, Klein et al. introduced an observer to predict the Li-ion battery behaviour and its properties. This simple model is derived from a combination of the P2D model and the temperature equations based on two main assumptions: 1) the solid concentration equation is handled with the PP model; 2) the changes in the electrolyte concentration are ignored [45]. This model is however limited to low discharge rates (<2C).

In 2013, Luo et al. developed an extended single particle Model (ESPM). Contrary to the SPM, the ESPM assumes a non-uniform profile for pore wall flux (J_n, J_p). Moreover, it uses a simplified distribution for the electrolyte properties and for the solid potential function. In spite of some perturbations in the cell potential curves, the predictions of the ESPM show good agreement with those of the P2D model up to 4C discharge rates [86, 87].

In 2013, Marcicki et al. employed a Padé approximation to simplify all PDEs of the P2D model so as to develop a reduced model for control applications and parameter identification studies [88].

In 2013, Rahimian et al. proposed an extended version of the single particle model using the full physics-based model equations. As discussed in section 2.4, the assumption of constant electrolyte properties is the main cause of errors in the SPM. Therefore, polynomial profiles have been retained to predict the electrolyte potential and the concentration with the following time-dependent coefficients:

$$c_{e,p}\left(x_p,t\right)=a_1\left(t\right)x_p^3+b_1\left(t\right)x_p^2+c_1\left(t\right)x_p+d_1\left(t\right);\left(x_p=x/L_p \quad for \quad 0\le x\le L_p\right) \tag{2.18}$$

$$c_{e,s}\left(x_s,t\right)=a_2\left(t\right)x_s^2+b_2\left(t\right)x_s+c_2\left(t\right);\left(x_s=\left(x-L_p\right)/L_s \ for \ L_p\le x\le L_p+L_s\right) \tag{2.19}$$

$$c_{e,n}\left(x_n,t\right)=a_3\left(t\right)x_n^3+b_3\left(t\right)x_n^2+c_3\left(t\right)x_n+d_3\left(t\right);\left(x_n=\left(x-L_p-L_s/L_n\right) \ for \ L_p+L_s\le x\le L\right) \tag{2.20}$$

$$\Phi_{e,p}\left(x_p,t\right)=A_1\left(t\right)x_p^3+B_1\left(t\right)x_p^2+C_1\left(t\right)x_p+D_1\left(t\right);\left(x_p=x/L_p \quad for \quad 0\le x\le L_p\right) \tag{2.21}$$

$$\Phi_{e,n}\left(x_n,t\right)=A_2\left(t\right)x_n^3+B_2\left(t\right)x_n^2+C_2\left(t\right)x_n+D_2\left(t\right);\left(x_n=\left(x-L_p-L_s/L_n\right) \ for \ L_p+L_s\le x\le L\right) \tag{2.22}$$

Like SPM, the pore wall flux is assumed to be constant in the Butler-Volmer equation. However, it must be computed in an interior point for each electrode in order to increase the accuracy of the pore wall flux values. The predictions of the Rahimian model are comparable to those of COMSOL for the P2D and SP models in the range of 1C to 5C. Higher degree polynomial profiles are however needed for the accurate prediction of the electrolyte concentration and potential variations [9]. The main disadvantage of the Rahimian model is that it does not include a relationship between the coefficients and the battery age and temperature. In 2015, Tanim et al. presented a modified SPM by using the P2D model equations, namely the electrolyte enhanced single particle model (ESPM). The assumptions made in this model are similar to those of the SPM, except for a quadratic polynomial function for the electrolyte concentration in the three domains (anode, cathode and separator). The Laplace transform and integral method analysis (IMA) are employed to reduce the order of concentration and potential functions in the anode, separator, and cathode domains. The final model equation is a transfer function between the cell voltage and the

cell current consisting of 15 dependent variables. There is also a temperature dependent model (ESPM-T) in which the key properties of the ESPM are updated for the temperature with empirical correlations. Since the temperature is an input signal in the ESPM-T model, it is necessary to rely on a sensor to generate the on-line cell temperature. The results of the Tanim ESPM models demonstrate good agreement with the P2D outputs. However, high discharge rates (above 5C) and low temperature (below -10°C) cause considerable cell voltage errors when compared to the P2D model [42]. The ESPM models are fast enough for control applications. Their main limitation is that the current density is uniform as in the SPM. Aging formula for Li-ion batteries may be adapted to the model for predicting the solid electrolyte interphase (SEI) layer growth [95].

Majdabadi et al. introduced a simplified Li-ion battery model that takes into account the arbitrary number of active material particles in a $LiFePO_4$ positive electrode. The simplified electrochemical multi-particle (SEMP) model combines the multi particle (MP) model [43-44] to the polynomial profiles for the electrolyte properties. The model handles particles with various radii and changing properties [89]. The predictions of Majdabadi model show good agreement with experimental data up to 5C discharge rates. Simulations were however carried out for a half-cell containing Li foil and $LiFePO_4$ cathode material. Majdabadi et Al. did not consider the whole complexity of a complete Li-ion battery with graphite and $LiFePO_4$ materials.

Table 2.3 provides a summary of the models discussed above. It is seen that the PP model is the most popular method to reduce the P2D model along the r direction. Moreover, the common reduced technique along the x direction is to consider polynomial profiles for the electrolyte's concentration and potential. The PP techniques are popular for three main reasons. First, their structure is mathematically simple: PDEs of the P2D model are replaced with differential algebraic equations (DAEs). Second, they make the Li-ion battery model computationally fast and inexpensive. Third, the polynomial profiles for the electrolyte properties in the x direction enhance the accuracy of the SPM. However, the temperature- and age- independent coefficients and the use of simple functions for the profiles are two important drawbacks of polynomial profile techniques.

Table 2.3: Summary of different techniques used in simplified models

	SPM	Polynomial Profile				Re. Gro.	POD	K.F.	Lin. BV	Padé app.
		c_s	c_e	Φ_e	J_k					
Zhang et al. (2000) [54]	●									
Subramanian et al. (2001) [75]	●	●								
Subramanian et al. (2005) [76]	●	●								
Subramanian et al. (2007) [77]		●	●		●					
Smith et al. (2007) [43]						●				
Smith et al. (2008) [79]						●				
Domenico et al., (2008) [78]								●		
Cai et al. (2009) [80]							●			
Subramanian et al. (2009) [81]		●	●		●					
Smith et al. (2010) [82]						●		●		
Ramadesigan et al. (2010) [83]		●								
Guo et al., (2011) [64]	●									
Forman et al. (2011) [84]		●							●	●
Dao, et al. (2012) [44]		●	●	●						
Lee et al. (2012) [85]						●			●	
Klein et al. (2013) [45]		●								
Luo et al. (2013) [86, 87]	●	●	●	●						
Marcicki et al. (2013) [88]										●
Rahimian et al. (2013) [50]	●	●	●	●						
Tanim et al. (2015) [42]	●	●	●	●						
Majdabadi et al. (2015) [89]			●	●						

* Lin. BV: Linearized Butler Volmer, K.F.=Kalman Filter, Re. Gro.: Residue Grouping

2.7. Suggestions and challenges

Based on the above review of the open literature concerning the modeling of Li-ions batteries, here is a list of issues that should be addressed in future investigations:

1. The most popular technique for model reduction is to fit the operating variables such as c_s, c_e, Φ_e, J_k with polynomial profiles. This technique enables the conversion of PDEs to simpler DAEs and, as a result, the model may become suitable for control and real-time applications. To the authors' knowledge however, no study has investigated thoroughly the effect of these parameters. Also, many questions remain unanswered. For instance, what are the consequences on the calculated potential functions (Φ_e, Φ_s) [44, 50, 89]? What is the effect of fitting a polynomial function for the electrolyte potential on the calculated pore wall fluxes? Which parameter should be fit with a polynomial, which parameter should be calculated and which parameter should be approximated?

2. In spite of the fact that the internal parameters of Li-ion batteries behave nonlinearly, all the simplified models have been implemented with simple polynomial functions. We propose to combine linear and nonlinear profiles for the variables. For example, the solid concentration function on the surface of the particles could be modelled in terms of the cell current density in the following manner:

$$c_{s,k}^{surf} = c_{s,k}^{ini} + A(i) + B(i)t + C\,exp(-Dt);\ k = n, p \qquad (2.18)$$

i is the cell current density. This approach could also be applied to other variables such as the electrolyte properties and the pore wall flux.

3) According to Table 2.2, it is imperative to develop a simple and fast model that takes into account the thermal conditions of the battery. The model reported in reference [64] rests on the SPM and is suitable for low discharge rates. Since BMSs are required to simulate a whole range of operating conditions, it is necessary to pursue research efforts in this area. Additional issues such as the internal heat generation, temperature-dependent properties and the effect of complex battery pack geometry should also be investigated. Inverse heat transfer techniques are also a promising avenue for answering some of these challenges since these methods can predict the internal parameters of the battery from temperature measurements taken on its envelope.

4) Most of the electrochemical aging models have been developed from the SPM. Some of the shortcomings of these models could be alleviated by developing a simplified version of P2D model considering the aging sources, such as side reactions and Solid Electrolyte Interfaces (SEI) layer growth in the governing equations.

5) The battery properties change as it ages. These changes cannot be ignored in the electrochemical models. Real-time models should account for the online battery data such as the cell potential, the current and the surface temperature. With this information, the on-line monitoring, age prediction, SoC and SoH estimations and the battery control will be improved.

6) There is a lack of reliable models for simulating the Li-ion batteries with $LiFePO_4$ cathode material. The problem is that the Li insertion/extraction phenomena in the material are not fully understood. The microscopic and macroscopic models for $LiFePO_4$ cathodes have yet to be bridged. Features such as carbon coating around the particles and phase-change behavior must be included. Moreover, due to the flat plateau exhibited by the open circuit potential curve, it is difficult to estimate the different cathode electrochemical parameters. Efforts should be deployed to overcome these problems. Simplified versions of the P2D model with variable cathode parameters (i.e., solid diffusion coefficient $D_{s,p}$, reaction rate K_p dependent on the concentration profiles and temperature) are needed for accurate modeling and for on-line applications. The development of simplified P2D models should account for the relationship between the different electrochemical parameters with Li concentration, temperature and age. Moreover, it is important to consider the role of the graphite as the negative electrode in comparison to the $LiFePO_4$ as the positive electrode.

2.8. Conclusion

A review of the open literature has revealed that modeling the full-physics of the Li-ion battery is too complex and computationally time-consuming to be of practical use in real-time applications such as monitoring batteries inside electric vehicles. The challenge therefore is to develop simpler and faster models which predict faithfully the behavior of Li-ion batteries. Unfortunately, no such model seems to meet all the requirements.

In this paper, a thorough review of simplified P2D models was presented. The assumptions, calculation procedures, potential and shortcomings of the models were discussed and compared. The study has shown that polynomial profiles for solid concentration (c_s) are the most popular methods to reduce the P2D model in the r direction. Polynomial profiles for electrolyte concentration and potential are also employed. Models based on polynomials are mathematically simple and computationally fast. Their main drawback is that the assumed profile coefficients are temperature- and age- independent. As a result, the accuracy of the predictions is affected. According to the authors, the following aspects of the simplified PD2 model should be addressed in future investigations: 1) To determine and to rank the most influential parameters in the simplified Li-ion battery models; 2) to employ higher-order polynomial profiles for different variables; 3) to develop coupled electrochemical and thermal equations for real-time Li-ion models; 4) to develop simplified P2D models that take into account the aging phenomenon; 5) to develop real-time models for predicting the internal properties of Li-ion batteries based on inverse heat transfer methods. 6) to propose a simplified model compatible with the characteristics of $LiFePO_4$ cathode material.

Acknowledgements

The authors are very grateful to Hydro-Québec and to the Natural Sciences and Engineering Council of Canada (NSERC) for their financial supports.

CHAPITRE 3 : AVANT-PROPOS

Auteurs et affiliation:

- Ali Jokar: étudiant au doctorat, Université de Sherbrooke, Faculté de génie, Département de génie chimique et de génie biotechnologique.
- Barzin Rajabloo: étudiant au doctorat, Université de Sherbrooke, Faculté de génie, Département de génie chimique et de génie biotechnologique.
- Martin Désilets: professeur, Université de Sherbrooke, Faculté de génie, Département de génie chimique et de génie biotechnologique.
- Marcel Lacroix: professeur, Université de Sherbrooke, Faculté de génie, Département de génie mécanique.

Date d'acceptation: 22 octobre 2016

État de l'acceptation: version finale publiée

Revue: Journal of the Electrochemical Society

Référence: [13]

Titre français: Une méthode inverse pour l'estimation des paramètres électrochimiques des piles aux ions lithium, Partie I : Méthodologie

Contribution au document: Dans cet article, une méthode inverse est proposée pour estimer les paramètres électrochimiques de piles aux ions lithium. Une version simplifiée du modèle P2D est également développée et utilisée à l'intérieur d'une procédure d'identification de paramètres. Cette nouvelle méthode a été validée avec succès en s'appuyant sur des données de référence obtenues avec des taux de décharge bas et élevés. La méthode a ensuite été appliquée à l'identification de paramètres de piles fabriquées à partir de différents matériaux d'électrode positive incluant le $LiCoO_2$, le $LiMn_2O_4$ et le $LiFePO_4$.

Résumé français :

Cette étude présente l'estimation de paramètres électrochimiques pour des piles aux ions lithium (Li-ion) à base de différents matériaux. La méthodologie d'estimation de paramètres est développée dans la première partie de cette étude. Les défis posés par l'utilisation de différents matériaux pour l'électrode positive, incluant le $LiCoO_2$, le $LiMn_2O_4$ et le $LiFePO_4$, sont examinés dans la deuxième partie.

Les paramètres électrochimiques du pile Li-ion les plus influents sont estimés au moyen d'une méthode inverse qui repose sur 5 éléments : les paramètres d'entrée, un modèle direct,

les données de référence, une fonction-objectif et un optimiseur. L'identification de huit variables électrochimiques est visée par cette étude. Une version simplifiée du modèle pseudo-2D (P2D) est développée et utilisée comme modèle direct. Les prédictions de ce modèle couplée à une fonction de bruit aléatoire sont utilisées pour générer les données de référence, qui incluent le potentiel en fonction de la capacité de la pile et ce, pour des taux de décharge bas et élevés. Une fonction de type moindres carrés et un algorithme génétique sont respectivement utilisés comme fonction-objectif et optimiseur. Une étude de sensibilité, dans laquelle différents taux de décharge ont été étudiés, a été employée afin d'identifier le meilleur domaine pour l'identification de chaque paramètre. Les résultats montrent que la méthodologie développée reste efficace et stable tant à bas qu'à haut niveau de décharge.

3. An inverse method for estimating the electrochemical parameters of lithium-ion batteries, Part I: Methodology

3.1. Abstract

An electrochemical parameter estimation (PE) study of lithium-ion batteries for different materials is presented. The PE methodology is developed in Part I of the study and the challenges regarding the different materials for the positive electrode including $LiCoO_2$, $LiMn_2O_4$ and $LiFePO_4$ are examined in Part II.

The most influential electrochemical parameters of the Li-ion battery are estimated by means of an inverse method. The inverse method rests on five elements: the input parameters, a direct model, the reference data, an objective function and an optimizer. Eight electrochemical variables are considered as the target of the PE study. A simplified version of Pseudo-two-Dimensional (P2D) model is developed for the direct model. The P2D model predictions coupled to a random noise function are employed to generate the reference data. The data include the cell potential values with respect to the battery capacity at low and high discharge rates. The least-squared function and Genetic Algorithm are employed as the objective function and its optimizer, respectively. The best time domain for the estimation of each parameter is calculated by using a sensitivity analysis performed for different discharge curves. Results show that the methodology remains accurate and stable at both low and high discharge rates.

Keywords: Parameter estimation; Inverse method; Li-ion battery; Simplified P2D model; Sensitivity analysis, Genetic Algorithm (GA).

Nomenclature:

a_k	Specific surface area of electrode *k (k=p,n)*, m^2/m^3
$c_{s,k}$	Solid-state concentration of electrode *k (k=p,n)*, mol/m^3
$c_{e,k}$	Electrolyte concentration in region *k (k=p,s,n)*, mol/m^3
$c_{e,k,0}$	Initial condition of electrolyte concentration in region *k (k=p,s,n)*, mol/m^3
$c_{s,k}^{\max}$	Maximum concentration of Li^+ in the particle of electrode *k (k=p,n)*, mol/m^3
$c_{s,k}^{surf}$	Concentration of Li^+ on the surface of the particles of the electrode *k (k=p,n)*, mol/m^3
$D_{eff,k}$	Effective diffusion coefficient of Li^+ in electrolyte for region *k (k=p,s,n)*, m^2/s
$D_{s,k}$	Li^+ diffusion coefficient in the particle of electrode *k (k=p,n)*, m^2/s
e_i	Measurement error function of the cell potential, V
e_r	Relative error, %

e_s	Specific error function of the cell potential, V^2
F	Faraday's constant, C/mol
I	Applied current density, A/m^2
J_k	Wall flux of Li^+ on the particle of *k (k=p,n)*, mol/m^2s
J_{p_j}	Dimensionless sensitivity coefficient, V
K_k	Reaction rate constant of electrode *k (k=p,n)*, $m^{2.5}/mol^{0.5}s$
L	Total thickness, m
L_k	Thickness of region *k (k=p,s,n)*, m
n	Negative electrode
p	Positive electrode
P	Unknown parameter matrix
r	Radial coordinate, m
R	Universal gas constant, J/mol K
R_{cell}	Solution phase resistance, Ω
$R_{s,k}$	Radius of the particle of electrode *k (k=p,n)*, m
s	Separator
S	Objective function, V^2
S_k	Total electroactive area of electrode k, m^2
SOC_k	State Of Charge of electrode *k (k=p,n)*
$SOC_{k,0}$	Initial State Of Charge of electrode *k (k=p,n)*
t	Time, s
T	Absolute temperature, K
t_+	Li^+ transference number in the electrolyte
U_k	Open-circuit potential of electrode *k (k=p,n)*, V
w_k	Weight of the active material of electrode k, g
x	Spatial coordinate, m

Greek

ε_k	Porosity of region *k (k=p,s,n)*
$\kappa_{eff,k}$	Effective ionic conductivity of the electrolyte in region *k (k=p,s,n)*, S/m
$\mu_{s,k}$	Overpotential of electrode *k (k=p,n)*, V
$\sigma_{eff,k}$	Effective electronic conductivity of the solid phase of electrode *k (k=p,n)*, S/m
$\Phi_{s,k}$	Solid-phase potential of electrode k $(k = p, n)$, V
$\Phi_{e,k}$	Electrolyte potential in region *k (k=p,s,n)*, V

3.2. Introduction

The simultaneous high power and energy density of lithium-ion (Li-ion) batteries have made it the preferred device for storing electricity. As a result, Li-ion batteries are increasingly used in various applications including electronics and the automotive industry. Regardless of the shape and of the battery pack arrangement, the internal structure of the battery usually comprises four main components: positive electrode, negative electrode, an electrolyte, and a separator. These components are made of materials that have been gradually modified over

the years so as to improve the efficiency, safety and performance of the batteries and to reduce their cost [1-3].

A battery management system (BMS) is crucial for monitoring the operation of the battery pack. The BMS must interact with all the elements of the system in order to control it and to protect the Li-ion cells. The intelligence of the BMS is based on a mathematical model that simulates and predicts the different operating conditions of the Li-ion battery pack. In high tech and automotive industries, the BMS usually relies on empirical-based models. These models are simple and provide fast response. They cannot however predict the performance of the battery as it ages. Moreover, they are only applicable to a specific cell, i.e., they cannot be transposed to other battery packs without recalibration [8, 68, 96].

Electrochemical-based models of Li-ion batteries, on the other hand, overcome these shortcomings. These models rest on chemical/electrochemical kinetics and transport equations. These Li-ion battery models are more complicated and CPU time-consuming than empirical based models. They are, on the other hand, more versatile and they provide reliable and stable responses in a wide range of operating conditions and applications. Among the electrochemical Li-ion battery models, the pseudo-two-dimensional (P2D) model and the Single Particle Model (SPM) appear to be the most popular [1, 9, 28]. The P2D model rests on (1) porous electrode theory, (2) concentrated solution theory, and (3) kinetics equations. Its predictions are accurate and have shown repeatedly good agreement with experimental data [1, 9, 34]. The SPM, on the other hand, is a simplified version of the P2D model. The SPM ignores the change in the electrolyte properties. As a result, the CPU time of the SPM is much less than that of the P2D model [9, 37].

In order to run the electrochemical-based mathematical models, it is imperative to know the different electrochemical parameters of the battery. Experimental measurement of these parameters is a challenging task. Sometimes it requires the dismantling of the battery itself. Also, some parameters need to be monitored continuously due to the fact that they change as the battery ages. In order to overcome the difficulties of experimental measurements, various research strategies for parameter estimation (PE) have been deployed. Table 3.1 summarizes the characteristics of these Parameter Estimation (PE) studies that have been applied to Li-ion batteries.

In 2004, a PE study of a polymer electrolyte membrane fuel cell (PEMFC) cathode was presented by Guo et al. [97]. Based on this research, five internal parameters of the Li-ion battery were estimated by Santhanagopalan et al. in 2007. These parameters are the diffusivity of Li^+ ions in the positive electrode ($D_{s,p}$), the reaction rate constants at the

electrodes/electrolyte interface (K_n and K_p) and the initial state-of-charge of negative and positive electrodes ($SOC_{n,0}$ and $SOC_{p,0}$). The calculation procedure was implemented by minimizing the least squares objective function with the Levenberg-Marquardt (LM) technique. Note that the objective function is defined here as the difference between the predictions of the direct model and the experimental data for the charge/discharge (up to 2C). Both the SPM and the P2D model were employed as the direct model. The PE results showed that the SPM is reliable for low discharge rates (<1C), while the P2D model remains accurate over the entire range of discharge rates. The CPU time of the PE process for the P2D model is however prohibitive compared to that of the SPM [11].

Table 3.1: Parameter Estimation (PE) studies on Li-ion batteries

Author	Battery Material	Estimated Parameters	Cycle rate	Direct Model	Optimizer	Extra Description
Santhanagopalan et al., 2007 [11, 12]	$LiCoO_2$	$D_{s,p}$,K_n, K_p, $SoC_{n,0}$,$SoC_{p,0}$	C/5, C/2, 1C, 2C	SPM P2D	LM[(1)]	Good agreement for SPM up to 1C and for P2D up to 2C.
Santhanagopalan et al., 2008 [12]	$LiCoO_2$	w_p, w_n, $SoC_{n,0}$,$SoC_{p,0}$	C/33, 1C	SPM	LM	Considering capacity fading in different temperatures
Ramadesigan et al., 2011 [92]	-	D_e, $D_{s,n}$, $D_{s,p}$, K_n,K_p	1C	Reduced P2D	Gauss-Newton	Predicting the capacity fade
Forman et al., 2012 [93]	$LiFePO_4$	88 related Parameters	1C, 2.5C, 5C	P2D	GA[(2)]	Using Fisher information to assess parameter uncertainty
Marcicki et al., 2013 [88]	$LiFePO_4$	ε_n,ε_p,$D_{s,n}$,$D_{s,p}$	C/3,1C	Reduced P2D	Curve Fitting	Using different data set, open circuit potential and discharge curves
Zhang et al., 2014 [98]	$LiFePO_4$ $LiCoO_2$	All related Parameters	C/2,1C, 1.5C,2C	P2D	GA	Using a multi-objective function consisting of the cell potential and the surface temperature
Masoudi et al., 2015 [99]	-	$c_{e,p,0}$, $c_{e,n,0}$, $c_{e,s,0}$, σ_n, t_+, ε_s	1C	Reduced P2D	Homotopy O. M. [(3)]	Using full-order model outputs as the reference in objective function
Rahman et al., 2016 [100]	$LiCoO_2$	$D_{s,n}$, $D_{s,p}$, K_n, K_p	1C	Reduced P2D	PSO[(4)]	Using PSO for parameter estimation

[(1)] Levenberg-Marquardt method, [(2)]Genetic Algorithm, [(4)]Homotopy optimization method [(3)]Particle Swarm Optimization

In 2008, Santhanagopalan el al. made an attempt at estimating some inner parameters of the Li-ion battery in order to quantify its capacity fade. The SPM was used as the direct model to estimate the SOC of the negative and positive electrodes ($SOC_{n,0}$ and $SOC_{p,0}$) and the active material loading of electrodes (w_p and w_n). Experimental data were collected after five charge/discharge cycles (0, 100, 200, 300, 400, and 500) under different temperature conditions. The results showed good agreement with available discharge curves. No predictions were made however for the future battery curves [12].

In 2011, Ramadesigan et al. investigated the effect of five different parameters on the Li-ion battery capacity fade by means of discharge curves of different charge/discharge cycles. These parameters are the diffusion coefficients D_e, $D_{s,n}$ and $D_{s,p}$, and the electrochemical reaction rate constants for negative and positive electrodes (K_n and K_p). The authors employed a simplified version of the P2D model as the direct model. The Gauss-Newton technique was adopted for minimizing the sum-of-squared differences of the objective

function. The results revealed that the negative electrode properties are most influential on the battery aging process [92].

Forman et al. implemented a full parameter estimation using the P2D model as the forward model and a genetic algorithm (GA) as its optimizer. A total of 88 operational parameters and geometric characteristics were determined based on the charge/discharge curves [93]. Due to the fact that several Li-ion battery parameters are not identifiable with performance curves, this method can only provide a rough estimation. The predictive method could be improved with more accurate experimental data for the geometry and the material characteristics.

In 2013, Marcicki et al. used curve fitting to identify the Li-ion batteries parameters in three steps. First, the composition characteristics of the electrodes were determined by using an open circuit potential curve. Second, resistance parameters related to their reduced model were estimated from discharge curves under different temperature conditions. Third, the diffusion coefficients were estimated by tuning the model parameters [88].

In 2014, Zhang et al. conducted a multi-objective PE by virtue of the discharge curves and the surface temperatures of Li-ion batteries based on $LiCoO_2$ and $LiFePO_4$. The modified multi-objective genetic algorithm was employed to estimate 25 parameters. The simulated discharge curves and the predicted surface temperature profiles showed good agreement with experimental data for low discharge curves [98].

In 2015, Masoudi et al. presented another PE study for Li-ion battery based on a reduced order model of the P2D model. The homotopy optimization approach was chosen to estimate six parameters, namely the volume fraction of the separator (ε_s), the Li^+ transference number (t_+), the electrical conductivity of the solid phase of the negative electrode (σ_n), and the initial electrolyte concentration in three regions. The predictions of the P2D model showed good accuracy for low discharge rates [99].

Recently, Rahman et al. identified four electrochemical variables of a Li-ion battery based on $LiCoO_2$. A particle swarm optimization (PSO) was used as the optimizer and, a reduced P2D model was employed as the direct model. The PE study was carried out however with a low discharge curve only (1C) [100].

The present paper extends the aforementioned studies by proposing a new and a general inverse PE method to identify different electrochemical parameters of Li-ion batteries. The method is applicable to both low and high discharge rate curves and to different positive electrode materials. The PE methodology is based on (1) a simplified version of the P2D model; (2) sensitivity curves of all expected parameters; and (3) an inverse method.

Inverse methods have been applied in many problems of science and engineering. These methods identify the system characteristics by means of specific experimental data and predictions from a direct model. Based on the difference between the experimental data and the model predictions, an objective function is minimized by virtue of an optimizer [14, 15]. The present inverse methodology comprises five elements: the input electrochemical parameters, the direct model, the reference data, the objective function and the optimizer. These elements are described next.

Eight electrochemical variables were selected as the target for the PE study. These variables are the solid diffusion coefficients ($D_{s,n}$ and $D_{s,p}$), the intercalation/deintercalation reaction-rate constants (K_n and K_p), the initial SOC ($SOC_{n,0}$ and $SOC_{p,0}$), and the electroactive surface areas (S_n and S_p). All these variables are identifiable based on the Li-ion direct models. Their values are required for simulating the battery performance and for predicting the aging process. Also, to improve the accuracy of the predictions, the geometric and the material characteristics were assumed to be known. These parameters are usually available from the manufacturers of Li-ion batteries. They can also be determined experimentally.

To account for low as well as for high discharge curves, it is imperative to rely on a direct model that simulates the experimental data. Moreover, due to the numerous back and forth calls in the PE process, the direct model should be computationally efficient and fast. As a result, a simplified version of the pseudo-two-dimensional (P2D) model was developed as the forward model. This model exhibits three main features: (1) accuracy, i.e., it takes into account the electrolyte properties; (2) it is fast. The calculation procedure has been optimized; and (3) flexibility. The number of unknown coefficients to be determined in the PE process is variable.

In this work, the reference data for the PE study are generated with the P2D model. These data include the cell potential values with respect to the battery capacity for low and high discharge rates (C/10, C/2, 1C, 2C, 5C). In order to mimic the uncertainty that plagues experimental data, a noise function was employed to add random-based errors to the normal distribution of the reference data. The least-square function in the time domain was chosen as the objective function for this work. Moreover, due to the complexity of the system, a genetic algorithm (GA) was used to minimize the objective function. To increase the accuracy and to accelerate the calculation procedure, the best time domain of the estimation for each parameter was performed. It was determined by means of the sensitivity curves for all parameters with respect to discharge time. The dimensionless Jacobians are computed from the solution of the governing equations. These solutions provide the first derivative of

the cell potential in terms of the discharge time. Results reveal that the higher the Jacobian value, the better the estimation. The predicted simulation discharge curves show good agreement with the noisy reference data for both low and high discharge curves.

3.3. Direct models of Li-ion batteries

The macroscopic models of the Li-ion batteries can be classified into two groups: empirical-based and electrochemical engineering models. The main reason for developing such models is to determine SOC and SOH of the battery [8, 9, 28].

Empirical models rest on the battery past battery experimental data to predict its future states. Equivalent circuit-based and neural network models are the most popular empirical models. They are widely used in electronics and in the automotive industry [8, 29, 30]. The interest of empirical models is that they are computationally fast and relatively simple. Unfortunately, their range of applications is limited. For instance, the physics-based parameters cannot be determined. The battery characteristics are not updated as the battery ages. Also, the empirical model pertaining to a specific battery cannot be transposed to other types of batteries [31, 32].

Electrochemical models are, on the other hand, more sophisticated. These models are based on chemical/electrochemical kinetics and transport equations. They may be used to simulate the Li-ion battery characteristics and reactions [9]. The pseudo-two-dimensional (P2D) model and the Single Particle Model (SPM) are among the most popular electrochemical-based models. The P2D model rests on the porous electrode theory, the concentrated solution theory and the kinetics equations [33, 34]. The P2D model has been extensively used in Li-ion battery investigations [32]. Its predictions are accurate and it has shown repeatedly good agreement with experimental data [35, 36]. In order to reduce the computational times, a simplified version of the P2D model, called the SPM, has been developed. In the SPM, the electrolyte properties are ignored and the transport phenomena are treated in a simple manner [37].

In this paper, the PE study is implemented using both low and high discharge curves based on the inverse method. The optimization process is carried out iteratively. On one hand, the P2D model is unquestionably rigorous but it is too complicated and slow. The SPM, on the other hand, provides quick responses but it is inaccurate for simulating high discharge rates and thick electrodes. Therefore, a simplified version of the P2D model is proposed as a compromise between complexity and accuracy for the PE process.

3.3.1. The P2D model

In 1993, Doyle et al. introduced the pseudo-two-dimensional (P2D) model for Li-ion batteries using a combination of the porous electrode theory and the concentrated solution theory. To this day, this model remains the most popular Li-ion battery model. It has been thoroughly tested and validated [33]. Figure 3.1 depicts the structure used in this model. The electrodes are considered as a porous matrix. Their behavior is modeled with spherical particles surrounded by the electrolyte. The intercalation and the de-intercalation processes of the Li-ions are performed through the surface area of these particles. Also, the transfer processes are predominantly unidirectional. Consequently, a 1-D mathematical model (x axis) may be applied [1, 34].

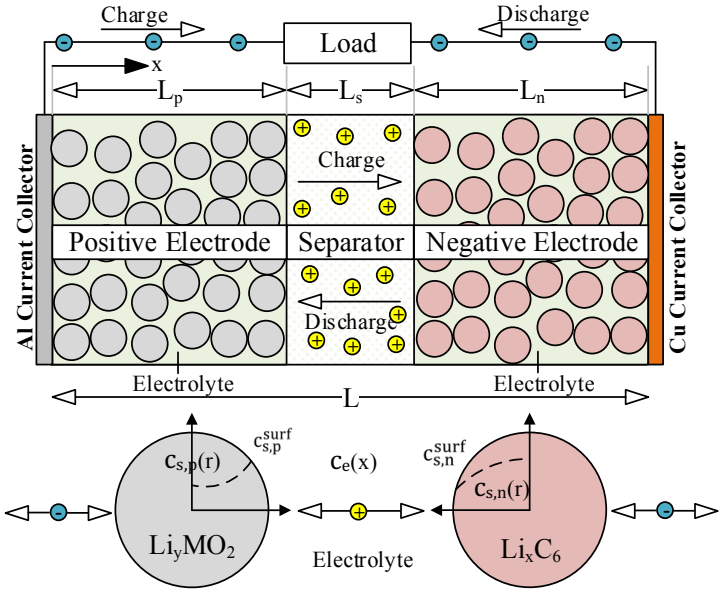

Figure 3.1: The Li-ion battery P2D model

The governing equations of the P2D model are reported in Table 3.2. The main features of these equations are: (1) solid-state Li^+ ion concentration (c_s) in the electrodes is derived from the Fick's law of diffusion for spherical particles; (2) liquid-phase Li^+ ion concentration (c_e) in the electrolyte and in the separator is based on the conservation of Li^+ ions; (3) solid-state potential (Φ_s) in the electrodes is derived from Ohm's law; (4) liquid-phase potential (Φ_e) in the electrolyte and in the separator is calculated using Kirchhoff's and Ohm's laws; (5) pore wall flux of Li+ ions (J) in the electrodes is described by the Butler-Volmer kinetics equation [34, 42].

Table 3.2: The governing equations of P2D Model [34]

Region	Eq. no.	Governing equations
Electrodes (k=n,p)	(3.1)	$\frac{\partial c_{s,k}(x,r,t)}{\partial t} = \frac{D_{s,k}}{r^2}\frac{\partial}{\partial r}\left(r^2 \frac{\partial c_{s,k}(x,r,t)}{\partial r}\right)$
	(3.2)	$\varepsilon_k \frac{\partial c_{e,k}(x,t)}{\partial t} = \frac{\partial}{\partial x}\left(D_{eff,k}\frac{\partial c_{e,k}(x,t)}{\partial x}\right) + a_k(1-t_+)J_k(x,t)$
	(3.3)	$\sigma_{eff,k}\frac{\partial^2 \Phi_{s,k}(x,t)}{\partial x^2} = a_k F J_k(x,t)$
	(3.4)	$-\sigma_{eff,k}\frac{\partial \Phi_{s,k}(x,t)}{\partial x} - \kappa_{eff,k}\frac{\partial \Phi_{e,k}(x,t)}{\partial x} + \frac{2\kappa_{eff,k}RT}{F}(1-t_+)\frac{\partial \ln c_{e,k}}{\partial x} = I$
	(3.5)	$J_k(x,t) = K_k\left(c_{s,k}^{\max} - c_{s,k}^{surf}\right)^{0.5}\left(c_{s,k}^{surf}\right)^{0.5} c_{e,k}^{0.5}\left[\exp\left(\frac{0.5F\mu_{s,k}(x,t)}{RT}\right) - \exp\left(-\frac{0.5F\mu_{s,k}(x,t)}{RT}\right)\right]$ $\mu_{s,k}(x,t) = \Phi_{s,k}(x,t) - \Phi_{e,k}(x,t) - U_k;\ V_{cell}(t) = \Phi_{s,k}(0,t) - \Phi_{s,k}(L,t)$
Separator (k=s)	(3.6)	$\varepsilon_k \frac{\partial c_{e,k}(x,t)}{\partial t} = \frac{\partial}{\partial x}\left(D_{eff,k}\frac{\partial c_{e,k}(x,t)}{\partial x}\right)$
	(3.7)	$-\kappa_{eff,k}\frac{\partial \Phi_{e,k}(x,t)}{\partial x} + \frac{2\kappa_{eff,k}RT}{F}(1-t_+)\frac{\partial \ln c_{e,k}}{\partial x} = I$

3.3.2. The Single Particle Model (SPM)

In 2000, Zhang et al. proposed a simplified version of the P2D model known as the Single Particle Model (SPM) for Li-ion batteries. The SPM rests on two main assumptions. First, each electrode is modeled as a spherical particle in which intercalation and de-intercalation phenomena occur. Second, variations of the electrolyte concentration and potential are ignored [54]. These equations comprise the solid-state concentration and the Butler-Volmer kinetics equations at both negative and positive electrodes. By using these equations, the cell potential function of the Li-ion batteries can be determined as [64]:

$$V_{cell} = \left(U_p - U_n\right) + \frac{2RT}{F}\ln\left(\frac{\sqrt{m_p^2+4}+m_p}{2}\right) + \frac{2RT}{F}\ln\left(\frac{\sqrt{m_n^2+4}+m_n}{2}\right) \tag{3.8}$$

$$m_p = \frac{I}{FK_p S_p c_{s,p}^{\max} c_e^{0.5}\left(1-SOC_p\right)^{0.5}\left(SOC_p\right)^{0.5}};\ S_p = \frac{3\varepsilon_p V_p}{R_p},\ SOC_p = \frac{c_{s,p}^{surf}}{c_{s,p}^{\max}} \tag{3.9}$$

$$m_n = \frac{I}{FK_n S_n c_{s,n}^{\max} c_e^{0.5}\left(1-SOC_n\right)^{0.5}\left(SOC_n\right)^{0.5}};\ S_n = \frac{3\varepsilon_n V_n}{R_n},\ SOC_n = \frac{c_{s,n}^{surf}}{c_{s,n}^{\max}} \tag{3.10}$$

$$SOC_k = SOC_{k,0} - \frac{J_k R_k}{c_{s,k}^{\max} D_{s,k}}\left[3\frac{D_{s,k}}{R_k^2}t + \frac{1}{5} - \sum_{k=1}^{\infty}\frac{2}{\lambda_k^2}\exp\left(-\frac{\lambda_k^2 D_{s,k}}{R_k^2}t\right)\right];\ \sin\left(\lambda_k\right) - \lambda_k\cos\left(\lambda_k\right) = 0 \tag{3.11}$$

The main advantages of the SPM are: (1) it is a simple model; (2) its solution requires minimum computational effort; (3) it can serve many purposes such as online estimation [37] and life modeling [55] of Li-ion batteries. Its main drawback is that it must be fine-

tuned according to the electrolyte properties in thick electrodes and at high discharge rates [9].

3.3.3. The Simplified P2D model

Several efforts have been deployed in the development of simplified models of Li-ion batteries. The complex governing equations of P2D model are reduced by using different mathematics- and physics-based techniques [10, 28]. In this paper, a reduced Li-ion battery model for the PE process is proposed. Two assumptions are made: first, the wall flux value in the electrodes (J_n and J_p) is considered constant as in the SPM; second, a linear function (Eq. 3.12) is employed to describe the electrolyte concentration behaviour as respect to the operation time and the position in three regions: the cathode, the separator and the anode.

$$c_{e,k}(x,t) = A_{1,k}(t)x + A_{2,k}(t);\ k = p,s,n,\ 0 \le x \le L \qquad (3.12)$$

A_1 and A_2 are assumed to be the time-dependent coefficients. The lengths L_p, L_s and L_n are illustrated in Figure 3.1. Applying the first assumption to the solid potential equation (Eq. 3.3) and to its boundary conditions, the constant wall fluxes may be calculated as follows:

$$J_p = \frac{I}{a_p F L_p};\ 0 \le x \le L_p \qquad (3.13)$$

$$J_n = \frac{-I}{a_n F L_n};\ L_p + L_S \le x \le L \qquad (3.14)$$

Moreover, the first derivative of the solid potential functions with respect to x are determined as follows:

$$\frac{\partial \Phi_{s,p}(x,t)}{\partial x} = \frac{I}{\sigma_p}\left(\frac{x}{L_p} - 1\right);\ 0 \le x \le L_p \qquad (3.15)$$

$$\frac{\partial \Phi_{s,n}(x,t)}{\partial x} = \frac{I}{\sigma_n L_n}\left(-x + L_p + L_s\right);\ L_p + L_s \le x \le L \qquad (3.16)$$

Eqs. 3.17 to 3.19 are immediately obtained by substitution of the second assumption into Eq. 3.2 and 3.6, that is,

$$\frac{dA_{1,k}}{dt} = 0;\ k = p,s,n \qquad (3.17)$$

$$A_{2,k} = \frac{a_k (1 - t_+) J_k}{\varepsilon_k} t;\ k = p,n \qquad (3.18)$$

$$\frac{dA_{2,s}}{dt} = 0 \qquad (3.19)$$

By using the boundary conditions of the electrolyte concentration profiles given by Eqs. 3.20 and 3.21, the values of the $A_{1,k}$ are equal to zero as shown in Eq. 3.22.

$$-D_p \frac{\partial c_{e,p}}{\partial x}\Big)_{x=0} = -D_n \frac{\partial c_{e,n}}{\partial x}\Big)_{x=L} = 0 \tag{3.20}$$

$$-D_p \frac{\partial c_{e,p}}{\partial x}\Big)_{x=L_p^-} = -D_s \frac{\partial c_{e,s}}{\partial x}\Big)_{x=L_p^+} \tag{3.21}$$

$$A_{1,k} = 0;\ k = p,s,n \tag{3.22}$$

Therefore, the electrolyte concentration profiles are computed by substituting Eqs. 3.18, 3.19 and 3.22 into Eq. 3.12.

$$c_{e,p}(t) = \frac{a_p (1-t_+) J_p}{\varepsilon_p} t = \frac{(1-t_+) I}{\varepsilon_p F L_p} t;\ 0 \le x \le L_p \tag{3.23}$$

$$c_{e,s}(t) = \text{Constant};\ L_p \le x \le L_p + L_s \tag{3.24}$$

$$c_{e,n}(t) = \frac{a_n (1-t_+) J_n}{\varepsilon_n} t = \frac{-(1-t_+) I}{\varepsilon_n F L_n} t;\ L_p + L_s \le x \le L \tag{3.25}$$

With the help of Eqs. 3.12 to 3.24 and the electrolyte potential governing equations (Eq. 3.4 and 3.7), we obtain:

$$\Phi_{e,p}(x,t) = \Phi_e(0) - I\left(\frac{x^2}{2\kappa_{eff,p} L_p}\right);\ 0 \le x \le L_p \tag{3.26}$$

$$\Phi_{e,s}(x,t) = \Phi_e(0) - I\left(\frac{x - L_p}{\kappa_{eff,s}} + \frac{L_p}{2\kappa_{eff,p}}\right);\ L_p \le x \le L_s + L_p \tag{3.27}$$

$$\Phi_{e,n}(x,t) = \Phi_e(0) - I\left(\frac{L_p}{2\kappa_{eff,p}} + \frac{L_s}{\kappa_{eff,s}} + \frac{-(x-L)^2 + L_n^2}{2\kappa_{eff,n} L_n}\right);\ L_s + L_p \le x \le L \tag{3.28}$$

The conductivity for the liquid/salt/polymer is approximated with a polynomial function of the form [81]:

$$\kappa_{eff,k}(x,t) = \varepsilon_p^{brugg}\left(\alpha_0 + \alpha_1 c_{e,k} + \alpha_2 c_{e,k}^2 + \ldots\right);\ 0 \le x \le L \tag{3.29}$$

α_i are constant coefficients for all regions. By incorporating Eqs. 3.15 to 3.28, the following electrolyte potential drop function between the positive and the negative electrodes is proposed:

$$(\Delta\Phi_e)_{0-L} = \Phi_{e,p}(0,t) - \Phi_{e,n}(L,t) \approx IR_{cell} = \frac{I}{a_0 + a_1 (It) + a_2 (It)^2 + \ldots} \tag{3.30}$$

The new constant coefficients (a_i) are determined by the PE process. By means of Eq. 3.5 & (3.30), the cell potential formula in SPM (Eq. 3.8) can be modified and calculated as a function of the electrochemical parameters and the unknown variables, that is,

$$V_{cell} \approx \left(U_p - U_n\right) + \frac{2RT}{F} \ln\left(\frac{\sqrt{m_p^2 + 4} + m_p}{2}\right) + \frac{2RT}{F} \ln\left(\frac{\sqrt{m_n^2 + 4} + m_n}{2}\right) + \frac{I}{a_0 + a_1 (It) + a_2 (It)^2 + \ldots} \tag{3.31}$$

This equation is applied in the PE process to estimate the electrochemical parameters and the unknown variables of the electrolyte potential drop function.

3.4. Parameter estimation process

3.4.1. Inverse method

Inverse methods are used for the PE of a system or for its functional identification. In the former, the unknown parameters can be estimated by means of experimental data. In the latter, the unknown functions can be determined in a finite or an infinite dimensional space [14]. The solution methods for inverse problems are usually more complicated than for direct problems. Direct problems are well-posed problems. The conditions that must be satisfied in a well-posed problem are that (1) the solution must exist; (2) it is unique and (3) it must be a continuous function. Inverse problems are, on the other hand, ill-posed problems. The solution of most inverse problems is highly dependent on the initial condition and on the boundary conditions as well as on the measured signals. There have been numerous attempts to tackle these difficulties and to convert inverse problems into well-posed problems [14-16].

In PE problems, the experimental signals play a key role in finding the expected parameters. These parameters must be measurable and accurate when compared with the direct model. In the identification of the Li-ion battery parameters, the time-varying cell potential values can be measured during the charge/discharge process. Figure 3.2 illustrates the relationship between the different elements of a PE study based on an inverse method. The objective function is defined here as the difference between the experimental data and the predictions of the direct model. A mathematical optimizer is employed to minimize the objective function so as to find the best values of the expected parameters.

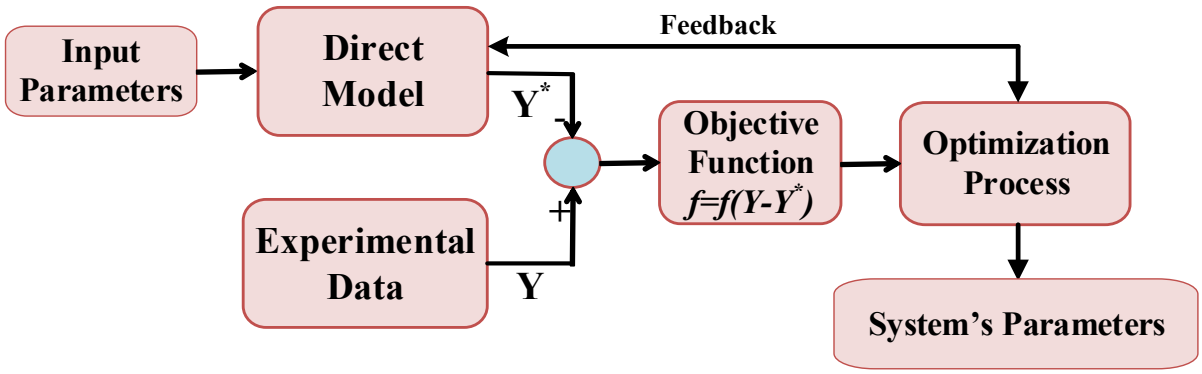

Figure 3.2: The solution procedure for inverse problems

3.4.2. PE equations

The inverse problem of the Li-ion battery can be defined as a "whole time domain" approach. This means that the experimental data can be measured in the small time interval between

zero to cut-off time ($0 < t \leq t_c$). The experimental data vector ($\boldsymbol{V}^*_{cell,m}$) relates to one charge/discharge process with N time intervals as shown in Eq. 3.32:

$$\mathbf{V}^*_{cell,m} = \begin{bmatrix} V_1^* \\ V_2^* \\ \vdots \\ V_N^* \end{bmatrix}_{N\times 1} ; t = t_1, t_2, ..., t_N \qquad (3.32)$$

The measurement of random errors is always a concern in the solution of inverse problems. The stability of the inverse method is sensitive to these errors. The solution technique for the inverse problem should be stable with the measurement errors and for small time intervals [14, 16]. In order to develop the mathematics for the inverse method, it is assumed that the measurement error (e_i) is a random and additive variable:

$$e_i = \left(\mathbf{V}^*_{cell,m}\right)_i - \left(\mathbf{V}^*_{cell,a}\right)_i ; \; t = t_1, t_2, ..., t_N \qquad (3.33)$$

The subscripts *m* and *a* represent the measurement and the actual variables, respectively. The objective function (S) is defined as the ordinary least-squares function of the measured data ($\mathbf{V}^*_{cell,m}$) and the calculated values ($\mathbf{V}_{\text{cell}}$) [14]:

$$S = \left(\mathbf{V}^*_{cell,m} - \mathbf{V}_{cell}(\mathbf{P})\right)^T \left(\mathbf{V}^*_{cell,m} - \mathbf{V}_{cell}(\mathbf{P})\right) = \sum_{i=1}^{N} \left(V^*_{cell,m,i} - V_{cell,i}(\mathbf{P})\right)^2 \qquad (3.34)$$

The superscript T indicates the transpose. Of course, the calculated ($\mathbf{V}_{\text{cell}}$) vectors must be derivable with respect to the unknown parameters (**P**). When experimental data are collected from M charge/discharge processes, Eq. 3.35 may be rewritten as [11]:

$$S = \left(\mathbf{V}^*_{cell,m} - \mathbf{V}_{cell}(\mathbf{P})\right)^T \left(\mathbf{V}^*_{cell,m} - \mathbf{V}_{cell}(\mathbf{P})\right) = \sum_{j=1}^{M} \sum_{i=1}^{N} \left(V^*_{cell,m,ij} - V_{cell,ij}(\mathbf{P})\right)^2 \qquad (3.35)$$

The objective function (3.35) is usually stable when only few parameters are unknown. It may become unstable when the inverse problem involves a larger number of unknown parameters. The instability is then reduced by adding regularization terms to the least-square objective function using Tikhonov's regularization and Alifanov's iteration regularization methods [14]. The expected parameters are estimated by solving the following optimization problem:

$$\min S = S(\mathbf{P}) \; subject\, to \; P_{j,low} \leq P_{j,1} \leq P_{j,high} \qquad (3.36)$$

$P_{j,low}$ and $P_{j,high}$ are the minimum and maximum of the P_j values respectively. Eq. 3.36 is solved for the unknown vector **P** as the system parameters. This process is implemented with an appropriate optimizer that finds the problem global minimum.

3.4.3. The Optimization process

Due to the numerous parameters used in the objective function of the present PE study, there may be several local minima in the vicinity of the global minimum. As a result, the optimization process for the inverse problem is mathematically challenging, slow to converge and computationally expensive [15]. Colaço et al. presented detailed description and comparison between different solution methods for inverse problems using the steepest descent method, the conjugate gradient method, the Newton-Raphson method, the quasi-Newton method, the Levenberg-Marquardt method (LM), Genetic Algorithms (GA), differential evolutions, the particle swarm method and the simulated annealing method [17]. In general, these optimization tools can be divided into two categories: deterministic techniques and stochastic methods. Although deterministic methods are usually faster than the stochastic methods, they easily fall into system local extrema and have complex structures. Stochastic-based optimization methods employ, on the other hand, random-based operation functions ideally suited for reaching the system global extremum [17, 18]. Therefore, in this paper, a genetic algorithm stochastic technique will be applied to the objective function in order to estimate the large number of electrochemical parameters of the Li-ion batteries.

GA is by far the most popular stochastic optimization technique used in all engineering fields. This method was officially introduced by Holland in the 1970s [101-103]. The GA originates from natural selection mechanisms. It starts from a strong random database, namely an initial population, and moves upward to many extremum points. Inspired by the living organism's structure, each member of the initial population is called chromosome containing some genes. Each chromosome represents a probabilistic answer of the optimization problem in which the number of variables is equivalent to the number of genes. In the GA, more fitted new populations replace older populations. Therefore, the algorithm requires a fitness function, which refers to the cost of a chromosome. After randomly generating the initial population, new populations are being produced by three genetic operators called pairing, mating and mutation:

(1) The pairing operator: This operator chooses the suitable parent chromosomes from the current population for pairing. The objective function determines the cost of each chromosome and its chance for selection.

(2) The mating operator: This operator produces one or more offspring from the selected pairs. After selecting the pairs, they are being mated by a random function and two children are produced.

(3) The mutation operator: This operator applies a random change in a small percent of genes in all chromosomes. Mutation results in introducing new characteristics to the chromosomes that did not exist in the previous ones. This operator avoids quick convergence to a local minimum especially for objective functions which have many local minima.

Figure 3.3 shows the GA flowchart with the relationships between all GA operators.

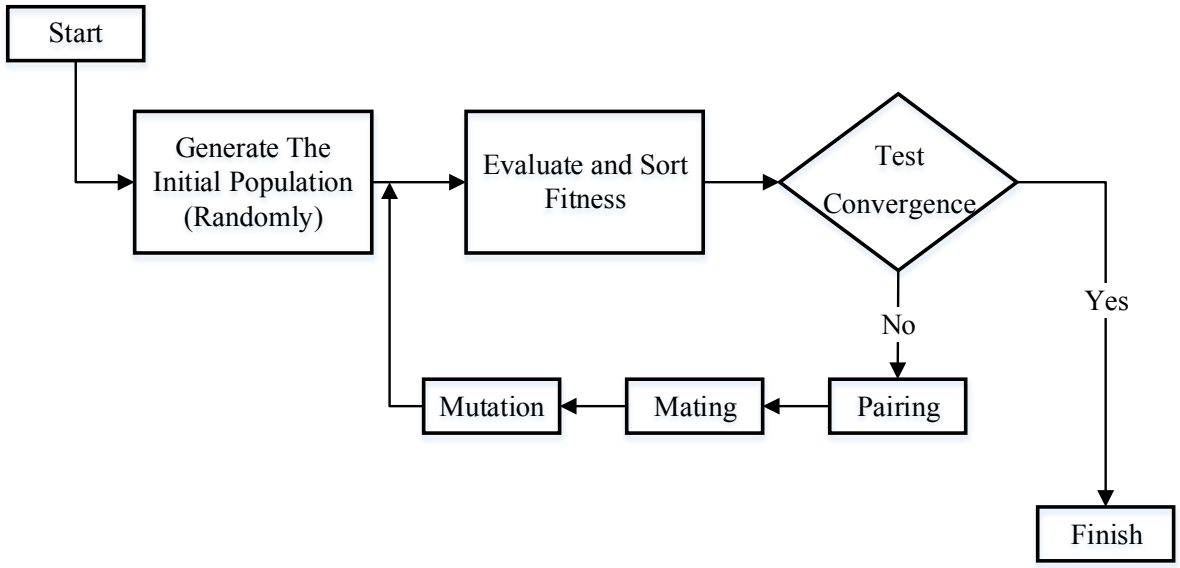

Figure 3.3: The Genetic Algorithm (GA) flowchart

3.5. Parameters and reference data

3.5.1. Expected parameters

The effective variables of the Li-ion battery performance can be classified into three groups: geometric, material and operational parameters. The geometric and material parameters can be easily obtained from direct measurements or from the datasheets provided by the manufacturer. The operational properties are, on the other hand, not easily available. Furthermore, some of them may vary according to the measurement techniques or the battery's age. Sometimes, the measurement of these parameters requires the dismantling of the battery itself. Therefore, eight electrochemical parameters, as the operational properties, were selected for the present PE study. These parameters are the solid diffusion coefficients ($D_{s,n}$ and $D_{s,p}$), the intercalation/deintercalation reaction-rate constants (K_n and K_p), the initial SOC ($SOC_{n,0}$ and $SOC_{p,0}$), and the electroactive surface areas (S_n and S_p). All these variables are identifiable based on the Li-ion direct models. Their values are needed to simulate the battery's performance and to predict its aging process. Table 3.3 provides the range for each parameter for a typical Li-ion battery with a $LiCoO_2$ positive electrode.

Table 3.3: Range of the electrochemical parameters for a Li-ion battery with $LiCoO_2$

Symbol	Unit	Low value	High value
$D_{s,n}$	m^2/s	1.5e-14	4.5e-14
$D_{s,p}$	m^2/s	0.5e-14	1.5e-14
K_n	$m^{2.5}/mol^{0.5}$ s	0.9e-11	2.7e-11
K_p	$m^{2.5}/mol^{0.5}$ s	3.3e-11	10e-11
$SOC_{n,0}$	-	0.65	0.85
$SOC_{p,0}$	-	0.4	0.6
S_n	m^2	0.6	1.3
S_p	m^2	0.6	1.3

3.5.2. Reference data

To identify the electrochemical parameters for the Li-ion battery, the reference data must be compared to the predictions of the direct model. In the present study, the reference data were generated with the P2D model available in COMSOL®Inc. Multiphysics 5.1. The reference data are composed of the cell potential values with respect to the battery capacity for low and high discharge rates, namely C/10, C/2, 1C, 2C, 5C. Moreover, to mimic real experimental data, random noise was added to the reference data (Eq. 3.37). The error profile is generated by a normal distribution random function multiplied by the accuracy of the measurement tools (0.001 V). The mean value and the standard deviation of the normal distribution are chosen to be 0 and 1, respectively. Due to the high accuracy of the experimental setup, the deviation value should even be lower. This means that the added error profile represents the worst case scenario. Figure 3.4 illustrates noisy reference data for different discharge curves.

$$V^*_{cell,ref.} = V^*_{cell,P2D}(t_i) + 0.001 \times rand(Normal\ distribution) \tag{3.37}$$

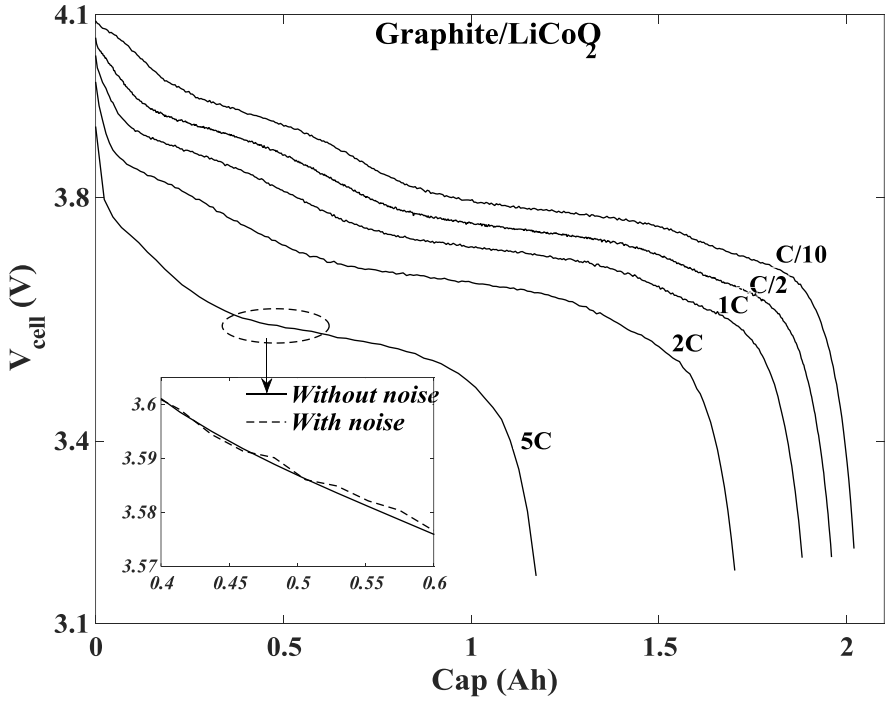

Figure 3.4: Noisy reference data for various discharge curves

3.6. Sensitivity Analysis

In order to increase the accuracy of the inverse method and to accelerate the parameter estimation process, the best time domain for the estimation of each parameter must be calculated. It is determined with the sensitivity curves for all parameters. The sensitivity or the Jacobian matrix (**J**) is defined as the first order partial derivatives of the calculated cell potential $\left(\boldsymbol{V}_{cell}(\boldsymbol{P})\right)$ with the respect to the unknown parameters ($\mathbf{P}_j$), that is:

$$\mathbf{J}\left(\mathbf{P}_j\right)=\left[\frac{\partial \mathbf{V}_{cell}^{T}}{\partial \mathbf{P}_j}\right]^{T} \tag{3.38}$$

In the present study, the governing equations for the SPM (Eqs. 3.8-3.11) are employed to calculate the sensitivity values. Due to the different order of magnitudes for these values, the dimensionless sensitivity coefficients are estimated as

$$J_{P_j}=P_j\frac{\partial V_{cell}}{\partial P_j} \tag{3.39}$$

It should be noted that the mean values of each parameter, extracted from Table 3.3, have been used to determine the sensitivity coefficients. Figures 3.5a to 3.5e show the sensitivity curves related to different discharge curves. The higher the Jacobian value, the better the estimation. The Jacobian values for each parameter vary with the discharge time and the discharge rate. Figure 3.5f presents a schematic of the best time domain for estimating of electrochemical parameters for Li-ion batteries based on graphite/$LiCoO_2$. Regardless of the

discharge rates, the discharge curves may be divided into three distinct regions for the best time domain including (1) the beginning of the discharge process; (2) the discharge cell voltage plateau; and (3) the end of the process with decreasing cell potential. Note that due to the various open circuit potentials, these results would be affected by the positive electrode materials, which will be shown in the next paper. According to the sensitivity analysis curves, the best time domain for the PE of different electrochemical parameters is as follows:

- $D_{s,n}$, k_n and k_p: For both low and high discharge rates, region 2 appears to be the best time domain to estimate these electrochemical parameters.
- $D_{s,p}$: Region 2 is best for identifying D_p at low discharge rates. However, by using the SPM as the direct model, the region 3 seems more appropriate for identifying $D_{s,p}$ at high discharge rates. This change is because of the dramatic increase of the first derivative of the cathode open circuit potential function (U_p) with respect to $D_{s,p}$ at the end of the discharge process in high C-rates. Since ($\partial U_p/\partial D_{s,p}$) profile is a material characteristic, its behavior may be change when using other cathode materials. This effect will be shown in the next part of this paper.
- S_n, $SOC_{n,0}$: Region 3 is the best time range for estimating both these parameters for all discharge rates.
- S_p, $SOC_{p,0}$: The best time domains for these parameters are in regions 1 and 3 for both low and high discharge rates.

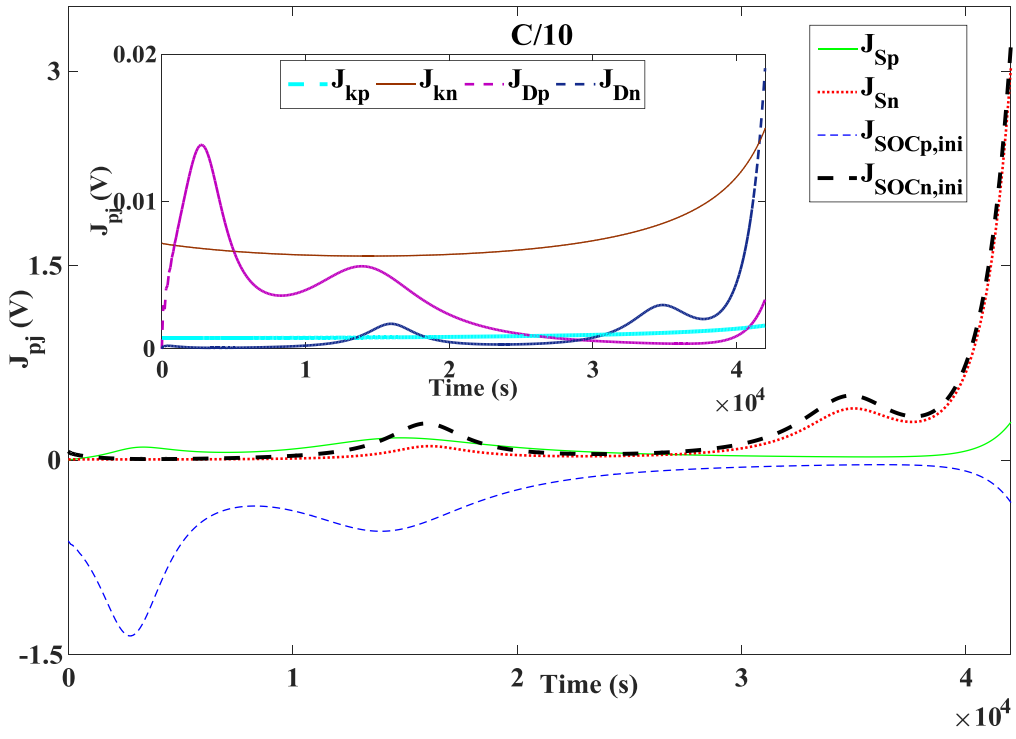

(a)

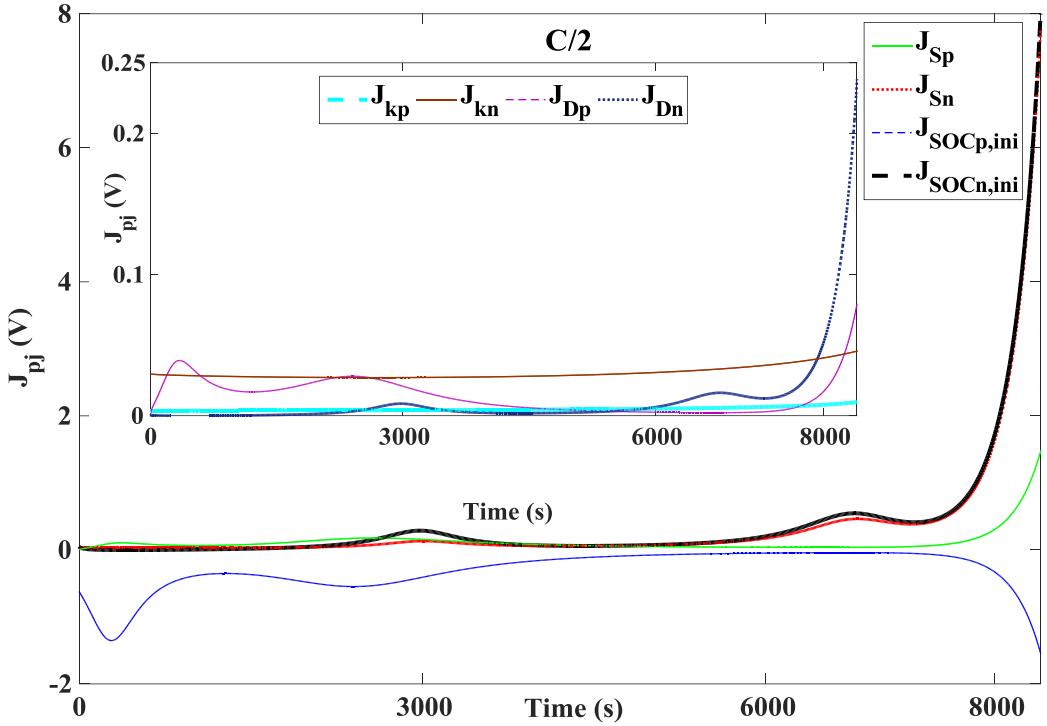
C/2
J_kp J_kn J_Dp J_Dn
J_Sp
J_Sn
J_SOCp,ini
J_SOCn,ini
J_pj (V)
Time (s)

(b)

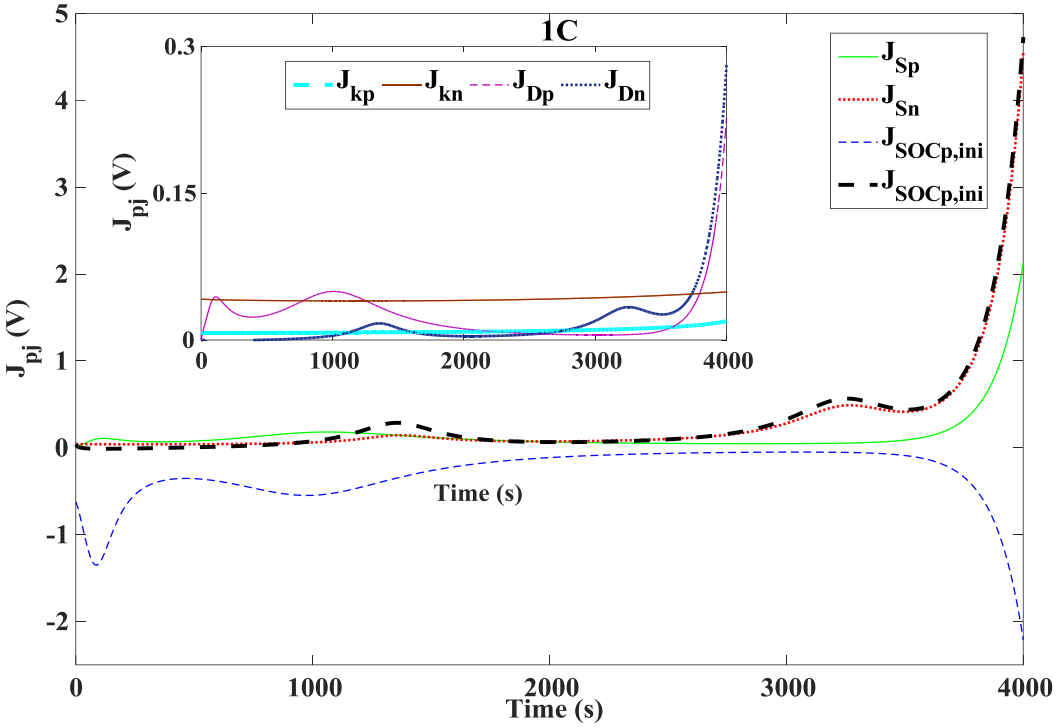
1C
J_kp J_kn J_Dp J_Dn
J_Sp
J_Sn
J_SOCp,ini
J_SOCp,ini
J_pj (V)
Time (s)

(c)

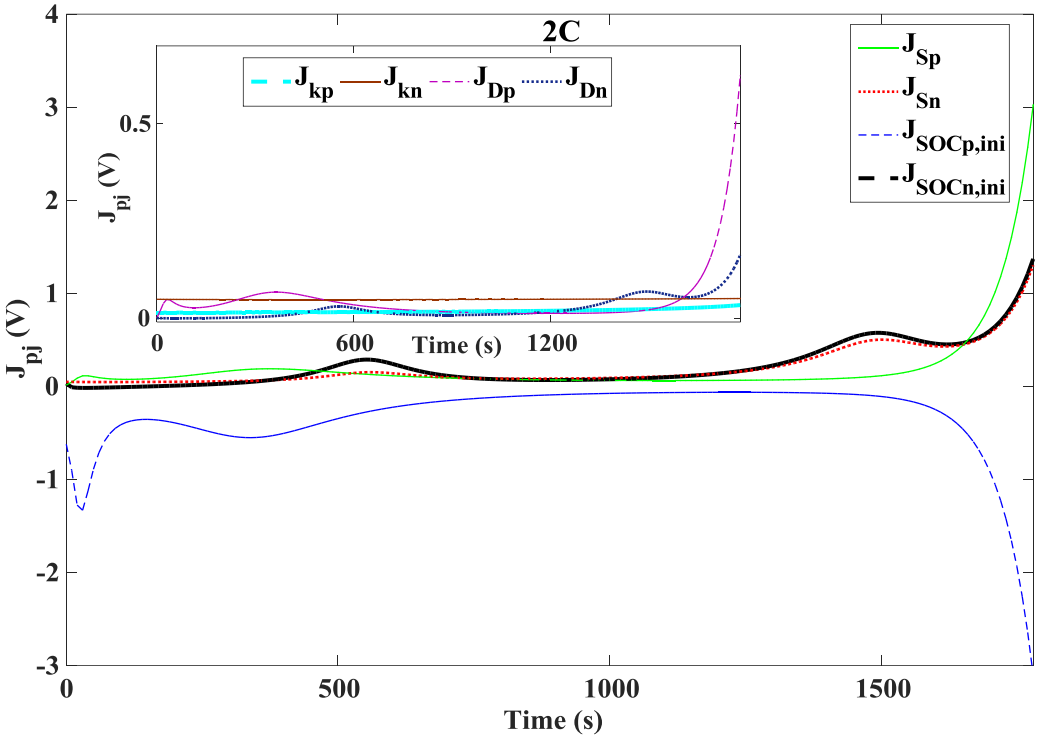
2C
J_kp
J_kn
J_Dp
J_Dn
J_pj (V)
Time (s)
J_Sp
J_Sn
J_SOCp,ini
J_SOCn,ini
J_pj (V)
Time (s)

(d)

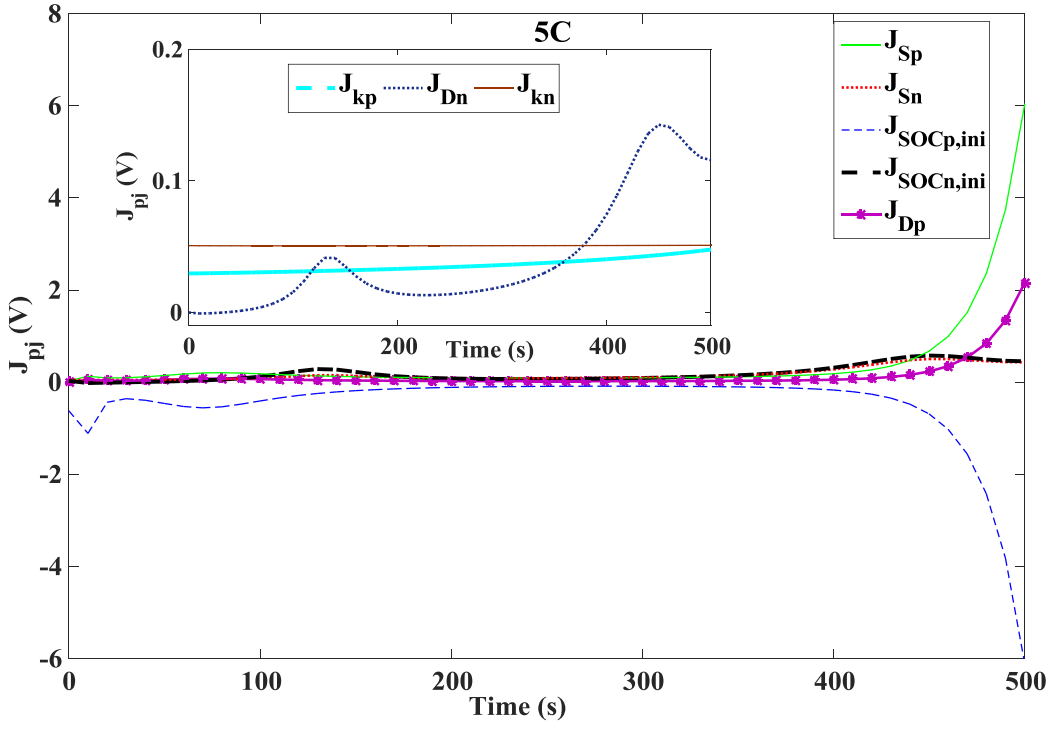
5C
J_kp
J_Dn
J_kn
J_pj (V)
Time (s)
J_Sp
J_Sn
J_SOCp,ini
J_SOCn,ini
J_Dp
J_pj (V)
Time (s)

(e)

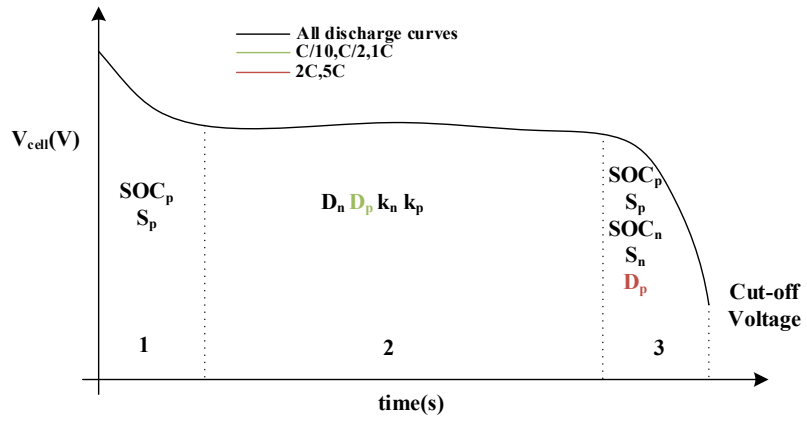

(f)

Figure 3.5: Sensitivity curves (a-e) and best time domain (f) for estimating the electrochemical parameters

3.7. Results

Six different scenarios for the PE study were investigated. Two scenarios were examined at low discharge rates (C/10), with and without a sensitivity analysis. Four additional scenarios were simulated for discharge curves of C/2, 1C, 2C and 5C.

3.7.1. Sensitivity analysis effects

It is observed, for low battery discharge rates (in the present case C/10), that the changes in the electrolyte properties are negligible along the x-direction. As a result, the SPM is accurate enough to be the direct model. The PE process was performed for two different scenarios, with and without a sensitivity analysis. Figures 3.6a,b illustrate the flow chart of both these scenarios.

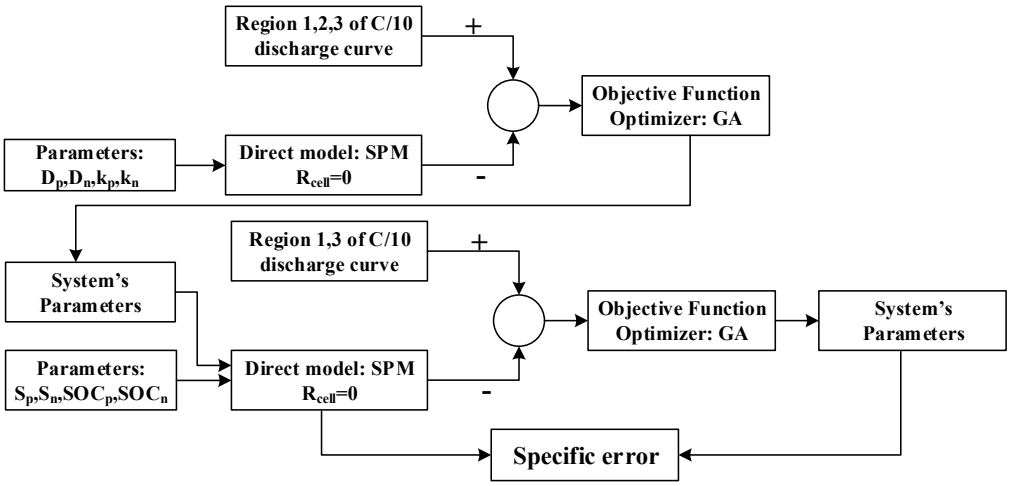

(a)

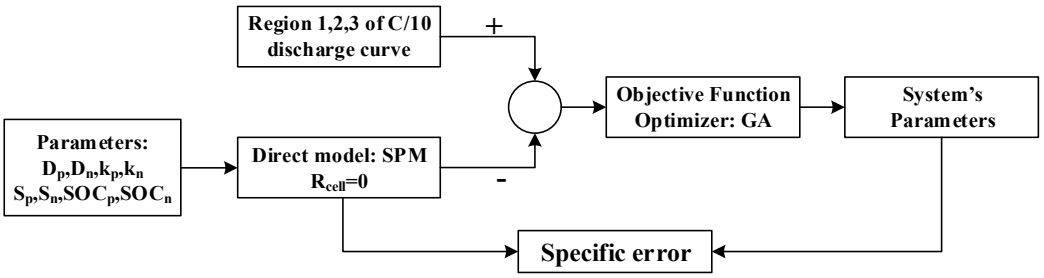

(b)

Figure 3.6: Flow chart of two scenarios for the PE (a) with and (b) without sensitivity analysis

The objective function used in both scenarios is defined in Eqs. 3.34 and 3.36. It means that the least-squared objective function is applied to only one discharge curve. The parameter constraints for the optimization process are provided in Table 3.3. The characteristics and the main results of these simulations are reported in Table 3.4. The specific error function is defined as

$$e_S = \left(\frac{1}{N}\right)\sum_{i=1}^{N}\left(V^{*}_{cell,m,i} - V_{cell,i}(\mathbf{P})\right)^2 \tag{3.40}$$

Table 3.4: Characteristics and results for the 1st and 2nd scenarios with and without sensitivity analysis

Parameter	Unit	1st	2nd
Initial population	-	800	800
Mutation Rate	%	5	5
GA iteration	-	100	100
Specific error	V^2	5.19e-6	3.56e-5

Examination of Table 3.4 reveals that the sensitivity analysis in the first scenario increases the accuracy of the predicted cell potential function as compared to the reference data. Moreover, the order of magnitude of the specific error for this scenario is 10 times lower than that for the second scenario.

3.7.2. Parameter estimation

In order to identify the electrochemical parameters of the Li-ion battery, four additional discharge curves, including high and low discharge rates, were examined. The objective function is based on Eqs. 3.31 and 3.35 and the constraints are summarized in Table 3.3. In other words, for each scenario, the objective function is simultaneously taking into account all discharge curves (C/2, 1C, 2C and 5C). The characteristics of the simulated scenarios are reported in Table 3.5. The results of the PE using both normal and noisy data are depicted in Figure 3.7.

Table 3.5: The characteristics and results of different scenarios of PE study

Sc.	Data Discharge Rate	Direct Model	Sensitivity Analysis	Initial population	Mutation Rate (%)	GA iteration	No. of Parameters
3	C/2,1C 2C,5C	Reduced model (one unknown variable a_0)	No	800	5	100	9
4			Yes	800	5	100	9
5		Reduced model (two unknown variable a_0 a_1)	No	800	5	100	10
6			Yes	800	5	100	10

The following conclusions may be drawn from Figure 3.7:

1. The computational methodology remains stable and accurate in all cases, including the worst case scenario with noisy data.

2. The magnitude of the specific errors for scenarios 3 and 5 and scenarios 4 and 6 shows that the higher the number of unknown parameters, the lower the error. Also, as expected, the performance of a sensitivity analysis improves the accuracy of the predictions.

3. The last scenario, scenario no. 6, is the best for the PE study of the Li-ion battery. It is based on the simplified model with two unknown parameters and it relies simultaneously on the sensitivity analysis.

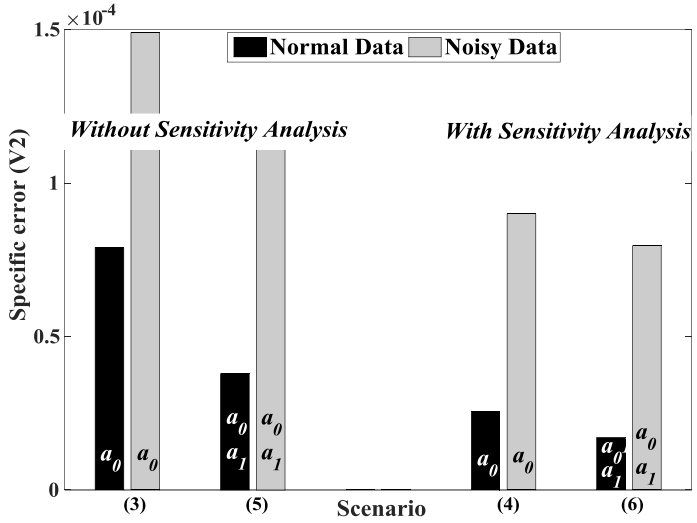

Figure 3.7: PE results using both normal and noisy data

Using the estimated parameters for the best scenario, the discharge curves for the Li-ion battery were determined by running the simplified model. Figures 3.8a and 3.8b show the simulation results for the normal and the noisy reference data respectively. It is seen that the predictions remain accurate for all discharge curves and for noisy reference data.

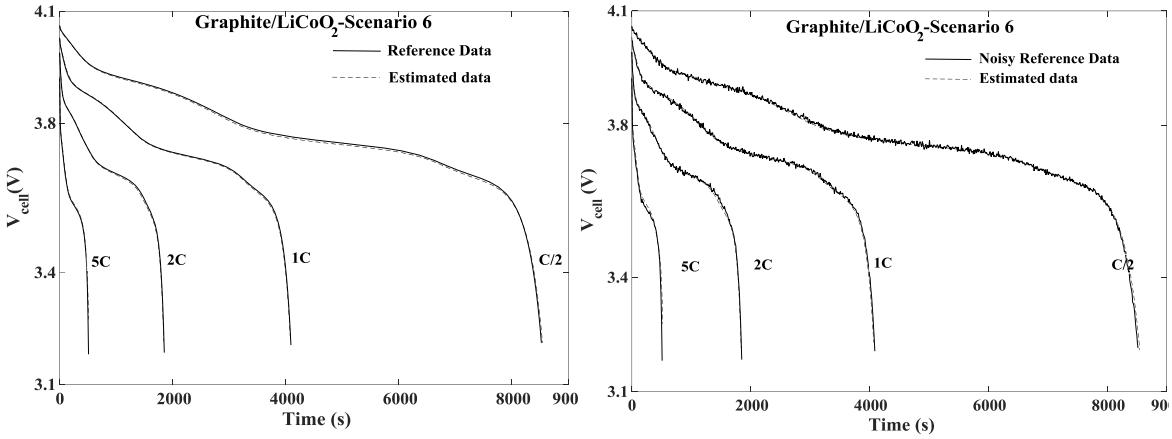

(a) (b)

Figure 3.8: Estimated discharge curves of the Li-ion battery using both normal (a) and noisy (b) reference data

Figure 3.9 illustrates the relative error (e_r) for the best scenario using normal and noisy data (Eq. 3.41). The relative error values were obtained by comparing with the real parameters ($P_{j,real}$) which are used to generate the reference data with the P2D COMSOL model.

$$e_r = \left| \frac{P_{j,PE} - P_{j,real}}{P_{j,real}} \right| \times 100 \qquad (3.41)$$

Figure 3.9 reveals that the relative errors for the constant rates (K_p and K_n) are higher than those for the other parameters. On other hand, according to Figures 3.5a-e their sensitivity coefficients are very low when compared to others. As a result, their effect on the cell potential function of the battery remains insignificant.

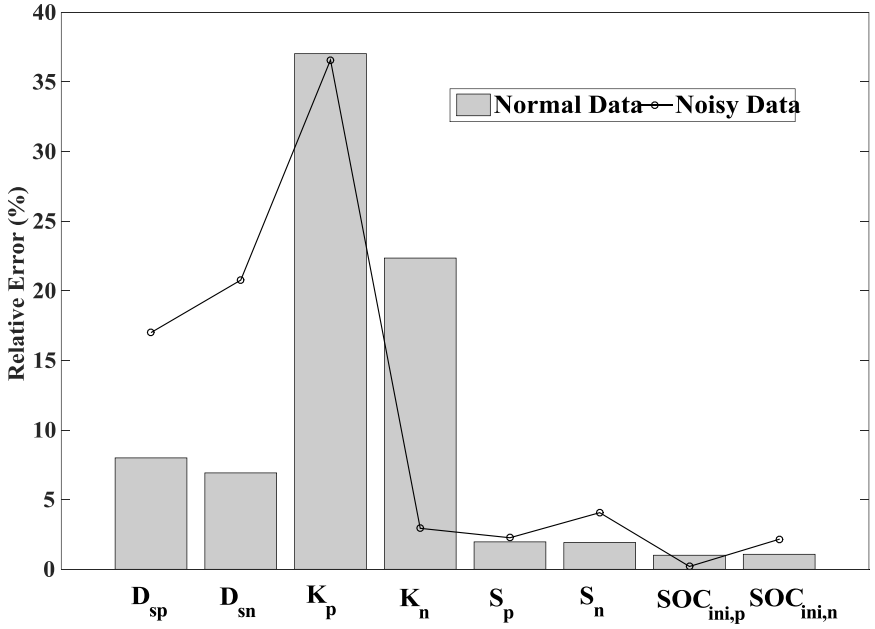

Figure 3.9: Relative error for the best scenario using normal and noisy data

The final values of the expected electrochemical parameters are presented in Table 3.6. It is seen that all parameters are in the expected range and compatible with the data available in the open literature.

Table 3.6: The final electrochemical parameter values of the Li-ion battery with $LiCoO_2$

Symbol	Unit	Reference Value	Value with normal data	Value with noisy data
$D_{s,p}$	m^2/s	1.0e-14	1.08e-14	1.17e-14
$D_{s,n}$	m^2/s	3.9e-14	3.63e-14	3.09e-14
K_p	$m^{2.5}/mol^{0.5}$ s	6.67e-11	4.2e-11	4.23e-11
K_n	$m^{2.5}/mol^{0.5}$ s	1.7e-11	2.08e-11	1.65e-11
S_p	m^2	1.117	1.139	1.0917
S_n	m^2	0.782	0.767	0.8138
$SOC_{p,0}$	-	0.495	0.500	0.496
$SOC_{n,0}$	-	0.742	0.750	0.726

3.8. Model validation

To validate the presented model, the electrochemical parameters of three Li-ion batteries with the LMO, the LCO, and the LFP cathode material are estimated. It is noted that, these results are presented in [104] as the second of part of this paper.

Similar to the Figure 3.5, the schematics of the best time domain for estimating of electrochemical parameters for Li-ion batteries with the LMO and the LFP cathode are presented in Figures 3.10 and 3.11, respectively.

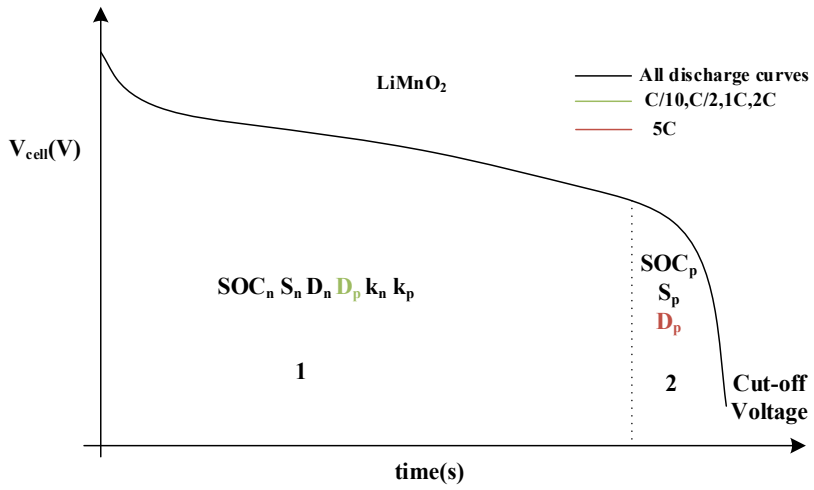

Figure 3.10: Schematic curve generated from a sensitivity analysis for Graphite/$LiMn_2O_4$

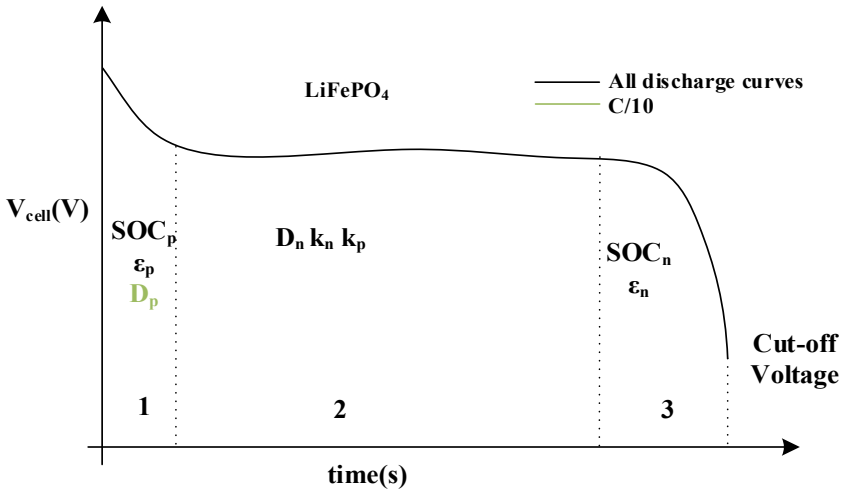

Figure 3.11: Schematic curve of sensitivity analysis for Graphite/$LiFePO_4$

As discussed in Section 3.7.2, the electrochemical parameters are identified for three commercial Li-ion batteries with different cathode materials. The range used and the estimated values of these parameters are presented in Tables 3.7, 3.8, and 3.9 for the Li-ion batteries with the LMO, the LCO, and the LFP cathode, respectively.

Table 3.7: Estimated parameters for the Graphite/$LiCoO_2$ cell

Symbol	Units	Range		Estimated value
		min	max	
$D_{s,p}$	m^2/s	1.0e-15	1.0e-13	9.9451e-14
$D_{s,n}$	m^2/s	1.0e-15	1.0e-13	4.9270e-14
K_p	$m^{2.5}/mol^{0.5}$ s	1.0e-12	1.0e-10	4.1618e-11
K_n	$m^{2.5}/mol^{0.5}$ s	1.0e-12	1.0e-10	2.1138e-11
S_p	m^2	0.6	1.3	1.02
S_n	m^2	0.6	1.3	0.81
$SOC_{p,0}$	-	0.4	0.6	0.53
$SOC_{n,0}$	-	0.6	0.8	0.68

Table 3.8: Estimated parameters for the Graphite/ $LiMn_2O_4$ cell

Symbol	Units	Range		Estimated value
		min	max	
$D_{s,p}$	m^2/s	1.0e-15	1.0e-12	6.7259e-13
$D_{s,n}$	m^2/s	1.0e-15	1.0e-12	7.5502e-13
K_p	$m^{2.5}/mol^{0.5}$ s	1.0e-12	1.0e-10	1.8324e-11
K_n	$m^{2.5}/mol^{0.5}$ s	1.0e-12	1.0e-10	2.8141e-11
S_p	m^2	0.9	1.6	1.39
S_n	m^2	0.9	1.6	1.42
$SOC_{p,0}$	-	0.17	0.3	0.22
$SOC_{n,0}$	-	0.65	0.85	0.71

Table 3.9: Estimated parameters for the Graphite/$LiFePO_4$ cell

Symbol	Unit	Range		Estimated value
		min	max	
$D_{s,p}$	m^2/s	1.0e-19	1.0e-17	4.0064e-18
$D_{s,n}$	m^2/s	1.0e-16	1.0e-14	4.6450e-15
K_p	$m^{2.5}/mol^{0.5}$ s	1.0e-13	1.0e-11	9.2287e-12
K_n	$m^{2.5}/mol^{0.5}$ s	1.0e-12	1.0e-10	3.4281e-12
ε_p	-	0.3	0.45	0.39
ε_n	-	0.4	0.6	0.60
$SOC_{p,0}$	-	0.01	0.06	0.05
$SOC_{n,0}$	-	0.75	0.82	0.81

The cell potential functions of these Li-ion batteries can be calculated by means of the estimated values. Figures 3.12, 3.13, and 3.14 demonstrate a good agreement between the calculated cell potentials and the experimental data for all types of Li-ion battery. It is noted that the simplified model presented in Section 3.3.3 is employed for the LCO and the LMO cathode materials. However, a SPM model modified by the mosaic approach used for the Li-ion battery with the LFP cathode. The detail description of this model will be presented in Chapter 5.

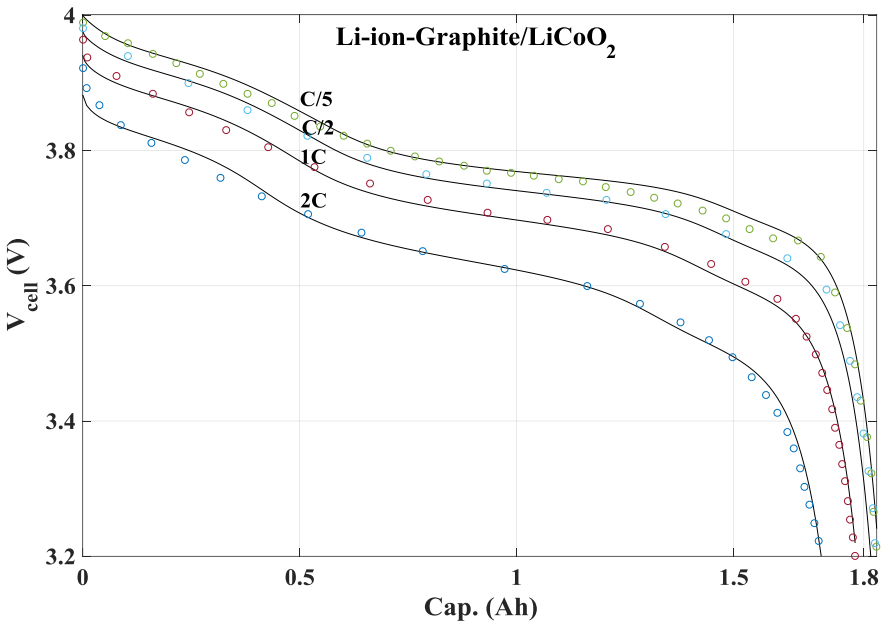

Figure 3.12: Simulated and experimental [11] discharge curves for the Graphite/$LiCoO_2$ cell

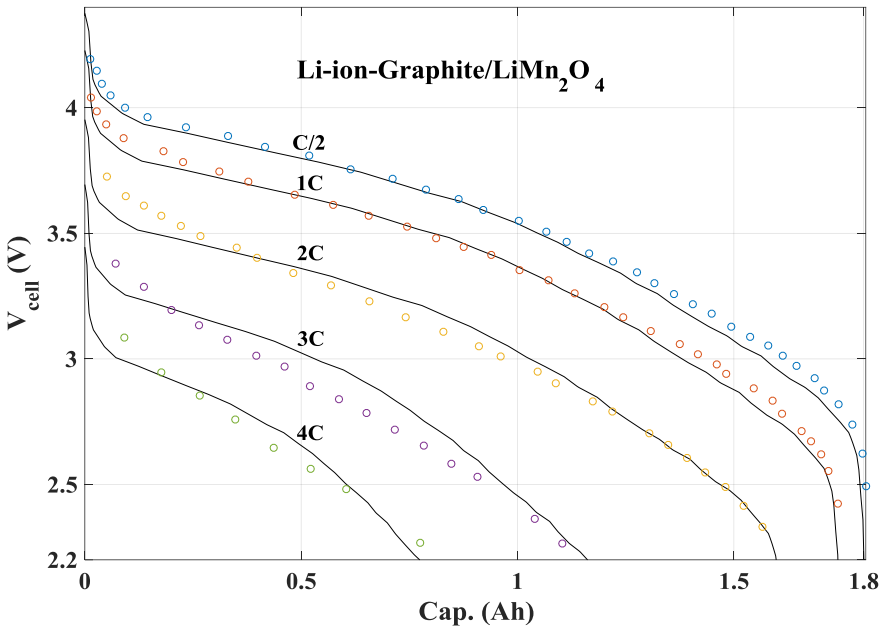

Figure 3.13: Simulated and experimental [34] discharge curves for the Graphite/$LiMn_2O_4$ cell

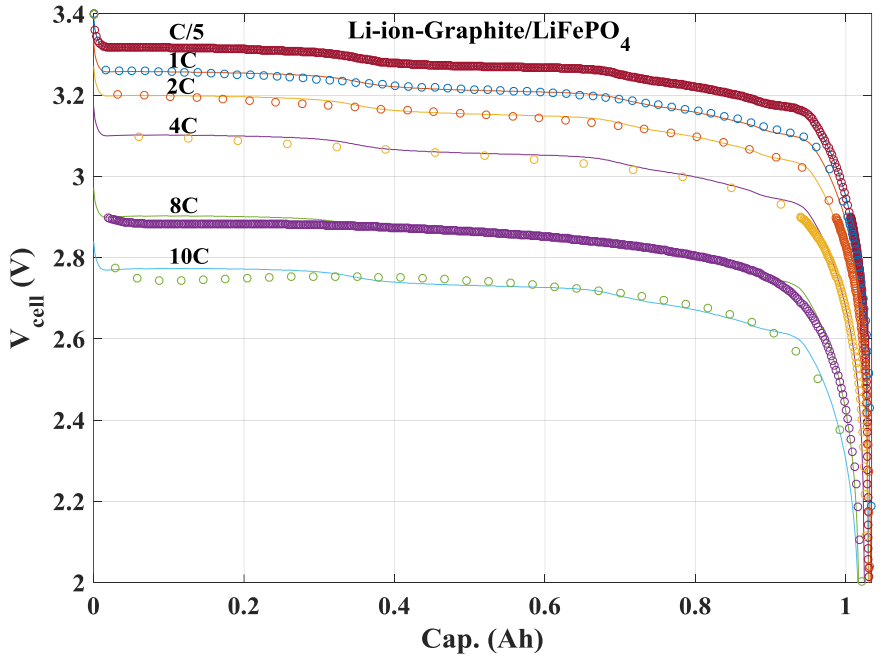

Figure 3.14: Simulated and experimental [105] discharge curves for the Graphite/ $LiFePO_4$ cell

3.9. Conclusion

An electrochemical Parameter Estimation (PE) of a Li-ion battery was conducted with an inverse method. The numerical procedure identifies eight key internal parameters of the Li-ion battery which are the solid diffusion coefficients ($D_{s,n}$ and $D_{s,p}$), the intercalation/deintercalation reaction-rate constants (K_n and K_p), the initial SOC ($SOC_{n,0}$ and

$SOC_{p,0}$), and the electroactive surface areas (S_n and S_p). A simplified version of the P2D model was developed for the PE study. Noisy reference data are generated by the COMSOL®Inc. Multiphysics 5.1 and a Gaussian random function. These data include five discharge curves, namely C/10, C/2, 1C, 2C, 5C. To increase the accuracy and the computational speed of the PE process, the best time domain for the identification of each parameter is determined. This is conducted by means of a sensitivity analysis for all parameters with respect to the cell potential. A least square function and the Genetic Algorithm (GA) are chosen as the objective function and the optimizer for the inverse method, respectively.

Using this methodology, six comparative scenarios are examined. In the 1st and 2nd scenarios, the effect of the sensitivity analysis on the PE process is investigated by using C/10 discharge curve. The results reveal that the sensitivity analysis increases the accuracy of the predicted cell potential function as compared to the reference data. Moreover, the order of magnitude of the specific error for the scenario with considering sensitivity analysis is 10 times lower than that for the regular scenario. In the other four scenarios, the effect of the developed simplified model and of the sensitivity analysis on the identification process is simultaneously examined for both low and high discharge rates. Results show that the larger the number of unknown coefficients in the simplified model, the lower the error. The best PE predictions are obtained when the reduced model calculations are coupled to a sensitivity analysis.

The method developed is applied to estimate the unknown parameters of three types of Li-ion batteries with different cathode materials. The comparison of the calculated cell potentials and the experimental data shows that the method is successful.

Acknowledgements

The authors are very grateful to Hydro-Québec and to the Natural Sciences and Engineering Council of Canada (NSERC) for their financial supports

CHAPITRE 4 : AVANT-PROPOS

Auteurs et affiliation:

- Ali Jokar: étudiant au doctorat, Université de Sherbrooke, Faculté de génie, Département de génie chimique et de génie biotechnologique.
- Martin Désilets: professeur, Université de Sherbrooke, Faculté de génie, Département de génie chimique et de génie biotechnologique.
- Marcel Lacroix: professeur, Université de Sherbrooke, Faculté de génie, Département de génie mécanique.

Revue: Journal of energy storage

Titre français: Une méthode inverse pour l'estimation de paramètres électrochimiques et pour la prédiction du comportement des piles aux ions lithium cylindriques

Contribution au document: Cet article scientifique traite de l'estimation des propriétés thermophysiques par méthode inverse d'une pile cylindrique aux ions lithium. La méthode a été utilisée avec succès pour identifier les principales propriétés thermophysiques et prédire le comportement thermique de la pile. Un modèle direct de transfert de chaleur a également dû être mis au point afin d'estimer la température de surface de la pile au moyen du modèle.

Résumé français :

Une estimation des propriétés thermophysiques d'une pile aux ions lithium (Li-ion), basée sur une méthode inverse et ne nécessitant la disponibilité préalable d'aucuns paramètres électrochimiques, est effectuée. Les cinq paramètres prédits sont la chaleur spécifique, la conductivité thermique, le coefficient de transfert de chaleur par convection, et les états de charge initial et final (SOC). L'identification de ces paramètres est nécessaire pour calculer la génération interne d'énergie et le champ de température, variables essentielles pour prédire le comportement thermique de la pile. Afin d'estimer les paramètres thermophysiques, un modèle direct de transfert de chaleur représentant la pile Li-ion cylindrique a été développé et utilisé pour simuler les données expérimentales, incluant les profils de température de surface à différents taux de décharge. Ces données proviennent de la mesure de pile Li-ion commerciales. Le modèle comprend à la fois les termes réversibles et irréversibles de génération d'énergie thermique. Les mesures expérimentales du potentiel de la pile sont également utilisées dans l'estimation de la distribution de température. Une relation approximative, indépendante des paramètres électrochimiques, est proposée pour représenter la variation du potentiel de la pile en fonction de la température ambiante. Par la suite, une méthode inverse en transfert thermique basée sur l'utilisation d'un algorithme

génétique est utilisée pour estimer les paramètres inconnus. Les résultats montrent que la méthode proposée est fiable, robuste et précise pour tous les taux de décharge.

4. An inverse method for estimating the thermophysical parameters and predicting the behavior of cylindrical lithium-ion batteries

4.1. Abstract

An inverse parameter estimation of the thermophysical properties of a cylindrical lithium-ion (Li-ion) battery is conducted with no need to the electrochemical parameters availability. The five predicted parameters are the heat capacity, thermal conductivity, convection heat transfer coefficient, and the initial and final states-of-charge. The identification of these parameters is necessary for calculating the internal heat generation and the temperature distribution, and therefore, for predicting the thermal behavior of the battery. To estimate the thermophysical parameters, a direct heat transfer model of the cylindrical Li-ion battery was developed that is applied to simulate experimental data including the surface temperature profiles for different discharge rates. The experimental data are collected from a commercial cylindrical Li-ion battery. The model contains both reversible and irreversible heat generation terms. It also employs the experimental cell potential function as an input to account for the temperature distribution. An approximate relation, independent of the electrochemical parameters, is proposed for the cell potential change with ambient temperature. Next, an inverse heat transfer method based on a genetic algorithm is employed for estimating the unknown parameters. The results show that the proposed method is reliable, robust and accurate at all discharge rates.

Keywords: Parameter estimation; Thermophysical parameters; Inverse method; Cylindrical Li-ion battery; Sensitivity analysis; LiFePO4 (LFP) cathode material; Genetic Algorithm (GA).

Nomenclature:

$c_{s,k}$	Solid-state concentration of Li^+ of electrode *k (k=p,n)*, mol m^{-3}
c_e	Concentration of electrolyte in the solution phase, mol m^{-3}
$c_{s,k}^{\max}$	Maximum concentration of Li^+ in the particle of electrode *k (k=p,n)*, mol m^{-3}
$c_{s,k}^{surf}$	Concentration of Li^+ on the surface of the particles of the electrode *k (k=p,n)*, mol m^{-3}
$D_{s,k}$	Li^+ diffusion coefficient in the particle of electrode *k (k=p,n)*, m^2s^{-1}
E	Voltage of the cell, V
$E_{0,k}$	Open-circuit potential of the electrode *k (k=p,n)*, V

F	Faraday's constant, C mol^{-1}
h	Convection coefficient between the cylindrical battery and its surroundings, $Wm^{-2}K^{-1}$
I	Applied current density, A m^{-2}
J_k	Wall flux of Li^+ at the surface of the particles of electrode *k (k=p,n)*, mol $m^{-2}s^{-1}$
k	Thermal conductivity of the cylindrical battery, $Wm^{-1}K^{-1}$
K_k	Reaction rate constant of the electrode *k (k=p,n)*, $m^{2.5}mol^{-0.5}s^{-1}$
L_c	Length of the cylindrical battery, m
n	Negative electrode
p	Positive electrode
P	Unknown parameter matrix
$\dot{Q}$	Total heat generation of the cylindrical battery, W
$\dot{q}$	Volumetric heat generation of the cylindrical battery, W m^{-3}
R	Universal gas constant, J $mol^{-1}K^{-1}$
r	Radial coordinate, m
R_c	Radius of the cylindrical battery, m
$R_{s,k}$	Radius of the particles of the electrode *k (k=p,n)*, m
s	Separator
S	Objective function, K^2
S_k	Total electroactive area of the electrode k, m^2
SOC_k	State Of Charge of the electrode *k (k=p,n)*
$SOC_{k,0}$	Initial State Of Charge of the electrode *k (k=p,n)*
t	Time, s
t_c	Time at the end of the discharge, s
T	Absolute temperature, K
T^*	Experimental surface temperature of the cylindrical battery, K
T_{sur}	Surrounding temperature, K
V_t	Total volume of the cylindrical battery, m^3
$V_{s,k}$	Total volume of the electrode k, m^3
x	Spatial coordinate, m
Greek	
α	Thermal diffusivity of the cylindrical battery, m^2 s^{-1}
ε_k	Porosity of the region *k (k=p,s,n)*
μ_k	Overpotential of the electrode *k (k=p,n)*, V
$\Phi_{s,k}$	Solid-phase potential of the electrode *k (k=p,n)*, V

4.2. Introduction

Lithium-ion (Li-ion) battery packs play a key role for storing electricity and for delivering electric power on demand. The reliability of these storage systems is strongly dependent on the safety and the robustness of the batteries. To ensure the continuous operation of the Li-ion battery pack, battery management systems (BMSs) are usually employed that monitor, control, and manage the thermal performance of the batteries, as well as check their safety and integrity. The interactions between the battery pack and other system components are also monitored by the BMS. One of the important tasks of the BMS is to keep the battery

temperature within appropriate limits under all circumstances. The BMS must handle challenging situations such as rapid charge and discharge processes and extreme ambient conditions [7, 10, 68, 72, 73, 106]. For instance, in hot environments, the thermal management system must be able to efficiently remove the heat generated by the battery pack during the charge and discharge processes. The rate of heat dissipated increases linearly with the operating temperature, and as a result, natural heat dissipation may not suffice to ensure the safety and integrity of the battery pack. Alternative cooling methods must then be devised to avoid battery thermal runaways [68, 107, 108].

Thermal management systems usually rest on rigorous heat transfer models. In 1985, Bernardi et al. performed an overall energy balance to develop a heat transfer model for battery systems. Their model assumes a uniform temperature distribution inside the cell. However, the temperature distribution is dependent on the electrochemical reactions, system heat capacity, phase changes, mixing enthalpy, electrical connections, and the heat transfer to the surroundings [38].

Pals and Newman incorporated a similar energy balance in their pseudo-two-dimensional (P2D) model to compute the heat generation rate of a stack of Li-ion cells [60, 61]. Other solutions were also obtained for thermal and electrochemical equations under the assumption of uniform temperature conditions [9, 36].

In 2011, Guo et al. coupled a single particle model (SPM) with the energy balance equations to develop a reduced heat transfer model of Li-ion batteries. Their numerical predictions showed good agreement with experimental data for low discharge rates [64].

The aforementioned approaches were used to simulate different Li-ion battery configurations such as cylindrical, prismatic and pouch types. Based on the work of Bernardi et al. [38], two heat generation sources were considered to calculate the temperature distribution inside the Li-ion battery: the reversible term which accounts for the battery entropy change associated with the reversible reactions, and the irreversible term which is due to the battery polarization. The change in the mixing enthalpy is neglected to simplify the heat transfer model. In spite of the fact that the temperature inside the sandwich layer was assumed uniform, temperature profiles between these layers could be predicted in the cylindrical and prismatic batteries.

The present paper addresses the parameter estimation of cylindrical Li-ion batteries, and a literature review on the heat transfer models for this type of battery is presented Table 4.1.

Table 4.1: Heat transfer studies for cylindrical Li-ion batteries.

Author	Type	Cathode Material	Cycle rate	Thermal Model	Extra Description
Inui et al., 2007 [109]	Cylindrical Prismatic	$LiCoO_2$	C/2, 1 C	2D	Empirical-based approach.
Muratori et al., 2010 [110]	Cylindrical	$LiFePO_4$	-	1D	Reversible term is neglected.
Forgez et al., 2010 [111]	Cylindrical	$LiFePO_4$	6 C	1D	Lumped approach.
Zhang, 2011 [112]	Cylindrical	$LiMn_2O_4$	1.7 C	1D	Coupled electrochemical-thermal model.
Jeon and Baek, 2011 [113]	Cylindrical	$LiCoO_2$ $LiNiCoMnO_2$	1 C	3D	Using polynomial fit function for entropy changes.
Lin et al., 2013 [114]	Cylindrical	$LiFePO_4$	-	1D	Using thermal resistance.
Kim et al., 2013 [115]	Cylindrical	$LiFePO_4$	-	1D	Using a simplified model.
Saw et al., 2013 [116]	Cylindrical	$LiFePO_4$	1 C,3C,5 C	3D	Coupled P2D model and 3D thermal equations.

Inui et al. developed two simulation codes for calculating the transient temperature distribution inside cylindrical and prismatic Li-ion batteries. The first model is a 2D axisymmetric model and the second model is a full 3D model. Both heat transfer models calculate the internal heat generation by employing measurements of the internal equivalent resistance and entropy changes. Although their numerical results showed good agreement with experimental data for low discharge rates (C/2,1 C), the models rely heavily on empirical data. Consequently, they cannot be transposed to other types of batteries that operate under different conditions [109].

Muratori et al. employed the Laplace transformation to simplify the heat transfer equations of a model of cylindrical Li-ion batteries with a $LiFePO_4$ (LFP) cathode material. The authors assumed that the reversible heat generation term for the LFP is negligible. The results of their study were validated with a finite element model (FEM) for low discharge rates. Their numerical predictions were not, however, compared to experimental data [110].

A lumped heat transfer model was proposed by Forgez et al. to simulate cylindrical Li-ion batteries. Their model depends on three parameters: the heat transfer resistance inside and outside the cell and the battery heat capacity. These parameters were estimated using the temperatures measured at the surface and center of the cylindrical batteries. In spite of its success, the model is limited because it ignores the temperature distribution along the length of the cylindrical battery [111].

Zhang applied a coupled electrochemical-thermal approach to model a cylindrical Li-ion battery. In this model, the electrochemical parameters are considered to be temperature-independent. Nevertheless, the model was successfully validated with experimental data at low discharge rates (1,7 C) [112].

Jeon and Baek investigated the thermal performance of cylindrical Li-ion batteries by means of a 3D model. Polynomial fit functions were used for estimating the entropy changes in the

heat generation equation. Simulations were performed for a wide range of discharge rates. However, the validation was only conducted for a low discharge rate (1 C) [113].

Lin et al. employed a simple thermal resistance model to predict the behavior of cylindrical batteries. Since their main goal was to estimate the centerline temperature, the governing equations included the surface and center temperature functions only. The model takes into account the heat generation source at the centerline, and the thermal resistance is determined experimentally [114].

Kim et al. proposed a reduced heat transfer model for real-time applications of cylindrical Li-ion batteries. They developed a 1D model in which the reversible heat generation term is neglected. A polynomial approximation is assumed for the temperature distribution along the radius. The time-dependent coefficients of the polynomials are determined by a volume-averaging technique [115].

Saw et al. employed a combination of the P2D model with a 3D heat conduction equation to model cylindrical Li-ion batteries. In this model, the thermophysical parameters, including thermal conductivity, density and heat capacity, are assumed to be anisotropic. The effects of the outer shell and the contact resistance on the battery thermal performance were examined. However, the dependence of the electrochemical parameters on the battery operating temperature was not taken into account [116].

All the heat transfer models described above can predict, with more or less success, the thermal behaviour of Li-ion batteries provided that their thermophysical parameters such as the specific heat capacity (C_p), thermal conductivity (k), battery density (ρ), thermal diffusivity (α) and inside heat generation are known. But there is a multitude of commercial Li-ion batteries containing different materials, electrolyte solutions, separators, current collectors, battery cans and terminals. Consequently, determining these thermophysical parameters from experimental data is, as Maleki et al. [66] and Hong et al. [117] have shown, a painstaking and tedious task.

The present paper proposes an alternative approach for estimating the thermophysical parameters of commercial cylindrical Li-ion batteries (Figure 4.1) to overcome some of these limitations. This approach rests on an inverse heat transfer method [14, 15].

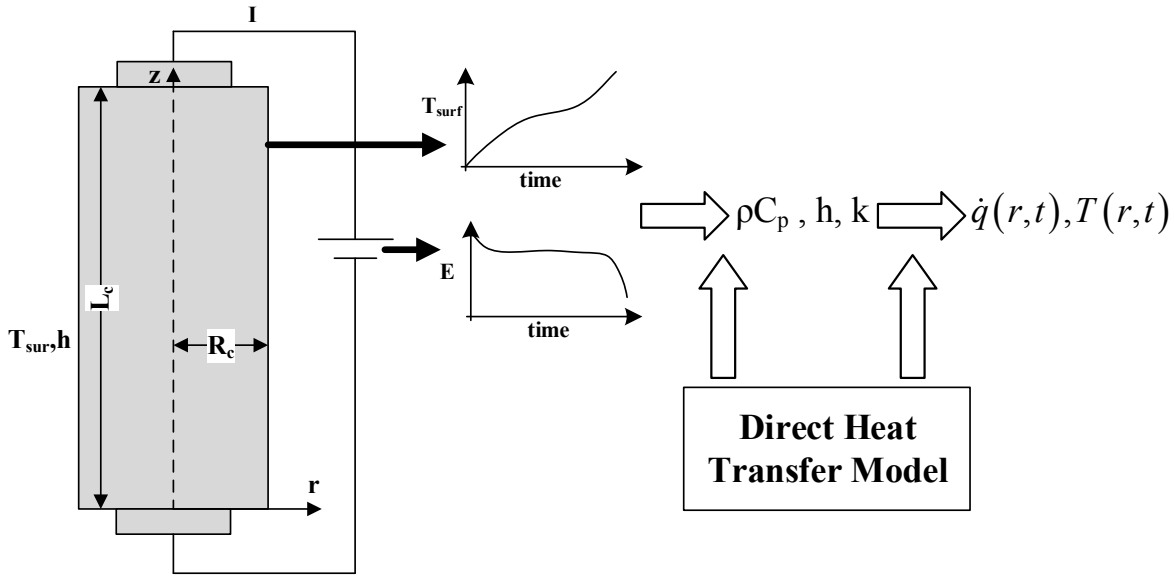

Figure 4.1: Overall thermophysical parameter estimation used in this study

4.3. Experimental data

The experimental data from a commercial 1.05 Ah 18650 Li_xC_6/Li_yFePO_4 cylindrical Li-ion battery were provided by Hydro-Québec. The experiments were conducted meticulously in order to generate the cell potential and the surface temperature as a function of the charge/discharge time, as shown in Figures 4.2a and 4.2b. The temperature of the climate chamber was kept constant at 25°C. The thermophysical parameters were estimated from the discharge experimental data. This is justified by the following facts: (1) the sharpest and noisiest operating temperature rise occur during the discharge process and (2) high battery discharge rates are found in many applications. The cell potential and the surface temperature curves are depicted in Figures 4.2a and 4.2b, respectively [105]. The higher the discharge rate, the higher the temperature rise. Therefore, only the data for high discharge rates at 2C, 4C, 8C, 10C, and 15C are considered. Figure 4.2b indicates that the surface temperature exceeds the safe temperature of 35°C for discharge rates of 10C and above. In these cases, operating the battery pack without an effective thermal management system would threaten the integrity and safety of the storage system.

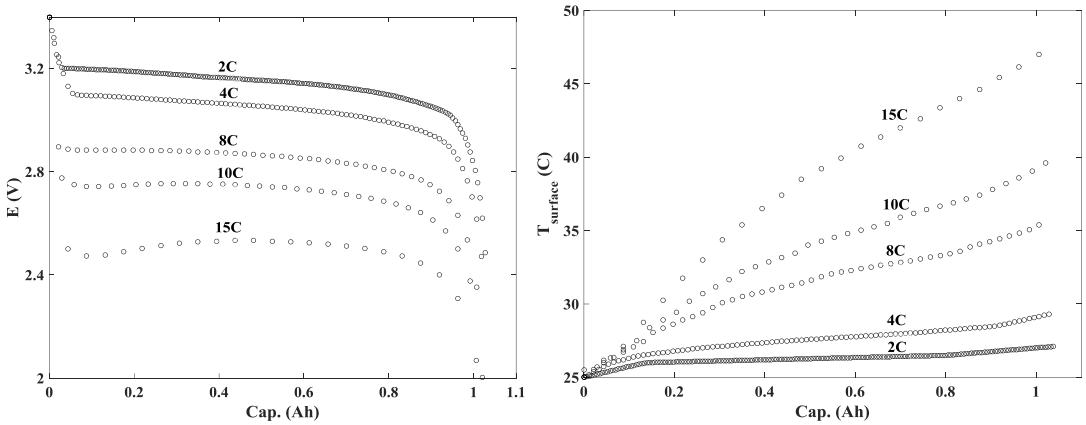

(a) **(b)**

Figure 4.2: (a) Cell potential and (b) surface temperature curves of the Li-ion battery [105]

4.4. Direct heat transfer model

The direct heat transfer model predicts the temperature distribution across the battery (the output) provided that its thermal and geometric properties, the initial condition and the boundary conditions are all known (the inputs).

The cylindrical Li-ion battery is made of sandwich layers. A layer is composed of a cathode, a separator, an anode and current collectors encapsulated into a protective cylindrical case. Regardless of the battery height, its cross section area has a spiral shape [109, 118].

4.4.1. Direct model equations

The direct heat transfer model of the battery proposed in this study rests on the following assumptions:

(1) The temperature gradient in the z-direction is much smaller than that in the r-direction, as has been assumed in previous studies [111, 113, 116]. As a result, a one-dimensional r-direction model is adopted ($T(z,r,t) \approx T(r,t)$).

(2) The mathematical model is radial (concentrated model) and not spiral. There is no gap and no contact resistance between the sandwiched layers [118].

(3) All materials are homogeneous and isotropic. Also, there is no bulk motion.

(4) The heat capacity (ρC_p), thermal conductivity (k) and convection heat transfer coefficient (h) are considered to be constant.

(5) The heat transfer across the battery shell case is neglected.

(6) The heat generation varies with time, but is assumed to be uniform in each layer.

(7) Radiation heat transfer is negligible.

Based on the aforementioned assumptions, the governing heat transfer equation for the temperature distribution T(r,t) across the cylindrical Li-ion battery is stated as [109, 110]:

$$k\frac{\partial^2 T(r,t)}{\partial r^2}+\frac{k}{r}\frac{\partial T(r,t)}{\partial r}+\dot{q}(r,t)=\left(\rho C_p\right)\frac{\partial T(r,t)}{\partial t};\ 0\le r\le R_c \tag{4.1}$$

where $\dot{q}$ is the volumetric heat generation of the cylindrical Li-ion battery. It comprises reversible ($\dot{q}_{rev}$) and irreversible ($\dot{q}_{irrev}$) components:

$$\dot{q}=\dot{q}_{irrev}+\dot{q}_{rev} \tag{4.2}$$

The reversible term is associated with the entropy change of the battery reactions and, the irreversible term to the battery polarization. These terms are defined as [38]:

$$\dot{q}_{irrev}=\frac{I}{V_t}\left(E_0(t)-E(t)\right);\ 0\le t\le t_c \tag{4.3}$$

$$\dot{q}_{rev}=\frac{I}{V_t}\left(-T(r,t)\frac{\partial E_0(t)}{\partial T}\right);\ 0\le t\le t_c, 0\le r\le R_c \tag{4.4}$$

V_t, I and t_c are the cylinder volume, charge/discharge current and cut-off process time, respectively. E(t) is the cell potential function and $E_0(t)$ is the open-circuit function. Note that the reversible heat generation is a function of the radius (r) and the charge/discharge time (t). Its magnitude can be either positive or negative according to the direction of the battery reactions. Because of assumption 6, the irreversible term is time-dependent only and it is always positive.

The boundary condition at the cylinder centerline is symmetrical:

$$\frac{\partial T(0,t)}{\partial r}=0;\ 0\le t\le t_c \tag{4.5}$$

A convective heat transfer boundary condition is applied on the cylinder surface:

$$\frac{\partial T(R_c,t)}{\partial r}=-\frac{h}{k}\left(T(R_c,t)-T_{sur}\right);\ 0\le t\le t_c \tag{4.6}$$

where h is the convection heat transfer coefficient.

The initial condition for the temperature of the Li-ion battery is:

$$T(r,0)=T_{sur};\ 0\le r\le R_c \tag{4.7}$$

T_{sur} is the temperature of the surroundings.

For the present study, the experimental cell potential functions E(t) are available for different discharge rates at a temperature of 25°C. These data are used in the direct model. The open-circuit potential functions for the negative (graphite) [64] and positive (LFP) [119] electrodes are determined from the state-of-charge (SOC) based on curves available in the open literature (Figures 4.3a and 4.3b). Similarly, the ($\partial E_0/\partial T$) values for graphite [64] and LFP [120] are computed from these data and presented in Figures 4.3c and 4.3d.

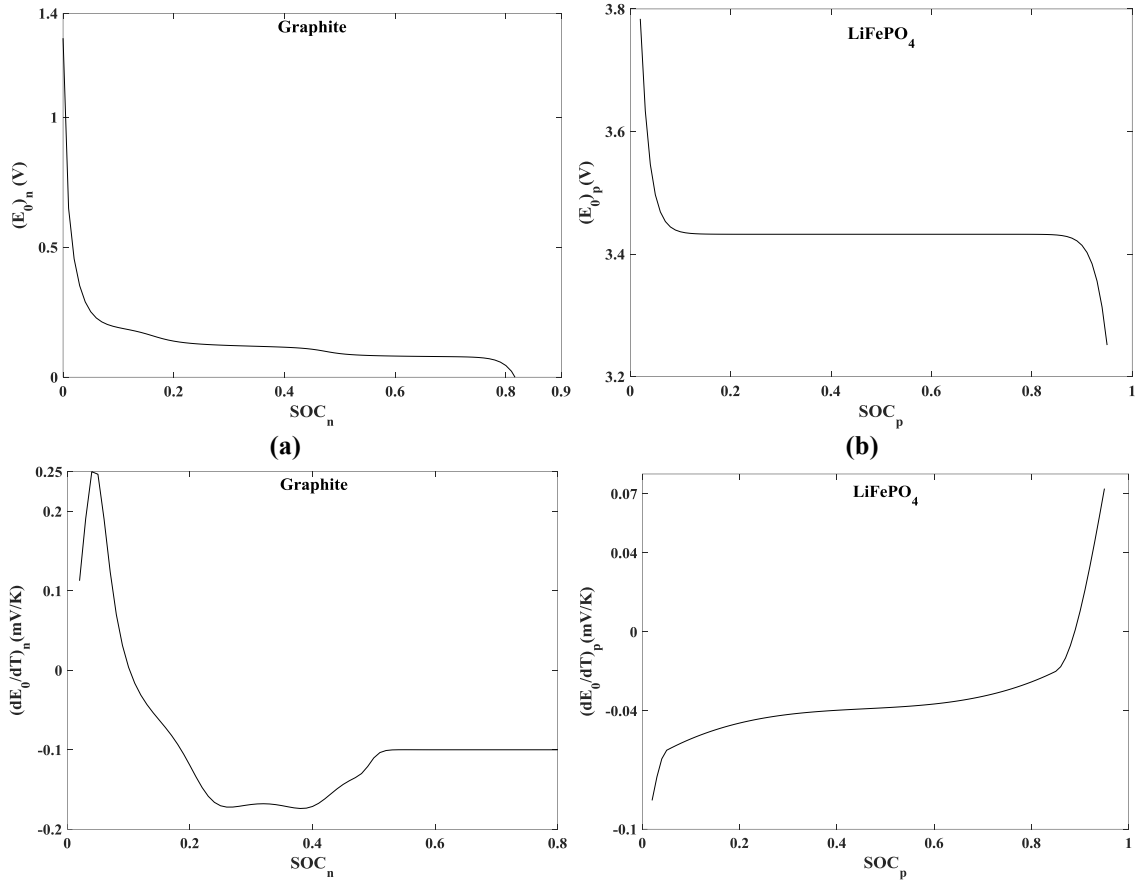

Figure 4.3: Open circuit potential (a,b) and entropic heat change (c,d) as a function of SOC for Graphite[64] and LFP[119, 120]

The set of Eqs. 4.1 to 4.7 is solved based on the mesh grid presented in Figure 4.4 with the Crank Nicolson Finite Difference Method [121] for which,

$$\frac{\partial^2 T}{\partial r^2} = \frac{T_{m+1}^n - 2T_m^n + T_{m-1}^n}{\Delta r^2} \tag{4.8}$$

$$\frac{\partial T}{\partial r} = \frac{T_{m+1}^n - T_{m-1}^n}{2\Delta r} \tag{4.9}$$

$$\frac{\partial T}{\partial t} = \frac{T_m^{n+1} - T_m^n}{\Delta t} \tag{4.10}$$

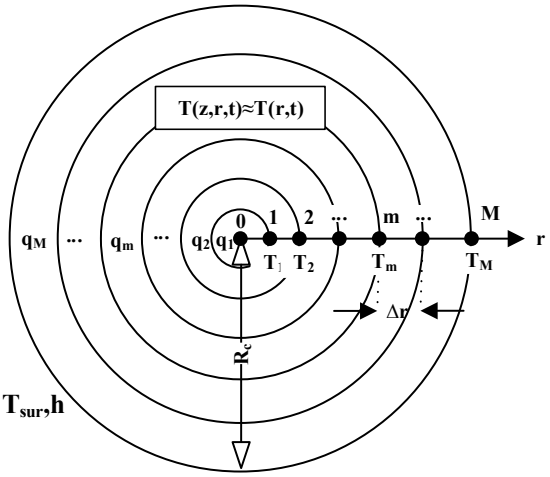

Figure 4.4: Finite difference mesh used for the cylindrical Li-ion battery

where the increment Δr is considered to be small relative to the total sandwich layer thickness. The volumetric heat generation term is computed for each layer. It is estimated with the average temperature between the inside and outside surface of each layer.

$$\dot{q}_m^n = \frac{I}{V}\left(E_0^n - E^n - \left(\frac{T_m^n + T_{m-1}^n}{2} \right)\left(\frac{\partial E_0}{\partial T} \right)^n \right) \tag{4.11}$$

Also, the finite difference equations for the boundary and initial conditions are:

$$T_0^{n+1}\left(1 + \frac{\left(\rho C_p\right)\Delta r^2}{k\Delta t} \right) - T_1^{n+1} = T_0^n \left(\frac{\left(\rho C_p\right)\Delta r^2}{k\Delta t} - 1 \right) + T_1^n \tag{4.12}$$

$$T_{M+1}^n = T_M^n \left(-\frac{2h\Delta r}{k} \right) + T_{M-1}^n + \frac{2h\Delta r T_{sur}}{k} \tag{4.13}$$

$$T_m^0 = T_{sur};\ m = 1,2,...,M \tag{4.14}$$

The open-circuit potential (E_0) and ($\partial E_0/\partial T$) are estimated from the open-circuit potential vs SOC curves of the electrodes.

The above set of finite difference equations is closed with a relationship between the SOC and battery discharge time. In the present study, it is assumed that the SOC functions vary linearly with respect to the discharge time. Moreover, due to the higher Li-ion capacity storage of LFP compared to graphite, the SOC_n will be close to zero at the end of the discharge period. The resulting SOC_n for the negative electrode is then expressed as:

$$SOC_n = SOC_{n,0}\left(1 - \frac{t}{t_c}\right);\ t_c = \frac{3600}{\left(I / I_{1C}\right)},\ SOC_{n,Final} \approx 0 \tag{4.15}$$

$SOC_{n,0}$ is the initial SOC_n . t_c is the final discharge time. I_{1C} is the 1 C discharge current.

In a similar manner, the SOC for the positive electrode is assumed to increase linearly with time. According to the literature, the SOC at the beginning of discharge is nearly zero (≈0.01-

0.05) [122, 123]. In this paper, the initial value of the SOC was set equal to 0.05. The resulting SOC_p exhibits the following relation with the discharge time:

$$SOC_p = SOC_{p,0} + \left(SOC_{p,Final} - SOC_{p,0}\right)\left(\frac{t}{t_c}\right);\ t_c = \frac{3600}{\left(I / I_{1C}\right)},\ SOC_{p,0} \approx 0.05 \qquad (4.16)$$

With the above information, the direct heat transfer model is able to predict the temperature distribution inside the cylindrical Li-ion battery. A schematic of the overall calculation procedure is depicted in Figure 4.5. The inputs to the direct model are classified into two groups: the known variables, which are provided by the experimental data, and the unknown parameters, which must be determined. The first group comprises the discharge current (I), surrounding temperature (T_{sur}), total volume of the cylindrical battery (V_t), and battery discharge curve (E). The second group includes the heat capacity (ρC_p), thermal conductivity (k), convection heat transfer coefficient (h), initial value of the SOC_n, and final SOC_p. These unknown parameters are estimated with the inverse heat transfer method discussed in section 4.5.

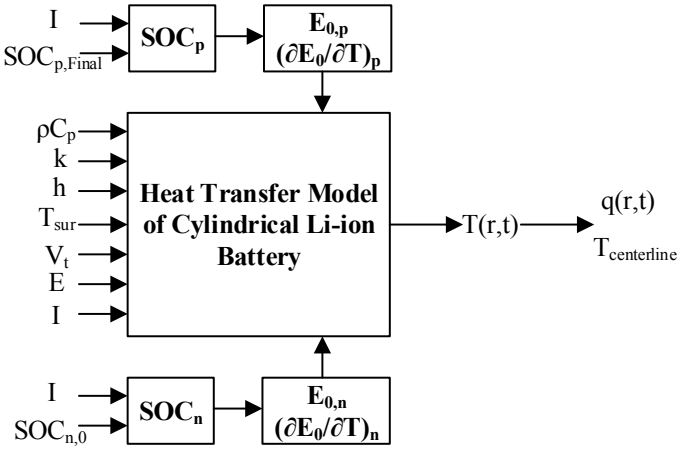

Figure 4.5: Schematic of the direct heat transfer model

4.4.2. The total heat generation terms

The heat generation during the discharge of a Li-ion battery plays a key role in the thermal management of the battery pack. The BMS employs this variable to maintain the battery operating temperature within reasonable limits. Once the temperature distribution is predicted by the direct model, the variation of the heat generation during the discharge period is estimated with the inverse method results. To achieve this goal, a relation for calculating the total heat generation is proposed. As discussed earlier, the total heat generation comprises two terms: the reversible heat generation term ($\dot{Q}_{rev}$) and the irreversible heat generation term ($\dot{Q}_{irrev}$). Therefore,

$$\dot{Q}_t = \dot{Q}_{irrev} + \dot{Q}_{rev} = \left(\dot{q}_1 V_1 + ... + \dot{q}_M V_M\right)_{irrev} + \left(\dot{q}_1 V_1 + ... + \dot{q}_M V_M\right)_{rev}; m = 1,2,...,M \quad (4.17)$$

where V_m is the volume of layer m. The magnitude of V_m is determined from,

$$V_m = 2\pi\left(\frac{m\Delta r + (m-1)\Delta r}{2}\right)\Delta r L = \pi\left(2m-1\right)\Delta r^2 L;\ m = 1,2,...,M \quad (4.18)$$

The substitution of Eqs. 4.3, 4.4 and 4.18 into Eq. 4.17 yields

$$\dot{Q}_{irrev} = \sum_{m=1}^{M} \frac{IV_m}{V_t}\left(E_0(t) - E(t)\right) = I\left(E_0(t) - E(t)\right) \quad (4.19)$$

$$\dot{Q}_{rev} = \sum_{m=1}^{M} \frac{IV_m}{V_t}\left(-T_m \frac{\partial E_0}{\partial T}\right) = -I\left(\frac{\Delta r}{R}\right)^2 \left(\frac{\partial E_0}{\partial T}\right)\sum_{m=1}^{M}(2m-1)T_m \quad (4.20)$$

The total heat generation ($\dot{Q}_t$) is a function of the battery discharge time. It is estimated from the voltage curve and the temperature distribution (T_m) across the cylindrical Li-ion battery. Eq. 4.19 shows that the irreversible heat generation of the battery is always positive (the cell potential (E) is always less than the open-circuit potential (E_0)). On the other hand, Eq. 4.20 shows that the reversible heat generation term is a heat source or a heat sink depending on the sign of the ($\partial E_0/\partial T$) term.

4.4.3. The effect of T_{sur}

The experimental data were collected at the standard surrounding temperature of 25°C. The direct heat transfer model may accommodate other surrounding temperatures according to the following scenarios:

Scenario 1. If the cell potential (E) is measured at a temperature different from 25°C, then the open-circuit potential (E_0) should be updated. These functions are approximated with a Taylor series expansion [64]:

$$E_{0,j}\left(SOC_j, T_{sur}\right) = E_{0,j}\left(SOC_j, T_{ref}\right) + \left.\frac{\partial E_{0,j}}{\partial T}\right|_{SOC_j, T_{ref}} \left(T_{sur} - T_{ref}\right);\ j = n, p;\ T_{ref} = 25°C \quad (4.21)$$

Scenario 2. If the cell potential (E) is measured at the standard surrounding temperature of 25°C, both the open-circuit potential (E_0) and the cell-potential (E) should be updated in order to predict the Li-ion battery behavior for different surrounding temperatures. E_0 may then be updated with Eq. 4.21. In the present paper, a new relation for the cell potential is proposed. To develop this relation, we resort to the governing equations of the single particle model (SPM) [64]:

$$\frac{\partial c_{s,k}(\hat{r},t)}{\partial t} = \frac{D_{s,k}}{\hat{r}^2}\frac{\partial}{\partial \hat{r}}\left(\hat{r}^2 \frac{\partial c_{s,k}(\hat{r},t)}{\partial \hat{r}}\right) \quad (4.22)$$

$$E = \left[E_{0,p} - E_{0,n} \right] + \frac{2RT}{F} \left(ln \left(\frac{\sqrt{m_p^2 + 4} + m_p}{2} \right) + ln \left(\frac{\sqrt{m_n^2 + 4} + m_n}{2} \right) \right) \tag{4.23}$$

$$J_k = 2K_k \left(c_{s,k}^{max} - c_{s,k}^{surf} \right)^{0.5} \left(c_{s,k}^{surf} \right)^{0.5} c_e^{0.5} \, sinh \left(\frac{0.5F\mu_k}{RT} \right); J_p = \frac{I}{F S_p}, J_n = -\frac{I}{F S_n} \tag{4.24}$$

$$\mu_k = \Phi_{s,k} - E_{0,k}; \; E = \Phi_{s,p} - \Phi_{s,n} \tag{4.25}$$

$$m_p = \frac{I}{FK_p S_p c_{s,p}^{\max} c_e^{0.5} \left(1 - SOC_p \right)^{0.5} \left(SOC_p \right)^{0.5}}; \; S_p = \frac{3\varepsilon_p V_{s,p}}{R_{s,p}}, SOC_p = \frac{c_{s,p}^{surf}}{c_{s,p}^{\max}} \tag{4.26}$$

$$m_n = \frac{I}{FK_n S_n c_{s,n}^{\max} c_e^{0.5} \left(1 - SOC_n \right)^{0.5} \left(SOC_n \right)^{0.5}}; \; S_n = \frac{3\varepsilon_n V_{s,n}}{R_{s,n}}, SOC_n = \frac{c_{s,n}^{surf}}{c_{s,n}^{\max}} \tag{4.27}$$

where $\hat{r}$ is the radial coordinate along the positive and negative particles. Here, it is noted that, the SPM does not work properly for Li-ion batteries with LFP cathode material [19]. However, it can be able to model them by considering the mosaic approach as implemented by Prada et al. [123]. In the mosaic approach, it is assumed that the Li^+ intercalation/deintercalation processes into LFP particles occur at different sites with identical spherical shapes. The effective radius or the Li^+ ion diffusion coefficient of the LFP particle is adjusted depending on the battery discharge/charge rates [123, 124].

The cell potential profile is already available at T_{sur}=25°C. Therefore, to estimate the cell potential for other surrounding temperatures, the Taylor series expansion is invoked:

$$E\left(T_{sur}\right) = E\left(T_{ref}\right) + \left.\frac{\partial E}{\partial T}\right|_{T_{ref}} \left(T_{sur} - T_{ref} \right); \; T_{ref} = 25°C \tag{4.28}$$

The second term of the right side of Eq. 4.28 is calculated with Eq. 4.23:

$$\left.\frac{\partial E}{\partial T}\right|_{T_{ref}} = \left.\frac{\partial E_0}{\partial T}\right|_{T_{ref}} + \frac{2R}{F} \left(\ln \left(\frac{\sqrt{m_p^2 + 4} + m_p}{2} \right) + \ln \left(\frac{\sqrt{m_n^2 + 4} + m_n}{2} \right) \right) \tag{4.29}$$

Of course, it is assumed that the electrochemical parameters are temperature-independent. The last step is to determine the magnitude of the second term of the right side of Eq. 4.29. It is calculated by Eq. 4.23 at the reference temperature (T_{ref}), that is,

$$\frac{2R}{F} \left(\ln \left(\frac{\sqrt{m_p^2 + 4} + m_p}{2} \right) + \ln \left(\frac{\sqrt{m_n^2 + 4} + m_n}{2} \right) \right) = \frac{E\left(T_{ref}\right) - E_0\left(T_{ref}\right)}{T_{ref}} \tag{4.30}$$

By substituting Eq. 4.30 into Eq. 4.29, the cell potential function (E) is estimated for different surrounding temperatures:

$$E\left(T_{sur}\right) = E\left(T_{ref}\right) + \left(\frac{\partial E_0}{\partial T} + \frac{E - E_0}{T} \right)\Bigg|_{T_{ref}} \left(T - T_{ref} \right); \; T_{ref} = 25C \tag{4.31}$$

The interesting feature of Eq. 4.31 is that the cell potential function (E) is estimated at any surrounding temperature without the use of other electrochemical parameter for the Li-ion battery.

4.5. Inverse heat transfer model

We have seen in section 4.4 above that the direct heat transfer model predicts the temperature distribution across the battery provided that its thermophysical properties and parameters, the initial condition and boundary conditions are all known.

Unfortunately, some of the properties and parameters of the battery are typically unknown. These unknowns include the heat capacity (ρC_p), thermal conductivity (k), convection heat transfer coefficient (h), initial SOC_n, and final SOC_p. These parameters can, however, be determined with the proposed inverse method.

Inverse heat transfer problems (IHTP) deal with the identification of unknown thermal characteristics by means of experimental data [14]. Three types of signals are measured from an operating Li-ion battery during the charge/discharge processes: the cell potential, current, and surface temperature T. In the present study, the surface temperature is used to estimate the unknown parameters.

Figure 4.6 provides an overall view of the inverse heat transfer procedure. The aim of the inverse method is to minimize an objective function (S) to determine the unknown parameters. The objective function (S) is defined as the difference between the computed temperature (**T(t)**) and the measured temperature (**T^*(t)**) at the surface of the battery. Once the objective function is satisfactorily minimized, the unknown parameters are automatically determined.

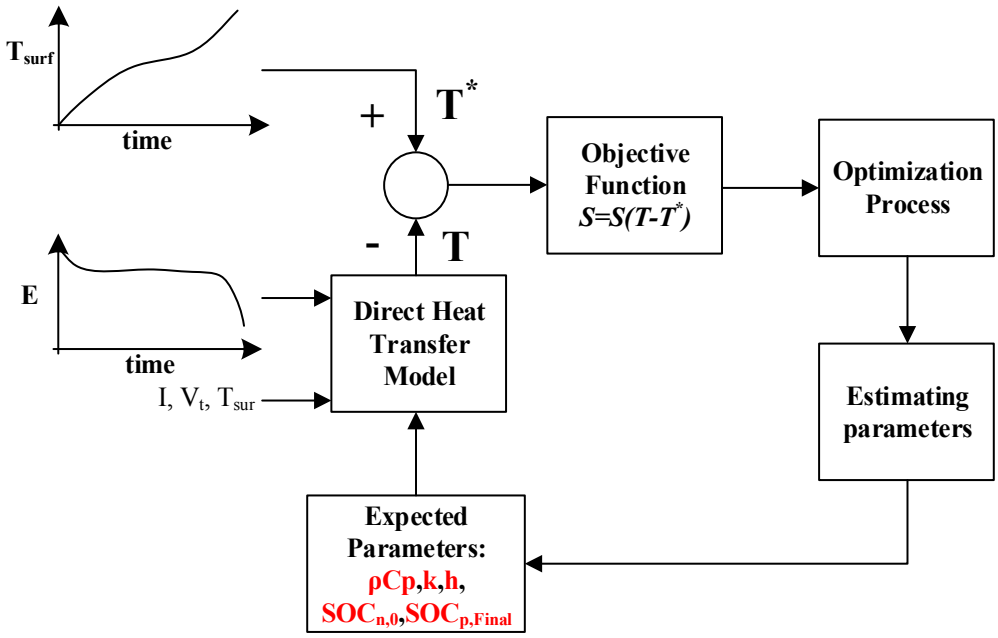

Figure 4.6: Schematic of the inverse heat transfer procedure

The inverse heat transfer problem for the Li-ion battery involves a "whole time domain" approach. This means that the experimental data are measured in small time intervals between zero and the cut-off time ($0 < t \leq t_c$). The temperature vector with N time intervals during one charge/discharge process is written as

$$\mathbf{T}^* = \begin{bmatrix} T_1^* \\ T_2^* \\ \vdots \\ T_N^* \end{bmatrix}_{N\times 1} ; t = t_1, t_2, ..., t_N \qquad (4.32)$$

The least-square objective function (S) for one charge/discharge process is then expressed as [14].

$$S = \left(\mathbf{T}^* - \mathbf{T}(\mathbf{P})\right)^T \left(\mathbf{T}^* - \mathbf{T}(\mathbf{P})\right) = \sum_{i=1}^{N} \left(\mathrm{T}_i^* - \mathrm{T}_i(\mathbf{P})\right)^2 \qquad (4.33)$$

The superscript T indicates the transpose of the matrix. For M charge/discharge processes, Eq. 4.33 is generalized as:

$$S = \left(\mathbf{T}^* - \mathbf{T}(\mathbf{P})\right)^T \left(\mathbf{T}^* - \mathbf{T}(\mathbf{P})\right) = \sum_{j=1}^{M}\sum_{i=1}^{N} \left(T_{ij}^* - T_{ij}(\mathbf{P})\right)^2 \qquad (4.34)$$

The calculated temperature vector (**T(t)**) is computed in terms of the unknown parameters (**P**). The parameters (**P**) are determined by minimizing the objective function (S) in the following manner:

$$\min S = S(\mathbf{P}) \; subject\; to\; P_{j,low} \leq P_j \leq P_{j,high} \qquad (4.35)$$

$P_{j,low}$ and $P_{j,high}$ are the minimum and the maximum of the P_j values, respectively. Eq. 4.35 is solved with an optimizer that determines the global minimum.

The optimization process for inverse problems is mathematically challenging, slow converging and computationally expensive [15]. Colaço et al. reviewed different solution methods for inverse problems among which we find the steepest descent method, conjugate gradient method, Newton-Raphson method, quasi-Newton method, Levenberg-Marquardt method (LM), genetic algorithms (GA), differential evolutions, particle swarm method and the simulated annealing method [17]. In general, these optimization methods are divided into two categories: deterministic methods and stochastic methods. The deterministic methods are usually faster than stochastic methods. However, their searches tend to become trapped in local extrema. On the other hand, stochastic-based optimization methods employ random-based operation functions that are ideally suited for reaching the system global extremum [17, 18].

In this paper, due to the complexity of the governing equations of the direct model (Eqs. 4.1 to 4.7), a stochastic technique called the genetic algorithm (GA) is adopted for minimizing the objective function and estimating the thermophysical parameters of the Li-ion battery.

The method was first introduced by Holland in the 1970s [101]. The GA originates from natural selection mechanisms. It starts from a strong random database, namely an initial population, and moves upward to many extremum points. Inspired by the structure of living organisms, each member of the initial population is called a chromosome containing some genes. Each chromosome represents a probabilistic solution to the optimization problem in which the number of variables is equivalent to the number of genes.

In the GA, more fitted new populations replace older populations. Therefore, the algorithm requires a fitness function, which refers to the cost of a chromosome. After generating randomly the initial population, new populations are produced by three genetic operators called pairing, mating and mutation:

(1) The pairing operator chooses the suitable parent chromosomes from the current population for pairing. The objective function determines the cost of each chromosome and its chance for selection.

(2) The mating operator produces one or more offspring from the selected pairs. After selecting the pairs, they are mated by a random function and two children are produced.

(3) The mutation operator applies a random change in a small proportion of genes in all chromosomes. Mutation results in introducing new characteristics to the chromosomes that

did not exist in the previous ones. This operator avoids quick convergence to a local minimum especially for objective functions which have many local minima.

4.6. Sensitivity analysis

The solution to all inverse problems involves a sensitivity analysis. For inverse heat transfer problems, the sensitivity or the Jacobian matrix (**J**) is calculated by taking the first order partial derivatives of the calculated temperature with respect to the expected (or the sought) parameters ($\mathbf{P}_j$) at time t_i (Eq. 4.34) [13, 14, 16, 104].

$$\mathbf{J}\left(\mathbf{P}_j\right)=\left[\frac{\partial \mathbf{T}^T}{\partial \mathbf{P}_j}\right]^T \tag{4.36}$$

J_{ij} is called the sensitivity coefficient, which indicates how $T(t_i)$ changes with respect to P_j. In the present study, the sensitivity analysis is carried out for the five parameters: ρC_p, k, h, $SOC_{n,0}$, $SOC_{p,F}$. Due to the difference in magnitude of these parameters, it is convenient to use the relative sensitivity coefficient defined as:

$$J_{ij} = P_j \frac{\partial T_i}{\partial P_j} \tag{4.37}$$

The sensitivity coefficients are computed with a finite-difference approximation

$$J_{ij} \cong P_j \frac{T_i\left(P_1,P_2,...,P_j+\varepsilon P_j,...\right)-T_i\left(P_1,P_2,...,P_j-\varepsilon P_j,...\right)}{2\varepsilon P_j} \tag{4.38}$$

ε is an arbitrarily small number of the order of $\sim 10^{-5}$ [14]. Figures 4.7a, b, c, d and e illustrate the sensitivity coefficients for the five expected parameters at different discharge rates. The sensitivity curves indicate that the higher the discharge rate, the larger the magnitude of the sensitivity coefficients for these parameters. Therefore, it is recommended to conduct the parameter estimation at higher discharge rates. Moreover, the curves represent that the order of magnitude of the sensitivity coefficients of the thermophycal parameters (ρC_p, k, h) is 10 and 100 higher than that of $SOC_{n,0}$, and $SOC_{p,Final,}$ respectively.

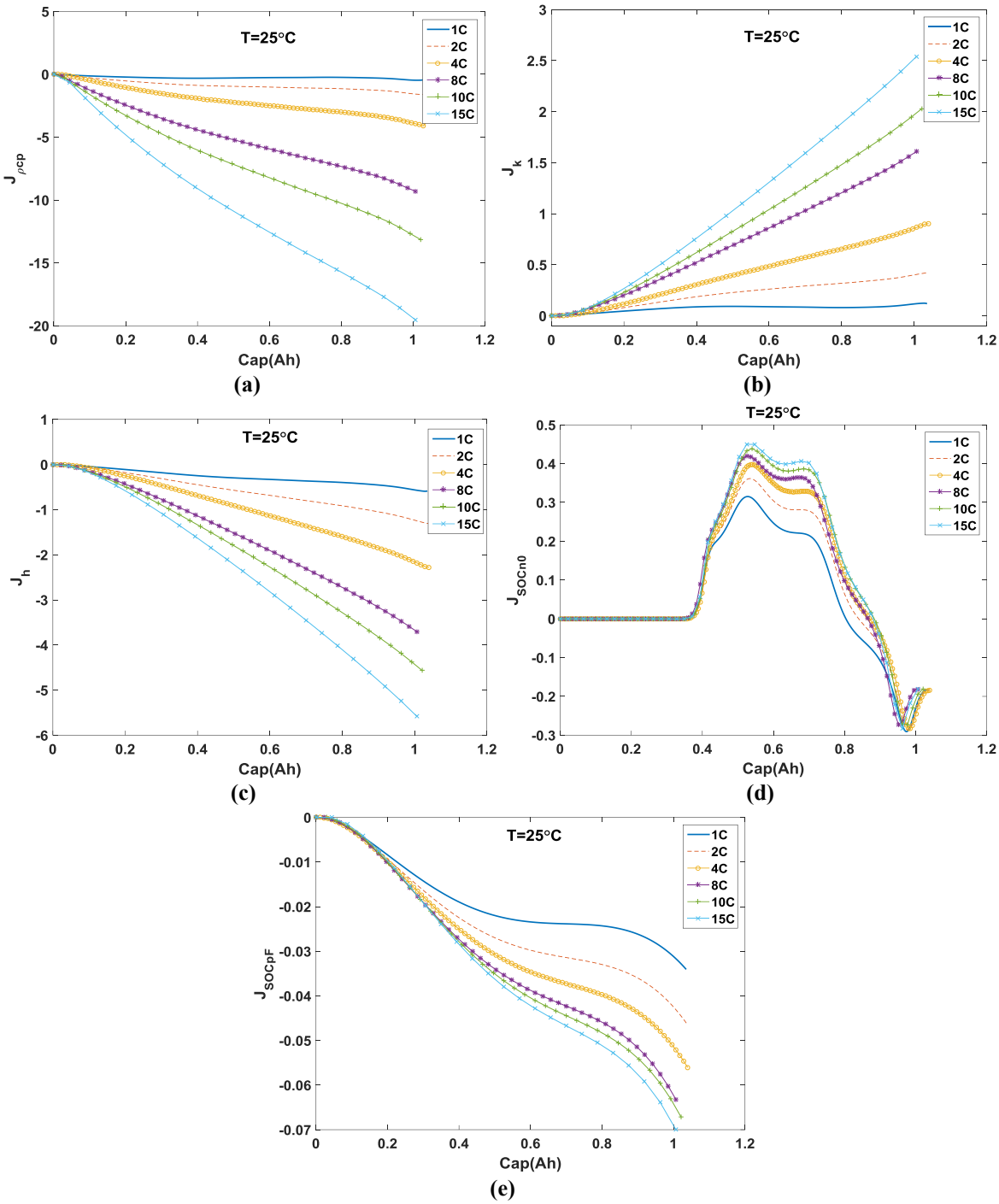

Figure 4.7: Relative sensitivity coefficients. (a) Heat capacity ($J_{\rho Cp}$); (b) Thermal conductivity(J_k); (c) Convection heat transfer coefficient (J_h); (d) Initial SOC of the negative electrode; (e) Final SOC of the positive electrode

4.7. Results

The parameters of the Li-ion battery are provided in Table 4.2. The range of the five parameters, i.e., ρC_p, k, h, $SOC_{n,0}$, and $SOC_{p,Final}$, as reported in the open literature, are summarized in Table 4.3 [66, 117, 122, 123]. The experimental data are provided for five discharge curves (2C, 4C, 8C, 10C and 15C). Eq. 4.34 is employed to minimize the objective function of the inverse problem.

Table 4.2: Parameters for the direct model

Parameter	Unit	Value
Radius of the cylinder	m	0.0129
Height of the cylinder	m	0.0542
Sandwich layer thickness	m	4.6e-4
T_{sur}	°C	25
I_{1C}	A	1.05
I_{2C}	A	2.1
I_{4C}	A	3.94
I_{8C}	A	7.88
I_{10C}	A	10.50
I_{15C}	A	15.75

Table 4.3: Range of the expected parameters for the inverse model

Symbol	Unit	Min	Max
ρC_p	J/m^3K	1.5e+6	5e+6
k	W/mK	0.05	5
h	W/m^2K	1	20
$SOC_{n,0}$	-	0.7	0.9
$SOC_{p,Final}$	-	0.6	0.8

The GA optimization procedure was initiated with a population of 400 chromosomes and a mutation rate of 5%. The resulting estimated parameters are provided in Table 4.4 which demonstrate good agreement with the values used in previous studies [110, 111, 125]. The estimated and measured surface temperatures are also compared in Figure 4.8. The agreement between the predictions and experimental data is very reasonable, considering the fact that the measurement error is 0.5ºC.

Table 4.4: Estimated parameters

Symbol	Unit	Value
ρC_p	J/m^3K	3.25e+6
k	W/mK	0.1052
h	W/m^2K	15.65
$SOC_{n,0}$	-	0.81
$SOC_{p,Final}$	-	0.61

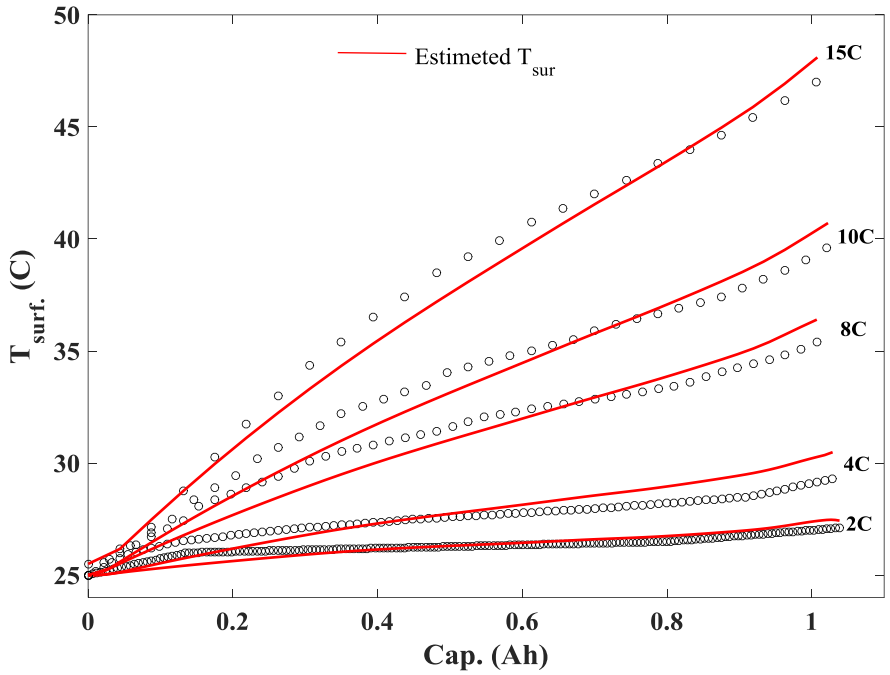

Figure 4.8: Estimated and measured surface temperature

Figure 4.9a illustrates the time-varying the maximum (near to centerline) and surface temperature profiles of the cylindrical Li-ion battery for a discharge rate of 10C. As expected, the temperature near to the center of the battery is higher than that at the surface. At the end of discharge, the temperature difference is 6ºC which is compatible with results of other experimental research [109, 126]. The heat generation functions are also calculated using the predicted temperature distribution and Eqs. 4.19 and 4.20. Figure 4.9b depicts the total, reversible, and irreversible heat generation terms of the cylindrical Li-ion battery at 10C discharge rate. As discussed previously, the reversible heat generation term may be either negative or positive. Due to the existence of a plateau in the LFP open- circuit potential, the mean total heat generation during most of the discharge period remains equal to 6.0 (W). It reaches 8.0 (W) at the end of discharge, and with a significant increase of the reversible heat generation. This thermal behavior must be taken into account when designing a thermal management system for the battery.

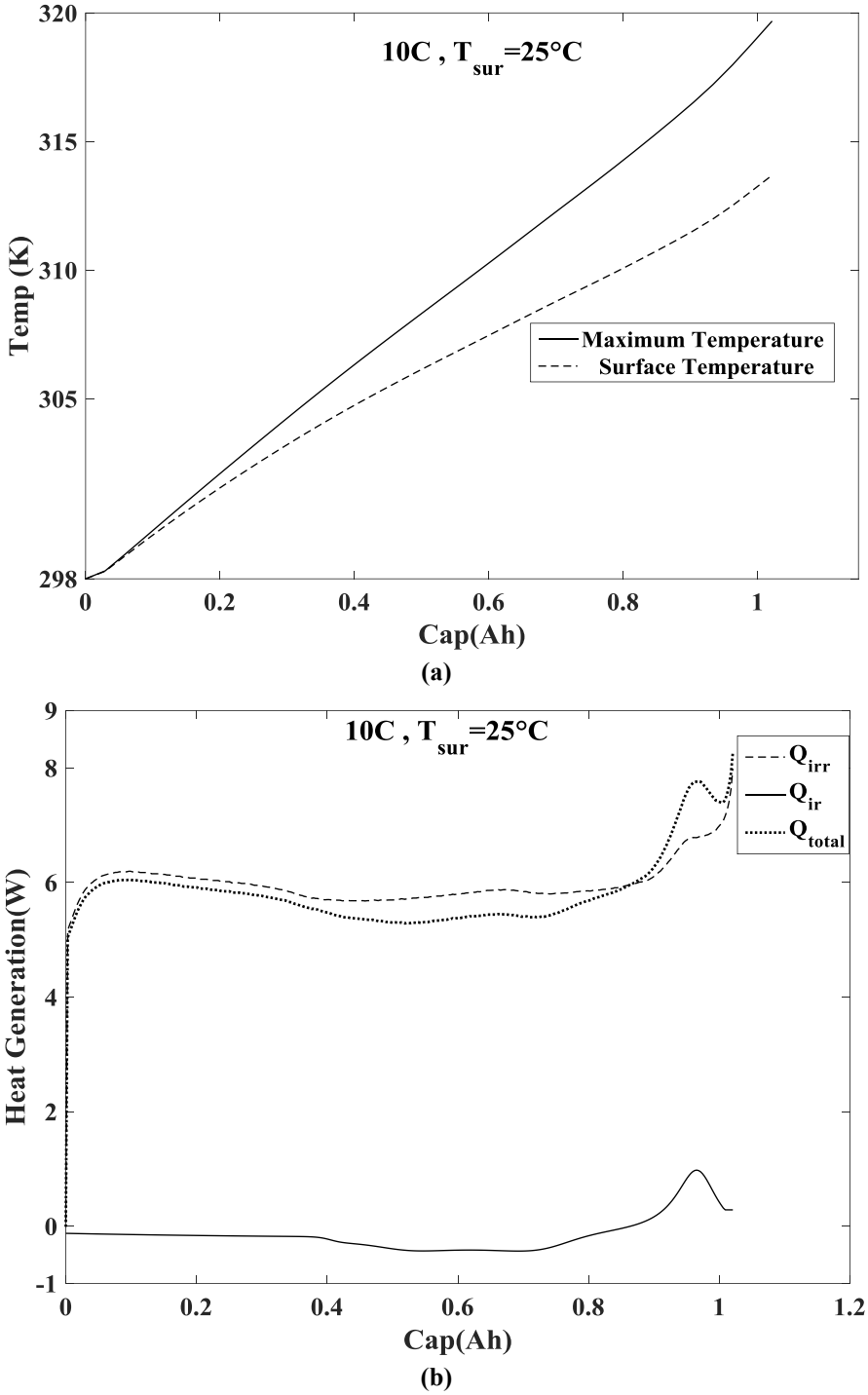

Figure 4.9: (a) Center and surface temperature at 15C discharge rate; (b) Predicted total, reversible, and irreversible heat generation terms.

The effect of the convection heat transfer coefficient on the centerline temperature of the battery (the maximum temperature), is depicted in Figure 4.10a. This figure reveals that the maximum temperature diminishes from 50°C to 35°C for a ten-fold increase in the heat transfer coefficient.

The surrounding temperature (T_{sur}) is another parameter that must be considered for when designing the battery thermal management system. As T_{sur} increases, the battery

performance is negatively affected. The effect of T_{sur} on the battery centerline temperature for a discharge rate of 8 C is illustrated in Figure 4.10b. Obviously, increasing the heat transfer coefficient (h) is beneficial to reducing the maximum temperature. But this action seems pointless when the ambient temperatures exceeds 50°C. In this case, another battery cooling technique must be devised.

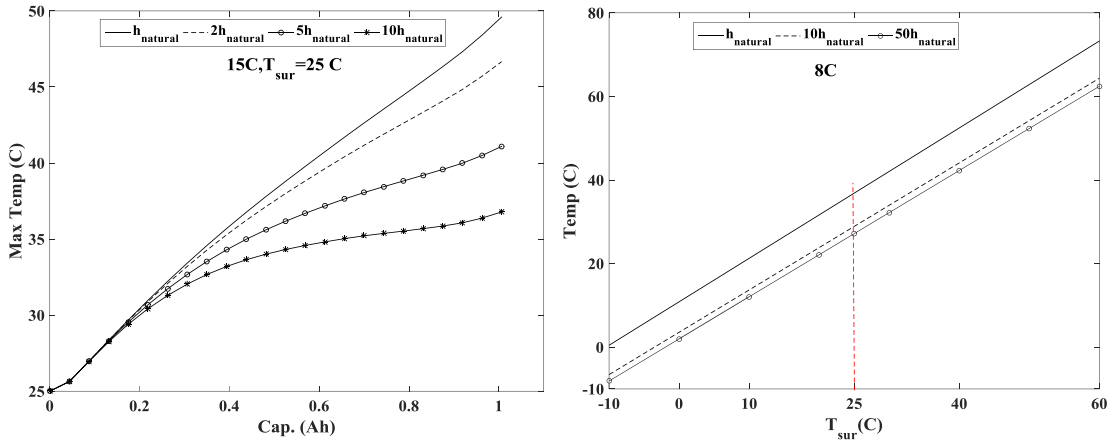

(a) (b)

Figure 4.10: Effect of (a) h, (b) T_{sur} and h on the battery maximum temperature

4.7. Conclusion

An inverse parameter estimation of the thermophysical properties of a cylindrical lithium-ion (Li-ion) battery was conducted. The identification of these parameters is necessary for predicting the thermal behavior of the battery. A direct heat transfer model of the cylindrical Li-ion battery was developed to estimate the thermophysical parameters. The direct model was then applied to simulate experimental data including surface temperature profiles for different discharge rates. The experimental data were collected from a commercial cylindrical Li-ion battery containing a LFP cathode material. The model contains both reversible and irreversible heat generation terms. It also employs the experimental cell potential function as an input to account for the temperature dependence of the electrochemical parameters such as the diffusion coefficients and reaction rate constant of the electrodes. An approximate relation, independent of the electrochemical parameters, was proposed for the cell potential change with the ambient temperature. An inverse heat transfer method based on a Genetic Algorithm (GA) was employed for estimating the five unknown parameters. The results show that the proposed parameter estimation method is reliable, robust and accurate for all discharge rates. Recommendations were also made concerning the effect of the convection heat transfer coefficient on the Battery Management Systems (BMSs) performance.

Acknowledgements

The authors are very grateful to Hydro-Quebec and to the Natural Sciences and Engineering Council of Canada (NSERC) (grant number RDCPJ 429143-11) for their financial supports.

CHAPITRE 5 : AVANT-PROPOS

Auteurs et affiliation:

- Ali Jokar: étudiant au doctorat, Université de Sherbrooke, Faculté de génie, Département de génie chimique et de génie biotechnologique.
- Barzin Rajabloo: étudiant au doctorat, Université de Sherbrooke, Faculté de génie, Département de génie chimique et de génie biotechnologique.
- Martin Désilets: professeur, Université de Sherbrooke, Faculté de génie, Département de génie chimique et de génie biotechnologique.
- Marcel Lacroix: professeur, Université de Sherbrooke, Faculté de génie, Département de génie mécanique.
- Karim Zaghib: Institut de recherche d'Hydro-Québec (IREQ), Varennes, Qc, Canada, J3X 1S1.

Revue: Electrochimica Acta

Titre français: Un modèle mosaïque modifié (MM) pour les piles aux ions lithium commerciales basées sur le $LiFePO_4$/Graphite

Contribution au document: Un nouveau modèle mathématique, permettant d'estimer les propriétés électrochimiques et thermophysiques de piles aux ions lithium comprenant des électrodes positives de LFP, est présenté et utilisé pour l'analyse de leur performance. Ce modèle a permis de combiner un modèle électro-thermique simplifié de pile aux ions lithium avec les équations mathématiques du modèle mosaïque modifié (MM).

Résumé français :

Un nouveau modèle mathématique est présenté pour l'analyse des piles aux ions lithium (Li-ion) commerciales basées sur le $LiFePO_4$/Graphite. Le modèle est développé en couplant un modèle électro-thermique simplifié de pile Li-ion avec les équations mathématiques représentant le modèle mosaïque modifié (MM). Le modèle électro-thermique repose sur un modèle à particule unique (SPM) modifié et sur une équation de conservation d'énergie. Dans le modèle MM, le processus d'intercalation et de désintercalation du Li^+ dans les particules de LFP est supposé se produire à différents sites identiques de forme sphérique. Le rayon effectif ou de façon équivalente le coefficient de diffusion solide du Li^+ dans les particules de LFP est considéré comme variable en fonction du taux de charge/décharge. Le modèle ne prétend pas représenter les mécanismes réels d'insertion et d'extraction des ions Li^+ au sein des particules de LFP. Toutefois, il simule avec succès le comportement

macroscopique de la pile. Quatre différents scénarios sont étudiés, dépendant de l'électrode dominante et du mode de fonctionnement de la pile, en charge ou en décharge. Le modèle MM est utilisés pour analyser le comportement de trois piles Li-ion commerciales avec des capacités différentes et opérées sous diverses conditions. Les résultats montrent que leur comportement peut être simulé avec précision tant à bas qu'à haut niveau de décharge.

5. A Modified Mosaic (MM) Model for Commercial Li-ion Batteries Based on $LiFePO_4$/Graphite

5.1. Abstract

A novel mathematical model is presented for analyzing commercial lithium-ion (Li-ion) batteries based on $LiFePO_4$(LFP)/graphite. The model is developed by coupling a simplified electro-thermal Li-ion battery model with the Modified Mosaic (MM) mathematical equations. The electro-thermal model rests on a modified Single Particle Model (SPM) and the energy balance equation. In the MM model, it is assumed that the Li^+ intercalation/deintercalation processes into LFP particles occur at different sites with identical spherical shapes. The effective radius or the Li^+ ion diffusion coefficient of the LFP particle is considered to be dependent on the battery discharge/charge rates. The model does not support the actual insertion/extraction mechanism of Li^+ ions at the LFP particles on the micro-scale (particle-by-particle process), however, it is successful in simulating the battery behavior at a macro-scale. Four different scenarios are investigated depending on which electrode is dominant during the charge and/or discharge processes. The MM model is employed to investigate the behavior of three commercial Li-ion batteries operated under different conditions and battery capacity. The results show that their behavior is accurately simulated for both low and high discharge rates.

Keywords: Li-ion battery; Li-ion battery model; LiFePO4 (LFP) electrode; Modified Mosaic model.

Nomenclature:

A_{cell}	Total cell surface area exposed to surroundings, m^2
$c_{s,k}$	Solid-state concentration of Li^+ of electrode *k (k=p,n)*, mol/m^3
$c_{e,k}$	Electrolyte concentration of Li^+ in region *k (k=p,s,n)*, mol/m^3
$c_{s,k}^{ini}$	Initial concentration of Li^+ in the particles of electrode *k (k=p,n)*, mol/m^3
$c_{s,k}^{\max}$	Maximum concentration of Li^+ in the particles of electrode *k (k=p,n)*, mol/m^3
$c_{s,k}^{surf}$	Concentration of Li^+ on the surface of the particles of the electrode *k (k=p,n)*, mol/m^3
C_k	Capacity of the electrode *k (k=p,n)*, Ah
$C_k^{\max}$	Maximum capacity of the electrode *k (k=p,n)*, Ah
$D_{s,k}$	Li^+ diffusion coefficient in the particles of electrode *k (k=p,n)*, m^2/s
$D_{s,k}^{ref}$	$D_{s,k}$ at reference temperature *(k=p,n)*, m^2/s
$Ea_{D,k}$	Solid phase diffusion activation energy *(k=p,n)*, kJ/mol

$Ea_{K,k}$	Reaction rate constant activation energy *(k=p,n)*, kJ/mol
F	Faraday's constant, C/mol
h	Convection coefficient between the battery and its surroundings, W/m^{2}K
I	Applied current, A
J_k	Wall flux of Li^+ in the particles of *k (k=p,n)*, mol/m^{2}s
K_k	Reaction rate constant of electrode *k (k=p,n)*, m$^{2.5}$/mol$^{0.5}$s
K_k^{ref}	K_k at reference temperature *(k=p,n)*, m$^{2.5}$/mol$^{0.5}$s
n	Negative electrode
N	The charge or discharge rate
$\dot{q}$	Volumetric heat generation, W/m^3
p	Positive electrode
r	Radial coordinate, m
R	Universal gas constant, J/mol K
R_c	Cell radius, m
R_{cell}	Solution phase resistance, Ω
$R_{s,k}$	Radius of the particles of electrode *k (k=p,n)*, m
s	Separator
S_k	Total electroactive area of electrode k *(k=p,n)*, m^2
SOC_k	State Of Charge of electrode *k (k=p,n)*
$SOC_{k,0}$	Initial State Of Charge of electrode *k (k=p,n)*
$SOC_{k,0}^{Dis.}$	Initial discharge State Of Charge of the electrode *k (k=p,n)*
t	Time, s
t^*	End time of the charge/discharge process, s
t_{1C}^*	End time of the battery discharge process at 1C, s
T	Absolute temperature, K
T_{ref}	Reference temperature, K
T_{sur}	Surrounding temperature, K
U_k	Open-circuit potential of electrode *k (k=p,n)*, V
U_k^{ref}	U_k at reference temperature *(k=p,n)*, V
V_{cell}	Voltage of the cell, V
$V_{s,k}$	Total volume of the electrode k *(k=p,n)*, m^3
V_t	Total volume of the battery, m^3
x	Spatial coordinate, m

Greek

ε_k	Porosity of the electrode *k (k=p,n)*
λ_j	jth eigenvalue
$\mu_{s,k}$	Overpotential of electrode *k (k=p,n)*, V
ρc	Battery heat capacity, J/m^{3}K
$\Phi_{s,k}$	Solid-phase potential of electrode *k (k=p,n)*, V
$\Phi_{e,k}$	Electrolyte potential in region *k (k=p,s,n)*, V

5.2. Introduction

Lithium-ion (Li-ion) batteries play a key role in the development of green technologies. This type of battery exhibits high power and high energy density. This is why Li-ion batteries are employed in many applications for storing electricity and delivering electric power on demand.

Li-ion batteries are available in different shapes including cylindrical, prismatic, coin and pouch types. The internal structure of the battery usually comprises four main components: two electrodes (positive and negative), electrolyte and separator. Over the years, the design, structure, materials and operating conditions of these batteries have been modified so as to improve their efficiency, safety and performance, as well as to drive down their cost [7, 127].

One of the most important advances in Li-ion battery technology has been the introduction of $LiFePO_4$ (LFP) as the cathode material [22]. The electronic and ionic conductivities of LFP powder were improved by decreasing the grain size to nanoscale and by using a conductive carbon-coating to encapsulate the LFP particles [19, 128]. Stable and safe olivine LFP has become an attractive cathode material in batteries for electric vehicles [22, 129]. The discharge/charge curves of LFP exhibit a voltage plateau at 3.5 (V) which is independent of the electrode State-Of-Charge (SOC). This behavior occurs because of the two-phase condition inside the LFP particles [22, 130, 131].

Most electrochemical models available in the open literature, for example the Pseudo-Two-Dimensional (P2D) model and the Single Particle Model (SPM), cannot adequately simulate the behavior of batteries with LFP cathodes [19]. The main reason is that these models rely on Fick's law which does not take into account the intercalation/deintercalation of Li^+ ions in the LFP particles. To overcome this difficulty, alternative approaches have been proposed.

In 1997, Padhi et al. suggested the shrinking-core idea to describe the insertion and the extraction processes of Li^+ ions at the surface of LFP particles (Figure 5.1a). They considered a shrinking interface inside the LFP particles where the two-phase mechanism occurs. The interface around the $FePO_4$ core shrinks during Li^+ ion insertion, and grows back during Li^+ ion extraction [22].

Anderson and Thomas presented a radial model based on the shrinking-core concept. They considered an inactive region in the center of spherical LFP particles (Figure 5.1b). They assumed that this inactive region is responsible for first-cycle capacity loss in the LFP electrode [124].

Srinivasan and Newman employed the shrinking-core concept and implemented these two-phase phenomena in LFP spherical particles into the porous electrode theory. They

determined the two-phase interface position by incorporating a mass balance between Li-rich (shell) and Li-poor (core) regions [131].

The shrinking-core porous electrode model has been developed to identify LFP electrode behavior in macro-scale and by assuming the isotropic diffusion of the LFP particles [19, 132]. Different experiments showed, however, an anisotropic ionic mobility of the Li^+ ion inside the LFP crystal. Therefore, the shrinking-core two-phase concept cannot describe the intercalation/deintercalation of Li^+ ions at the surface of LFP particles at the micro scale [133, 134]. Chen et al. showed that the Li^+ ions migrate along 1D channels inside the LFP particles (the *b* direction at the phase boundary) [133]. Based on this fact, Laffont et al. presented a "new core-shell" conceptual model (Figure 5.1c) [135]. By means of the X-ray diffraction and electron microscopy, Delmas et al. reported a simultaneous existence of fully intercalated and fully deintercalted LFP particles in the electrode. They proposed a "domino-cascade" mechanism representing the phase boundary displacement during charge/discharge process (Figure 5.1d) [136].

To simulate the hysteresis and the phase transition behaviour in LFP electrode, Dreyer et al. developed a thermodynamic-based model, namely "many-particle" model (Figure 5.1e). A non-monotonic chemical potential function profile is considered for each LFP single particle. The approach is, then, applied to all particles by allowing the Li^+ ion exchange between particles. The results show that the lithiation/delithiation process of LFP occurs in a sequential particle-by-particle at low rates. However, two critical drawbacks remain with this model: the slow and quasi-static charge/discharge process, and lack of the transport and kinetic phenomena effects [137, 138]. Inspired by the many-particle model, Farkhondeh et al. developed a mesoscopic model in which the LFP electrode is discretized into meso-scale units. An ohmic overpotential is defined for each unit, while the unit volume fraction is calculated by virtue of a Gaussian distribution. Despite the many-particle approach, this model can be used for higher rates [137, 139]. Recently, they have also applied this method to the porous-electrode theory to simulate a Li/LFP cell. The results are promising and represent that the Li^+ ion intercalation/deitercalation processes at higher rates switch to a mixed sequential-parallel regime at lower rates [140]. Meanwhile, Bazant groups developed the phase-field models in order to predict the displacement of the phase boundaries inside the LFP nanoparticles. These models rest on the non-equilibrium thermodynamics based on the Cahn-Hilliard phase-field models. While the approach is expensive and time-consuming to simulate the whole LFP electrode, it is powerful to explain different LFP crystal behaviors during the Li^+ intercalation/deintercalation process [141-144].

The main drawback of the aforementioned models is that they are slow and expensive for simulating the performance of the LFP electrode in the commercial Li-ion batteries. All equations should be separately solved for each particle or unit. Therefore, they can be useful for off-line applications but cannot be applied to the Battery Management System (BMS) to be used for the on-line monitoring, the parameter estimation, etc.

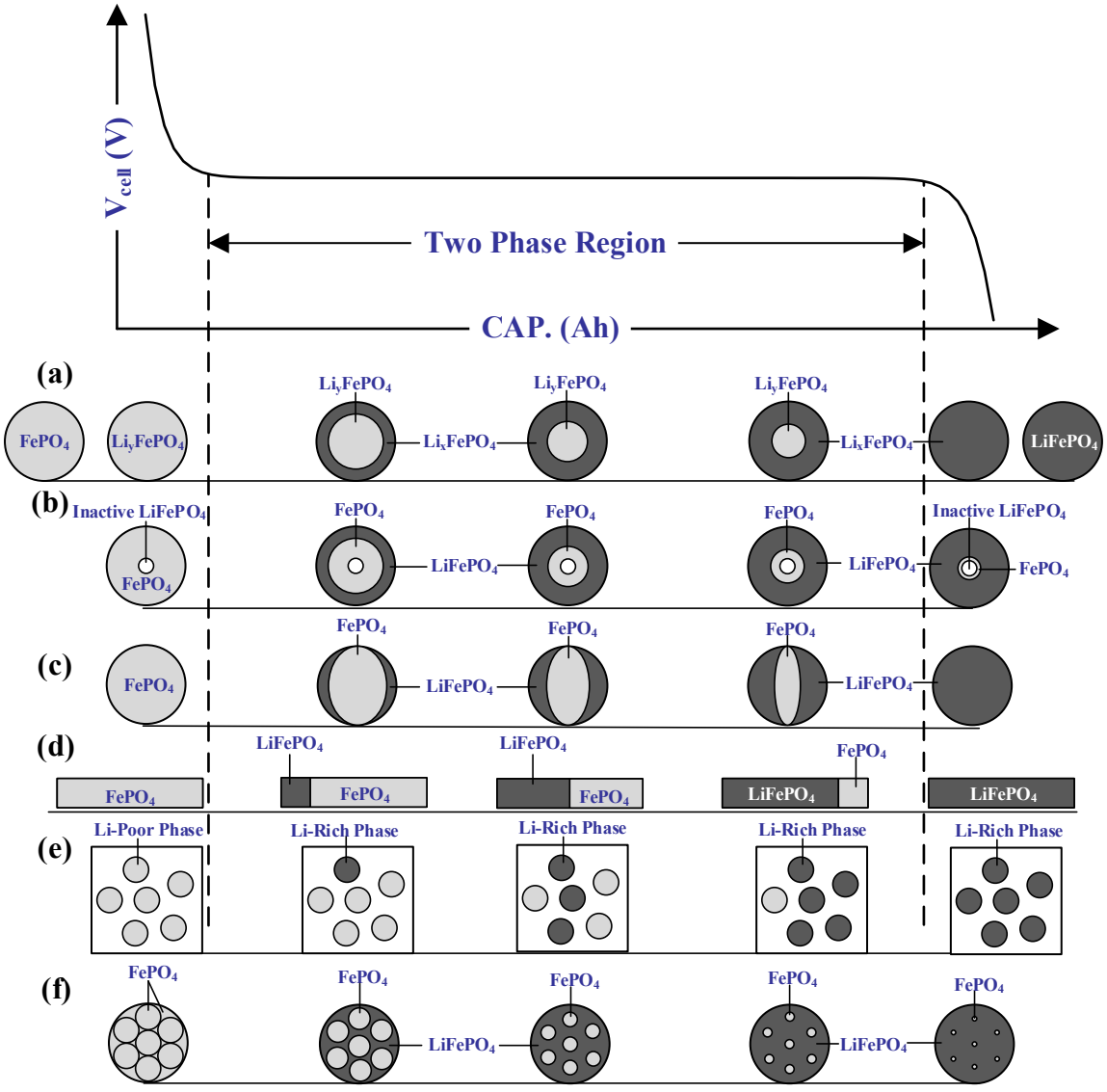

Figure 5.1: Schematic representation of different LFP models (a) shrinking-core, (b) radial, (c) new core-shell, (d) domino-cascade, (e) many-particle, and (f) mosaic.

Anderson and Thomas proposed a mosaic model for describing the intercalation/deintercalation mechanisms of Li^+ ions at the surface of LFP spheres (Figure 5.1f). This model assumes that the shrinking-core process occurs at different nucleation sites inside a LFP particle. It also assumes that the sites have identical spherical shapes with smaller radius compared to the LFP particle. According to the mosaic model, the effective

radius of LFP particles is different from the real particle radius, and it is dependent on the battery discharge/charge rates. In other words, the diffusion coefficient for the Li^+ ions in the LFP particle varies according to the current density. Anderson and Thomas did not, however, present a mathematical model for the calculation of the mosaic particles [124].

Delacourt and Safari applied this approach to model the early stages of discharge curves of a Li/LFP cell. The Li^+ ion diffusion coefficient was maintained constant while the LFP particle radii were adjusted to achieve the best fitting between experimental and calculated data for different discharge rates. The authors did not reveal the mathematical relation between the effective radius of the LFP particles and the current density. They show, however, that the higher the current density, the lower the effective radius of the LFP particles. This means that the number of nucleation sites inside the LFP particles increases with the discharge rate [145]. Prada et al. presented a simplified electro-thermal model by using a simplified P2D model and the mosaic concept to simulate a commercial Li-ion battery based on LFP/Graphite. They adjusted the effective radius not only for the LFP particles, but also for graphite particles at different discharge/charge rates. The diffusion coefficients were kept constant. Once again, the inverse relation between the current density and the effective radius for both electrodes was illustrated. Prada et al. believed that since the insertion/extraction Li^+ ions are faster in smaller particles, it is possible to model the overpotential for different discharge/charge rates. Their model was validated with experimental data. No mathematical equations were suggested, however, for the mosaic model [123]. Recently, Maheshwari et al. applied the mosaic method to simulate, with two approaches, a Li-ion battery based on LFP/Graphite. First, the effective radius of the LFP particles was considered. The effective radius of the graphite particles remained however constant. This is due to the fact that the positive electrode is typically the dominant electrode in the Li-ion battery while the negative electrode is typically overdesigned. Second, the positive diffusion coefficient was adjusted with the current density while the LFP radius was maintained constant. The simulation results showed good agreement with experimental data for both approaches. Moreover, a quadratic correlation was observed between the LFP effective radius and the diffusion coefficient at each current density. All of the adjusted parameters were estimated so as to achieve the best fitting for the battery discharge curves. Once again, the authors did not provide any mathematical models for the mosaic approach [146].

In a nutshell, while the actual insertion/extraction mechanism of Li^+ ions at the LFP particles (the particle-by-particle process) is not supported by the mosaic model, the best results have

been achieved by virtue of the mosaic model implemented by Prada et al. for the Li-ion commercial cell [123]. Mathematical equations of the mosaic model for the simulation of commercial Li-ion cells based on LFP/Graphite still need to be developed. This is precisely the purpose of the present paper, which proposes a porous electrode model coupled with the mathematical equations of the Modified Mosaic (MM) concept. A combination of the SPM and the battery energy balance equations is employed to develop the electro-thermal model. The SPM accuracy at high current densities is increased by adding an electrolyte resistance term in the overpotential function. In order to develop the MM model, the electro-thermal governing equations are then modified based on the LFP battery behavior according to the mosaic concept. The results show that commercial Li-ion batteries are successfully simulated by considering the mosaic model at low and high discharge rates.

5.3. Modified Mosaic (MM) model development

The macroscopic Modified Mosaic (MM) model is developed for Li-ion batteries with LFP as the cathode material. It employs the mosaic approach and an electro-thermal model for modeling the Li-ion batteries based on LFP/Graphite.

The main reason for developing electrochemical models is to predict the electrochemical and the thermal performances of the Li-ion batteries [9, 10]. They can be classified into two groups: empirical-based models and electrochemical engineering models.

Empirical models utilize electrochemical experimental data to predict the battery performance. Equivalent circuit-based and neural network models are the most popular empirical models. They are widely used in the electronics and automotive industries. However, they cannot simulate the performance of aging batteries or batteries operated in harsh ambient conditions [9]. Electrochemical models are, on the other hand, more sophisticated and also more predictive. These models are based on chemical/electrochemical kinetics and transport equations. They are used to simulate the Li-ion battery characteristics and reactions [9, 10]. The Pseudo-two-Dimensional (P2D) model [34] and the Single Particle Model (SPM) [54] are among the most popular electrochemical-based models. The P2D model developed by Doyle et al. was extensively used in Li-ion battery investigations [34]. The P2D model includes aspects of the porous electrode theory, concentrated solution theory and resolution of kinetics equations. Its predictions are accurate and it has shown repeatedly good agreement with experimental data [9, 10, 34].

In order to reduce the computational time, a simplified version of the P2D model, called the SPM, was developed by Zhang et al. [54]. In the SPM, the electrolyte properties are ignored and the transport phenomena are treated in a simple manner [9, 10, 54].

In the present study, a combination of the SPM and the battery energy balance equations is employed to develop the electro-thermal model. The SPM accuracy at high current densities is increased by adding an electrolyte resistance term in the overpotential function, and by considering the battery temperature effects. In order to develop the MM model, the electro-thermal governing equations are then modified based on the LFP battery behavior according to the mosaic concept.

5.3.1. Electro-thermal model

The SPM rests on two main assumptions: (*i*) each electrode (Figure 5.2) is modeled as a spherical particle in which intercalation and deintercalation occur, and (*ii*) variations in the electrolyte properties are ignored [54, 64]. Due to its simple equations and the low computational time, the SPM model is useful in many practical applications such as parameter estimation, real-time control modeling and life cycle modeling of Li-ion batteries [10].

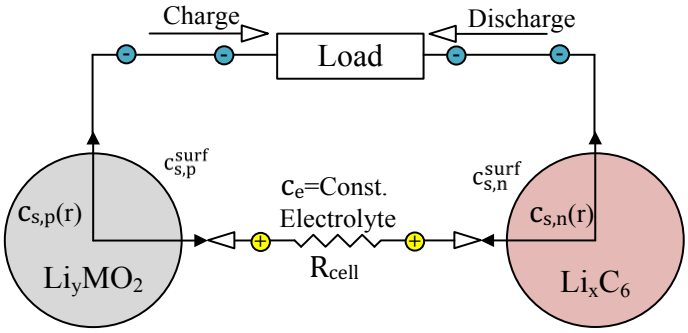

Figure 5.2: Schematic of the Single Particle Model (SPM)

The main equation of the SPM is the solid-state concentration which is calculated by Fick's second law for both the negative and the positive spherical particles [64]:

$$\frac{\partial c_{s,k}(r,t)}{\partial t} = \frac{D_{s,k}}{r^2}\frac{\partial}{\partial r}\left(r^2 \frac{\partial c_{s,k}(r,t)}{\partial r}\right) \tag{5.1}$$

Eq. 5.1 is solved by using the initial and the boundary conditions for each particle [64]:

$$c_{s,k}(r, t=0) = c_{s,k}^{ini} \tag{5.2}$$

$$D_{s,k}\frac{\partial c_{s,k}(r=0,t)}{\partial r} = 0 \tag{5.3}$$

$$D_{s,k}\frac{\partial c_{s,k}\left(r=R_{s,k},t\right)}{\partial r}=-J_k \tag{5.4}$$

J_k is the wall flux of Li^+ ions on the surface of each particle, and it is constant in the SPM. This parameter is calculated by using Eq. 5.5 for each electrode.

$$J_n=-\frac{I}{F\,S_n},J_p=\frac{I}{F\,S_p},S_k=\frac{3\varepsilon_k V_{s,k}}{R_{s,k}} \tag{5.5}$$

The battery current (I) has a negative value when the battery is being discharged. The Butler-Volmer kinetics equation makes a connection between the wall flux (J_k), the over potential function ($\mu_{s,k}$) and the Li^+ surface concentration at each particle [64]:

$$J_k=K_k\left(c_{s,k}^{\max}-c_{s,k}^{surf}(t)\right)^{0.5}\left(c_{s,k}^{surf}(t)\right)^{0.5}c_{e,k}^{0.5}\left[\exp\left(\frac{0.5F\mu_{s,k}(t)}{RT}\right)-\exp\left(-\frac{0.5F\mu_{s,k}(t)}{RT}\right)\right] \tag{5.6}$$

The overpotential function is the difference between the actual and the equilibrium potential of the battery. The overpotential function and the battery cell potential are calculated as follows [64]:

$$\mu_{s,k}(t)=\Phi_{s,k}(t)-\Phi_{e,k}(t)-U_k(t);\ V_{cell}(t)=\Phi_{s,p}(t)-\Phi_{s,n}(t) \tag{5.7}$$

In order to improve the SPM accuracy, the potential drop between the positive and negative electrodes in the electrolyte is simplified with the following equation [64]:

$$\Phi_{e,p}-\Phi_{e,n}=I\,R_{cell} \tag{5.8}$$

Note that the diffusion coefficients ($D_{s,k}$) and the reaction rate constants (K_k) are temperature-dependent parameters which are connected to the Arrhenius' equation [64].

$$D_{s,k}(T)=D_{s,k}^{ref}\exp\left[\frac{Ea_{D,k}}{R}\left(\frac{1}{T}-\frac{1}{T_{ref}}\right)\right] \tag{5.9}$$

$$K_k(T)=K_k^{ref}\exp\left[\frac{Ea_{K,k}}{R}\left(\frac{1}{T}-\frac{1}{T_{ref}}\right)\right] \tag{5.10}$$

All the experimental data for the present study were gathered at the reference temperature (ambient temperature) T_{ref} = 25°C. The open circuit potential function (U_k) is also updated with the battery operation temperature in the following manner [64]:

$$U_k(T)=U_k^{ref}+\left.\frac{\partial U_k}{\partial T}\right|_{T_{ref}}\left(T-T_{ref}\right) \tag{5.11}$$

Guo et al. presented a solution for Eqs. 5.5 to 5.8 to determine the cell potential function of the Li-ion battery [64]:

$$V_{cell}=\left(U_p-U_n\right)+\frac{2RT}{F}\ln\left(\frac{\sqrt{m_p^2+4}+m_p}{2}\right)+\frac{2RT}{F}\ln\left(\frac{\sqrt{m_n^2+4}+m_n}{2}\right)+IR_{cell} \tag{5.12}$$

$$m_p = \frac{I}{FK_p S_p c_{s,p}^{\max} c_e^{0.5} \left(1 - SOC_p\right)^{0.5} \left(SOC_p\right)^{0.5}};\ SOC_p = \frac{c_{s,p}^{surf}}{c_{s,p}^{\max}} \tag{5.13}$$

$$m_n = \frac{I}{FK_n S_n c_{s,n}^{\max} c_e^{0.5} \left(1 - SOC_n\right)^{0.5} \left(SOC_n\right)^{0.5}};\ SOC_n = \frac{c_{s,n}^{surf}}{c_{s,n}^{msx}} \tag{5.14}$$

Moreover, they derived an analytical solution for the electrode State-Of-Charge (SOC) in the constant current (I) and cell temperature (T) conditions [64]:

$$SOC_k = SOC_{k,0} - \frac{J_k R_{s,k}}{c_{s,k}^{\max} D_{s,k}} \left[3\frac{D_{s,k}}{R_{s,k}^2} t + \frac{1}{5} - \sum_{j=1}^{\infty} \frac{2}{\lambda_j^2} \exp\left(-\frac{\lambda_j^2 D_{s,k}}{R_{s,k}^2} t \right) \right]; \sin\left(\lambda_j\right) - \lambda_j \cos\left(\lambda_j\right) = 0 \tag{5.15}$$

It is noted that, to evaluate the SOC at variable temperature condition (T), Eqs. 5.1 to 5.4 should be simultaneously solved by numerical methods, such as Finite Difference Method (FDM). In order to calculate the cell potential function, it is imperative to consider the battery operating temperature in Eqs. 5.9 to 5.14. The temperature distribution inside the Li-ion battery is, however, non-uniform and depends on the geometry. For the present study, a lumped heat transfer model is employed to cover all shapes of Li-ion batteries. The thermal model equations must, of course, be adapted according to the specific geometry. The governing heat transfer equations for the battery are as follows [109]:

$$\frac{dT}{dt} = \frac{1}{(\rho c)} \left(\dot{q}_{irrev} + \dot{q}_{rev} - \dot{q}_{conv.} \right) \tag{5.16}$$

$$\dot{q}_{irrev} = \frac{-I}{V_t} \left(U_p - U_n - V_{cell} \right) \tag{5.17}$$

$$\dot{q}_{rev} = \frac{IT}{V_t} \left(\frac{\partial U_p}{\partial T} - \frac{\partial U_n}{\partial T} \right) \tag{5.18}$$

$$\dot{q}_{conv.} = hA_{cell} \left(T - T_{sur} \right) \tag{5.19}$$

$$T\left(0\right) = T_{sur} \tag{5.20}$$

V_t and A_{cell} are the total volume and external surface area of the battery, respectively. The current is negative when the battery is being discharged. Figures 5.3 and 5.4 depict the open circuit potential functions (U_k) and the ($\partial U_k/\partial T$) values for the graphite and LFP used in this paper.

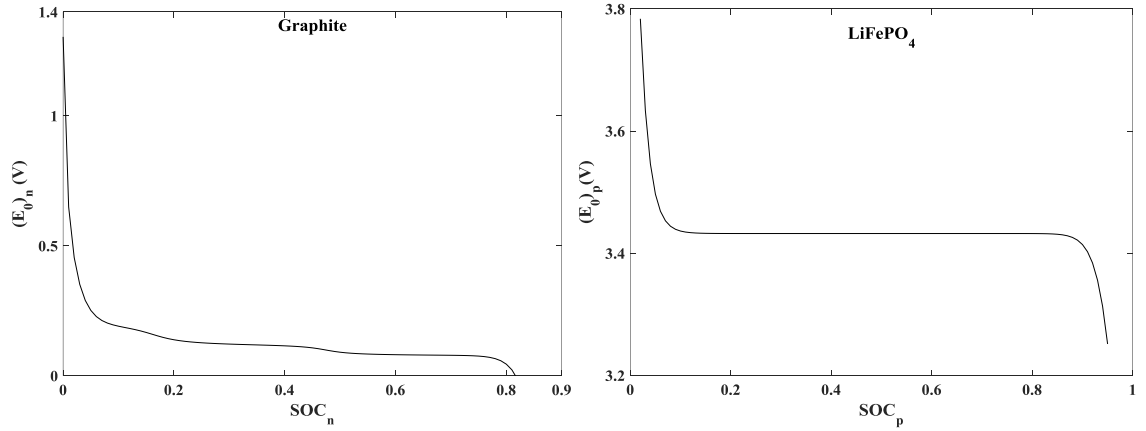

Figure 5.3: Open circuit potential function as a function of SOC for graphite (a) [64] and LFP (b) [119]

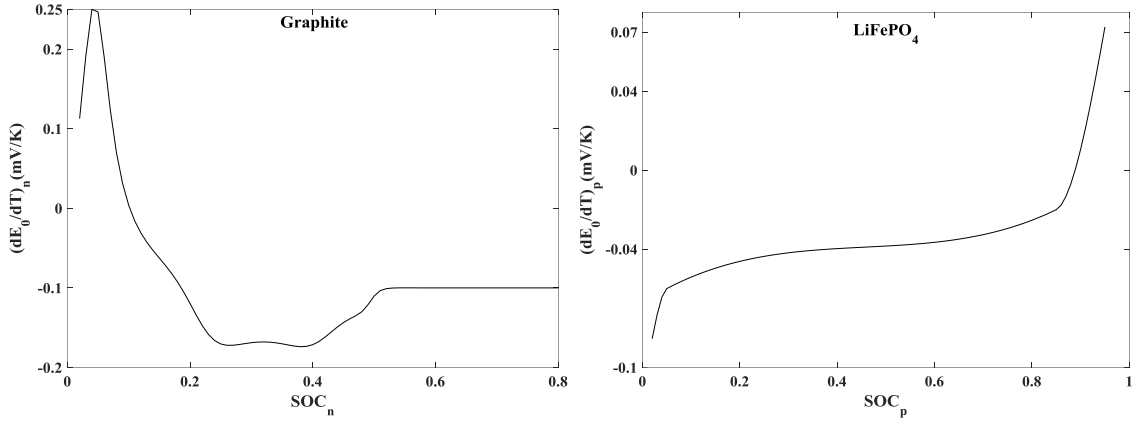

Figure 5.4: Entropic heat change as a function of SOC for graphite (a) [64] and LFP (b) [120]

5.3.2. LFP/graphite designs

In order to take into account the two-phase region in the LFP intercalation/deintercalation process, the mathematical model developed in the previous section must be refined further. It is seen in Fig. 3b that the prominent feature of the open-circuit potential curve for LFP is the plateau around 3.5 (V). This is the potential characteristic that differentiates LFP from other cathode materials such as $LiCoO_2$ and $LiMn_2O_4$.

In Li-ion batteries with LFP/Graphite, the cell potential curve is dependent on the electrode capacity. The capacity (C_k) of each electrode can be calculated from the active material volume and the difference in the SOC [123]:

$$C_k = \varepsilon_k F V_{s,k} c_{s,k}^{\max} \left| SOC_{k,Final} - SOC_{k,0} \right| / 3600 \tag{5.21}$$

The difference in the SOC defines the operating window of the battery. These conditions become more restrictive as the battery ages and/or the solid electrolyte interphase (SEI) layer grows. Note that the initial and final SOC values are determined according to the battery charge/discharge process. The discharge process is initiated from $SOC_{p,0}^{Dis}$ and $SOC_{n,0}^{Dis}$. But the end points are dependent on the electrode capacity. If the positive electrode capacity (C_p)

is lower than the negative electrode capacity (C_n), the final SOC_p value may reach 1 as the positive electrode is fully charged. If, on the other hand, C_p is higher than C_n, the final SOC_n value may become zero as the negative electrode is fully discharged. Therefore, the SOC_p varies from $SOC_{p,0}^{Dis}$ to 1, while the SOC_n varies from zero to $SOC_{n,0}^{Dis}$. The maximum value of the electrodes capacity can then be calculated as follows:

$$C_p^{\max} = \varepsilon_p F V_{s,p} c_{s,p}^{\max} \left(1 - SOC_{p,0}^{Dis.}\right) \tag{5.22}$$

$$C_n^{\max} = \varepsilon_n F V_{s,n} c_{s,n}^{\max} SOC_{n,0}^{Dis.} \tag{5.23}$$

Figure 5.5 illustrates the different possible conditions for the battery charge/discharge processes depending on the maximum values of the electrode capacity.

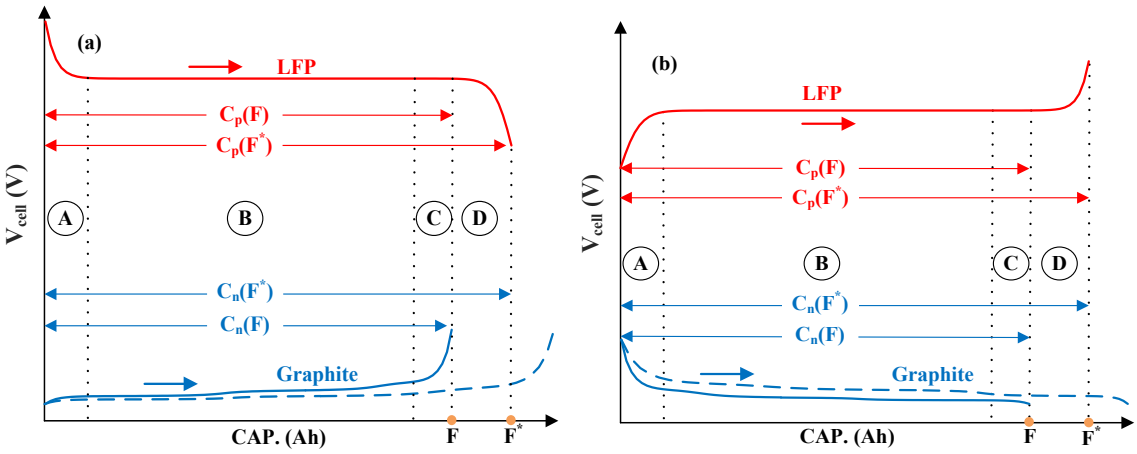

Figure 5.5: Schematic presentation of different possible conditions for Li-ion batteries with LFP/Graphite during (a) discharge (b) charge processes.

Four different regions are identified during the charge and discharge processes:

- Region A (early stage): During discharge, the initial open-circuit potential of graphite is negligible compared to that of LFP (3.8 V). Therefore, the effect of the positive electrode (LFP) is dominant over that of the negative electrode (graphite). On the other hand, during charge, the effect of both electrodes is important for determining the cell potential curve.
- Part B (LFP plateau): The open-circuit potential of the LFP is approximately constant due to the two-phase processes. This means that the shape of the cell potential curve is dictated by the graphite open-circuit potential and the battery polarization functions.
- Part C (later stage): If the negative electrode capacity (C_n) is lower than that of the positive electrode (C_p), the charge/discharge processes will terminate at point F. In other words, the negative electrode is dominant at the end of the battery charge/discharge process. During discharge, the final value of the SOC_n at point F tends toward zero and, the lack of Li^+ ions

in the negative electrode eventually stops the process. During charge, the Li^+ ion saturation of the negative electrode eventually interrupts the charge. The open-circuit potential of the LFP remains constant and the positive electrode has the capacity for further reaction.

- Part D (final stage): If the negative electrode capacity (C_n) is higher than that of the positive electrode (C_p), the charge/discharge processes will terminate at point F^*. In this case, the positive electrode is dominant at the end of the battery charge/discharge process. The SOC_p value at point F^* tends towards 1 at the end of discharge, and towards $SOC_{p,0}^{Dis}$ at the end of charge. The lack of the positive electrode capacity interrupts the process.

The overall cell potential profile of Li-ion batteries with LFP/Graphite differs according to the dominant electrode (Fig. 5.6). When the negative electrode is dominant (Fig. 5.6a), the different discharge curves converge to one point. This happens because the SOC_n can drop to zero while the final SOC_p reaches a plateau (region C). On the other hand, when the positive electrode is dominant (Fig. 6b), the end point shifts towards the left side as the discharge process reaches the end of the LFP curve. In this region, the polarization is significant [147]. It is noted that, as the battery ages, the active material is consumed and/or the SEI layer grows on the negative electrode. Thus, it is possible for the battery to change the dominant electrode condition.

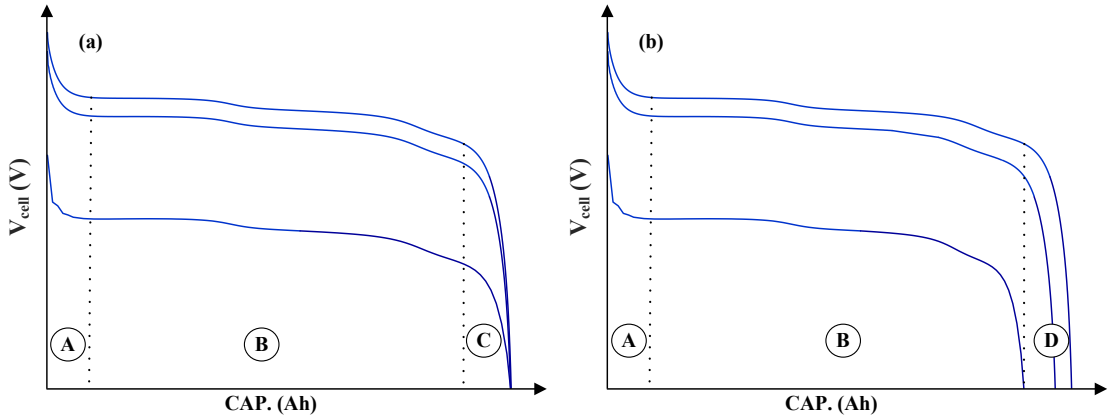

Figure 5.6: The schematic cell potential shape of Li-ion battery with LFP/Graphite at different C-rates when (a) the negative and (b) positive electrode is dominant

5.3.3. Modified Mosaic (MM) model

In this section, the electro-thermal model is modified so that it can be used to simulate the behavior of commercial Li-ion batteries with LFP/Graphite. The electro-thermal model modification is implemented for four different scenarios that depend on the charge and discharge processes, and the relative capacities of each electrode in the Li-ion batteries. It is

noted that, in all scenarios, the effective radii of both electrodes are first calculated at the cell temperature (T) condition, and then used for the variable operation temperature conditions.

Scenario 1: Process: discharge; Dominant electrode: negative (point F in Figure 5.5a).
In this scenario, the cell potential function converges to one point for different discharge rates. This point corresponds to the maximum capacity of the negative electrode. It is estimated as follows:

$$C = |I| t^* \approx |I_{1C}| t^*_{1C} \tag{5.24}$$

I_{1c} and t^*_{1C} are the current and the discharge time (approximately 3600 s), respectively when the battery discharge rate is 1C. The final SOC_n is near zero at the end of discharge. For the negative electrode, Eq. 5.15 becomes:

$$\frac{3\varepsilon_n V_{s,n} Fc^{\max}_{s,n} D_{s,n} SOC^{Dis.}_{n,0}}{I R^2_{s,n}} = \sum_{j=1}^{\infty} \frac{2}{\lambda_j^2} \exp\left(-\frac{\lambda_j^2 D_{s,n}}{R^2_{s,n}} t\right) - \frac{1}{5} - \frac{3D_{s,n}}{R^2_{s,n}} t^* \tag{5.25}$$

$SOC^{Dis}_{n,0}$ is the initial SOC_n at the beginning of discharge. According to our calculations, the first term on the right-hand side of Eq. 5.25 is negligible with respect to the other terms. Therefore, Eq. 5.25 can be rearranged to provide the effective radius of the graphite particles in the MM model:

$$\frac{R^2_{s,n}}{D_{s,n}} = -15 \frac{\varepsilon_n V_{s,n} Fc^{\max}_{s,n} SOC^{Dis.}_{n,0} + I_{1C} t^*_{1C}}{N I_{1C}} = 15 \frac{\varepsilon_n V_{s,n} Fc^{\max}_{s,n} SOC^{Dis.}_{n,0} - |I_{1C}| t^*_{1C}}{N |I_{1C}|} \tag{5.26}$$

$$R_{s,n} = \sqrt{\frac{\varepsilon_n V_{s,n} Fc^{\max}_{s,n} SOC^{Dis.}_{n,0} - |I_{1C}| t^*_{1C}}{N |I_{1C}| / 15} D_{s,n}} \tag{5.27}$$

N is the battery discharge rate and I_{1c} has a negative sign during discharge. These equations show the relation between the radius and the diffusion coefficient for the negative electrode particles. It is seen that the higher the discharge rate, the lower the effective graphite radius. This relation is compatible with the effective graphite radius adjusted by Prada et al [123].
The calculation for the effective radius for the LFP particles is tricky when the negative electrode is dominant. As illustrated in Figure 5.5a, the operating point for the LFP electrode falls on the plateau at the end of discharge. The LFP potential curve is insensitive to the SOC_p on the plateau. This makes it difficult to determine precisely the location of the end point on the LFP potential curve. To solve this problem, the relation for the electrode capacity at point F in Fig. 5a is employed:

$$C_n(@F) = C_p(@F) \tag{5.28}$$

By substituting Eq. 5.21 into Eq. 5.28, the operation window for the positive electrode can be estimated as follows:

$$\left(SOC_{p,@F} - SOC_{p,0}^{Dis.}\right) = \left(\frac{\varepsilon_n}{\varepsilon_p}\right)\left(\frac{V_{s,n}}{V_{s,p}}\right)\left(\frac{c_{s,n}^{\max}}{c_{s,p}^{\max}}\right) SOC_{n,0}^{Dis.};\ SOC_{n,@F} \approx 0 \tag{5.29}$$

Moreover, by substituting Eq. 5.29 into Eq. 5.15 and using a similar approach, the effective radius for the LFP particles in the MM model can be determined as follows:

$$\frac{R_{s,p}^2}{D_{s,p}} = -15\frac{\varepsilon_n V_{s,n} F c_{s,n}^{\max} SOC_{n,0}^{Dis.} + I_{1C} t_{1C}^*}{N\, I_{1C}} = 15\frac{\varepsilon_n V_{s,n} F c_{s,n}^{\max} SOC_{n,0}^{Dis.} - |I_{1C}| t_{1C}^*}{N|I_{1C}|} = \frac{R_{s,n}^2}{D_{s,n}} \tag{5.30}$$

$$R_{s,p} = R_{s,n}\sqrt{\frac{D_{s,p}}{D_{s,n}}} \tag{5.31}$$

Eq. 5.31 shows how the negative electrode dictates the effective radius of the positive electrode.

Scenario 2: Process: charge; Dominant electrode: negative (point F in Figure 5.5b).

A schematic of this scenario is depicted in Figure 5.5b with the end point F. It is assumed that the SOC_n increases from zero to $SOC_{n,0}^{Dis}$ during charge. Using an approach similar to that of scenario 1, the effective negative and positive radius equation is calculated with Eqs. 5.27 and 5.31, respectively. In order to avoid overcharging, the charge process may be interrupted before the SOC_n reaches $SOC_{n,0}^{Dis}$.

Scenario 3: Process: discharge; Dominant electrode: positive (point F^* in Figure 5.5a):

Since the capacity of the positive electrode is lower than that of the graphite electrode, the final SOC_p tends toward 1 at point F^*. Eq. 5.24 is not valid for this scenario since the LFP discharge curves are shifted to the left side (see Figure 5.6b) when the discharge current is increased. Therefore, the cut-off time (t^*) in each discharge rate should be employed instead of t_{1C}^*. The effective radius of the LFP particles in the MM model is then calculated as follows:

$$\frac{R_{p,n}^2}{D_{s,p}} = 15\frac{-\varepsilon_p V_{s,p} F c_{s,p}^{\max}\left(1 - SOC_{p,0}^{Dis.}\right) - It^*}{N\, I_{1C}} = 15\frac{\varepsilon_p V_{s,p} F c_{s,p}^{\max}\left(1 - SOC_{p,0}^{Dis.}\right) - |I| t^*}{N|I_{1C}|} \tag{5.32}$$

$$R_{s,p} = \sqrt{\frac{\varepsilon_p V_{s,p} F c_{s,p}^{\max}\left(1 - SOC_{p,0}^{Dis.}\right) - |I| t^*}{N|I_{1C}|/15} D_{s,p}} \tag{5.33}$$

These equations show the relation between the radius and the diffusion coefficient of the positive electrode particles. The higher the discharge rate, the smaller the effective positive

radius. This relation is compatible with the effective radius for positive particles as adjusted according to the analyses of Delacourt and Safari [145], Prada et al. [123], and Maheshwari et al. [146]. The electrode capacities have the same value at point F* in Figure 5.6a, that is,

$$C_p\left(@F^*\right)=C_n\left(@F^*\right) \tag{5.34}$$

By substituting Eq. 5.21 into Eq. 5.34, the operation window for the negative electrode can be estimated as follows:

$$\left(SOC_{n,0}^{Dis.}-SOC_{n,@F*}\right)=\left(\frac{\varepsilon_p}{\varepsilon_n}\right)\left(\frac{V_{s,p}}{V_{s,n}}\right)\left(\frac{c_{s,p}^{\max}}{c_{s,n}^{\max}}\right)\left(1-SOC_{p,0}^{Dis.}\right);\ SOC_{p,@F*}\approx 1 \tag{5.35}$$

By substituting Eq. 5.35 into Eq. 5.15, the effective radius for the graphite particles in the MM model can be determined from Eq. 5.37.

$$\frac{R_{s,n}^2}{D_{s,n}}=-15\frac{\varepsilon_p V_{s,p}Fc_{s,p}^{\max}\left(1-SOC_{p,0}^{Dis.}\right)+It^*}{N\,I_{1C}}=15\frac{\varepsilon_p V_{s,p}Fc_{s,p}^{\max}\left(1-SOC_{p,0}^{Dis.}\right)-|I|t^*}{N\left|I_{1C}\right|}=\frac{R_{s,p}^2}{D_{s,p}} \tag{5.36}$$

$$R_{s,n}=R_{s,p}\sqrt{\frac{D_{s,n}}{D_{s,p}}} \tag{5.37}$$

Eq. 5.37 shows how the positive electrode dictates the effective radius of the negative electrode.

Scenario 4: Process: charge; Dominant electrode: positive (point F* in Fig. 5b):

The schematic of this scenario is shown in Fig. 5b with the end point F*. It is assumed that SOC_p decreases from one to $SOC_{p,0}^{Dis.}$ during charge. The effective positive and negative radius equations are achieved with Eqs. 5.33 and 5.37, respectively. In order to avoid overcharging, the charge process may be interrupted before the SOC_p reaches $SOC_{p,0}^{Dis.}$.

The overall MM model is summarized in Figure 5.7.

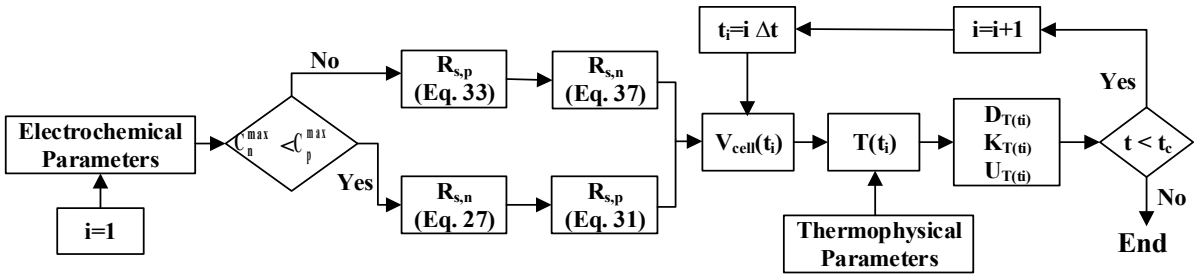

Figure 5.7: Flowchart of the MM model

5.4. Model Validation

The MM model was validated for three different Li-ion batteries based on LFP/Graphite at low and high discharge rates. Table 5.1 reports the data needed to run these tests. The results of the simulations are presented in the following sections.

Table 5.1: Electrochemical and thermophysical parameters for the three different Li-ion batteries

Parameter	Symbol	Unit	Case A		Case B		Case C	
			p	n	p	n	p	n
Cell Radius	R_c	cm	1.29†		1.29▼		-	
Cell lateral surface	A_{cell}	cm^2	43.93†		63.4▼		55*	
1C current density	I_{1C}	A	1.05		2.3		6.0	
Solid diffusion coefficient (25ºC)	$D_{s,k}$	m^2/s	9.66×10^{-18}*	9.06×10^{-15}*	5.9×10^{-20}▼	3.0×10^{-15}▼	2.2×10^{-14}▪	3.9×10^{-14}▪
Reaction rate constant (25ºC)	K_k	$m^{2.5}/mol^{0.5}s$	1.86×10^{-12}*	1.98×10^{-11}*	2.98×10^{-12}*	2.53×10^{-11}*	1×10^{-9}▪	2×10^{-11}▪
Porosity	ε_k	-	0.383*	0.566*	0.374▼	0.58▼	0.1805▪	0.46▪
Initial SOC	$SOC_{k,0}$	-	0.013*	0.813*	0.035▼	0.811▼	0.00001▪	0.5▪
Maximum solid phase concentration	$c_{s,k}^{max}$	mol/m^3	22806▼	31370•	22806▼	30555▼	22806▪	31370▪
Average electrolyte concentration	c_e	mol/m^3	1000•		1200▼		1000▪	
Electrode volume	$V_{s,k}$	cm^3	5.14†	2.7†	14.4▼	6.12▼	51.37*	35.00*
Solution phase resistanc	R_{cell}	Ω	0.049*		0.018*		0.0051*	
Heat capacity	ρc	J/m^3K	$3.53\times10^{+6}$*		$3\times10^{+6}$*		$2.028\times10^{+6}$▪	
Convection coefficient	h	w/m^2K	19.5*		10*		5▪	
Surrounding temperatur	T_{sur}	ºC	25†		23▼		27▪	
Solid phase diffusion activation energy	$Ea_{D,k}$	kJ/mol	39▼	35•	39▼	35▼	35▪	35▪
Reaction rate constant activation energy	$Ea_{K,k}$	kJ/mol	13▼	20•	13▼	20▼	20▪	20▪
1C charge/discharge duration	t_{1C}^*	s	3550†		3600▼		3300▪	
Maximum electrode capacity value	C_k^{max}	Ah	1.1565▲	1.0952▲	3.1766▲	2.3574▲	5.6684▲	6.7681▲
Dominant electrode			Negative▲		Negative▲		Positive▲	

* Parameter Estimation, † Measurement, ▲ Calculation, ▼ Ref. [123], • Ref. [64], ▪ Ref. [146].

5.4.1. Case A

The experimental data for case A come from a commercial 1.05 Ah 18650 Li_xC_6/Li_yFePO_4 cylindrical Li-ion cell, which was provided by the industrial partner for the present research project. Experiments were conducted to generate the cell potentials and the surface temperatures as a function of the discharge time. The surrounding temperature in the climatic chamber was constant at 25°C [105]. The electrochemical parameters were estimated with a calculation methodology reported in previous studies [13, 104]. The dominant electrode was determined following the MM model flowchart (Figure 5.7). According to Table 5.1, the positive electrode capacity is higher than that of the negative electrode. As a result, the graphite electrode is dominant. Eqs. 5.30 and 5.31 are then used to calculate the cell potential and the surface temperature profiles. Figures 5.8 and 5.9 indicate a good agreement between the numerical predictions and the experimental data for the cell potential and the surface temperature. Moreover, Figure 5.10 shows the $(R^2/D)_k$ for both electrodes with respect to

the discharge rates. As expected, the higher the discharge rate, the lower the effective radius for a constant diffusion coefficient.

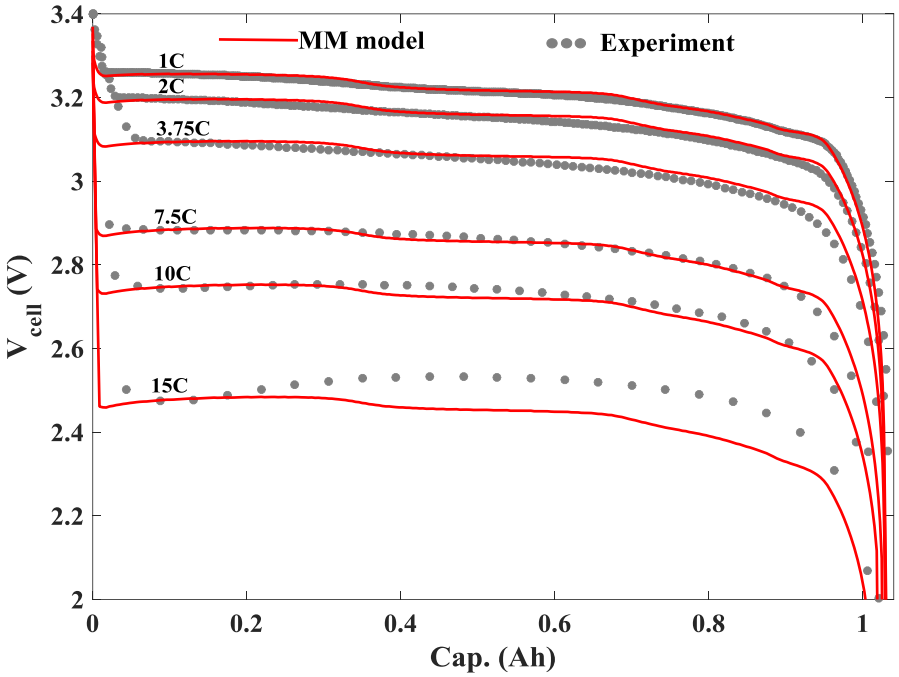

Figure 5.8: MM model predictions versus experimental data for the cell potential (case A) [105]

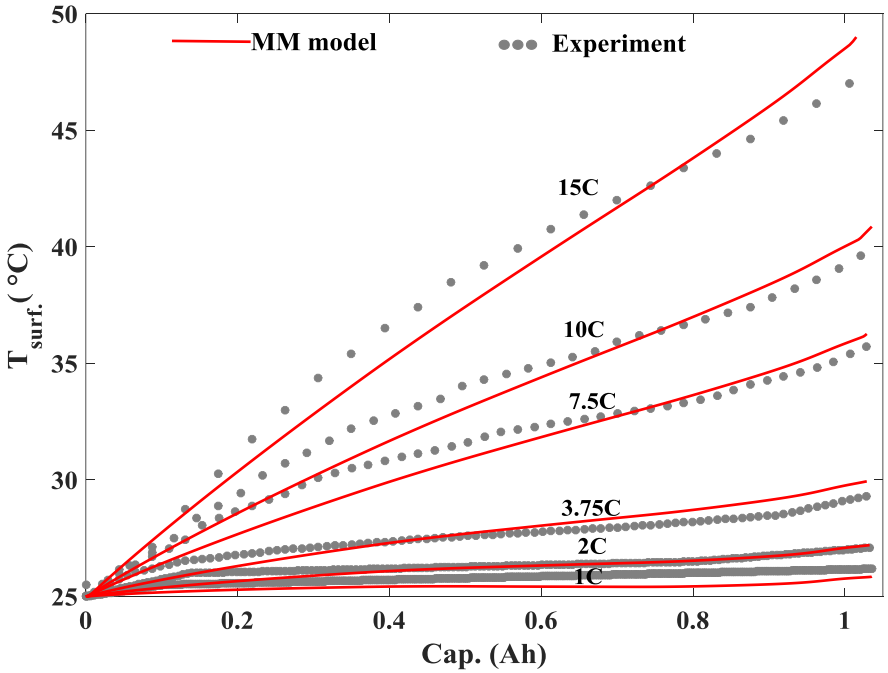

Figure 5.9: MM model predictions versus experimental data for the surface temperature (case A) [105]

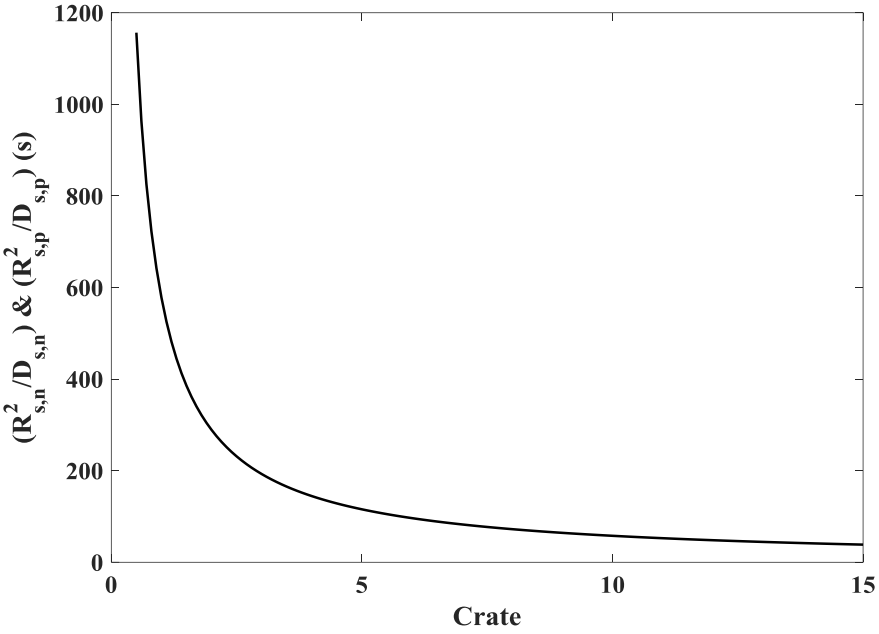

Figure 5.10: MM model calculations of $(R^2/D)_k$ versus Crate (case A)

5.4.2. Case B

This case represents the Li-ion battery used by Prada et al. to validate their model. The battery is a commercial LFP/Graphite cell with 2.3 Ah capacity that was provided by A123 Systems [123]. The main parameters for the battery are reported in Prada's paper. According to Table 5.1, the graphite electrode is dominant. As a result, Eqs. 5.30 and 5.31 are employed to calculate the cell potential and the surface temperature profiles. The good agreement between the model predictions and the experimental data is depicted in Figures 5.11 and 5.12. Figure 5.13 illustrates the $(R^2/D)_k$ for both electrodes with respect to the discharge rates.

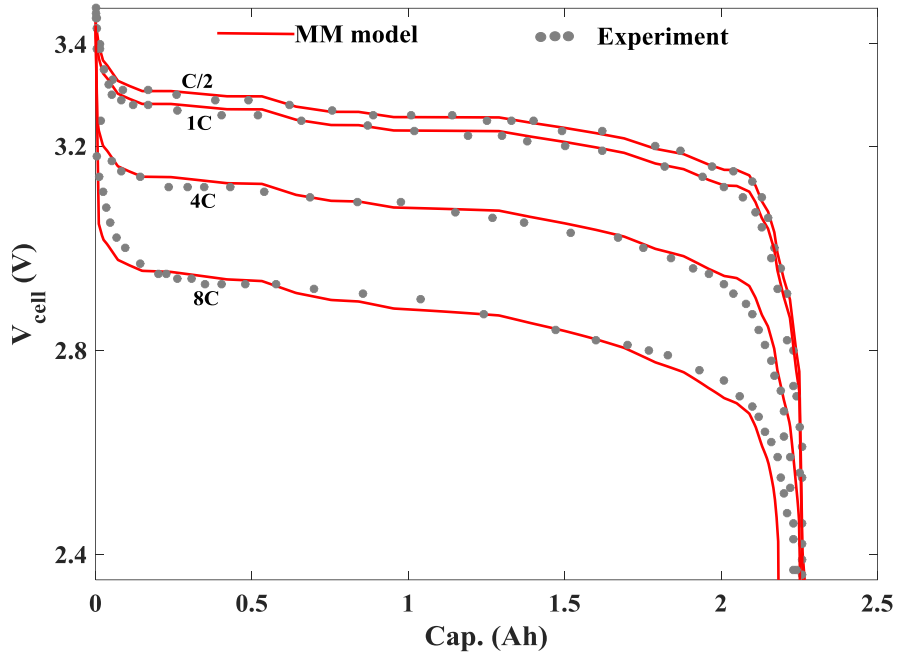

Figure 5.11: MM model predictions versus experimental data for the cell potential (case B) [123]

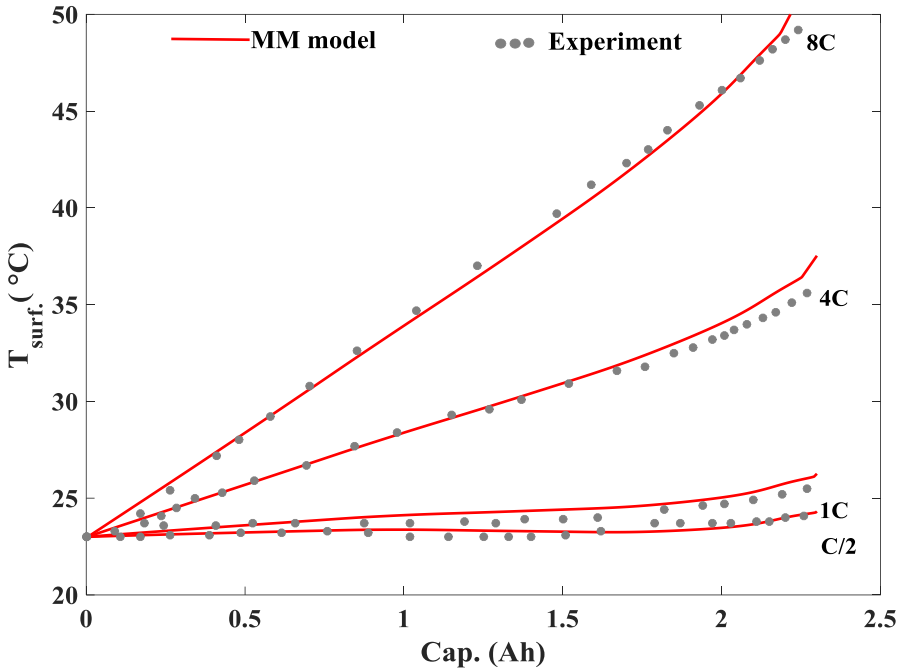

Figure 5.12: MM model predictions versus experimental data for the surface temperature (case B) [123]

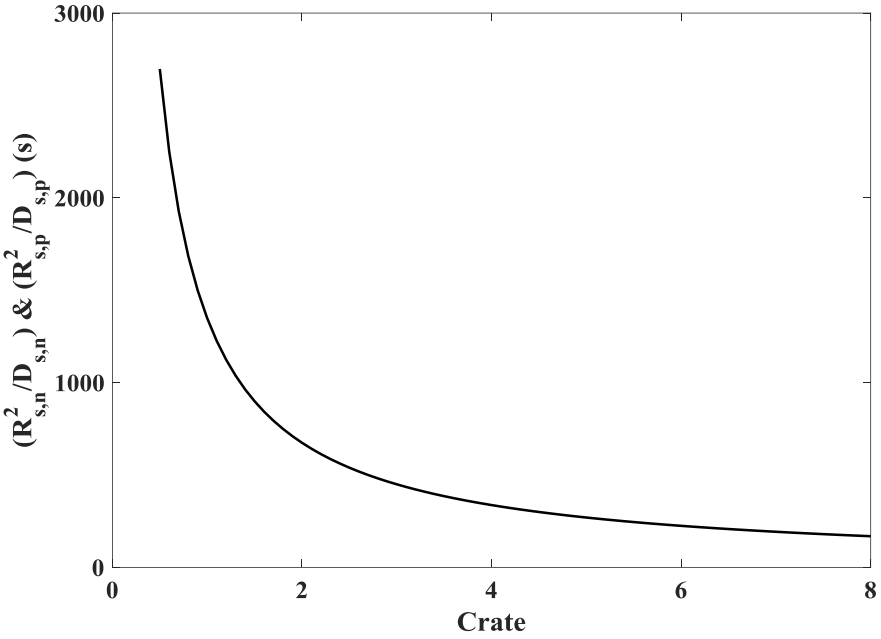

Figure 5.13: MM model calculations of $(R^2/D)_k$ versus Crate (case B)

5.4.3. Case C

This case represents the Li-ion battery used by Maheshwari et al. to validate their model. The battery is a commercial LFP/Graphite cell with 6 Ah capacity. It is provided by Lithops S.r.l [146]. The main parameters for the battery are reported in Maheshwari's paper. Contrary to the previous two cases, the LFP electrode is dominant, according to Table 2.1. Therefore, Eqs. 5.36 and 5.37 are used to calculate the cell potential and the surface temperature profiles. Figure 5.14 shows that the model predictions for the cell potential are in excellent agreement with the experimental data. According to Figure 5.15, the MM model could successfully predict the maximum cell temperatures at the end of discharge. However, to increase the calculation accuracy during discharge process, it is necessary to consider the geometry effects on the heat transfer equations. The results also reveal that the LFP electrode performance curve shifts to the left with increasing discharge rate leading to a change in the cut-off time with C-rate. By using t^* in each discharge rate, Figure 5.16 shows the $(R^2/D)_k$ for both electrodes with respect to the discharge rates.

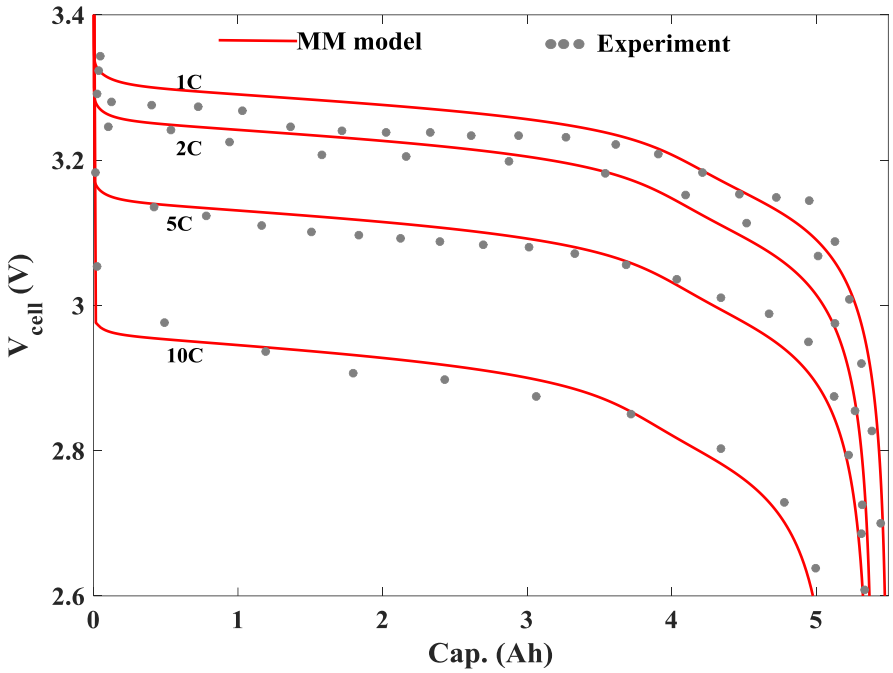

Figure 5.14: MM model predictions versus experimental data for the cell potential (case C) [146]

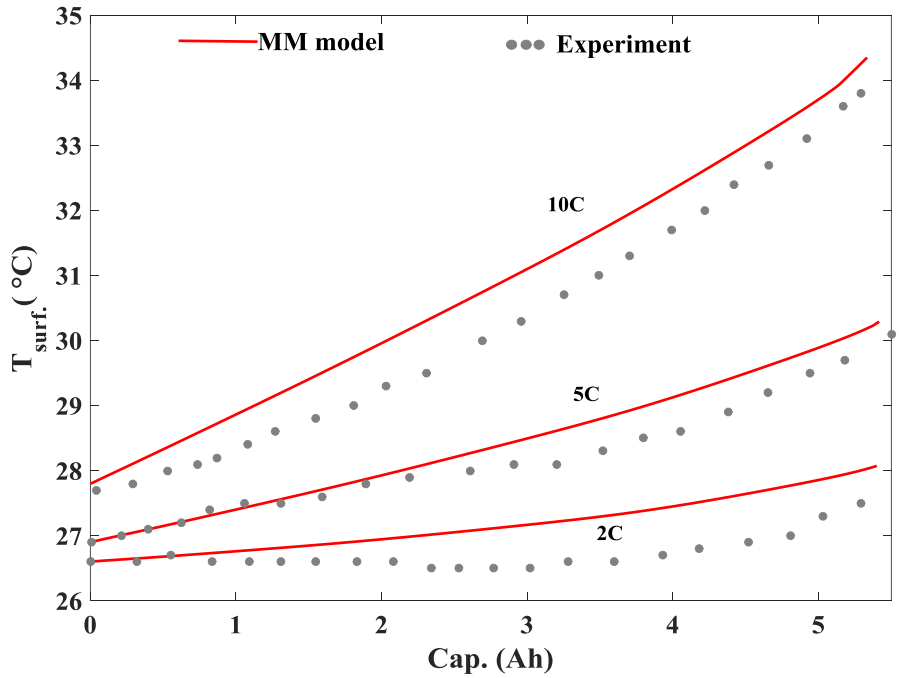

Figure 5.15: MM model predictions versus experimental data for the surface temperature (case C) [146]

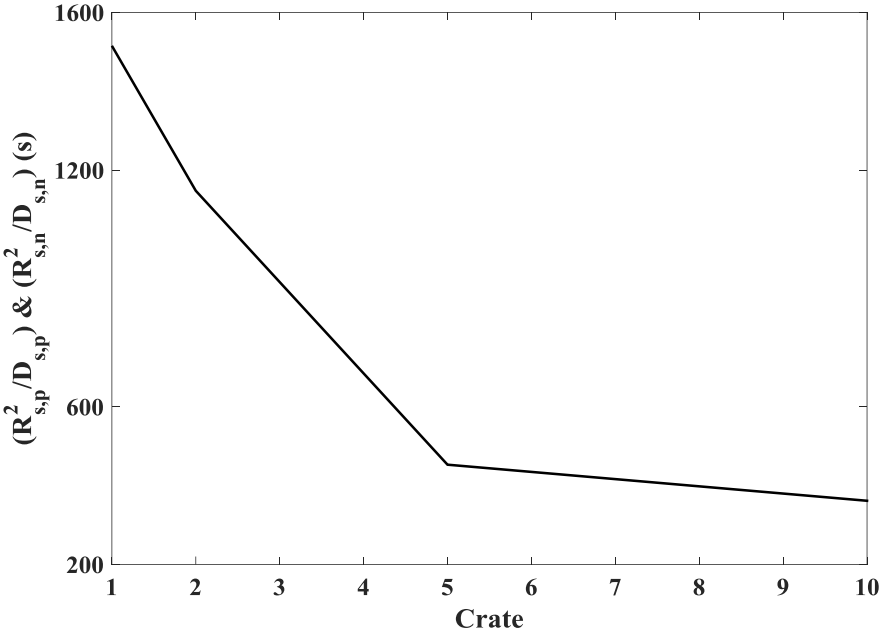

Figure 5.16: MM model calculations of $(R^2/D)_k$ versus Crate (case C)

5.5. Conclusion

A novel mathematical approach was presented for modeling commercial lithium-ion (Li-ion) batteries based on $LiFePO_4$(LFP)/graphite technology. The model was developed by coupling a simplified electro-thermal Li-ion battery model with the modified mosaic (MM) mathematical equations. The electro-thermal model rests on a modified Single Particle Model (SPM) and the energy balance equations. In the mosaic approach, it is assumed that the Li^+ intercalation/deintercalation processes into LFP particles occur at different sites with identical spherical shapes. The effective radius or the Li^+ ion diffusion coefficient in the LFP particles is considered to be dependent on the battery discharge/charge rates. The model does not support the actual insertion/extraction mechanism of Li^+ ions at the LFP particles in the micro-scale (particle-by-particle process), however, it is successful to simulate the battery behavior in macro-scale. Four different scenarios were investigated that consider which electrode is dominant during the charge and/or discharge processes. The MM model was employed to investigate the behavior of three commercial Li-ion batteries with different capacities that operated under different conditions. The results showed that their behavior may be simulated with accuracy at both low and high discharge rates. By applying the MM model to a Li-ion battery based on LFP/Graphite technology, it is possible to estimate its parameters, to simulate its performance in a battery pack, and to evaluated its behavior to be used in a Battery Management System (BMS).

Acknowledgements

The authors are very grateful to Hydro-Québec and the Natural Sciences and Engineering Council of Canada (NSERC) for their financial support.

CHAPITRE 6 : AVANT-PROPOS

Auteurs et affiliation:

- Ali Jokar: étudiant au doctorat, Université de Sherbrooke, Faculté de génie, Département de génie chimique et de génie biotechnologique.
- Martin Désilets: professeur, Université de Sherbrooke, Faculté de génie, Département de génie chimique et de génie biotechnologique.
- Marcel Lacroix: professeur, Université de Sherbrooke, Faculté de génie, Département de génie mécanique.
- Karim Zaghib: Institut de recherche d'Hydro-Québec (IREQ), Varennes, Qc, Canada, J3X 1S1.

Revue: Journal of the Electrochemical Society

Titre français: Une méthode inverse pour l'estimation couplée des paramètres électro-thermiques des piles cylindriques aux ions lithium basées sur le LFP-Graphite

Contribution au document: Cet article présente une étude d'estimation de paramètres dans laquelle les paramètres électrochimiques et thermophysiques d'une pile cylindrique Lithium-ion, faite à partir d'électrodes de graphite et de $LiFePO_4$ (LFP), sont simultanément déterminés. Les paramètres inconnus comprennent neuf paramètres électrochimiques et trois paramètres thermophysiques.

Résumé français :

Une étude d'estimation de paramètres est effectuée pour déterminer simultanément les paramètres électrochimiques et thermophysiques d'une pile cylindrique aux ions lithium (Li-ion) fait à partir d'électrodes de graphite et de $LiFePO_4$ (LFP). Les inconnues incluent neuf paramètres électrochimiques et trois propriétés thermophysiques. Les paramètres électrochimiques sont les coefficients de diffusion solide ($D_{s,n}$ et $D_{s,p}$), les constantes des réactions d'intercalation et de désintercalation (K_n et K_p), les états de charge initiaux ($SOC_{n,0}$ et $SOC_{p,0}$), les porosités (ε_n et ε_p) et la résistance de la solution électrolytique (R_{cell}). Les paramètres thermophysiques sont la capacité calorifique (ρC_p), la conductivité thermique (k) et le coefficient de convection thermique (h). Un problème inverse multi-objectif est défini en utilisant le potentiel de la pile et les températures de surface. Les données expérimentales sont tirées de tests menés à des taux de décharge variant entre 1C et 15 C. Un modèle de type mosaïque modifié (MM) est proposé pour simuler les données expérimentales. Le

modèle direct MM comprend un sous-modèle électro-thermique représentant le comportement des particules de LFP. Une fonction multi-objectif basée sur la différence normalisée entre les prédictions du modèle direct et les données expérimentales est défini. Les paramètres recherchés sont déterminés en minimisant la fonction objective à l'aide d'un algorithme génétique. En dépit de la complexité des équations et du nombre élevé de paramètres inconnus, les prédictions inverses sont en excellent accord avec les mesures expérimentales et ce, pour tous les taux de décharge. Finalement, la méthode inverse proposée pour l'estimation de paramètres est prometteuse pour le design des systèmes de gestion thermique des batteries.

6. An inverse method for the coupled electro-thermal parameter estimation of cylindrical lithium-ion batteries based on LFP/Graphite

6.1. Abstract

A parameter estimation study is conducted to determine simultaneously the electrochemical and the thermophysical parameters of a cylindrical lithium-ion (Li-ion) battery made with graphite/$LiFePO_4$ (LFP) electrodes. The unknown parameters include nine electrochemical and three thermophysical parameters. The electrochemical parameters are the solid diffusion coefficients ($D_{s,n}$ and $D_{s,p}$), the intercalation/deintercalation reaction-rate constants (K_n and K_p), the initial SOC ($SOC_{n,0}$ and $SOC_{p,0}$), the porosities (ε_n and ε_p), and the solution phase resistance (R_{cell}). The thermophysical parameters are the heat capacity (ρC_p), the thermal conductivity (k), and the convection heat transfer coefficient (h). A multi-objective inverse problem is defined by using the cell potential and the surface temperature profiles. Experimental data are taken from tests conducted at discharge rates ranging from 1C to 15C. To simulate the experimental data, a Modified Mosaic (MM) model is proposed. The MM direct model comprises an electro-thermal model that mimics the behaviour of LFP particles. A multi-objective function based on the normalized discrepancy between the predictions of the direct model and the experimental data is defined. The sought-after parameters are determined by minimizing the objective function with a genetic algorithm (GA). In spite of the complexity of the equations and the large number of unknown parameters, the inverse predictions show excellent agreement with the experimental data for all discharge rates. As a result, the proposed parameter estimation inverse method is a promising tool for the design of battery thermal management systems.

Keywords: Multi-objective parameter estimation; Thermophysical parameters; Electrochemical parameters; Inverse method; Cylindrical Li-ion battery; LiFePO4 (LFP) positive electrode material.

Nomenclature:

$c_{s,k}$	Solid-state concentration of Li^+ of electrode *k (k=p,n)*, mol/m^3
$c_{e,k}$	Electrolyte concentration of Li^+ in region *k (k=p,s,n)*, mol/m^3
$c_{s,k}^{ini}$	Initial concentration of Li^+ in the particles of electrode *k (k=p,n)*, mol/m^3

$c_{s,k}^{\max}$	Maximum concentration of Li^+ in the particles of electrode *k (k=p,n)*, mol/m^3
$c_{s,k}^{surf}$	Concentration of Li^+ on the surface of the particles of the electrode *k (k=p,n)*, mol/m^3
$D_{s,k}$	Li^+ diffusion coefficient in the particles of electrode *k (k=p,n)*, m^2/s
$D_{s,k}^{ref}$	$D_{s,k}$ at reference temperature *(k=p,n)*, m^2/s
$Ea_{D,k}$	Solid phase diffusion activation energy *(k=p,n)*, kJ/mol
$Ea_{K,k}$	Reaction rate constant activation energy *(k=p,n)*, kJ/mol
F	Faraday's constant, C/mol
h	Convection coefficient between the battery and its surroundings, W/m^{2}K
I	Applied current, A
J_k	Wall flux of Li^+ in the particles of electrode *k (k=p,n)*, mol/m^{2}s
k	Thermal conductivity of the cylindrical battery, W/mK
K_k	Reaction rate constant of electrode *k (k=p,n)*, m$^{2.5}$/mol$^{0.5}$s
K_k^{ref}	K_k at reference temperature *(k=p,n)*, m$^{2.5}$/mol$^{0.5}$s
n	Negative electrode
O.F.	Objective function
$\dot{Q}$	Total heat generation of the cylindrical battery, W
$\dot{q}$	Volumetric heat generation, W/m^3
p	Positive electrode
r	Radial coordinate (micro grid), m
r^*	Radial coordinate (macro grid), m
R	Universal gas constant, J/mol K
R_{cell}	Solution phase resistance, Ω
$R_{s,k}$	Radius of the particles of electrode *k (k=p,n)*, m
R_c	Radius of the cylindrical battery, m
s	Separator
S_k	Total electroactive area of electrode k *(k=p,n)*, m^2
SOC_k	State Of Charge of electrode *k (k=p,n)*
$SOC_{k,0}$	Initial State Of Charge of electrode *k (k=p,n)*
t	Time, s
t_{1C}^*	End of discharge time of the battery at 1C, s
T	Absolute temperature, K
T_{ref}	Reference temperature, K
T_{sur}	Surrounding temperature, K
T_{surf}	Battery surface temperature, K
T'_{surf}	Normalized battery surface temperature
U_k	Open-circuit potential of electrode *k (k=p,n)*, V
U_k^{ref}	U_k at reference temperature *(k=p,n)*, V
V_{cell}	Voltage of the cell, V
V'_{cell}	Normalized voltage of the cell
$V_{s,k}$	Total volume of the electrode k *(k=p,n)*, m^3
V_t	Total volume of the battery, m^3
x	Spatial coordinate, m

Greek

ε_k	Porosity of the electrode *k (k=p,n)*
λ_j	jth eigenvalue
$\mu_{s,k}$	Overpotential of electrode *k (k=p,n)*, V
ρC_p	Battery heat capacity, J/m^{3}K
$\Phi_{s,k}$	Solid-phase potential of electrode *k (k=p,n)*, V
$\Phi_{e,k}$	Electrolyte potential in region *k (k=p,s,n)*, V

6.2. Introduction

The demand for the storage of electricity using lithium-ion (Li-ion) batteries is growing. This trend is supported by the numerous applications in electronics and in electric vehicles. In order to maintain their operation uninterrupted, and to ensure their reliability, the electric storage devices usually rely on a battery management System (BMS). The BMS is employed to monitor, to control, and to manage the performance of the batteries, as well as to check their safety and integrity. The interactions between the battery pack and the other system components are also monitored by the BMS. Moreover, the BMS keeps the operational temperature of the battery pack within limits so as to avoid battery thermal runaways and to maintain good energy efficiencies. Sometimes, the BMS must face challenging operating conditions such as rapid charge and discharge processes and extreme ambient conditions. As a result, it is imperative for the BMS to receive feedback from the working environment, and to predict the electrochemical and the thermal performance of the batteries. To achieve this goal, the BMS relies on electro-thermal models that simulate the Li-ion battery performance [7, 68, 72, 106].

In the high tech industry and in the automotive industry, the BMS is usually constructed with empirical-based models. These models are simple and provide fast response. They cannot however predict the performance of the battery as it ages. Moreover, they are only applicable to a specific cell, i.e., they cannot be transposed to other battery technologies without recalibration [9, 10]. On the other hand, more complex and rigorous electrochemical models of Li-ion batteries based on electrochemical kinetics and mass and energy transport have been developed. They overcome the shortcomings of empirical models and are more accurate and robust.

Among the electrochemical Li-ion battery models, the pseudo-two-dimensional (P2D) model and the Single Particle Model (SPM) appear to be the most popular. These models will be discussed in Section 3 [9, 10, 34, 54].

The success of the electrochemical Li-ion battery models is strongly dependent on the precise knowledge of the electrochemical parameters and the thermophysical properties of the battery. These parameters and properties may be classified into three groups: geometry, materials and operating conditions [11, 13]. The thermophysical properties belong to the second group. These properties can be obtained from experimental measurements. They may also be available from the manufacturer. The third group comprises electrochemical parameters that are more difficult to obtain. Indeed, the direct experimental measurement of these physical properties is a tedious task. It usually requires the dismantling of the battery. To make matters more complicated, the measured properties may also depend on the battery age and may vary according to the measurement technique.

One interesting alternative for overcoming the difficulties of measuring the battery properties is to resort to inverse methods. Inverse methods estimate the unknown parameters of a system by means of easily measurable data. The parameter estimation methodology usually comprises five elements: input parameters, direct model, experimental data, objective function and optimizer. Such a methodology is based on optimization algorithms whose aim is to minimize the discrepancy between the predictions of a direct model (including the estimated parameters) and the experimental data [14, 15].

Many computational investigations have been conducted for identifying the operational parameters of Li-ion batteries. Most of these studies focused however on the estimation of the electrochemical parameters only. The coupling of the thermophysical parameters to the electrochemical variables has been largely ignored.

In 2007, Santhanagopalan et al. estimated five electrochemical parameters of the Li-ion battery by minimizing the least-square objective function with the Levenberg-Marquardt (LM) technique. The parameters include the diffusivity of Li^+ ions in the positive electrode ($D_{s,p}$), the reaction rate constants at the electrode/electrolyte interfaces (K_n and K_p) and the initial state-of-charge of the negative and positive electrodes ($SOC_{n,0}$ and $SOC_{p,0}$). The authors employed both the SPM and the P2D model as the direct models to develop the objective function [11].

Ramadesigan et al. performed a parameter estimation study to investigate the effect of five electrochemical parameters on the Li-ion battery capacity fade by studying the discharge curves at different charge/discharge rates. Their direct model is a simplified version of the P2D model. The parameters are the diffusion coefficients D_e, $D_{s,n}$ and $D_{s,p}$, and the electrochemical reaction rate constants for the negative and positive electrodes (K_n and K_p) [92].

Forman et al. implemented a full electrochemical parameter estimation using the P2D model as the forward model and a genetic algorithm (GA) as its optimizer. The electrochemical parameters and the geometric characteristics were extracted from the charge/discharge curves [93].

Marcicki et al. used curve fitting to identify the Li-ion battery parameters. The composition characteristics of the electrodes were determined with an open circuit potential curve. The resistance parameters were estimated from discharge curves for different temperature conditions. The diffusion coefficients were estimated by tuning the model parameters [88].

Zhang et al. conducted a multi-objective parameter estimation study by virtue of the discharge curves and the surface temperatures of Li-ion batteries. Only the electrochemical parameters were identified. The thermo-physical variables were not estimated. A modified multi-objective genetic algorithm was employed. Their results showed good agreement with experimental data only for low discharge curves [98].

Masoudi et al. reported another parameter estimation study for a Li-ion battery based on a reduced order model of the P2D model. The homotopy optimization approach was chosen to estimate six electrochemical parameters, namely the volume fraction of the separator (ε_s), Li^+ transference number (t_+), electrical conductivity of the solid phase of the negative electrode (σ_n), and the initial electrolyte concentration in three regions [99].

Rahman et al. identified four electrochemical variables by using the Particle Swarm Optimization (PSO) method [100].

Jokar et al. presented a method for the estimation of eight electrochemical parameters of Li-ion batteries by using a sensitivity analysis for three common positive electrode materials: $LiCoO_2$, $LiMn_2O_4$ and $LiFePO_4$ (LFP) [13, 104].

Despite the electrochemical parameter estimation studies, the identification of the thermophysical properties of the Li-ion battery is rare. A lumped heat transfer model was proposed by Forgez et al. to simulate cylindrical Li-ion batteries. The resistance parameters were estimated using the temperatures measured at the surface and at the center of the cylindrical batteries [111]. Jeon and Baek employed polynomial fitting functions for estimating the entropy changes in the heat generation equation inside a cylindrical Li-ion battery [113].

The present paper pursues the aforementioned studies by tackling a more challenging problem. It proposes an inverse method for estimating simultaneously the electrochemical parameters and the thermophysical properties of Li-ion batteries. The sought-after parameters include nine electrochemical parameters and three thermophysical properties.

The electrochemical parameters are the solid diffusion coefficients ($D_{s,n}$ and $D_{s,p}$), intercalation/deintercalation reaction-rate constants (K_n and K_p), initial SOC ($SOC_{n,0}$ and $SOC_{p,0}$), porosities (ε_n and ε_p), and solution phase resistance (R_{cell}). The thermophysical properties are heat capacity (ρC_p), thermal conductivity (k), and convection heat transfer coefficient (h). To estimate these parameters and properties, two experimental data sets for a graphite/LFP cylindrical Li-ion battery are employed. The data include the cell potential and the surface temperature profiles for different discharge rates. The Modified Mosaic (MM) model is adopted as the direct model. The MM model includes an electro-thermal model and a mathematical form of the mosaic approach that mimics the behaviour of the LFP particles. The electro-thermal model is developed from the SPM and the heat transfer equations for cylindrical Li-ion batteries. A multi-objective function is defined by means of the normalized values of the cell potential and of the surface temperatures. Due to the complexity of the system, a genetic algorithm (GA) is used to minimize the objective function and to calculate the sought-after parameters.

6.3. Experimental data

The experimental data were obtained from a commercial 1.05 Ah 18650 Li_xC_6/Li_yFePO_4 cylindrical Li-ion battery, Figure 6.1 [105]. The data were kindly provided by Hydro-Québec. The experiments were conducted so as to generate the cell potentials and the surface temperatures as a function of the discharge time. The electrochemical/thermochemical parameters were estimated with these experimental data for both low and high discharge rates (1C, 2C, 4C, 8C, 10C, and 15C). The surrounding temperature in the climatic chamber was kept constant at 25°C. Figures 6.2a and 6.2b present the cell potential and the surface temperature with respect to the discharge capacity, respectively. Figure 6.2b indicates that the surface temperature exceeds the safe temperature of 35°C for discharge rates of 10C and above. Operating the battery pack under these conditions without an effective thermal management system is obviously not recommended. The integrity and the safety of the storage system would be threatened.

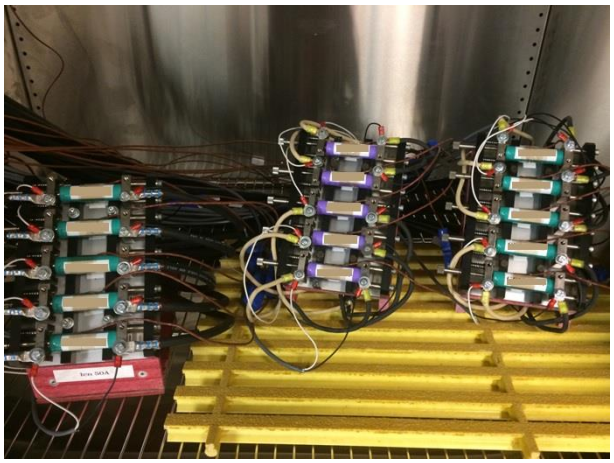

Figure 6.1: Experimental setup used for testing cylindrical Li-ion batteries [105]

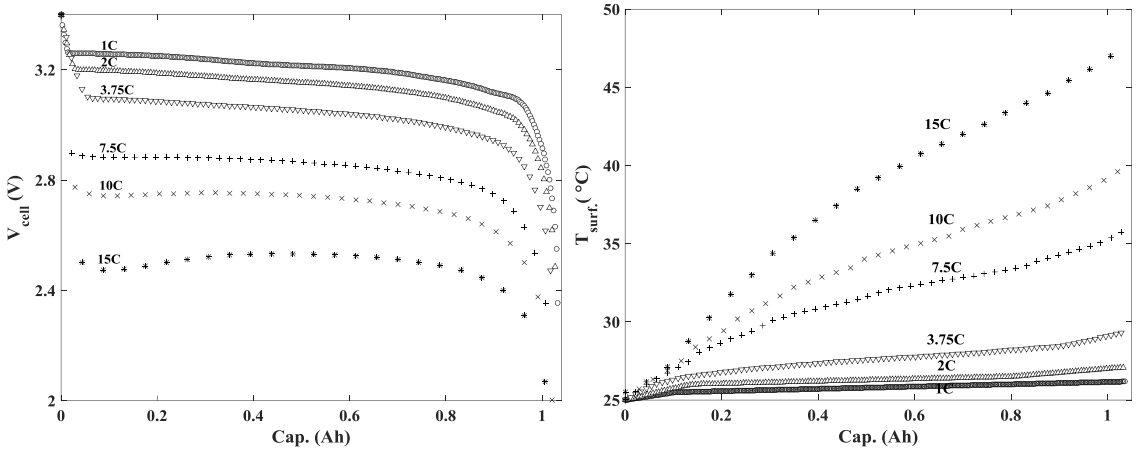

(a) **(b)**

Figure 6.2: (a) Cell potential and (b) surface temperature curves of the Li-ion battery [105]

6.4. The direct model

The electro-thermal direct model predicts simultaneously the cell potential and the surface temperature. It couples an electrochemical model to the heat transfer conservation equation. As mentioned above, electrochemical models can be classified into empirical-based models and electrochemical engineering models [9, 10]. Empirical models, such as the equivalent circuit-based models and the neural network models, rest entirely on experimental data. These models are widely used in electronics and in the automotive industry. They are simple and computationally fast. They cannot however simulate the performance of aging batteries or batteries that are operated in harsh ambient conditions [9, 28]. On the other hand, electrochemical engineering models are more sophisticated. They are based on the chemical/electrochemical kinetics and transport equations. They may be used to simulate the the electrochemical behaviour of Li-ion batteries. The Pseudo-two-Dimensional (P2D) model and the Single Particle Model (SPM) are among the most popular electrochemical-based models [9, 10]. The P2D model developed by Doyle et al. has been extensively used

for Li-ion battery investigations. It rests on the porous electrode and concentrated solution theories and uses kinetic equations to represent intercalation/desintercalation phenomena [34]. Its predictions are accurate and it has shown repeatedly good agreement with experimental data [9]. To reduce the computational time, a simplified version of the P2D model, called the SPM, has been developed by Zhang [54]. In the SPM, the electrolyte properties are ignored and the transport phenomena are treated in a simple manner [10, 54]. Most electrochemical models available in the open literature, such as the P2D model and the SPM, cannot simulate properly the behavior of batteries with LFP positive electrode.

The main reason is that they rest on Fick's law which does not take into account the two-phase region in the LFP intercalation/deintercalation process. To overcome this shortcoming, Padhi et al. suggested the shrinking-core idea to describe the insertion and the extraction processes of Li^+ ions at the surface of LFP particles. They considered a shrinking interface inside the LFP particles where the two-phase mechanism occurs [22]. Srinivasan and Newman employed the shrinking-core concept and implemented these two-phase phenomena in LFP spherical particles into the porous electrode theory. They determined the two-phase interface position by incorporating a mass balance between Li-rich (shell) and Li-poor (core) regions [131]. The shrinking-core porous electrode model has been developed to identify LFP electrode behavior on a macro-scale and by assuming the isotropic diffusion of the LFP particles. Different experiments showed, however, that the Li^+ ions migrate along 1D channels inside the LFP particles (the *b* direction at the phase boundary) leading an anisotropic ionic mobility of the Li^+ ion inside the LFP crystal and a particle-by-particle intercalation/deintercalation of Li^+ ions [133, 134]. Therefore, based on this study, it is concluded that the shrinking-core two-phase concept cannot describe the intercalation/deintercalation of Li^+ ions at the surface of LFP particles at the micro scale. Alternative approaches have been proposed to simulate the micro-scale behavior of the LFP particles, such as the new core-shell model [135], domino-cascade model [136], many-particle model [138], and phase-field models [141, 142, 144]. However, the main drawback of these models is that they are slow and expensive for simulating the performance of the LFP electrode in full scale commercial Li-ion batteries. All equations should be separately solved for each particle or unit. Therefore, they can be useful for off-line applications but cannot be applied for the coupled electro-thermal parameter estimation of cylindrical lithium-ion batteries.

In the present study, the mosaic model is employed to simulate the performance of the battery. The mosaic model was first proposed by Anderson and Thomas [124]. The model

assumes that the shrinking-core process can occur at different nucleation sites inside a LFP particle. It also assumes that the sites have identical spherical shapes with a radius smaller than that of LFP particles. According to the mosaic model, the effective radius of LFP particles is dependent on the battery discharge/charge rates. In other words, the diffusion coefficient for the Li^+ ions in the LFP particle varies according to the current density [124]. The model does not support the actual insertion/extraction mechanism of Li^+ ions in the LFP particles at the micro-scale (particle-by-particle process). However, it is successful to simulate the battery behavior at macro-scale. Different studies have been conducted with this model for investigating commercial Li-ion batteries for both negative and positive electrode particles. However, these studies did not provide any mathematical models for the mosaic approach. They simply tuned the effective radii of the LFP and the graphite particles at different discharge/charge rates to predict the batteries performance [123, 145, 146].

In the present paper, a Modified Mosaic (MM) model is employed. The MM model is a mathematical model that combines the mosaic approach to an electro-thermal model of the Li-ion battery. The electro-thermal model is developed by combining the SPM and the battery energy balance equations. To increase the SPM accuracy, an electrolyte resistance term is considered in the overpotential function. The details of this model are presented elsewhere [148].

6.4.1. The electro-thermal model

The SPM rests on two main assumptions: First, each electrode (Figure 6.3) is modeled as a spherical particle in which intercalation and de-intercalation phenomena occur. Second, variations of the electrolyte properties are ignored. Due to its simple equations and the low computational time, the SPM model is befitting many practical applications such as parameter estimation, real-time control modeling and lifetime modeling of Li-ion batteries [9, 10, 54].

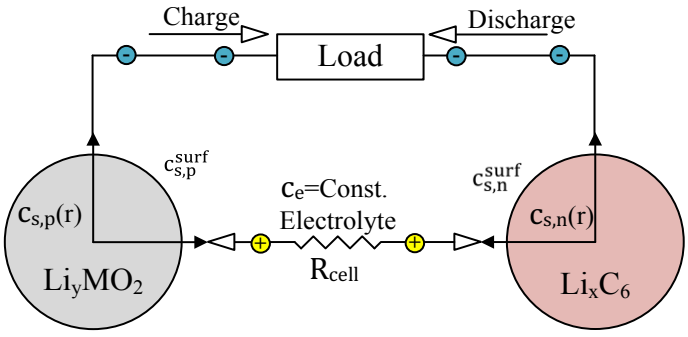

Figure 6.3: Schematic of the Single Particle Model (SPM)

The main equation of the SPM is the solid-state concentration. It is calculated with Fick's second law for both the negative and the positive spherical particles [64].

$$\frac{\partial c_{s,k}(r,t)}{\partial t} = \frac{D_{s,k}}{r^2}\frac{\partial}{\partial r}\left(r^2 \frac{\partial c_{s,k}(r,t)}{\partial r}\right) \tag{6.1}$$

Eq. 6.1 can be solved knowing the initial and the boundary conditions for each particle [64]:

$$c_{s,k}(r, t=0) = c_{s,k}^{ini} \tag{6.2}$$

$$D_{s,k}\frac{\partial c_{s,k}(r=0,t)}{\partial r} = 0 \tag{6.3}$$

$$D_{s,k}\frac{\partial c_{s,k}(r=R_{s,k},t)}{\partial r} = -J_k \tag{6.4}$$

J_k is the wall flux of Li^+ ions on each particle. The wall flux is assumed to be constant in the SPM. This parameter is calculated by using Eq. 6.5 for each electrode.

$$J_n = -\frac{I}{F S_n}, J_p = \frac{I}{F S_p}, S_k = \frac{3\varepsilon_k V_{s,k}}{R_{s,k}} \tag{6.5}$$

The battery current (I) is negative when the battery is discharged. The Butler-Volmer kinetics equation makes a connection between the wall flux (J_k), the over potential ($\mu_{s,k}$) and the Li^+ surface concentration at each particle [64]:

$$J_k = K_k\left(c_{s,k}^{\max} - c_{s,k}^{surf}(t)\right)^{0.5}\left(c_{s,k}^{surf}(t)\right)^{0.5} c_{e,k}^{0.5}\left[\exp\left(\frac{0.5F\mu_{s,k}(t)}{RT}\right) - \exp\left(-\frac{0.5F\mu_{s,k}(t)}{RT}\right)\right] \tag{6.6}$$

The over potential is the difference between the actual and the equilibrium potential of the battery. The over potential and the battery cell potential are calculated as follows:

$$\mu_{s,k}(t) = \Phi_{s,k}(t) - \Phi_{e,k}(t) - U_k(t);\ V_{cell}(t) = \Phi_{s,p}(t) - \Phi_{s,n}(t) \tag{6.7}$$

In order to improve the SPM accuracy, the potential drop between the positive and the negative electrodes in the electrolyte is simplified with the following equation [64]:

$$\Phi_{e,p} - \Phi_{e,n} = I R_{cell} \tag{6.8}$$

Note that the diffusion coefficients ($D_{s,k}$) and the reaction rate constants (K_k) are temperature-dependent parameters which are updated by virtue of an Arrhenius equation [64].

$$D_{s,k}(T) = D_{s,k}^{ref}\exp\left[\frac{Ea_{D,k}}{R}\left(\frac{1}{T} - \frac{1}{T_{ref}}\right)\right] \tag{6.9}$$

$$K_k(T) = K_k^{ref}\exp\left[\frac{Ea_{K,k}}{R}\left(\frac{1}{T} - \frac{1}{T_{ref}}\right)\right] \tag{6.10}$$

In this study, all the experimental data were collected at the reference temperature (ambient temperature) of T_{ref}=25ºC. The open circuit potential function (U_k) was also updated with the battery operation temperature in the following manner [64]:

$$U_k(T) = U_k^{ref} + \left.\frac{\partial U_k}{\partial T}\right|_{T_{ref}} \left(T - T_{ref}\right) \tag{6.11}$$

Guo et al. presented a solution for Eqs. 6.5 to 6.8 to determine the cell potential of the Li-ion battery [64]:

$$V_{cell} = \left(U_p - U_n\right) + \frac{2RT}{F}\ln\left(\frac{\sqrt{m_p^2+4}+m_p}{2}\right) + \frac{2RT}{F}\ln\left(\frac{\sqrt{m_n^2+4}+m_n}{2}\right) + IR_{cell} \tag{6.12}$$

$$m_p = \frac{I}{FK_pS_pc_{s,p}^{\max}c_e^{0.5}\left(1-SOC_p\right)^{0.5}\left(SOC_p\right)^{0.5}};\ SOC_p = \frac{c_{s,p}^{surf}}{c_{s,p}^{\max}} \tag{6.13}$$

$$m_n = \frac{I}{FK_nS_nc_{s,n}^{max}c_e^{0.5}\left(1-SOC_n\right)^{0.5}\left(SOC_n\right)^{0.5}};\ SOC_n = \frac{c_{s,n}^{surf}}{c_{s,n}^{max}} \tag{6.14}$$

It is noted that, to compute the SOC at the variable cell temperature condition (T), Eqs. 6.1 to 6.4 should be simultaneously solved by numerical methods, such as Finite Different Method (FDM). In order to calculate the cell potential function, it is imperative to consider the battery operating temperature in Eqs. 6.9 to 6.14. For the present study, the Li-ion battery is cylindrical. Therefore, the thermal model is developed with the energy conservation formulated in cylindrical coordinates. The model rests on the following assumptions: (1) The temperature gradient is dominant in the radial direction (r*); (2) The model is radial and not spiral; (3) There is no gap and no contact resistance between the sandwiched layers; (4) The materials are homogeneous and isotropic; (5) The thermophysical properties are considered to be constant; (6) The heat transfer across the battery external shell case is neglected; (7) The heat generation is uniform in each layer; and (8) Radiation heat transfer is negligible.

Figure 6.4 shows a schematic of the cylindrical Li-ion battery used in solving the thermal model equations.

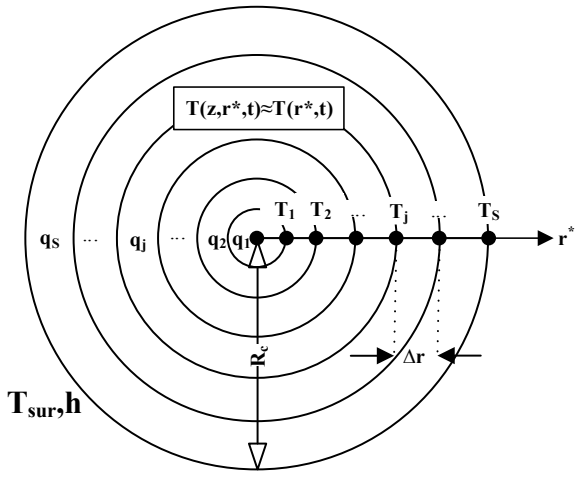

Figure 6.4: Concentric model for the cylindrical Li-ion battery

The governing heat transfer equations for the temperature distribution T(r*,t) across the cylindrical Li-ion battery may be stated as follows [109]:

$$k\frac{\partial^2 T}{\partial r^{*2}}+\frac{k}{r^*}\frac{\partial T}{\partial r^*}+\dot{q}=\left(\rho C_p\right)\frac{\partial T}{\partial t};\ 0\le r^*\le R_c \tag{6.15}$$

$$\dot{q}=\dot{q}_{irrev}+\dot{q}_{rev} \tag{6.16}$$

$$\dot{q}_{irrev}=\frac{-I}{V_t}\left(U_p-U_n-V_{cell}\right) \tag{6.17}$$

$$\dot{q}_{rev}=\frac{IT}{V_t}\left(\frac{\partial U_p}{\partial T}-\frac{\partial U_n}{\partial T}\right) \tag{6.18}$$

The current is negative when the battery is being discharged. The initial and boundary conditions for the heat transfer model are presented in Eqs. 6.19 to 6.21.

$$\frac{\partial T\left(0,t\right)}{\partial r^*}=0 \tag{6.19}$$

$$\frac{\partial T\left(R_c,t\right)}{\partial r}=-\frac{h}{k}\left(T\left(R_c,t\right)-T_{sur}\right) \tag{6.20}$$

$$T\left(r^*,0\right)=T_{sur} \tag{6.21}$$

T_{sur} is the temperature of the surroundings. The set of Eqs. 6.15 to 6.21 is solved with a Crank Nicolson Finite Difference Method based on the grid presented in Figure 6.4 [121].

The variation of the heat generation during the charge/discharge period can now be estimated by using the temperature distribution. The total heat generation comprises two terms: the reversible heat generation term ($\dot{Q}_{rev}$) and the irreversible heat generation term ($\dot{Q}_{irrev}$). Referring to Figure 6.4,

$$\dot{Q}_t=\dot{Q}_{irrev}+\dot{Q}_{rev}=\left(\dot{q}_1V_1+\ldots+\dot{q}_jV_j+\ldots+\dot{q}_SV_S\right)_{irrev}+\left(\dot{q}_1V_1+\ldots+\dot{q}_jV_j+\ldots+\dot{q}_SV_S\right)_{rev} \tag{6.22}$$

where V_j is the volume of layer j. The magnitude of V_j is determined from,

$$V_j=2\pi\left(\frac{j\Delta r+(j-1)\Delta r}{2}\right)\Delta rL=\pi\left(2j-1\right)\Delta r^2L;\ j=1,2,\ldots,S \tag{6.23}$$

Substitution of Eqs. 6.17, 6.18 and 6.23 into Eq. 6.22 yields,

$$\dot{Q}_{irrev}\left(t\right)=\sum_{j=1}^{S}\frac{-IV_j}{V_t}\left(U_p\left(t\right)-U_n\left(t\right)-V_{cell}\left(t\right)\right)=-I\left(U_p\left(t\right)-U_n\left(t\right)-V_{cell}\left(t\right)\right) \tag{6.24}$$

$$\dot{Q}_{rev}\left(t\right)=\sum_{j=1}^{S}\frac{IV_j}{V_t}T_j\left(\frac{\partial U_p\left(t\right)}{\partial T}-\frac{\partial U_n\left(t\right)}{\partial T}\right)=I\left(\frac{\Delta r}{R_c}\right)^2\left(\frac{\partial U_p\left(t\right)}{\partial T}-\frac{\partial U_n\left(t\right)}{\partial T}\right)\sum_{j=1}^{S}\left(2j-1\right)T_j\left(t\right) \tag{6.25}$$

Figures 6.5 and 6.6 depict the open circuit potential functions (U_k) and the ($\partial U_k/\partial T$) values for the graphite and for the LFP.

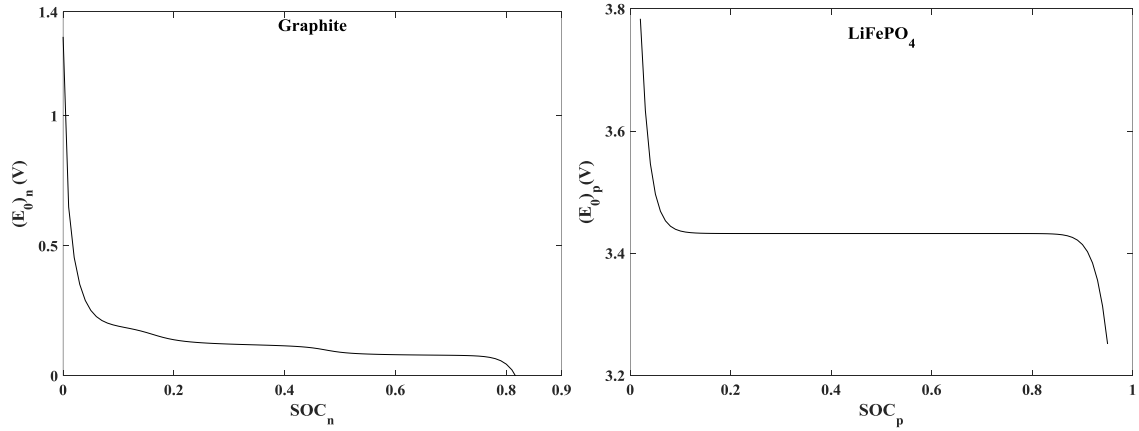

Figure 6.5: Open circuit potential function as a function of SOC for (a) Graphite [64] and (b) LFP [119]

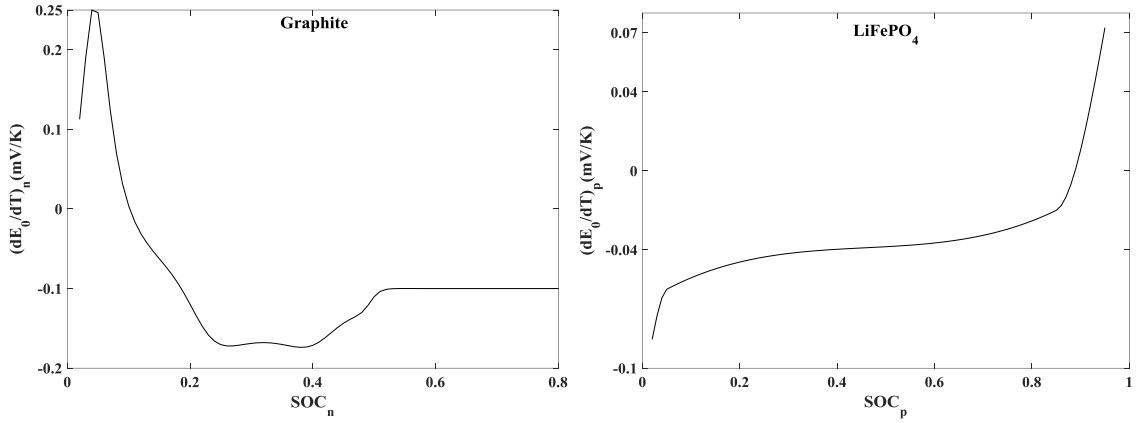

Figure 6.6: Entropic heat change as a function of SOC for (a) Graphite [64] and (b) LFP [120]

6.4.2. The Modified Mosaic (MM) model

The mosaic approach allows us to change the particle radius instead of the diffusion coefficient in order to represent the specific behavior of graphite/LFP Li-ion batteries at different current density. The MM model employs a mathematical approach to find the appropriate effective radii to be used in the porous electrode theory. This approach is based on the identification of the dominant electrode which is the electrode with the lowest quantity of active material. Depending on which electrode is dominant, the effective radius is calculated by considering the battery behavior on its discharge/charge curves [148]. For the batteries tested in this study, the negative electrode has been identified as the dominant electrode. Therefore, the effective radii of the negative and of the positive particles can be calculated as follows [148]:

$$R_{s,n} = \sqrt{\frac{\varepsilon_n V_{s,n} F c_{s,n}^{\max} SOC_{n,0} - |I_{1C}| t_{1C}^*}{N|I_{1C}|/15} D_{s,n}} \tag{6.26}$$

$$R_{s,p} = R_{s,n} \sqrt{\frac{D_{s,p}}{D_{s,n}}} \tag{6.27}$$

I_{1C} and t_{1C}^{*} are the current and the end of discharge time (approximately 3600 s) respectively, both at a dischange intensity of 1C. N is the battery discharge rate. The overall MM model used to simulate the discharge process is illustrated in Fig. 6.7.

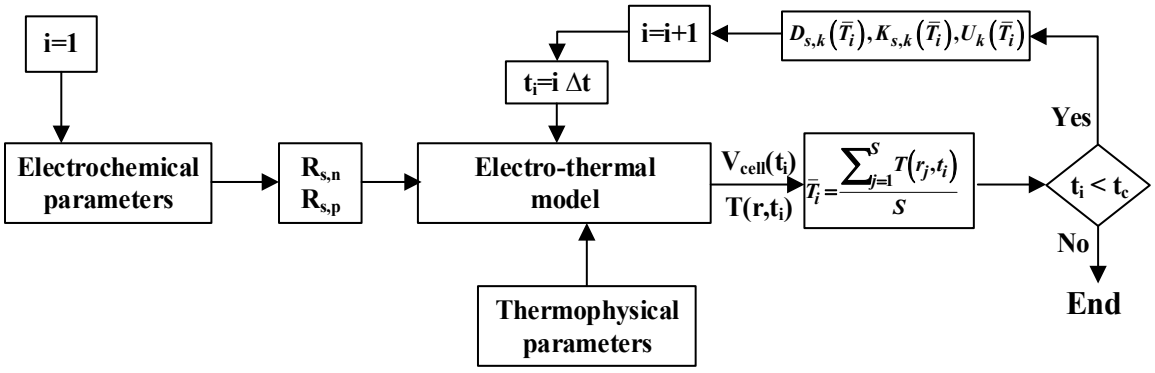

Figure 6.7: The overall MM model used to simulate the discharge process

6.5. The inverse method

The cell potential and the temperature distribution along the cylindrical Li-ion battery can be determined by means of the direct model presented in section 6.4. To run the model, it is necessary to know the different electrochemical and thermophysical parameters. Unfortunately, some of the properties and parameters of the battery are unknown. Furthermore, their magnitudes may change as the battery ages. To determine the unknown parameters, an inverse method is employed. The inverse method is fed with experimental data for the cell potential and the surface temperature of the battery. The main advantage of the inverse method is to be able to identify the sought-after parameters without resorting to invasive measurements techniques or without dismantling the battery. In the present study, the surface temperature profiles are the sole experimental data that are used for estimating the thermophysical parameters.

The unknown parameters include nine electrochemical parameters and three thermophysical properties. The electrochemical parameters are the solid diffusion coefficients ($D_{s,n}$ and $D_{s,p}$), intercalation/deintercalation reaction-rate constants (K_n and K_p), initial SOC ($SOC_{n,0}$ and $SOC_{p,0}$), porosities (ε_n and ε_p), and solution phase resistance (R_{cell}). The thermophysical properties are the heat capacity (ρC_p), thermal conductivity (k), and convection heat transfer coefficient (h).

Figure 6.8 provides an overall view of the proposed inverse procedure. The aim of the inverse method is to minimize the objective function (O.F.) in order to determine the unknown parameters and properties. As there are two kinds of experimental data, the

objective function is defined as a multi-objective function. Once the objective function is satisfactorily minimized, the unknown parameters and properties are automatically determined.

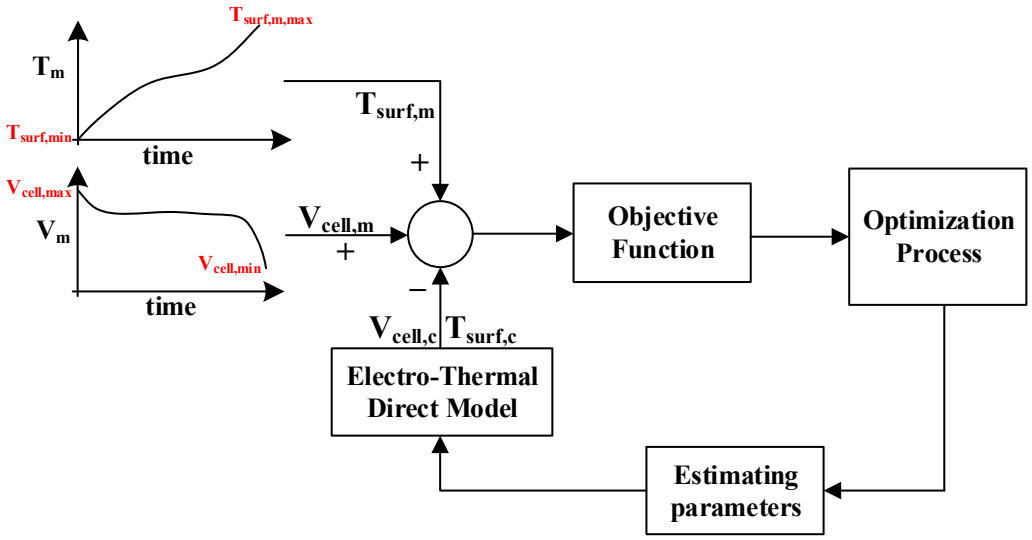

Figure 6.8: Schematic of the inverse procedure for the coupled electro-thermal parameter estimation

The experimental data for the Li-ion battery were recorded at a constant time interval between zero and the cut-off time ($0 < t \leq t_c$). Therefore, the procedure used for the inverse method involves a "whole time domain" approach.

To derive a general multi-objective function, let us start with one charge/discharge curve. The measured cell potential ($\mathbf{V}_{cell,m}$) and the surface temperature ($\mathbf{T}_{surf,m}$) vectors with N time intervals during one charge/discharge process may be written as,

$$\mathbf{V}_{cell,m} = \begin{bmatrix} V_{cell,1} \\ V_{cell,2} \\ \vdots \\ V_{cell,N} \end{bmatrix}_{N\times 1} ; t = t_1, t_2, \ldots, t_N \tag{6.28}$$

$$\mathbf{T}_{surf,m} = \begin{bmatrix} T_{surf,1} \\ T_{surf,2} \\ \vdots \\ T_{surf,N} \end{bmatrix}_{N\times 1} ; t = t_1, t_2, \ldots, t_N \tag{6.29}$$

As the order of magnitude and the physics of these two vectors are very different, it is necessary to normalize their values into the range [0, 1]:

$$\mathbf{V}'_{cell,m} = \frac{\mathbf{V}_{cell,m} - \mathrm{V}_{cell,\min}}{\mathrm{V}_{cell,\max} - \mathrm{V}_{cell,\min}} \tag{6.30}$$

$$\mathbf{T}'_{surf,m} = \frac{\mathbf{T}_{surf,m} - \mathrm{T}_{surf,min}}{\mathrm{T}_{surf,m,max} - \mathrm{T}_{surf,min}} \tag{6.31}$$

The minimum surface temperature is set equal to the initial temperature. The maximum temperature depends however on the charge/discharge rate. A similar approach is considered for the normalization of both the calculated cell potential ($\mathbf{V}_{cell,c}$) and the surface temperature ($\mathbf{T}_{surf,c}$) functions that were determined by the direct model:

$$\mathbf{V}'_{cell,c}(\mathbf{P}) = \frac{\mathbf{V}_{cell,c}(\mathbf{P}) - \mathrm{V}_{cell,min}}{\mathrm{V}_{cell,max} - \mathrm{V}_{cell,min}} \tag{6.32}$$

$$\mathbf{T}'_{surf,c}(\mathbf{P}) = \frac{\mathbf{T}_{surf,c}(\mathbf{P}) - \mathrm{T}_{surf,min}}{\mathrm{T}_{surf,m,max} - \mathrm{T}_{surf,min}} \tag{6.33}$$

The vector **P** comprises the sought-after parameters. The most common form of the objective function in inverse problems is the least-square objective function [14, 15]. Here, there are two least-square functions that correspond to the normalized cell potential and to the normalized surface temperature. Therefore, the inverse problem is a multi-objective optimization. The *Weighted global criterion method* [149] is invoked to define the multi-objective function for one charge/discharge rate in a matrix form:

$$O.F. = \frac{1}{2}\left[\left(\mathbf{V}'_{cell,m} - \mathbf{V}'_{cell,c}(\mathbf{P})\right)^T \left(\mathbf{V}'_{cell,m} - \mathbf{V}'_{cell,c}(\mathbf{P})\right)\right] + \frac{1}{2}\left[\left(\mathbf{T}'_{surf,m} - \mathbf{T}'_{surf,c}(\mathbf{P})\right)^T \left(\mathbf{T}'_{surf,m} - \mathbf{T}'_{surf,c}(\mathbf{P})\right)\right] \tag{6.34}$$

The superscript *T* indicates the transpose of the function. The weights in this multi-objective objective function are set equal to 0.5. This means that the relative importance of the cell potential and of the surface temperature functions is similar. The objective function can be rewritten in the following explicit form:

$$O.F. = \frac{1}{2}\sum_{i=1}^{N}\left[\left(V'_{cell,m,i} - V'_{cell,c,i}(\mathbf{P})\right)^2 + \left(T'_{surf,m,i} - T'_{surf,c,i}(\mathbf{P})\right)^2\right] \tag{6.35}$$

By substituting Eqs. 6.30 to 6.33 into Eq. 6.35, the objective function becomes

$$O.F. = \frac{1}{2}\sum_{i=1}^{N}\left[\left(\frac{V_{cell,m,i} - V_{cell,c,i}(\mathbf{P})}{V_{cell,max} - V_{cell,min}}\right)^2 + \left(\frac{T_{surf,m,i} - T_{surf,c,i}(\mathbf{P})}{T_{surf,m,max} - T_{surf,min}}\right)^2\right] \tag{6.36}$$

For M charge/discharge curves (at different rates), the objective function is then:

$$O.F. = \frac{1}{2}\sum_{j=1}^{M}\sum_{i=1}^{N}\left[\left(\frac{V_{cell,m,ij} - V_{cell,c,ij}(\mathbf{P})}{V_{cell,max} - V_{cell,min}}\right)^2 + \left(\frac{T_{surf,m,ij} - T_{surf,c,ij}(\mathbf{P})}{T_{surf,m,max} - T_{surf,min}}\right)^2\right] \tag{6.37}$$

The electrochemical and the thermophysical parameters (**P**) are determined by minimizing the objective function (O.F.) in the following manner:

$$\min O.F. = O.F.(\mathbf{P}) \text{ subject to } P_{j,low} \le P_j \le P_{j,high} \tag{6.39}$$

$\mathrm{P_{j,low}}$ and $\mathrm{P_{j,high}}$ are the minimum and the maximum values of $\mathrm{P_j}$ values, respectively. Eq. 6.38 is solved with an optimizer that determines the global minimum.

The optimization process for inverse problems is usually mathematically challenging, slow converging and computationally expensive [15]. Colaço et al. reviewed different solution methods for inverse problems among which we find the steepest descent method, the conjugate gradient method, the Newton-Raphson method, the quasi-Newton method, the Levenberg-Marquardt method (LM), the Genetic Algorithms (GA), differential evolutions, the particle swarm method and the simulated annealing method [17]. In general, these optimization methods are divided into two categories: the deterministic methods and the stochastic methods. Deterministic methods are usually faster than stochastic methods. However, they easily fall onto local extrema and have complex structures. On the other hand, stochastic-based optimization methods employ random-based operation functions that are ideally suited for reaching system global extrema [17, 18].

Due to the complexity of the governing equations (Eqs. 6.1 to 6.27) and due to the number of sought-after parameters, a stochastic technique called the Genetic algorithm (GA) was adopted in the present study. The GA minimizes the objective function and estimates the electrochemical and the thermophysical parameters of the Li-ion battery.

The Genetic algorithm (GA) was first introduced by Holland in the 1970s [101]. The GA originates from natural selection mechanisms. It starts from a strong random database, namely an initial population, and moves upward to many extremum points. Inspired by the living organism's structure, each member of the initial population is called a chromosome containing some genes. Each chromosome represents a probabilistic solution to the optimization problem in which the number of variables is equivalent to the number of genes. In the GA, more fitted new populations replace older populations. Therefore, the algorithm requires a fitness function, which refers to the cost of a chromosome. After generating the initial population randomly, new populations are produced by three genetic operators called pairing, mating and mutation.

6.6. Results

The numerical simulations conducted with the direct model adopted the following physical characteristics for the battery (Table 6.1)

Table 6.1: Characteristics of the battery

Symbol	Unit	Case A	
		p	n
R_c	cm	1.29†	
A_{cell}	cm^2	43.93†	
I_{1C}	A	1.05	
$c_{s,k}^{max}$	mol/m^3	22806[123]	31370[64]
c_e	mol/m^3	1000[64]	
$V_{s,k}$	cm^3	5.14†	2.7†
T_{sur}	ºC	25†	
$Ea_{D,k}$	kJ/mol	39[123]	35[64]
$Ea_{K,k}$	kJ/mol	13[123]	20[64]
t_{1C}^{*}	s	3550†	
$V_{cell,min}$	V	2.0	
$V_{cell,max}$	V	3.4	
$T_{surf,min}$	ºC	25.0	
$T_{surf,1C,max}$	ºC	26.2	
$T_{surf,2C,max}$	ºC	27.2	
$T_{surf,3.75C,max}$	ºC	29.5	
$T_{surf,7.5C,max}$	ºC	35.4	
$T_{surf,10C,max}$	ºC	39.6	
$T_{surf,15C,max}$	ºC	47.0	

† Measurement

The GA optimization procedure was initiated with a population of 400 chromosomes and a mutation rate of 5%. The initial chromosomes were generated by using a random function that spans the range of each sought-after parameter as reported in the open literature. The range of each parameter was also employed to update the chromosome during mutation. The objective function (Eq. 6.38) was then minimized by using the genetic operators and the experimental data for the six discharge curves (1C, 2C, 3.75C, 7.5C, 10C and 15C). The sought-after parameters were finally determined at the optimum point. Table 6.2 reports the range and the estimated values for both the electrochemical parameters and the thermophysical properties.

Table 6.2: Electrochemical and thermophysical parameters estimated for the Li-ion battery

Symbol	Unit	Min	Max	Value
Electrochemical Parameters				
$D_{s,p}$	m^2/s	1.00×10^{-18}	10.00×10^{-18}	9.66×10^{-18}
$D_{s,n}$	m^2/s	1.00×10^{-15}	10.00×10^{-15}	9.06×10^{-15}
K_p	$m^{2.5}/mol^{0.5}$ s	1.00×10^{-12}	10.00×10^{-12}	1.86×10^{-12}
K_n	$m^{2.5}/mol^{0.5}$ s	1.00×10^{-11}	10.00×10^{-11}	1.98×10^{-11}
ε_p	-	0.30	0.40	0.383
ε_n	-	0.50	0.60	0.566
$SOC_{p,0}$	-	0.01	0.06	0.013
$SOC_{n,0}$	-	0.75	0.85	0.810
R_{cell}	Ω	0.010	0.100	0.049
Thermophysical Parameters				
ρC_p	J/m^3K	$1.0\times10^{+6}$	$5.0\times10^{+6}$	$3.53\times10^{+6}$
k	W/mK	0.10	2.00	0.24
h	W/m^2K	0.1	30	19.50

To check the accuracy of the estimated parameters and properties, they were fed back as input data to the direct model. The predictions of the direct model were then compared to the experimental data (Figs. 6.9 and 6.10). The agreement between the predictions and the experimental data is excellent.

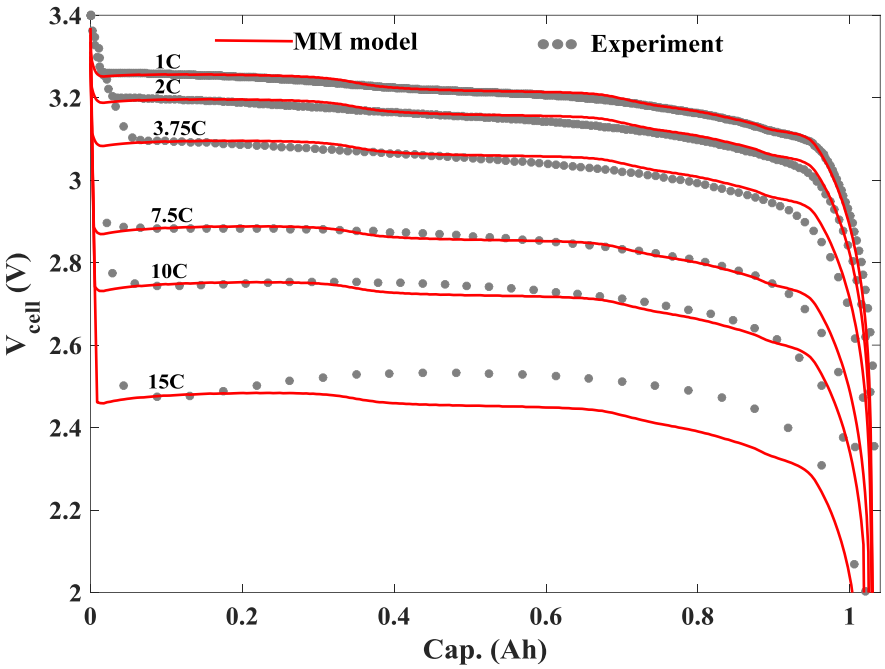

Figure 6.9: Predictions of the cell potentials versus experimental data

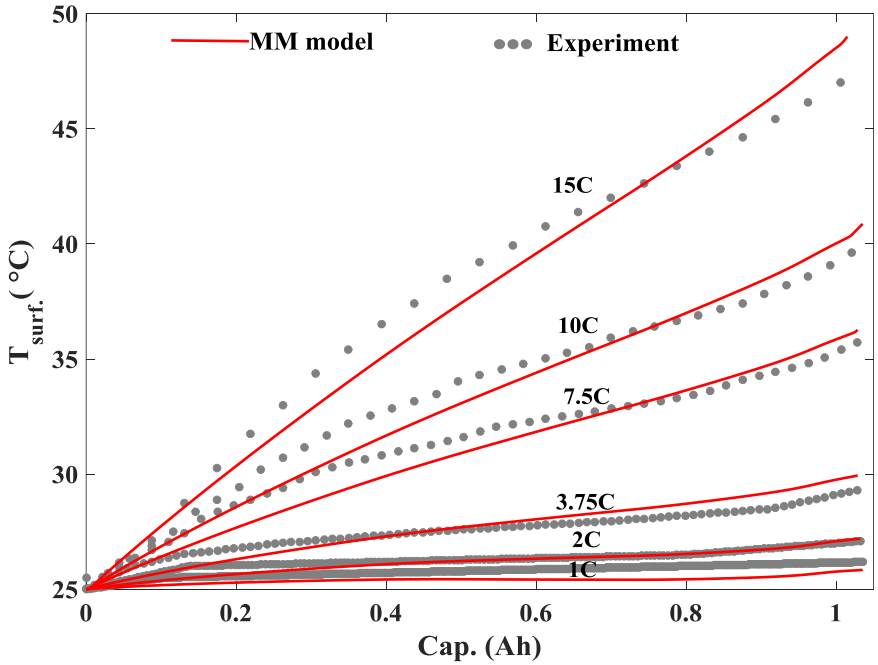

Figure 6.10: Predictions of the surface temperatures versus experimental data

By using the predicted temperature distribution and Eqs. 6.24 and 6.25, the heat generation functions were calculated for different discharge rates. Figure 6.11 depicts the total heat generation term of the cylindrical Li-ion battery. Due to the existence of a plateau in the LFP open-circuit potential, each heat generation profile has a plateau during most of the discharge period. Moreover, the higher the discharge rate, the higher is the heat generation value. The small jump at the end of heat generation curves corresponds to the jump of the graphite entropic heat change curve at low values of the SOCn. As a result, the simultaneous estimation of the electro-thermal parameters allows the heat generation profile to be taken into account in the design of the battery thermal management system.

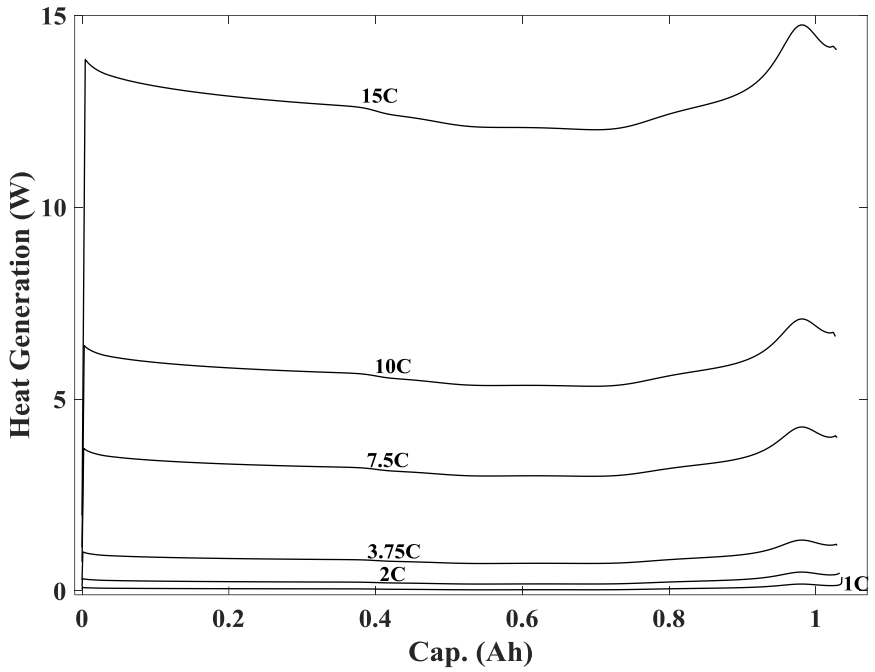

Figure 6.11: Prediction of the heat generation for different discharge rates

6.7. Conclusion

A parameter estimation study was conducted to determine simultaneously the electrochemical and the thermophysical parameters of a cylindrical Lithium-ion (Li-ion) battery made with graphite/$LiFePO_4$ (LFP) electrodes. The unknown parameters include nine electrochemical and three thermophysical parameters. The electrochemical parameters are the solid diffusion coefficients ($D_{s,n}$ and $D_{s,p}$), the intercalation/deintercalation reaction-rate constants (K_n and K_p), the initial SOC ($SOC_{n,0}$ and $SOC_{p,0}$), the porosities (ε_n and ε_p), and the solution phase resistance (R_{cell}). The thermophysical parameters are the heat capacity (ρC_p), the thermal conductivity (k), and the convection heat transfer coefficient (h). A multi-objective inverse problem was defined by using the cell potential and the surface temperature profiles. Experimental data were collected from tests conducted at discharge rates ranging from 1C to 15C. To simulate the experimental data, a Modified Mosaic (MM) model was proposed. The MM direct model comprises an electro-thermal model that mimics the behaviour of LFP particles. A multi-objective function based on the normalized discrepancy between the predictions of the direct model and the experimental data was defined. The sought-after parameters were determined by minimizing the objective function with a Genetic Algorithm (GA). In spite of the complexity of the mathematical equations and the large number of unknown parameters, the inverse predictions show excellent agreement with

the experimental data for all discharge rates. The proposed parameter estimation method was shown to be a promising tool for the design of battery thermal management systems.

Acknowledgements

The authors are very grateful to Hydro-Québec and to the Natural Sciences and Engineering Council of Canada (NSERC) for their financial support.

CHAPITRE 7 : AVANT-PROPOS

Auteurs et affiliation:

- Ali Jokar: étudiant au doctorat, Université de Sherbrooke, Faculté de génie, Département de génie chimique et de génie biotechnologique.
- Martin Désilets: professeur, Université de Sherbrooke, Faculté de génie, Département de génie chimique et de génie biotechnologique.
- Marcel Lacroix: professeur, Université de Sherbrooke, Faculté de génie, Département de génie mécanique.
- Karim Zaghib: Institut de recherche d'Hydro-Québec (IREQ), Varennes, Qc, Canada, J3X 1S1.

Revue: Journal of Power Sources

Titre français: Modèle mésoscopique et estimation de paramètres d'une pile aux ions lithium basée sur le LFP/Graphite

Contribution au document: Un nouveau modèle mésoscopique, permettant de simuler les phénomènes d'intercalation et de désintercalation du Li^+ à l'intérieur des particules de LFP et de représenter le comportement d'une pile aux ions lithium à base de $LiFePO_4$/Graphite, est présenté. Ce modèle est basé sur le modèle à particule unique (SPM) couplé à une approche mésoscopique afin de prendre correctement en compte les électrodes à base de $LiFePO_4$ (LFP).

Résumé français :

Un nouveau modèle numérique simulant le comportement des piles aux ions lithium (Li-ion) basées sur le $LiFePO_4$/graphite est présenté. Ce modèle est basé sur le modèle à particule unique modifié (SPM) couplé à une approche mésoscopique prenant en compte les électrodes à base de $LiFePO_4$ (LFP). Le modèle comprend une particule sphérique représentant l'électrode de graphite et N unités de LPF représentant l'électrode positive. Toutes les équations du modèle SPM sont gardées pour simuler la performance de l'électrode négative. Le modèle mésoscopique, de son côté, s'appuie sur des conditions thermodynamiques de non-équilibre et fait usage d'un potentiel à circuit ouvert non-monotone pour chaque unité de LFP. Une étude d'estimation de paramètres est également conduite pour identifier tous les paramètres requis dans le modèle. Les inconnues identifiées sont le coefficient de diffusion solide de l'électrode négative ($D_{s,n}$), la constante des réactions

d'intercalation et de désintercalation de l'électrode négative (K_n), la porosité des électrodes négative et positive (ε_n et ε_n), l'état initial de charge de l'électrode négative ($SOC_{n,0}$), la composition partielle initiale des unités de LFP ($y_{k,0}$), Les résistances minimum et maximum des unités de LFP (R_{min} et R_{max}) et la résistance électrique de la solution (R_{cell}). Les résultats montrent que le modèle mésoscopique peut simuler avec succès le comportement électrique des piles Li-ion tant à bas qu'à haut taux de décharge. Les prédictions du modèle sont en parfait accord avec les données expérimentales utilisées. Le modèle peut aussi décrire adéquatement le processus de lithiation/délithiation se déroulant au sein des particules de LFP. La principale limitation de ce nouveau modèle vient du temps de calcul élevé, surtout lorsque comparé à un modèle de type macroscopique.

7. Mesoscopic modeling and parameter estimation of a lithium-ion battery based on LFP/Graphite

7.1. Abstract

A novel numerical model for simulating the behavior of lithium-ion batteries based on $LiFePO_4$/Graphite is presented. The model is based on the modified Single Particle Model (SPM) coupled to a mesoscopic approach for the $LiFePO_4$ (LFP) electrode. The model comprises one representative spherical particle as the graphite electrode, and N LFP units as the positive electrode. All the SPM equations are retained to model the negative electrode performance. The mesoscopic model rests on non-equilibrium thermodynamic conditions and uses a non-monotonic open circuit potential for each unit. A parameter estimation study is also carried out to identify all the parameters needed for the model. The unknown parameters are the solid diffusion coefficient of the negative electrode ($D_{s,n}$), intercalation/deintercalation reaction-rate constant of the negative electrode (K_n), negative and positive electrode porosity (ε_n and ε_n), initial State Of Charge of the negative electrode ($SOC_{n,0}$), initial partial composition of the LFP units ($y_{k,0}$), minimum and maximum resistance of the LFP units (R_{min} and R_{max}), and solution resistance (R_{cell}). The results show that the mesoscopic model can simulate successfully the electric behavior of lithium-ion batteries at low and high charge/discharge rates. The predictions of the model are in excellent agreement with the experimental data. The model can also describe adequately the lithiation/delithiation of the LFP particles. The main limitation of the model is that it is computationally expensive compared to macro-based models.

Keywords: Parameter estimation; Electrochemical parameters; Mesoscopic model; Inverse method; Cylindrical Li-ion battery; LiFePO4 (LFP) positive electrode material.

Nomenclature:

A,B	The coefficients of the Murgules equations
A_p	Total area of the positive electrode, m^2
$c_{s,n}$	Solid-state concentration of Li^+ of the negative electrode, mol/m^3
$c_{s,p}$	Solid-state concentration of Li^+ of the positive electrode, mol/m^3
c_e	Electrolyte concentration of Li^+, mol/m^3
$c_{s,n}^{ini}$	Initial concentration of Li^+ in the particle of the negative electrode, mol/m^3
$c_{s,k}^{\max}$	Maximum concentration of Li^+ in the particle of electrode k $(k=p,n)$, mol/m^3
$c_{s,n}^{surf}$	Concentration of Li^+ on the surface of the particle of the negative electrode, mol/m^3
$D_{s,n}$	Li^+ diffusion coefficient in the particle of the negative electrode, m^2/s

F	Faraday's constant, C/mol
i_k	Partial current of the kth LFP unit per mole of the active material, A/mol
I	Applied current, A
J_n	Wall flux of Li^+ in the particle of the negative electrode, mol/m^{2}s
K_n	Reaction rate constant of the negative electrode, m$^{2.5}$/mol$^{0.5}$s
L_p	Total thickness of the positive electrode, m
n	Negative electrode
$O.F.$	Objective function
p	Positive electrode
r	Radial coordinate (micro grid), m
R	Universal gas constant, J/mol K
$\overline{R}$	Mean Ohmic resistance of the LFP units, Ω mol
R_{cell}	Solution phase resistance, Ω
R_{max}	Maximum Ohmic resistance of the kth LFP unit, Ω mol
R_{min}	Minimum Ohmic resistance of the kth LFP unit, Ω mol
R_k	Ohmic resistance of the kth LFP unit, Ω mol
$R_{s,n}$	Radius of the particle of the negative electrode, m
S	Standard deviation of the Ohmic resistance of the LFP units, Ω mol
S_n	Total electroactive area of the negative electrode, m^2
SOC_n	State Of Charge of the negative electrode
$SOC_{n,0}$	Initial State Of Charge of the negative electrode
t	Time, s
T	Absolute temperature, K
U_0	Standard equilibrium potential of the LFP, V
U_n	Open-circuit potential of the negative electrode, V
U_k	Open-circuit potential of the kth LFP unit, V
V_{cell}	Voltage of the cell, V
$V_{s,n}$	Total volume of the negative electrode, m^3
y_k	Li^+ partial composition in the kth LFP unit
$y_{p,0}$	Initial partial composition of the LFP units

Greek

ε_k	Fraction of active material in the kth LFP unit
ε_n	Porosity of the negative electrode
ε_p	Porosity of the positive electrode
$\mu_{s,n}$	Overpotential of the negative electrode, V
$\mu_{s,k}$	Overpotential of the kth LFP unit, V
$\Phi_{s,k}$	Solid-phase potential of electrode *k (k=p,n)*, V
$\Phi_{e,k}$	Electrolyte potential in region *k (k=p,n)*, V

7.2. Introduction

The high power and high energy density of lithium-ion (Li-ion) batteries make them attractive for storing electricity and delivering electric power on demand. Over the years, the design, structure, materials and operating conditions of these batteries have been continuously improved. As a result, their cost has been driven down and their efficiency, safety and performance have steadily increased [7, 127].

One of the most important advances in Li-ion battery technology has been the introduction of $LiFePO_4$ (LFP) as the cathode material [22]. The electronic and ionic conductivities of LFP powder has been improved by decreasing the grain size to nanoscale and by introducing a conductive carbon-coating to encapsulate the LFP particles [19, 128]. Moreover, stable and safe olivine LFP has become an attractive cathode material in batteries for electric

vehicles [22, 129]. The discharge/charge curves of LFP exhibit a voltage plateau at 3.5 (V) which is independent of the electrode state-of-charge (SOC). This behavior occurs because of the two-phase condition inside the LFP particles [22, 130, 131].

Nowadays, mathematical modelling has become an inescapable tool for the design, operation and control of Li-ion batteries. Two of the most popular electrochemical models available in the open literature are the Pseudo-Two-Dimensional (P2D) model and the Single Particle Model (SPM). In spite of the fact that that these models have been employed extensively for predicting the behavior of Li-ion batteries, they cannot, however, handle LFP cathodes [19]. The main reason is that the P2D and SP models rely on Fick's law which ignores the intercalation/deintercalation of Li^+ ions in the LFP particles. To overcome this difficulty, alternative approaches have been proposed.

In 1997, Padhi et al. suggested the shrinking-core idea to describe the insertion and the extraction processes of Li^+ ions at the surface of LFP particles. A shrinking interface inside the LFP particles is considered where the two-phase mechanism occurs. The interface around the $FePO_4$ core shrinks during Li^+ ion insertion, and grows back during Li^+ ion extraction [22]. Srinivasan and Newman employed the shrinking-core concept and implemented these two-phase phenomena in LFP spherical particles into the porous electrode theory [131]. They then determined the two-phase interface position by incorporating a mass balance between the Li-rich shell and the Li-poor core regions.

By assuming isotropic diffusion of the LFP particles, the shrinking-core porous electrode model was used to identify the behavior of the LFP electrode at macro-scale [19, 132]. Experiments showed, however, an anisotropic ionic mobility of the Li^+ ion inside the LFP crystal. As a result, the shrinking-core two-phase concept could not describe the intercalation/deintercalation of Li^+ ions at the surface of LFP particles [133, 134].

Chen et al. showed that the Li^+ ions migrate inside the LFP particles along 1D channels (the *b* direction at the phase boundary) [133]. Based on this fact, Laffont et al. suggested a "new core-shell" conceptual model [135]. By means of X-ray diffraction and electron microscopy, Delmas et al. reported the simultaneous existence of fully intercalated and fully deintercalted LFP particles in the electrode [136]. They proposed a "domino-cascade" mechanism for representing the phase boundary displacement during a charge/discharge process.

To simulate the hysteresis and the phase transition behaviour in LFP electrodes, Dreyer et al. [137] developed a thermodynamic-based model called the "many-particle" model. A non-monotonic chemical potential function profile was considered for each LFP single particle. The approach was then applied to all particles by allowing Li^+ ion exchanges between the

particles. The results showed that the lithiation/delithiation process of LFP occurs in a sequential particle-by-particle at low rates. Their model is however plagued by two limitations: the charge/discharge process is quasi-static and the transport and kinetic phenomena are ignored [137, 138]. Inspired by the many-particle model, Farkhondeh et al. [139] developed a mesoscopic model in which the LFP electrode is discretized into meso-scale units. An ohmic overpotential is defined for each unit, while the unit volume fraction is calculated by virtue of a Gaussian distribution. Despite the many-particle approach, the mesoscopic model can be used for higher charge/discharge rates [139].

Recently, the authors simulated a Li/LFP cell with the mesoscopic model coupled to the porous-electrode theory. Their results are promising. They showed that the Li^+ ion intercalation/deitercalation processes at higher rates switch to a mixed sequential-parallel regime [140]. Meanwhile, the team of Bazant developed "phase-field" models for predicting the displacement of the phase boundaries inside the LFP nanoparticles [141-144]. These models rest on non-equilibrium thermodynamics based on the Cahn-Hilliard phase-field models. In spite of the fact that this approach is expensive and time-consuming, it can predict successfully the micro behavior of LFP crystal during the Li^+ intercalation/deintercalation process [141-144].

The main drawback of all the aforementioned Li-ion battery models is that their computations are slow and expensive. All the conservation equations are solved separately for each particle or unit. As a result, these simulation models are useful for off-line applications. They cannot be implemented into Battery Management Systems (BMS) for on-line monitoring.

Anderson and Thomas proposed a mosaic model for describing the intercalation/deintercalation mechanisms of Li^+ ions at the surface of LFP spheres. This model assumes that the shrinking-core process occurs at different nucleation sites inside a LFP particle. It also assumes that the sites have identical spherical shapes with smaller radius compared to the LFP particle. Moreover, the effective radius is dependent on the battery discharge/charge rates. In other words, the diffusion coefficient for the Li^+ ions in the LFP particle varies according to the current density [124]. Different works have employed the mosaic approach to model the Li-ion battery with the LFP cathode materials [123, 145]. The results are promising. Unfortunately, the actual insertion/extraction mechanisms of Li^+ ions at the LFP particles (the *b* direction at the phase boundary and the particle-by-particle process) are not supported by this approach.

The purpose of the present paper is to model a commercial Li-ion battery by means of a mesoscopic approach for the LFP electrode. An isothermal model resting on the modified SPM with the mesoscopic model is developed. A parameter estimation study is performed in order to identify the parameters needed to run the model. The model is then employed to predict the battery performance at low and high charge/discharge rates.

7.3. Experimental data

The experimental data stem from a commercial 1.05 Ah 18650 Li_xC_6/Li_yFePO_4 cylindrical Li-ion battery. The data were kindly provided by Hydro-Québec. The experiments were conducted so as to generate the cell potential as a function of the discharge time. The electrochemical parameters were estimated for both low and high discharge rates (1C, 2C, 3.75C, 7.5C, 10C, and 15C). The experiments were performed in a climatic chamber where the temperature was maintained at 25°C. Figure 7.1 illustrates the measured cell potential functions with respect to the discharge capacity.

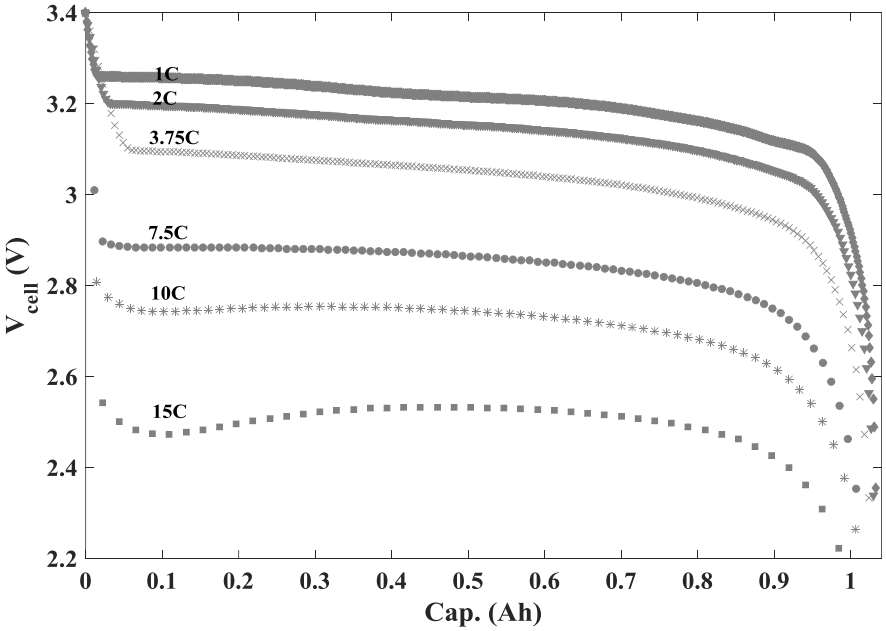

Figure 7.1: Cell potential curves of the Li-ion battery with respect to the capacity [105]

7.4. Model development

The "many-particle" model [137] twinned with the mesoscopic approach [139] was retained for simulating the unit-by-unit Li^+ intercalation/deintercalation processes inside LFP particles. The SPM was applied to model the negative electrode behavior. The negative electrode is represented by a spherical particle with the R_n radius. An equivalent surface area

is considered for the total electroactive area of the negative electrode (S_n). In order to improve the SPM accuracy, the potential drop between the positive and negative electrodes in the electrolyte is mimicked with a constant resistance (R_{cell}). Figure 7.2 illustrates the schematic of the model. As it can be seen, the whole graphite electrode is modelled as a spherical particle of radius R_n into which intercalation and deintercalation occur. The positive (LFP) electrode is comprised of different active units surrounded by carbon.

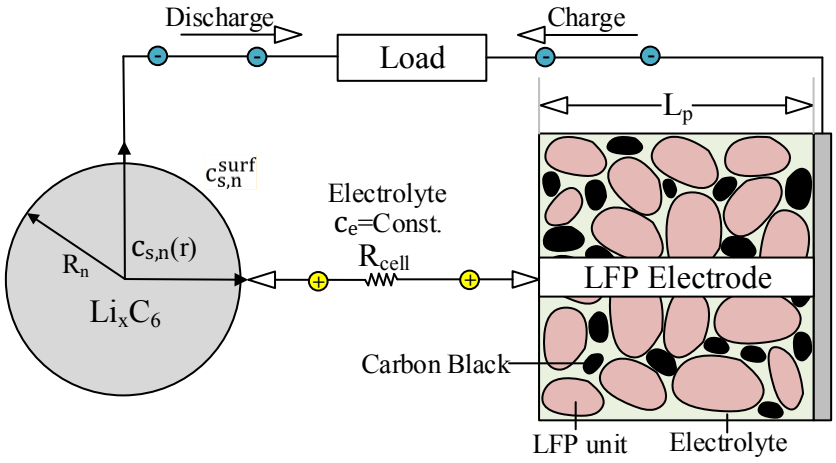

Figure 7.2: Schematic of the single particle and the mesoscopic model

7.4.1. The negative (C) electrode

The solid-state concentration of the negative spherical particle is estimated with Fick's second law [64]:

$$\frac{\partial c_{s,n}}{\partial t} = \frac{D_{s,n}}{r^2}\frac{\partial}{\partial r}\left(r^2 \frac{\partial c_{s,n}}{\partial r}\right) \tag{7.1}$$

Eq. 7.1 is solved by using the following initial and boundary conditions for the graphite particle [64]:

$$c_{s,n}(t=0) = c_{s,n}^{ini} \tag{7.2}$$

$$D_{s,n}\frac{\partial c_{s,n}(r=0)}{\partial r} = 0 \tag{7.3}$$

$$D_{s,n}\frac{\partial c_{s,n}(r=R_{s,n})}{\partial r} = -J_n \tag{7.4}$$

J_n is constant in the SPM. It is calculated as follows:

$$J_n = -\frac{I}{F\,S_n}, S_n = \frac{3\varepsilon_n V_{s,n}}{R_{s,n}} \tag{7.5}$$

Note that the battery current (I) takes a negative value when the battery is being discharged. The Butler-Volmer kinetics equation makes a connection between the wall flux (J_n), the over potential function ($\mu_{s,n}$) and the Li^+ surface concentration at the negative electrode [64]:

$$J_n = K_n \left(c_{s,n}^{\max} - c_{s,n}^{surf}\right)^{0.5} \left(c_{s,n}^{surf}\right)^{0.5} c_e^{0.5} \left[\exp\left(\frac{0.5F\mu_{s,n}}{RT}\right) - \exp\left(-\frac{0.5F\mu_{s,n}}{RT}\right)\right] \quad (7.6)$$

The over potential function of the negative electrode ($\mu_{s,n}$) is the difference between the actual and the equilibrium potential of the graphite particle:

$$\mu_{s,n} = \Phi_{s,n} - \Phi_{e,n} - U_n \quad (7.7)$$

Figure 7.3 depicts the open circuit potential function for the graphite (U_n) used in the present study [64].

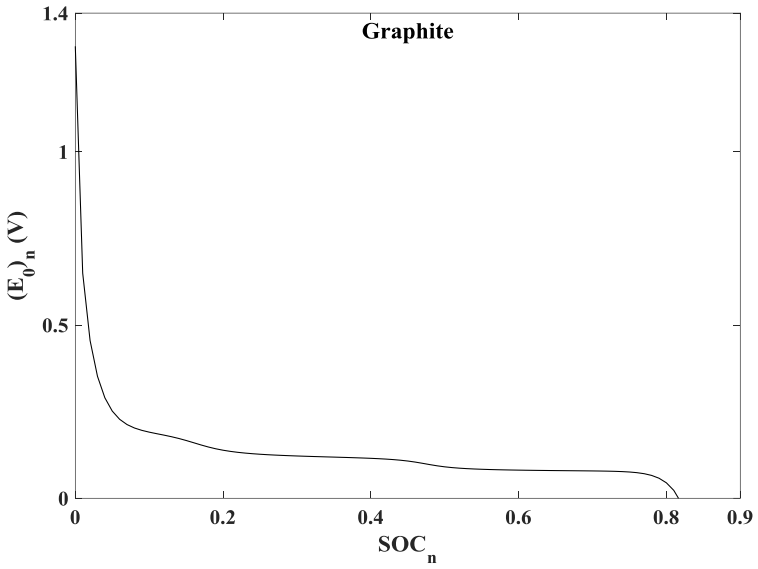

Figure 7.3: Open circuit potential function as a function of SOC for graphite [64]

7.4.2. The positive (LFP) electrode

Let us now define the concept of each unit in the LFP electrode as proposed by Dreyer *et al.* [137] and Farkhondeh *el al.* [139]. The LFP electrode is divided into *N "elementary lithiating/delithiating units"* (or *"units"* for short) with no specific geometry in the range of 50 to 1000 nm [137]. The size of each unit is small enough so that the intra-unit phase transition processes may be ignored, and large enough so that the Li^+ intercalation/deintecalation processes may take place.

By assuming the non-equilibrium condition and a homogenous lithiating/delithiating inside the units, a non-monotonic open circuit potential is considered for each unit. This function is calculated by taking the first derivative of the bulk free-energy density with respect to the

particle composition [137]. Here, a one-parameter Margules model is employed to compute the open circuit potential for the k^{th} unit as follows [150]:

$$U_k = U_0 + \frac{RT}{F} ln\left(\frac{1-y_k}{y_k}\right) + \frac{RT}{F}\left[A(2y_k - 1)\right];\ k \in \{1,2,...,N\} \tag{7.8}$$

U_0 and A are the standard equilibrium potential and the coefficient of the Margules model, respectively. The A value is positive as the intercalated Li^+ ions attract each other and as it tends to increase the system energy. It is noted that the two-parameter Margules equation (Eq. 7.9) can be also used to improve the model accuracy [150].

$$U_k = U_0 + \frac{RT}{F} ln\left(\frac{1-y_k}{y_k}\right) + \frac{RT}{F}\left[-A + 2Ay_k - B + 3By_k - \frac{3}{2}By_k^2\right];\ k \in \{1,2,...,N\} \tag{7.9}$$

The Li^+ partial composition (y_k) is defined as follows:

$$y_k = \frac{c_{s,p}}{c_{s,p}^{max}};\ k \in \{1,2,...,N\} \tag{7.10}$$

The unit partial composition function (y_k) is function of the charge/discharge time only. Figure 7.4 depicts the non-monotonic open circuit potential (U_k) of the single LFP unit with respect to the Li^+ partial composition (y_k). The points A and B define the spinodal region on the U_k curve. In this region, the LFP unit behavior is unstable. This means that the potential tends to jump from point A to point A^* when the battery is being discharged (or the LFP unit is being lithiated). The lower the discharge rate, the faster the jumping process as the discharge process gets closer to equilibrium conditions at low rates. On the other hand, the unit exhibits a rapid motion from point B to point B^* during the battery charge process (or the LFP unit delithiation). Based on this fact, Dreyer *et al.* were able to model the voltage hysteresis of the LFP electrode [137]. It is noted that the Li-poor region can be defined as $0 < y_k < 0.2$ (from the beginning of the discharge process to the point A). Also, the Li-rich region occurs from point B to the end of the discharge process (or $0.8 < y_k < 1.0$). Therefore, the lithiation/delithiation process at each LFP unit occurs between the Li-poor and the Li-rich conditions. The Li^+ ions insertion or extraction phenomena continue until all units reach to the Li-rich/Li-poor condition. This process occurs in a sequential unit-by-unit depending on the unit resistance.

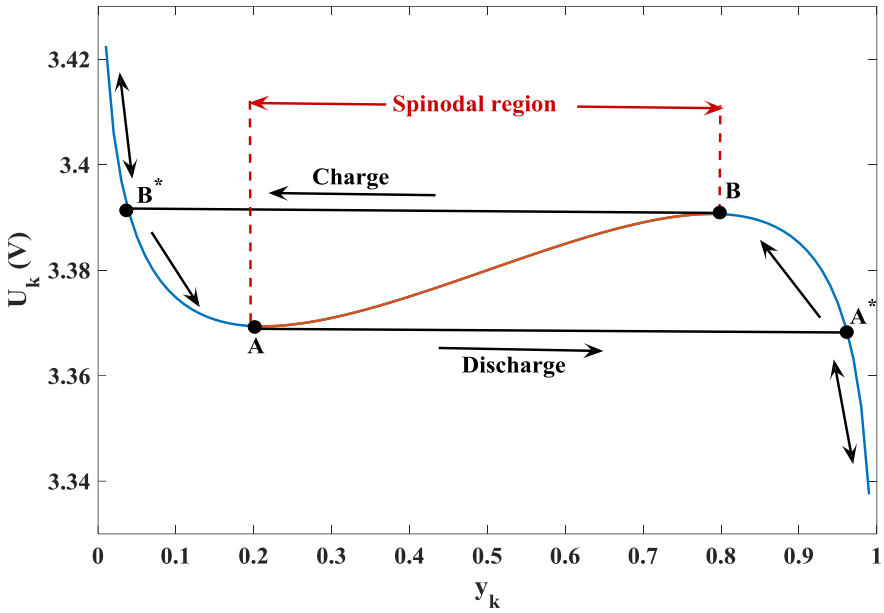

Figure 7.4: The U_k function of the single LFP unit versus y_k
(The blue and black lines show stable conditions and the red line unstable)

By defining an ohmic resistance (R_k), the polarization function ($\mu_{s,k}$) for each unit can be determined as [139]:

$$\mu_{s,k} = R_k i_k = \Phi_{s,p} - \Phi_{e,p} - U_k;\ k \in \{1,2,...,N\} \tag{7.11}$$

$\Phi_{s,p}$ and $\Phi_{e,p}$ are the solid-phase and the electrolyte potential of the LFP electrode respectively. The magnitudes of these potentials are the same for all units as they are connected to each other. It is assumed that the resistance values vary linearly between the minimum (R_{min}) and the maximum resistance (R_{max}). For consistency, the R_{min} and the R_{max} are assigned to the first and Nth unit, respectively.

Due to the fact that the Li^+ concentration is assumed uniform in each unit, the partial current (i_k) can be calculated by means of the material balance law [139],

$$i_k = -F\frac{dy_k}{dt};\ k \in \{1,2,...,N\} \tag{7.12}$$

The partial current (i_k) is calculated per mole of LFP material. This current is negative when the battery is being discharged. The total current density applied to the LFP electrode is equal to the sum of the partial currents, that is:

$$\frac{I}{A_p} = c_{s,p}^{max} L_p \varepsilon_p \sum_{k=1}^{N} \varepsilon_k i_k;\ k \in \{1,2,...,N\} \tag{7.13}$$

ε_p is the total active material volume fraction in the LFP electrode. Also, ε_k is the fraction of active material in the k^{th} unit ($\Sigma_k\ \varepsilon_k = 1$). In order to compute the ε_k values, a normal distribution function is suggested by Farkhondeh *et al.* based on the resistance values [139]:

$$\varepsilon_k = \frac{\frac{1}{S\sqrt{2\pi}} e^{\frac{-\left(R_k-\bar{R}\right)^2}{2S^2}}}{\sum_{k=1}^{N}\left[\frac{1}{S\sqrt{2\pi}} exp\left(\frac{-\left(R_k-\bar{R}\right)^2}{2S^2}\right)\right]} \tag{7.14}$$

S and $\bar{R}$ are the standard deviation and the mean resistance respectively. Eqs. 7.8 to 7.14 are solved simultaneously with the Newton–Raphson method for all units. Their solution yields the solid-phase potential of the LFP electrode. This solution procedure is however computationally slow and expensive compared to that of the macro-based model.

7.4.3. The electrolyte

As mentioned before, a constant resistance is employed for the electrolyte potential drop. This assumption increases the SPM accuracy for high charge/discharge rates and thick electrodes. As a result, the solution potential drop may be simplified with the following equation [64]:

$$\Phi_{e,p} - \Phi_{e,n} = I\, R_{cell} \tag{7.15}$$

Finally, the battery cell potential can be calculated as follows [64]:

$$V_{cell} = \Phi_{s,p} - \Phi_{s,n} \tag{7.16}$$

7.5. Parameter estimation method

In order to apply the model developed in Section 7.4 to commercial Li-ion batteries, it is imperative to specify the geometric and the electrochemical parameters. Unfortunately, some of these parameters are unknown. Moreover, their magnitude may change as the battery ages. To determine the unknown parameters, an inverse method is proposed. The inverse method is supplied with the experimental data for the cell potential of the battery. The inverse method is then able to identify the sought-after parameters without resorting to invasive measurements techniques or without dismantling the battery. A detailed description of the parameter estimation method employed in the present study is reported in [13, 104].

The nine unknown parameters are the solid diffusion coefficient of the negative electrode ($D_{s,n}$), the intercalation/deintercalation reaction-rate constant of the negative electrode (K_n), the negative and positive electrode porosity (ε_n and ε_p), the initial State Of Charge of the negative electrode ($SOC_{n,0}$), the initial partial composition of the LFP units ($y_{k,0}$), the minimum and maximum resistance of the LFP units (R_{min} and R_{max}), and the solution resistance (R_{cell}). The $SOC_{n,0}$ variable is defined as follows:

$$SOC_{n,0} = \frac{c_{s,n}^{surf}}{c_{s,n}^{max}} \tag{7.17}$$

The calculated cell potential is compared with the experimental cell potential for five discharge rates (1C, 2C, 3.75C, 7.5C, and 10C). The objective function (O.F.) is defined as the ordinary least-square function of the measured data ($\mathbf{V}_{cell,m}^{*}$) and the calculated values ($\mathbf{V}_{\text{cell}}$). The objective function for the inverse problem of N time intervals and M charge/discharge processes [13] is defined as:

$$O.F. = \left(\mathbf{V}_{cell,m}^{*} - \mathbf{V}_{cell}(\mathbf{P})\right)^{T}\left(\mathbf{V}_{cell,m}^{*} - \mathbf{V}_{cell}(\mathbf{P})\right) = \sum_{j=1}^{M}\sum_{i=1}^{N}\left(V_{cell,m,ij}^{*} - V_{cell,ij}(\mathbf{P})\right)^{2} \tag{7.18}$$

The superscript *T* indicates the transpose of the function. The expected parameters (**P**) are determined by minimizing the objective function (O.F.) in the following manner:

$$\min O.F. = O.F.(\mathbf{P}) \text{ subject to } P_{j,low} \le P_j \le P_{j,high} \tag{7.19}$$

$P_{j,low}$ and $P_{j,high}$ are the minimum and the maximum values of P_j, respectively.

Due to the complexity of the governing equations and due to the number of sought-after parameters, the objective function is minimized by means of a Genetic Algorithm (GA) [13].

7.6. Results

Numerical simulations with the direct model were carried out for a battery whose physical characteristics are summarized in Table 7.1.

Table 7.1: Known cell variables used in the model

Parameter	Symbol	Unit	Value
1C current density	I_{1C}	A	1.05
Max LFP solid phase concentration	$c_{s,p}^{max}$	mol/m^3	22806
Max graphite solid phase concentration	$c_{s,n}^{max}$	mol/m^3	31370
Average electrolyte concentration	c_e	mol/m^3	1000
Negative electrode volume	$V_{s,n}$	cm^3	2.7
Radius of the negative particle	R_n	m	1.0×10^{-6}
Positive electrode thickness	L_p	m	5.197×10^{-6}
Positive electrode surface	A_p	m^2	0.159
Number of unit	N	-	200
The standard deviation of the ε_k	S	Ω mol	1.28×10^{-3} [139]
The standard equilibrium potential	U_0	V	3.38
The Margules coefficient	A	-	3[139]
Surrounding temperature	T_{sur}	ºC	25

The GA optimization procedure was initiated with a population of 200 chromosomes and a mutation rate of 5%. The initial chromosomes were generated by using a random function

that spans the range of each sought-after parameter as reported in the open literature. The range of each parameter was also employed to update the chromosome during mutation. The objective function (Eq. 7.18) was then minimized by using the genetic operators and the experimental data for the six discharge curves (1C, 2C, 3.75C, 7.5C, 10C and 15C). The expected parameters were finally determined at the optimum point. Table 7.2 reports the range and the estimated values for the unknown parameters.

Table 7.2: Electrochemical parameters estimated for the Li-ion battery

Symbol	Unit	Min	Max	Value
$D_{s,n}$	m^2/s	1.00×10^{-15}	10.00×10^{-15}	9.7×10^{-15}
K_n	$m^{2.5}/mol^{0.5}\ s$	1.00×10^{-11}	10.00×10^{-11}	9.44×10^{-11}
ε_n	-	0.50	0.60	0.58
$SOC_{n,0}$	-	0.75	0.85	0.76
ε_p	-	0.30	0.40	0.376
$y_{p,0}$	-	0.01	0.06	0.044
R_{min}	$\Omega\ mol$	1.0×10^{-5}	10.0×10^{-5}	9.55×10^{-5}
R_{max}	$\Omega\ mol$	1.0×10^{-3}	10.0×10^{-3}	2.30×10^{-3}
R_{cell}	Ω	0.01	0.10	0.039

To check the accuracy of the estimated parameters, they were plugged back into the direct model. The predictions of the direct model were then compared to the experimental data (Figure 7.5).

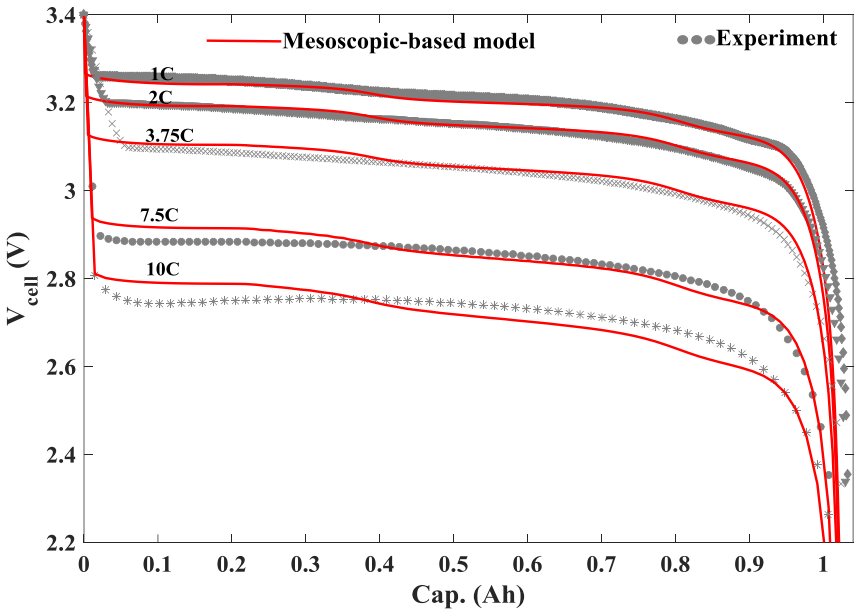

Figure 7.5: Predictions of the cell potentials versus experimental data

Fig. 7.5 shows that the agreement between the predictions and the experimental data is excellent. The computational time for the mesoscopic-based model was found, however, to be roughly 10 times larger than that for the Modified Mosaic (MM) model (the current-dependent radius). A detailed description of the MM model is provided in [148]. Figure 7.6 compares the results from the mesoscopic-based model to that from the MM model for discharge rates varying from 1C to 15C. Note that the mesoscopic-scale model is based on isotherm conditions, while the effects of the battery temperature change are taken into account in the MM model. It is seen that the predictions of both models are close to the experimental data for both low and high discharge rates. The bottom line is that the mesoscopic-based model is accurate but slow. Therefore, it would be helpful for off-line applications and the prediction of the LFP electrode behavior.

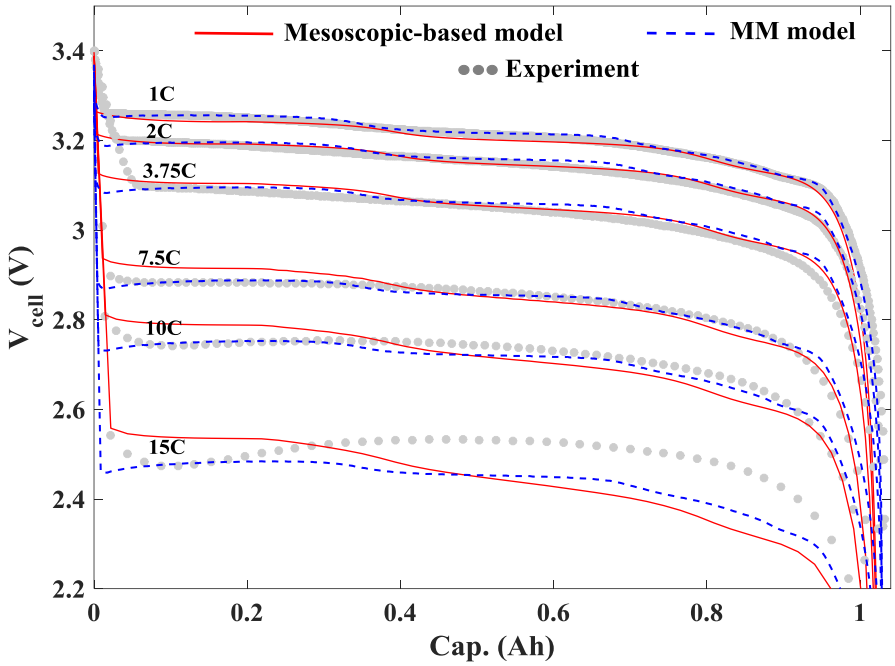

Figure 7.6: The mesoscopic-based model versus the MM model

Figure 7.7 shows the Li^+ partial composition (y_k) for all LFP units with respect to the discharge time at 1C rate. It also illustrates the evolution of the cell potential (V_{cell}). The y_k values are chiefly composed of two regions: the Li-poor (blue color) and Li-rich (yellow color). Only a few LFP units are in the spinodal region ($0.2 < y_k < 0.8$) at the end of discharge process. Due to the negative electrode capacity and/or due to the dominance of the negative electrode, the unstable condition in the spinodal region does not shift to the stable region.

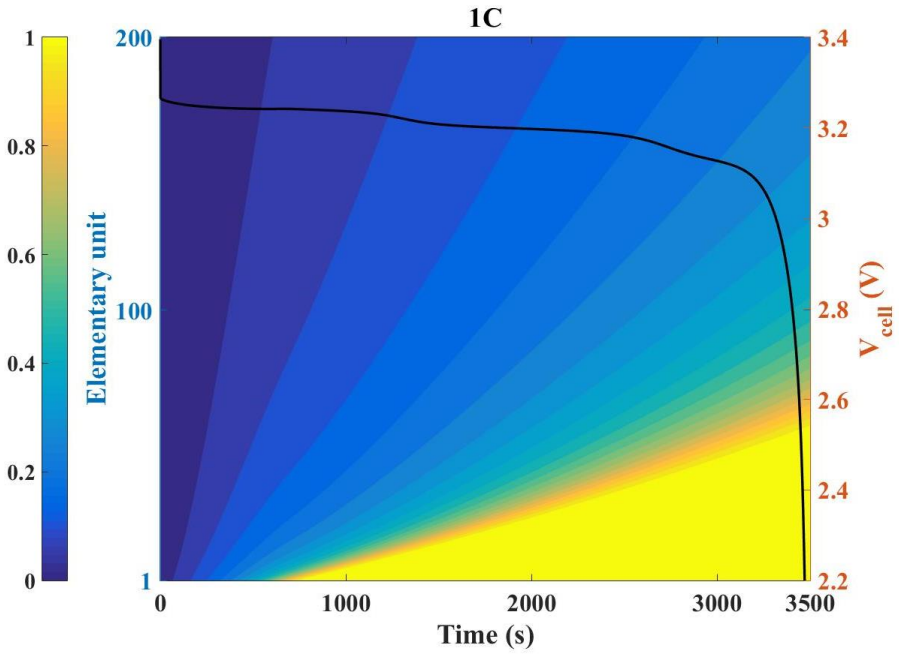

Figure 7.7: y_k values for all units and V_{cell} versus the discharge time at 1C rate

7.7. Conclusion

A novel numerical model for simulating the behavior of lithium-ion batteries was presented. The model is based on the modified Single Particle Model (SPM) coupled to a mesoscopic approach for the $LiFePO_4$ (LFP) electrode. The model comprises one representative spherical particle as the graphite electrode, and N LFP units as the positive electrode. All the SPM equations are retained to model the negative electrode performance. The mesoscopic model rests on non-equilibrium thermodynamic conditions and it uses a non-monotonic open circuit potential for each unit. A parameter estimation study was carried out to identify all the parameters needed for the model. The unknown parameters are the solid diffusion coefficient of the negative electrode ($D_{s,n}$), the intercalation/deintercalation reaction-rate constant of the negative electrode (K_n), the negative and positive electrode porosity (ε_n and ε_p), the initial State Of Charge of the negative electrode ($SOC_{n,0}$), the initial partial composition of the LFP units ($y_{k,0}$), the minimum and maximum resistance of the LFP units (R_{min} and R_{max}), and the solution resistance (R_{cell}). The results showed that the mesoscopic model can simulate successfully the electric behavior of lithium-ion batteries at low and high charge/discharge rates. The predictions of the model are in excellent agreement with the experimental data. The model can also mimic adequately the lithiation/delithiation of the LFP particles. The main limitation of the model is that it is computationally expensive compared to macro-based models.

7.8. Acknowledgements

The authors are very grateful to Hydro-Québec and to the Natural Sciences and Engineering Council of Canada (NSERC) for their financial support.

CHAPITRE 8 : AVANT-PROPOS

Auteurs et affiliation:

- Ali Jokar: étudiant au doctorat, Université de Sherbrooke, Faculté de génie, Département de génie chimique et de génie biotechnologique.
- Barzin Rajabloo: étudiant au doctorat, Université de Sherbrooke, Faculté de génie, Département de génie chimique et de génie biotechnologique.
- Martin Désilets: professeur, Université de Sherbrooke, Faculté de génie, Département de génie chimique et de génie biotechnologique.
- Marcel Lacroix: professeur, Université de Sherbrooke, Faculté de génie, Département de génie mécanique.

Date d'acceptation: 09 Sep. 2016

État de l'acceptation: version finale publiée

Revue: ECS Transactions

Référence: [151]

Titre français: Une étude d'estimation en ligne de paramètres électrochimiques de piles aux ions lithium basée sur l'utilisation de réseaux neuronaux

Contribution au document: Dans cet article scientifique, une méthode en temps réel est proposée pour l'estimation des propriétés électrochimiques d'une pile aux ions lithium. Cette technique repose sur l'utilisation de réseaux neuronaux qui sont entraînés à l'aide d'un modèle à particule unique.

Résumé français :

Une technique en ligne basée sur les réseaux neuronaux (NN) est proposée pour l'estimation de propriétés électrochimiques de piles aux ions lithium (Li-ion). Le modèle à particule unique (SPM) a été retenu pour entraîner le modèle NN, qui est ensuite utilisé pour l'estimation des coefficients de difusion ($D_{s,n}$ et $D_{s,p}$), des constantes pour les réactions d'intercalation et de désintercalation (K_n et K_p) aux électrodes, la résistance de l'électrolyte (R_{cell}) et la courbe de décharge. Les résultats montrent que le modèle NN proposé est précis, performant en terme de temps de calcul et donc approprié à l'estimation en ligne de paramètres. Le modèle NN peut aussi être adapté à l'estimation d'une quantité importante de paramètres d'entrée et de sortie. Finalement, il est probable que le modèle NN présenté trouve des applications au sein des systèmes de gestion des batteries.

8. An on-line electrochemical parameter estimation study of lithium-ion batteries using neural networks

8.1. Abstract

A real time neural network (NN) technique is presented for estimating the electrochemical properties of Li-ion batteries. The Single Particle Model is retained to train the NN model. The resulting NN model is then used to estimate the diffusion coefficients ($D_{s,n}$ & $D_{s,p}$) and the intercalation/deintercalation reaction-rate constants (K_n & K_p) of the electrodes, the electrolyte resistance of the battery (R_{cell}) and its discharge curve. The results show that the proposed NN model is computationally performant, accurate and befitting on-line parameter estimations. The NN model is also adaptable to a multitude of input variables and output parameters. As a result, it is expected that the present NN model will find applications in Battery Management Systems.

Keywords: On-line parameter estimation; Inverse method; Li-ion battery; Neural Networks; Battery management systems.

Nomenclature:

$c_{s,k}$	Solid-state concentration of electrode *k (k=p,n)*, mol/m^3
$c_{e,k}$	Electrolyte concentration in region *k (k=p,s,n)*, mol/m^3
$c_{s,k}^{\max}$	Maximum concentration of Li^+ in the particle of electrode *k (k=p,n)*, mol/m^3
$c_{s,k}^{surf}$	Concentration of Li^+ on the surface of the particles of the electrode *k (k=p,n)*, mol/m^3
$D_{s,k}$	Li^+ diffusion coefficient in the particle of electrode *k (k=p,n)*, m^2/s
d	Desired value in neural networks
E	Error function in neural networks
e_r	Relative error, %
F	Faraday's constant, C/mol
f_i	Activation function of neurons of neural networks
I	Applied current density, A/m^2
J_k	Wall flux of Li^+ on the particle of *k (k=p,n)*, mol/m^{2}s
K_k	Reaction rate constant of electrode *k (k=p,n)*, m$^{2.5}$/mol$^{0.5}$s
n	Negative electrode
O	Output variable in neural networks
p	Positive electrode
r	Radial coordinate, m
s	Separator
R	Universal gas constant, J/mol K
R_{cell}	Solution phase resistance, Ω
$R_{s,k}$	Radius of the particle of electrode *k (k=p,n)*, m

S_k	Total electroactive area of electrode k, m^2
SOC_k	State Of Charge of electrode *k (k=p,n)*
$SOC_{k,0}$	Initial State Of Charge of electrode *k (k=p,n)*
t	Time, s
T	Absolute temperature, K
U_k	Open-circuit potential of electrode *k (k=p,n)*, V
V_{cell}	Voltage of cell, V
V_k	Total volume of electrode k, m^3
w_{ij}	Weights between neurons of neural networks
x	Spatial coordinate, m

Greek

δ_i	Error of each neuron of neural network
ε_k	Porosity of region *k (k=p,s,n)*
η	Learning rate of neural networks
$\mu_{s,k}$	Overpotential of electrode *k (k=p,n)*, V
$\Phi_{s,k}$	Solid-phase potential of electrode k $(k = p, n)$, V
$\Phi_{e,k}$	Electrolyte potential in region *k (k=p,s,n)*, V

8.2. Introduction

Several studies have been devoted to the electrochemical modeling of lithium-ion (Li-ion) batteries. The pseudo-two-dimensional (P2D) model and the Single Particle Model (SPM) appear to be the most popular electrochemical models for this battery [1, 9, 10, 34]. The success of these models depends, among other things, on the precise knowledge of the electrochemical properties of the battery [11-13]. Direct measurement of these properties is, however, a tedious task. It typically requires the dismantling of the battery. Moreover, the measured properties are dependent on the battery's age and may vary according to the measurement technique.

To overcome the difficulties of measuring the battery properties, parameter estimation techniques coupled to inverse methods have been proposed. These techniques are based on optimization algorithms that aim at minimizing the discrepancy between the predictions of a direct model (including the estimated parameters) and the experimental data.

Santhanagopalan et al. employed a Levenberg-Marquardt (LM) technique to identify five internal parameters of Li-ion batteries [11]. Ramadesigan et al. investigated the effect of five different parameters on the capacity fade of Li-ion batteries using battery discharge curves and the Gauss-Newton technique [92]. Forman et al. implemented a full parameter estimation using the P2D model as the forward model and a Genetic Algorithm (GA) as the optimizer [93]. Zhang et al. conducted a multi-objective parameter estimation by means of

the discharge curves and the surface temperatures of Li-ion batteries made with $LiCoO_2$ and $LiFePO_4$ cathodes [98]. Masoudi et al. proposed a mathematical model based on a reduced order of the P2D model and the homotopy optimization approach. Their model was employed to estimate six internal parameters of the Li-ion batteries [99]. Rahman et al. identified four electrochemical variables of Li-ion batteries by using Particle Swarm Optimization (PSO) and a reduced P2D model [100]. More recently, the authors developed a parameter estimation method for conducting sensitivity analyses. Eight electrochemical parameters of Li-ion batteries made of different cathode materials were successfully identified, for both low and high discharge rates [13].

The major drawback of all the aforementioned inverse parameter estimation methods is that they are computationally expensive. This is due to the complexity of the model equations of the Li-ion battery and to the limited performance of the optimizers. As a result, the inverse parameter estimation methods are not pertinent for on-line control, monitoring and Battery Management Systems (BMSs). The promising alternative to these methods is the Artificial neural network (NN).

An artificial neural network (NN) is a computing system comprising many nonlinear processing elements connected to each other. These elements are called neurons. Each connection has a weight to be determined in the NN training. The training process is generally implemented by means of known experimental data. The data provide the input neurons. The trained NN may then simulate and identify the system by using a black box approach [102, 152, 153].

NNs have been employed in the past to investigate the performance of Li-ion batteries. Ulltah et al. proposed a neural-fuzzy approach to design a fast battery charger by using data from the characteristics curves of batteries [154]. Grewal and Grant applied the artificial NNs to a Li-ion battery pack for cellular phones. The model was employed to determine the State of Charge (SoC) of the battery pack [155]. Affanni et al. used the NN to estimate the SoC of a Li-ion battery pack in order to control electric vehicles [156]. Chau et al. employed a combination of the NNs and fuzzy concepts, namely adaptive neuro-fuzzy inference system, to calculate the state of available capacity of Li-ion batteries. The discharge capacity and the operating temperature were used for NN training [157]. Li et al. applied fuzzy NNs using B-spline membership into Li-ion battery. A genetic algorithm was also adopted for adjusting the free parameters and for computing the battery pack SoC [158]. Parthiban applied a NNs-based approach to a Co/Li cell in order to predict the charge/discharge capacity from charge/discharge cycle data. Parthiban was then able to predict accurately the

cell capacity after 50 cycles [159]. Charkhgard and Farrokhi employed radial basis function and neural networks coupled to Kalman filter (KF) to estimate the SoC of a Li-ion battery. Their results showed good agreement with experimental data. Unfortunately, their model could not account for the effect of the temperature and the aging process on the battery [160]. Finally, Eddahech et al. [161] and later Lin et al. [162] took on NNs to predict the State of Health (SoH) of Li-ion batteries.

Nearly all of the above mentioned studies were conducted however with the sole purpose of calculating the SoC or the SoH of Li-ion batteries. Furthermore, the data needed for training the NNs all rely on empirical battery models.

The present paper proposes a new NN method for real-time control and monitoring of Battery Management Systems (BMSs). The NN method identifies five electrochemical parameters: the diffusion coefficients of the electrodes ($D_{s,n}$ & $D_{s,p}$), their intercalation/deintercalation reaction-rate constants (K_n & K_p) and the electrolyte resistance of the battery (R_{cell}). The black box approach rests the 1C discharge curve of a Li-ion battery made with a $LiCoO_2$ cathode. The data needed for the training of the NN are generated with an improved SPM. The 1C discharge curves are first calculated for a range of the expected parameters. The data are then used to determine the weights and the functions of the NN.

8.3. Artificial Neural Networks

Artificial neural networks are comprised of many processing elements (neurons) connected to each other. A feed forward multilayer NN is commonly used for the simulation of physical systems. It consists of an input layer, an output layer and one or more hidden layers. The input variables are introduced to the network through the input neurons (Figure 8.1). The output information is then determined from the output neurons by means of nonlinear transformations in the hidden layer(s). The nonlinear transformations are composed of the weights of the connection between two neurons. A distinct nonlinear function pertains to each neuron [152, 163].

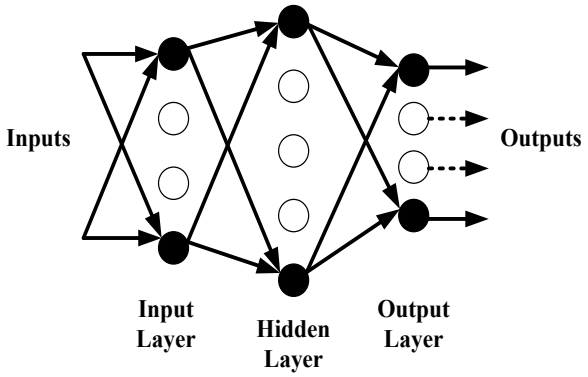

Figure 8.1: The overall schematic of a feed forward multilayer NN

The back-propagation error algorithm is a common method to obtain the optimum value of the weights in a NN. It minimizes a quadratic cost function by the gradient descent method. During the network training process, the weights are adjusted according to the inputs and the corresponding outputs. At the beginning of the training process, inputs are introduced into the network and propagated forward to generate the outputs. An error is generated by the difference between the computed and the desired outputs. The weights are then fine-tuned by the back-propagation error algorithm. The process is repeated until an acceptable tolerance error is achieved [152, 153]. The network weights are calculated by means of decreasing the network error function. This function is defined as follows [163]:

$$E_p = \frac{1}{2}\sum_{k=1}^{K}(d_{pk} - O_{pk})^2 \qquad (8.1)$$

E_p is the error function, d_{pk} is the desired value, and O_{pk} is the output variable. According to the back-propagation error algorithm, the output of each neuron is computed as follows [152]:

$$O_i = f_i(\sum_{j=0}^{m} w_{ij} O_j) \qquad (8.2)$$

O_i is the output of the i^{th} neuron from its layer, O_j is the output of the j^{th} neuron from the previous layer, f_i is the activation function of the i^{th} neuron, w_{ij} is the weight between the j^{th} and the i^{th} neuron and m is the total number of inputs applied to the i^{th} neuron including bias. The weights are adjusted by the back-propagation error algorithm according to the following rule [159]:

$$\Delta w_{ij}(n+1) = \eta(\delta_i . O_i) \qquad (8.3)$$

n indicates the number of iterations or epochs, η is the learning rate, and δ_i is the error on the i^{th} neuron. The value of δ_i for the output i^{th} neuron is the difference between the desired

values, i.e. d_i and O_i . The recommended range for the learning rate or for the convergence coefficient (η) is $10^{-4} < \eta < 1$ [152].

In this paper, the batch learning method is retained. This method is known to be memory efficient and it provides accurate training [163]. In spite of the fact that the batch learning method is computationally slower than the pattern-by-pattern learning method, it is not, however, sensitive to the order of the training pattern. Moreover, no data are dismissed in the network. Hence, during the first iteration of the training process (the first epoch), the network weights are trained by the entire data set in the following manner [163]:

$$\Delta w_j = \frac{1}{P}\sum_{i=1}^{P}\Delta w_{ij} \qquad (8.4)$$

p represents the number of training patterns. To alleviate the problem of slow convergence of the batch training method and to avoid falling into local minimums, an adaptive η approach is used. In this technique, η is computed based on the variations of training errors as follows:

$$\eta(i+1) = \begin{cases} k_1\eta(i) & \Delta E(i) > 0 \\ k_2\eta(i) & \Delta E(i) < 0 \end{cases} \qquad (5)$$

k_1 and k_2 are constant. Their magnitudes are in the range $0 < k_1 < 1 < k_2$. These constants depend on the type of data and the network size [163]. For the present study, they were estimated at k_1=0.94 and k_2=1.04 by means of a sensitivity analysis. Moreover, the optimum number of hidden layers and the optimum number of neurons are chosen according to the type of system under simulation and the number of training data [152]. Of course, the bigger the number of layers and the number of neurons, the longer the training run-times.

8.4. Single Particle Model

Electrochemical models of Li-ion batteries are more sophisticated that empirical-based models [10, 11]. To this day, the Pseudo-two-Dimensional (P2D) model appears to be the most accurate electrochemical-based model. This model was first developed by Doyle et al. [1, 34]. In order to reduce the computational time, Zhang et al. proposed a simplified version of the P2D model known as the Single Particle Model (SPM). The SPM rests on two main assumptions: First, each electrode (Figure 8.2) is modeled as a spherical particle in which intercalation and de-intercalation phenomena occur. Second, variations of the electrolyte properties are ignored [9, 54]. Due to its simple equations and the low computational time,

the SPM model is befitting many practical applications such as parameter estimation, real-time control modeling and life modeling of Li-ion batteries.

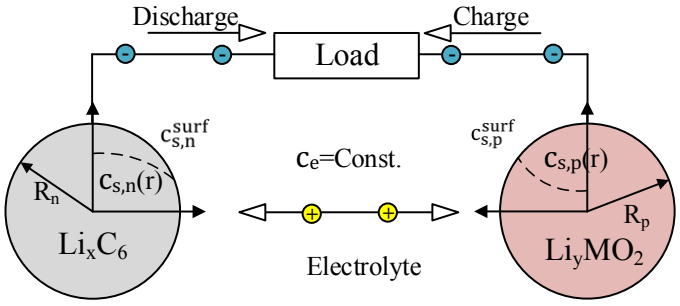

Figure 8.2: Schematic of the Single Particle Model (SPM)

Eqs. 8.6) and (8.7) show the governing equations of the SPM. These equations are comprised of the solid-state concentration and the Butler-Volmer kinetics relations for both the negative and the positive electrodes [54, 64].

$$\frac{\partial c_{s,k}(x,r,t)}{\partial t} = \frac{D_{s,k}}{r^2}\frac{\partial}{\partial r}\left(r^2 \frac{\partial c_{s,k}(x,r,t)}{\partial r}\right) \tag{8.6}$$

$$J_k(x,t) = K_k\left(c_{s,k}^{\max} - c_{s,k}^{surf}\right)^{0.5}\left(c_{s,k}^{surf}\right)^{0.5} c_{e,k}^{0.5}\left[\exp\left(\frac{0.5F\mu_{s,k}(x,t)}{RT}\right) - \exp\left(-\frac{0.5F\mu_{s,k}(x,t)}{RT}\right)\right] \tag{8.7}$$

$\mu_{s,k}$ is the over potential function of each electrode. It is calculated as follows:

$$\mu_{s,k}(x,t) = \Phi_{s,k}(x,t) - \Phi_{e,k}(x,t) - U_k;\ V_{cell}(t) = \Phi_{s,p} - \Phi_{s,n} \tag{8.8}$$

In order to improve the SPM accuracy, the potential drop between the positive and the negative electrodes in the electrolyte is simplified with the following equation [64]:

$$\Phi_{e,p} - \Phi_{e,n} = IR_{cell} \tag{8.9}$$

The cell potential function of the Li-ion battery can then be determined as [64]:

$$V_{cell} = \left(U_p - U_n\right) + \frac{2RT}{F}\ln\left(\frac{\sqrt{m_p^2+4}+m_p}{2}\right) + \frac{2RT}{F}\ln\left(\frac{\sqrt{m_n^2+4}+m_n}{2}\right) + IR_{cell} \tag{8.10}$$

$$m_p = \frac{I}{FK_pS_pc_{s,p}^{\max}c_e^{0.5}\left(1-SOC_p\right)^{0.5}\left(SOC_p\right)^{0.5}};\ S_p = \frac{3\varepsilon_pV_p}{R_p},\ SOC_p = \frac{c_{s,p}^{surf}}{c_{s,p}^{\max}} \tag{8.11}$$

$$m_n = \frac{I}{FK_nS_nc_{s,n}^{\max}c_e^{0.5}\left(1-SOC_n\right)^{0.5}\left(SOC_n\right)^{0.5}};\ S_n = \frac{3\varepsilon_nV_n}{R_n},\ SOC_n = \frac{c_{s,n}^{surf}}{c_{s,n}^{\max}} \tag{8.12}$$

If the SPM is to be retained for a BMS, it is imperative to know the geometric properties, the material properties and the operating parameters of the battery. The geometric and the material properties can be determined from direct measurements. They may also be provided

by the manufacturers. The operating parameters are, on the other hand, not readily available. Some of these parameters may vary according to the measurement techniques or the battery age. Moreover, the measurement of the parameters sometimes requires the dismantling of the battery. To avoid such a brute force solution and maintain the integrity of the battery, a NN parameter estimation method was developed for estimating five key parameters. These parameters are the diffusion coefficients ($D_{s,n}$ & $D_{s,p}$) and the intercalation/deintercalation reaction-rate constants (K_n & K_p) of the electrodes, and the electrolyte resistance (R_{cell}) of the battery. Table 8.1 lists the other cell variables used in the SPM. The open circuit potential functions for Li_yCoO_2 and Li_xC_6 cathodes are provided by Eqs. 8.13 and 8.14 respectively [64].

Table 8.1: Cell properties used in the SPM [64]

0	Unit	k=n	k=p
R	J/mol K	8.3143	
T	K	298	
F	C/mol	96485	
I	A/m^2	1.656	
c_e	mol/m^3	1000	
R_k	m	12.5e-6	8.5e-6
$SOC_{k,0}$	-	0.742	0.495
S_k	m^2	0.7824	1.1167
$c_{s,k}^{\max}$	mol/m^3	31833	51410

$$U_p = 4.04596 + \exp(-42.30027\ SOC_p + 16.56714) - 0.04880\arctan(50.01833\,SOC_p - 26.48897) - 0.05447\arctan(18.99678\,SOC_p - 12.32362) - \exp(78.24095\,SOC_p - 78.68074) \quad (8.13)$$

$$U_n = 0.13966 + 0.68920\exp(-49.20361\ SOC_n) + 0.41903\exp(-254.40067\,SOC_n) - \exp(49.97886\,SOC_n - 43.37888) - 0.028221\arctan(22.52300\,SOC_n - 3.65328) - 0.01308\arctan(28.34801\,SOC_n - 13.43960) \quad (8.14)$$

8.5. The on-line inverse PE

Inverse problems are ill-posed mathematical problems. As a result, their solution is usually more challenging than that for direct problems. Inverse problems are dependent on the initial and the boundary conditions, as well as on the measured signals [14, 15].

The inverse parameter estimation approach has been employed to identify the unknown characteristics of Li-ion batteries. This technique is based on optimization algorithms whose

aim is to minimize the discrepancy between the predictions of a direct model (including the estimated parameters) and the experimental data. The major drawback of inverse methods is that they are computationally expensive. The equations of Li-ion battery models are complex and the performance of the optimizers is limited. Consequently, inverse methods are poor candidates for on-line control, monitoring and/or Battery Management Systems (BMSs). Further details concerning inverse methods can be found in [11, 13].

To tackle this difficulty, an original inverse method resting on a trained NN was developed. This method is adapted to the on-line estimation of electrochemical parameters of Li-ion batteries. The input of the NN is comprised of a 1C discharge curve of a Li-ion battery made with a $LiCoO_2$ cathode. The input matrix is introduced into the NN as a time domain parameter that includes a small time interval between zero and the cut-off time ($0 < t \leq t_c$):

$$\mathbf{V}_{cell,1C} = \begin{bmatrix} V_1 \\ V2 \\ \vdots \\ V_N \end{bmatrix}_{N\times 1} ; t = t_1, t_2, ..., t_N \qquad (8.15)$$

N is the number of cell potential measurements. N is equal to the number of neurons in the NN input layer. The outputs of the model are the five electrochemical properties of the battery, that is, $D_{s,n}$, $D_{s,p}$, K_n , K_p and R_{cell}. Due to the matrix-based structure of the NN, the model estimates immediately the expected parameters after the training process. Figure 8.3 shows a schematic of the on-line estimator.

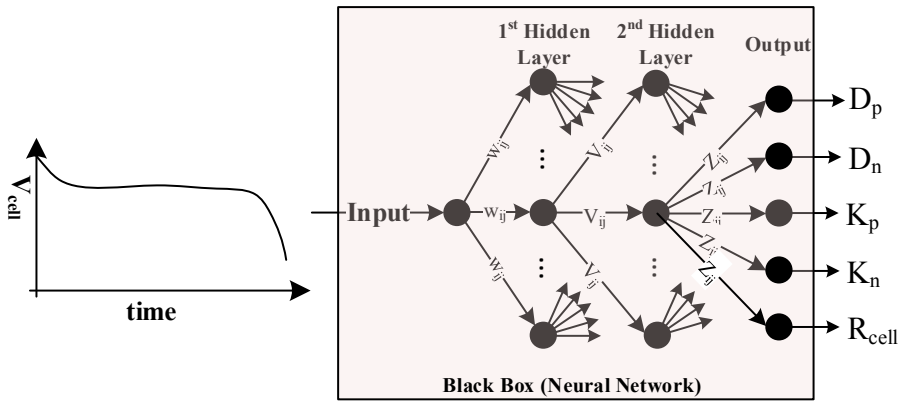

Figure 8.3: On-line parameter estimation for Li-ion batteries using neural network

8.6. The NN training

The NN modelling of Li-ion batteries was implemented with four different layers: one input layer, two hidden layers and one output layer. The input layer contains 37 neurons for the 1C discharge curve matrix. Measurements were taken at time intervals of 100 seconds over

a time period of one hour. Furthermore, two hidden layers comprising 50 and 75 neurons were employed in order to minimize the training error. The output layer provided the five signals that characterize the electrochemical properties. Figure 8.4 exemplifies the resulting network architecture.

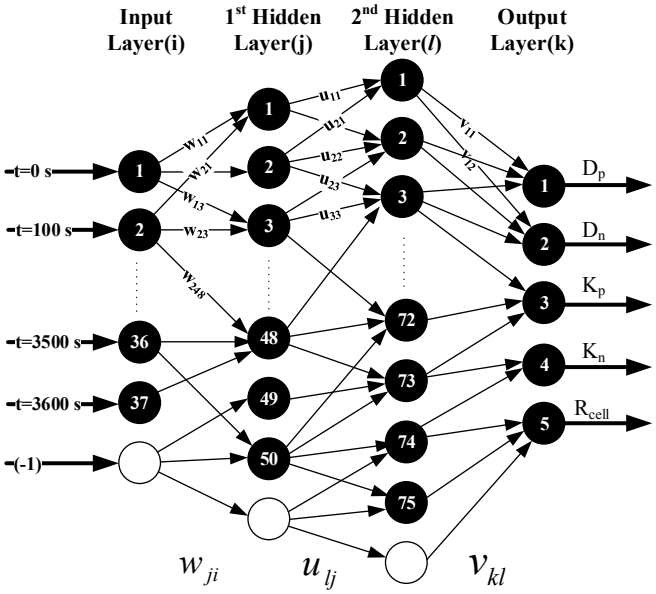

Figure 8.4: Network structure for the NN on-line parameter estimation of Li-ion batteries

The data needed for the training of the NN were generated with the SPM. The 1C discharge curves were first calculated for a range of the expected parameters. This range was delineated by considering five different values of each parameter (Table 8.2). As a result, the SPM was run for 3125 datasets (5^5) for computing the 1C discharge curves of the Li-ion battery.

Table 8.2: Range for the expected parameters

Symbol	Unit	Dataset				
		Min (1)	(2)	(3)	(4)	Max (5)
$D_{s,p}$	m^2/s	5.00e-15	7.50e-15	1.00e-14	1.25e-14	1.50e-14
$D_{s,n}$	m^2/s	1.50e-14	2.25e-14	3.00e-14	3.75e-14	4.50e-14
K_p	$m^{2.5}/mol^{0.5}$ s	3.30e-11	4.975e-11	6.65e-11	8.325e-11	1.00e-10
K_n	$m^{2.5}/mol^{0.5}$ s	9.00e-12	1.35e-11	1.80e-11	2.25e-11	2.70e-11
R_{cell}	Ω	0.01	0.0125	0.015	0.0175	0.02

The data were then employed to train the NN so as to determine the internal weights and functions. The training process was next deployed into three steps. First, all inputs and

outputs variables were normalized in the interval of [-1,1]. Second, the optimum number of training iterations (epochs) was calculated. Seventy percent (70 %) of the generated data was randomly employed to train the network. The remaining data (30%) were used to test the performance of the network. It was found that the 2000th epoch is the optimum training epoch, i.e., it is the epoch for which the computational cost is minimized. Figure 8.5 illustrates the training and the test error as a function of the training epoch number. Third, once the optimum number of iteration was determined, the model was trained once again for all the available data. Figure 8.6 shows the training error as a function of the number of training epochs. Finally, the resulting neural network was used to estimate the electrochemical properties for different 1C discharge curves.

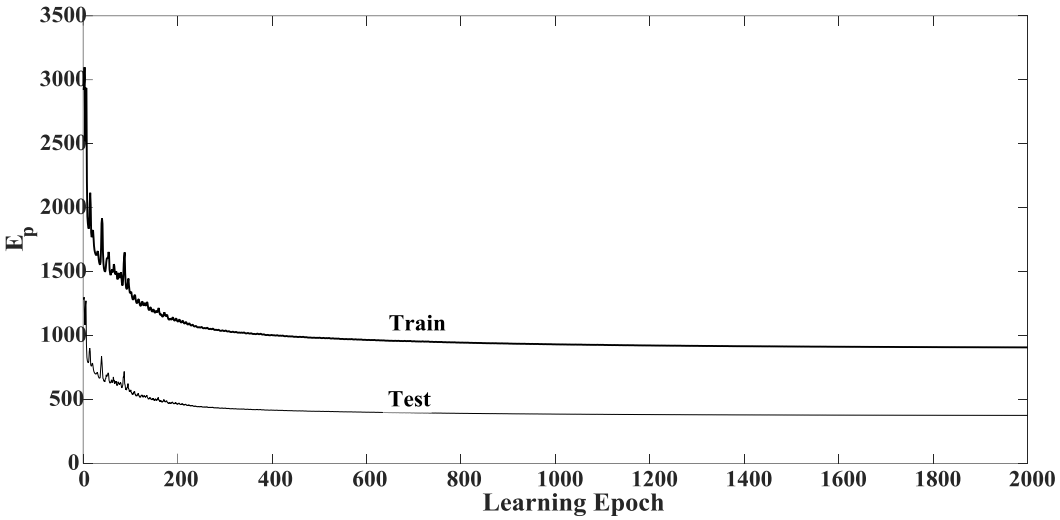

Figure 8.5: Training and test error as a function of the number of learning epochs

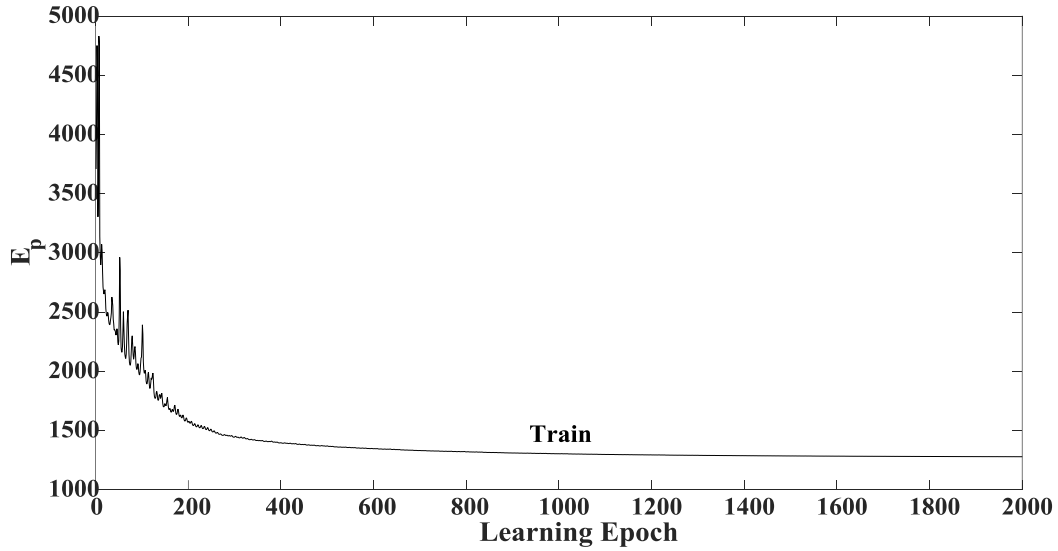

Figure 8.6: Training error as a function of the number of training epochs

8.7. Implementation

The performance of the on-line parameter NN estimator was tested for the following two scenarios.

8.7.1. Scenario 1: The calculated discharge curve

In this scenario, the NN-based model is compared to the computed data obtained with the SPM. First, the SPM is run to determine the calculated cell potential function by using the known parameters. Table 8.3 shows the values retained for the expected parameters. Second, the calculated cell potential function is introduced into the trained NN for estimating the expected variables. And third, the results for the parameters and the cell potential are compared. The flowchart of Scenario 1 is depicted in Figure 8.7.

Table 8.3: Known parameters used in scenario 1

Symbol	Unit	Value
$D_{s,p}$	m^2/s	1.0e-14
$D_{s,n}$	m^2/s	3.9e-14
K_p	$m^{2.5}/mol^{0.5}$ s	3.67e-11
K_n	$m^{2.5}/mol^{0.5}$ s	1.76e-11
R_{cell}	Ω	0.0162

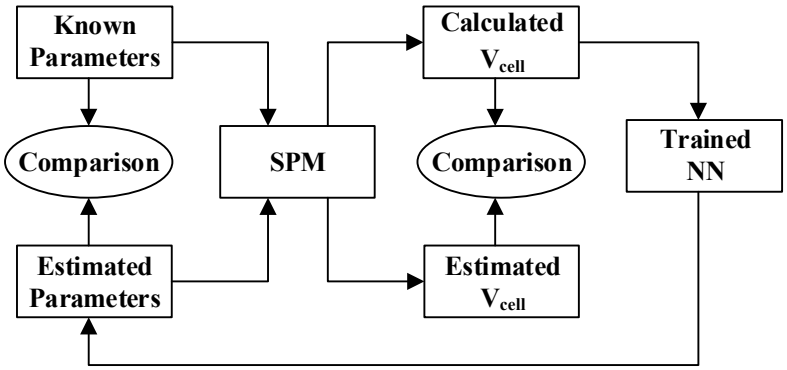

Figure 8.7: Flowchart of Scenario 1

Figure 8.8 illustrates the relative error for the estimated parameters. The relative error is defined as

$$e_r = \left| \frac{P_E - P_{real}}{P_{real}} \right| \times 100 \qquad (8.16)$$

P_E is the estimated parameter and P_{real} is the known parameter. Examination of Figure 8.8 reveals that the predictions of the NN are excellent.

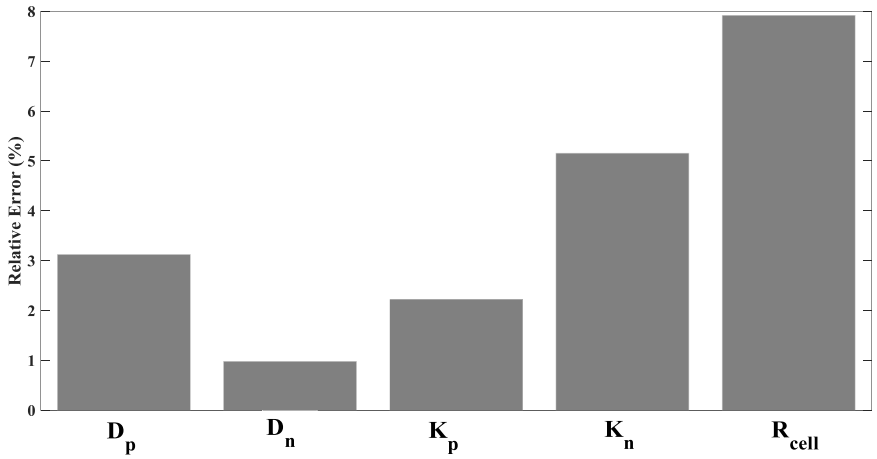

Figure 8.8: Relative error for the estimated parameters

Figure 8.9 compares the calculated and the estimated cell potential using the NN model and the SPM model. Once again, the results are in very good agreement.

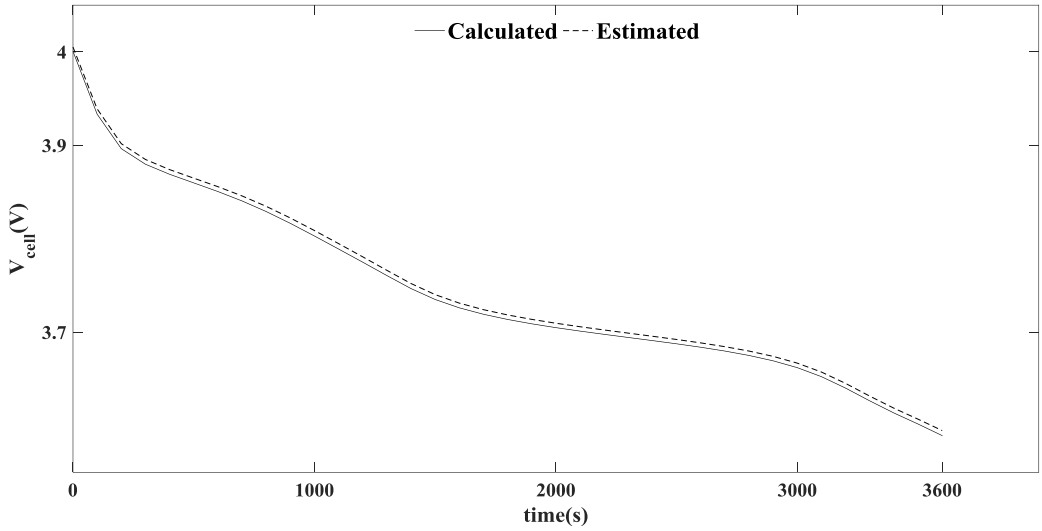

Figure 8.9: Calculated (SPM) and estimated (NN) cell potentials

8.7.2. Scenario 2: The experimental discharge curve

In Scenario 2, the NN-based parameter estimator is validated with an experimental discharge curve. The experimental data come from a Li-ion battery made with a $LiCoO_2$ cathode. The 1C discharge curve is provided in reference [11]. The other parameters are summarized in Table 8.1. Scenario 2 consists of two separate parameter estimation studies: One is

conducted with the NN-based model and the other is carried out with the regular parameter estimation model reported in reference [13]. The experimental cell potential was introduced into these models in order to determine the expected parameters. The flowchart of Scenario 2 is presented in Figure 8.10.

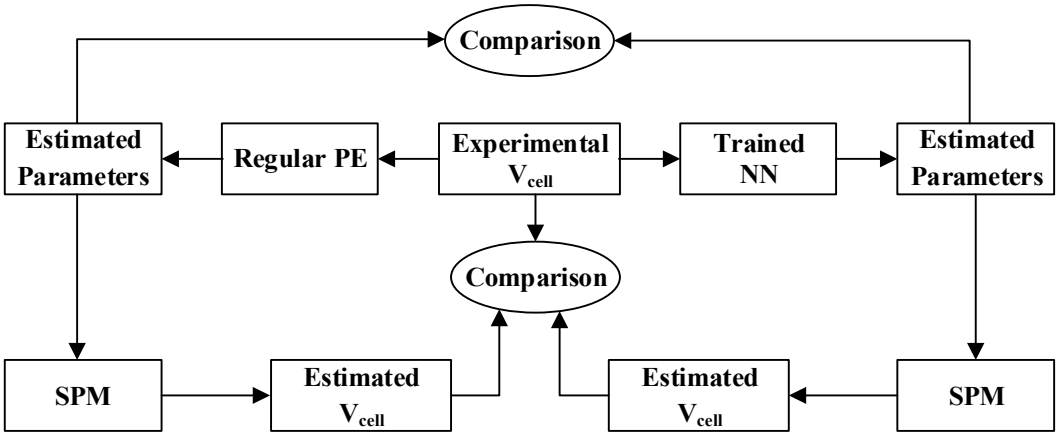

Figure 8.10: Flowchart of Scenario 2

Table 8.4 shows the estimated parameters from the two methods. Convergence of the NN PE method is achieved in 0.02 s while that of the regular parameter estimation method is obtained in 4 s. The former is 200 times faster than the latter! The predictions of the on-line NN estimator are also nearly indistinguishable from the predictions of the regular parameter estimation technique and the experimental cell potentials (Figure 8.11).

Table 8.4: Estimated parameters with the NN on-line model and the regular PE model

Symbol	Unit	Estimated Values	
		Regular PE	NN PE
$D_{s,p}$	m^2/s	0.895e-14	1.076e-14
$D_{s,n}$	m^2/s	1.968e-14	2.535e-14
K_p	$m^{2.5}/mol^{0.5}$ s	6.084e-11	6.676e-11
K_n	$m^{2.5}/mol^{0.5}$ s	1.894e-11	1.962e-11
R_{cell}	Ω	0.011	0.0147

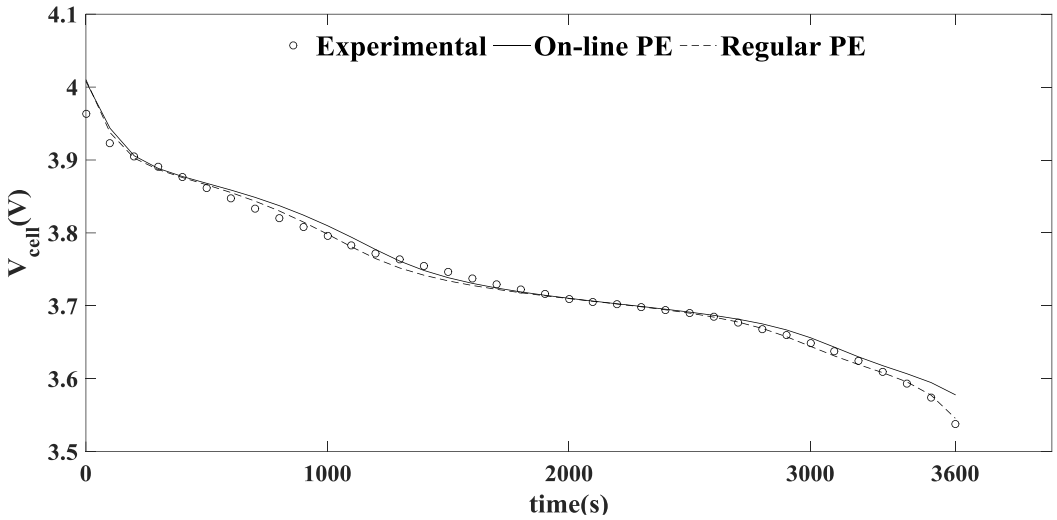

Figure 8.11: Estimated and experimental cell potentials

8.8. Conclusion

A real time Neural Network (NN) technique was presented for estimating the electrochemical properties of Li-ion batteries. The Single Particle Model was retained to train the NN model. The resulting NN model was then used to estimate the diffusion coefficients ($D_{s,n}$ & $D_{s,p}$) and the intercalation/deintercalation reaction-rate constants (K_n & K_p) of the electrodes, the electrolyte resistance of the battery (R_{cell}) and its discharge curve. The results showed that the proposed NN model is computationally performant, accurate and befitting on-line parameter estimations. The NN model is also adaptable to a multitude of input variables and output parameters. As a result, it is expected that the present NN model will find applications in Battery Management Systems. The NN model remains, however, bounded to the input variables adopted for the training scenario.

Acknowledgements

The authors are very grateful to Hydro-Quebec and to the Natural Sciences and Engineering Council of Canada (NSERC) with grant number RDCPJ 429143-11 for their financial supports.

9. Conclusion and future work

9.1. Conclusion

The main goal of this thesis was to develop a general method to simultaneously estimate different electrochemical and thermophysical parameters and to predict the performance of different types of Li-ion batteries. To achieve this goal, a technique based on the inverse method procedure was developed. The inverse method rests on five elements: (1) the reference data, (2) the expected parameters, (3) a direct model, (4) an objective function, and (5) an optimizer. Here are the important characteristics of all inverse method elements:

(1) The reference data: The experimental data provided by Hydro-Québec were selected depending on which parameters are supposed to be estimated. Two types of the experimental data belonging to different commercial Li-ion batteries were employed including the cell potential and the surface temperature at different charge/discharge rates.

(2) The expected parameters: Different electrochemical and thermophysical parameters were estimated in this thesis. In Chapter 3, eight electrochemical parameters were identified by using the cell potential experimental datasets. In Chapter 4, the thermophysical variables of the battery were only estimated independent of the electrochemical parameters. Finally, the coupled electro-thermal parameter estimation study was presented in Chapter 6. All of the estimation processes were carried out for different cathode materials.

(3) The direct model: Three kinds of Li-ion battery direct models were developed in this thesis to capture the electrochemical and thermal behavior of the battery. A simplified version of the P2D model was introduced for Li-ion batteries with LMO and LCO positive electrode materials. Also, two types of LFP models were developed for simulating the performance of these types of positive electrode material, namely the MM model and the mesoscopic-based model. It is noted that these models are useful in different applications like control, online-monitoring, BMSs, etc.

(4) The objective function: To estimate the expected parameters, it is necessary to define an objective function based on the normalized discrepancy between the predictions of the direct model and the experimental data. In Chapter 3, a novel method was presented to increase the accuracy of the inverse method and to accelerate the parameter estimation process. The best time domain for the estimation of each parameter was calculated. It was determined with the sensitivity curves for all parameters.

(5) The optimizer: Due to the numerous parameters used in the objective function of the study, the optimization process for the inverse problem is mathematically challenging, slow

to converge and computationally expensive. Therefore, the Genetic Algorithm (GA) is employed as a stochastic method to minimize the objective function.

By virtue of the inverse method, the parameter identification and performance study was conducted. The method was successful to simultaneously estimate the electrochemical and thermophysical parameters of a cylindrical Lithium-ion (Li-ion) battery. The cell potential and the surface temperature functions were also predicted at low and high charge/discharge rates. In spite of the complexity of the mathematical equations and the large number of unknown parameters, the inverse predictions show excellent agreement with the experimental data for all discharge rates. The proposed parameter estimation method was shown to be a promising tool for the design of battery thermal management systems. Finally in Chapter 8, a real time neural network (NN) technique was presented for estimating the Li-ion batteries properties. The results showed that the proposed NN model is computationally performant, accurate and befitting on-line parameter estimations. As a result, it is expected that the present NN model will find applications in Battery Management Systems. The NN model remains, however, bounded to the input variables adopted for the training scenario.

9.2. Conclusion in French

L'objectif principal de cette thèse était de développer une méthode générale permettant d'estimer simultanément différents paramètres électrochimiques et thermophysiques et de prédire les performances de différents types de batteries Li-ion. Pour atteindre cet objectif, une technique basée sur la méthode inverse a été développée. La méthode inverse repose sur cinq éléments: (1) les données de référence, (2) les paramètres attendus, (3) un modèle direct, (4) une fonction objective et (5) un optimiseur. Voici les caractéristiques importantes de tous les éléments de la méthode inverse:

(1) Les données de référence: Les données expérimentales fournies par Hydro-Québec ont été choisies en fonction des paramètres censés être estimés. Deux types de données expérimentales appartenant à différentes batteries commerciales au Li-ion ont été utilisés, y compris le potentiel de la cellule et la température de surface à différents taux de charge / décharge.

(2) Les paramètres attendus: Différents paramètres électrochimiques et thermophysiques ont été estimés dans cette thèse. Au chapitre 3, huit paramètres électrochimiques ont été identifiés en utilisant les ensembles de données expérimentales sur le potentiel mesuré. Au chapitre 4, les variables thermophysiques de la batterie ont été estimées indépendamment des paramètres électrochimiques. Enfin, l'étude d'estimation des paramètres

électrothermiques couplés a été présentée au chapitre 6. Tous les processus d'estimation ont été réalisés pour différents matériaux de cathodes.

(3) Le modèle direct: Trois types de modèles directs de batteries Li-ion ont été développés dans cette thèse pour capturer le comportement électrochimique et thermique de la batterie. Une version simplifiée du modèle P2D a été introduite pour les batteries Li-ion avec des matériaux d'électrode positive LMO et LCO. En outre, deux types de modèles LFP ont été développés pour simuler les performances de ces types de matériau d'électrode positive, à savoir le modèle MM et le modèle mésoscopique. Il est à noter que ces modèles sont utiles dans différentes applications comme le contrôle, la surveillance en ligne, les BMS, etc.

(4) La fonction objective: Pour estimer les paramètres attendus, il est nécessaire de définir une fonction objective basée sur l'écart normalisé entre les prédictions du modèle direct et les données expérimentales. Au chapitre 3, une nouvelle méthode a été présentée pour accroître la précision de la méthode inverse et accélérer le processus d'estimation des paramètres. Le meilleur domaine temporel pour l'estimation de chaque paramètre a été calculé. Il a été déterminé avec les courbes de sensibilité pour tous les paramètres.

(5) L'optimiseur: En raison des nombreux paramètres utilisés dans la fonction objective de l'étude, le processus d'optimisation du problème inverse est mathématiquement difficile, lent à converger et coûteux en calculs. Par conséquent, l'algorithme génétique (GA) est utilisé comme une méthode stochastique pour minimiser la fonction objective.

Cette méthode inverse a permis l'identification des paramètres, l'étude des performances et l’estimation simultanément des paramètres électrochimiques et thermophysiques d'une batterie cylindrique Lithium-ion (Li-ion). Les fonctions du potentiel de la cellule et de la température de surface ont également été prédites à des taux de charge / décharge faibles et élevés. Malgré la complexité des équations mathématiques et le grand nombre de paramètres inconnus, les prédictions inverses montrent un excellent accord avec les données expérimentales pour tous les taux de décharge. La méthode d'estimation des paramètres proposée s'est révélée être un outil prometteur pour la conception de systèmes de gestion thermique des batteries. Enfin, au chapitre 8, une technique de réseaux de neurones en temps réel (NN) a été présentée pour estimer les propriétés des batteries Li-ion. Les résultats ont montré que le modèle NN proposé est performant, précis et convenant aux estimations de paramètres en ligne. En conséquence, il est prévu que le modèle NN actuel trouvera des applications dans les systèmes de gestion de batterie. Le modèle NN reste cependant limité aux variables d'entrée retenues pour le scénario de formation.

9.3. Suggested future work

- A parameter estimation study is suggested to investigate the effect of battery aging on the parameters values. To conduct this study, it is vital to modify the direct model. The model should adjust with some age-dependent variables to model the side reactions and the active material consumption as the battery ages. Then, the parameter estimation study can be ready for charge/discharge curves with different battery cycles.
- It is suggested to complement the electro-thermal modeling with a mechanical model in order to investigate all concerns over the safety of the Li-ion batteries. The model would be useful to predict the battery mechanical failure and its effects on the battery performance. This model should employ a micro- and a macro-scale approach at the same time to be able to simulate both crack initiation in the electrode and the cell structural failure in a battery pack.
- The parameter estimation method developed in Chapter 3 could be applied to other electrochemical systems like Li-S battery. The sensitivity analysis should be performed to find out the best time estimation for each parameter.

9.4. Suggestions de travaux futurs

• Une étude d'estimation des paramètres est suggérée pour étudier l'effet du vieillissement de la batterie sur les valeurs des paramètres. Pour mener cette étude, il est indispensable de modifier le modèle direct. Le modèle doit s'ajuster avec certaines variables dépendantes de l'âge pour modéliser les réactions secondaires et la consommation de matière active au fur et à mesure que la pile vieillit. Ensuite, l'étude d'estimation des paramètres peut être prête pour représenter les courbes de charge / décharge avec différents cycles de charge / décharge des batteries Li-ion.

• Il est suggéré de compléter la modélisation électrothermique par un modèle mécanique afin d'étudier toutes les problèmes relatifs à la sécurité des batteries Li-ion. Le modèle serait utile pour prédire la défaillance mécanique de la batterie et ses effets sur les performances. Ce modèle devrait utiliser une approche micro- et macro-échelle en même temps pour simuler à la fois l'amorçage de la fissure dans l'électrode et la défaillance structurale de la pile dans une batterie.

• La méthode d'estimation des paramètres développée au chapitre 3 pourrait être appliquée à d'autres systèmes électrochimiques tels que les batteries Li-S. Une analyse de sensibilité devrait être menée afin de trouver la meilleure estimation en fonction du temps et ce, pour chaque paramètre.

References

[1] K.E. Thomas, J. Newman, R.M. Darling, Mathematical modeling of lithium batteries, in: Advances in lithium-ion batteries, Springer, 2002, pp. 345-392.

[2] D. Linden, T.B. Reddy, Handbook of Batteries, third ed., McGraw-Hill Book Co., New York, 2001.

[3] B. Dunn, H. Kamath, J.-M. Tarascon, Electrical Energy Storage for the Grid: A Battery of Choices, *Science*, **334** (2011) 928-935.

[4] J.M. Tarascon, M. Armand, Issues and challenges facing rechargeable lithium batteries, *Nature*, **414** (2001) 359-367.

[5] K. Xu, Nonaqueous Liquid Electrolytes for Lithium-Based Rechargeable Batteries, *Chemical Reviews*, **104** (2004) 4303-4418.

[6] C. Julien, A. Mauger, K. Zaghib, H. Groult, Comparative Issues of Cathode Materials for Li-Ion Batteries, *Inorganics*, **2** (2014) 132.

[7] C. Julien, A. Mauger, A. Vijh, K. Zaghib, Lithium Batteries: Science and Technology, Springer, 2015.

[8] J. Zhang, J. Lee, A review on prognostics and health monitoring of Li-ion battery, *Journal of Power Sources*, **196** (2011) 6007-6014.

[9] V. Ramadesigan, P.W.C. Northrop, S. De, S. Santhanagopalan, R.D. Braatz, V.R. Subramanian, Modeling and Simulation of Lithium-Ion Batteries from a Systems Engineering Perspective, *Journal of The Electrochemical Society*, **159** (2012) R31-R45.

[10] A. Jokar, B. Rajabloo, M. Désilets, M. Lacroix, Review of simplified Pseudo-two-Dimensional models of lithium-ion batteries, *Journal of Power Sources*, **327** (2016) 44-55.

[11] S. Santhanagopalan, Q. Guo, R.E. White, Parameter Estimation and Model Discrimination for a Lithium-Ion Cell, *Journal of The Electrochemical Society*, **154** (2007) A198-A206.

[12] S. Santhanagopalan, Q. Zhang, K. Kumaresan, R.E. White, Parameter Estimation and Life Modeling of Lithium-Ion Cells, *Journal of The Electrochemical Society*, **155** (2008) A345-A353.

[13] A. Jokar, B. Rajabloo, M. Désilets, M. Lacroix, An Inverse Method for Estimating the Electrochemical Parameters of Lithium-Ion Batteries: I. Methodology, *Journal of The Electrochemical Society*, **163** (2016) A2876-A2886.

[14] M. Ozisik, H. Orlande, A. Kassab, Inverse heat transfer: fundamentals and applications, *Applied Mechanics Reviews*, **55** (2002) 18.

[15] A. Tarantola, Inverse problem theory and methods for model parameter estimation, siam, 2005.

[16] J.V. Beck, K.J. Arnold, Parameter estimation in engineering and science, John Wiley and Sons, New York, 1977.

[17] M.J. Colaço, H.R. Orlande, G.S. Dulikravich, Inverse and optimization problems in heat transfer, *Journal of the Brazilian Society of Mechanical Sciences and Engineering*, **28** (2006) 1-24.

[18] J. Nocedal, S. Wright, Numerical optimization, Springer Science & Business Media, 2006.

[19] L.-X. Yuan, Z.-H. Wang, W.-X. Zhang, X.-L. Hu, J.-T. Chen, Y.-H. Huang, J.B. Goodenough, Development and challenges of LiFePO 4 cathode material for lithium-ion batteries, *Energy & Environmental Science*, **4** (2011) 269-284.

[20] A. Du Pasquier, I. Plitz, S. Menocal, G. Amatucci, A comparative study of Li-ion battery, supercapacitor and nonaqueous asymmetric hybrid devices for automotive applications, *Journal of Power Sources*, **115** (2003) 171-178.

[21] L. Hu, J.W. Choi, Y. Yang, S. Jeong, F. La Mantia, L.-F. Cui, Y. Cui, Highly conductive paper for energy-storage devices, *Proceedings of the National Academy of Sciences*, **106** (2009) 21490-21494.

[22] A.K. Padhi, K.S. Nanjundaswamy, J.B. Goodenough, Phospho-olivines as Positive-Electrode Materials for Rechargeable Lithium Batteries, *Journal of The Electrochemical Society*, **144** (1997) 1188-1194.

[23] J.B. Goodenough, A.K. Padhi, K. Nanjundaswamy, C. Masquelier, Cathode materials for secondary (rechargeable) lithium batteries, in, Google Patents, 1999.

[24] P.G. Bruce, B. Scrosati, J.-M. Tarascon, Nanomaterials for Rechargeable Lithium Batteries, *Angewandte Chemie International Edition*, **47** (2008) 2930-2946.

[25] A.S. Andersson, J.O. Thomas, B. Kalska, L. Häggström, Thermal Stability of LiFePO4 - Based Cathodes, *Electrochemical and Solid-State Letters*, **3** (2000) 66-68.

[26] B.A. Johnson, R.E. White, Characterization of commercially available lithium-ion batteries, *Journal of Power Sources*, **70** (1998) 48-54.

[27] G.M. Ehrlich, Lithium-ion batteries, Handbook of Batteries, McGraw Hill Books, New York, 2002.

[28] A. Seaman, T.-S. Dao, J. McPhee, A survey of mathematics-based equivalent-circuit and electrochemical battery models for hybrid and electric vehicle simulation, *Journal of Power Sources*, **256** (2014) 410-423.

[29] A.J. Salkind, C. Fennie, P. Singh, T. Atwater, D.E. Reisner, Determination of state-of-charge and state-of-health of batteries by fuzzy logic methodology, *Journal of Power Sources*, **80** (1999) 293-300.

[30] M.W. Verbrugge, R.S. Conell, Electrochemical and Thermal Characterization of Battery Modules Commensurate with Electric Vehicle Integration, *Journal of The Electrochemical Society*, **149** (2002) A45-A53.

[31] P.W.C. Northrop, B. Suthar, V. Ramadesigan, S. Santhanagopalan, R.D. Braatz, V.R. Subramanian, Efficient Simulation and Reformulation of Lithium-Ion Battery Models for Enabling Electric Transportation, *Journal of The Electrochemical Society*, **161** (2014) E3149-E3157.

[32] A.M. Bizeray, S. Zhao, S.R. Duncan, D.A. Howey, Lithium-ion battery thermal-electrochemical model-based state estimation using orthogonal collocation and a modified extended Kalman filter, *Journal of Power Sources*, **296** (2015) 400-412.

[33] J. Newman, K.E. Thomas-Alyea, Electrochemical systems, John Wiley & Sons, 2012.

[34] M. Doyle, T.F. Fuller, J. Newman, Modeling of Galvanostatic Charge and Discharge of the Lithium/Polymer/Insertion Cell, *Journal of The Electrochemical Society*, **140** (1993) 1526-1533.

[35] M. Doyle, J. Newman, A.S. Gozdz, C.N. Schmutz, J.M. Tarascon, Comparison of Modeling Predictions with Experimental Data from Plastic Lithium Ion Cells, *Journal of The Electrochemical Society*, **143** (1996) 1890-1903.

[36] K. Kumaresan, G. Sikha, R.E. White, Thermal Model for a Li-Ion Cell, *Journal of The Electrochemical Society*, **155** (2008) A164-A171.

[37] S. Santhanagopalan, Q. Guo, P. Ramadass, R.E. White, Review of models for predicting the cycling performance of lithium ion batteries, *Journal of Power Sources*, **156** (2006) 620-628.

[38] D. Bernardi, E. Pawlikowski, J. Newman, A General Energy Balance for Battery Systems, *Journal of The Electrochemical Society*, **132** (1985) 5-12.

[39] T.M. Bandhauer, S. Garimella, T.F. Fuller, A Critical Review of Thermal Issues in Lithium-Ion Batteries, *Journal of The Electrochemical Society*, **158** (2011) R1-R25.

[40] J. Newman, W. Tiedemann, Porous-electrode theory with battery applications, *AIChE Journal*, **21** (1975) 25-41.

[41] M. Doyle, Design and simulation of lithium rechargeable batteries, Ph.D. Thesis, in: Lawrence Berkeley National Laboratory, University of California, 1995.

[42] T.R. Tanim, C.D. Rahn, C.-Y. Wang, A Temperature Dependent, Single Particle, Lithium Ion Cell Model Including Electrolyte Diffusion, *Journal of Dynamic Systems, Measurement, and Control*, **137** (2014) 011005-011005-011011.

[43] K.A. Smith, C.D. Rahn, C.-Y. Wang, Control oriented 1D electrochemical model of lithium ion battery, *Energy Conversion and Management*, **48** (2007) 2565-2578.

[44] T.-S. Dao, C.P. Vyasarayani, J. McPhee, Simplification and order reduction of lithium-ion battery model based on porous-electrode theory, *Journal of Power Sources*, **198** (2012) 329-337.

[45] R. Klein, N.A. Chaturvedi, J. Christensen, J. Ahmed, R. Findeisen, A. Kojic, Electrochemical Model Based Observer Design for a Lithium-Ion Battery, *IEEE Transactions on Control Systems Technology*, **21** (2013) 289-301.

[46] G.G. Botte, V.R. Subramanian, R.E. White, Mathematical modeling of secondary lithium batteries, *Electrochimica Acta*, **45** (2000) 2595-2609.

[47] P.M. Gomadam, J.W. Weidner, R.A. Dougal, R.E. White, Mathematical modeling of lithium-ion and nickel battery systems, *Journal of Power Sources*, **110** (2002) 267-284.

[48] M.D. Beeney, Lithium Ion Battery Modeling using Orthogonal Projections And Descriptor Form, Doctoral dissertation,, in, The Pennsylvania State University, 2013.

[49] S.J. Moura, N.A. Chaturvedi, M. Krstic, PDE estimation techniques for advanced battery management systems — Part I: SOC estimation, in: 2012 American Control Conference (ACC), 2012, pp. 559-565.

[50] S. Khaleghi Rahimian, S. Rayman, R.E. White, Extension of physics-based single particle model for higher charge–discharge rates, *Journal of Power Sources*, **224** (2013) 180-194.

[51] L. Cai, R.E. White, Mathematical modeling of a lithium ion battery with thermal effects in COMSOL Inc. Multiphysics (MP) software, *Journal of Power Sources*, **196** (2011) 5985-5989.

[52] S. Atlung, K. West, T. Jacobsen, Dynamic Aspects of Solid Solution Cathodes for Electrochemical Power Sources, *Journal of The Electrochemical Society*, **126** (1979) 1311-1321.

[53] B.S. Haran, B.N. Popov, R.E. White, Determination of the hydrogen diffusion coefficient in metal hydrides by impedance spectroscopy, *Journal of Power Sources*, **75** (1998) 56-63.

[54] D. Zhang, B.N. Popov, R.E. White, Modeling Lithium Intercalation of a Single Spinel Particle under Potentiodynamic Control, *Journal of The Electrochemical Society*, **147** (2000) 831-838.

[55] G. Ning, B.N. Popov, Cycle Life Modeling of Lithium-Ion Batteries, *Journal of The Electrochemical Society*, **151** (2004) A1584-A1591.

[56] M. Farkhondeh, C. Delacourt, Mathematical Modeling of Commercial LiFePO4 Electrodes Based on Variable Solid-State Diffusivity, *Journal of The Electrochemical Society*, **159** (2011) A177-A192.

[57] M. Safari, C. Delacourt, Mathematical Modeling of Lithium Iron Phosphate Electrode: Galvanostatic Charge/Discharge and Path Dependence, *Journal of The Electrochemical Society*, **158** (2011) A63-A73.

[58] M. Farkhondeh, M. Safari, M. Pritzker, M. Fowler, T. Han, J. Wang, C. Delacourt, Full-Range Simulation of a Commercial LiFePO4 Electrode Accounting for Bulk and Surface Effects: A Comparative Analysis, *Journal of The Electrochemical Society*, **161** (2014) A201-A212.

[59] K. Chen, G. Unsworth, X. Li, Measurements of heat generation in prismatic Li-ion batteries, *Journal of Power Sources*, **261** (2014) 28-37.

[60] C.R. Pals, J. Newman, Thermal Modeling of the Lithium/Polymer Battery: I . Discharge Behavior of a Single Cell, *Journal of The Electrochemical Society*, **142** (1995) 3274-3281.

[61] C.R. Pals, J. Newman, Thermal Modeling of the Lithium/Polymer Battery: II . Temperature Profiles in a Cell Stack, *Journal of The Electrochemical Society*, **142** (1995) 3282-3288.

[62] W. Gu, C.-Y. Wang, Thermal and electrochemical coupled modeling of a lithium-ion cell, in: Proceedings of the ECS, 2000, pp. 748-762.

[63] S.C. Chen, C.C. Wan, Y.Y. Wang, Thermal analysis of lithium-ion batteries, *Journal of Power Sources*, **140** (2005) 111-124.

[64] M. Guo, G. Sikha, R.E. White, Single-Particle Model for a Lithium-Ion Cell: Thermal Behavior, *Journal of The Electrochemical Society*, **158** (2011) A122-A132.

[65] K.A. Murashko, A.V. Mityakov, J. Pyrhönen, V.Y. Mityakov, S.S. Sapozhnikov, Thermal parameters determination of battery cells by local heat flux measurements, *Journal of Power Sources*, **271** (2014) 48-54.

[66] H. Maleki, S.A. Hallaj, J.R. Selman, R.B. Dinwiddie, H. Wang, Thermal Properties of Lithium-Ion Battery and Components, *Journal of The Electrochemical Society*, **146** (1999) 947-954.

[67] S. Al Hallaj, H. Maleki, J.S. Hong, J.R. Selman, Thermal modeling and design considerations of lithium-ion batteries, *Journal of Power Sources*, **83** (1999) 1-8.

[68] L. Lu, X. Han, J. Li, J. Hua, M. Ouyang, A review on the key issues for lithium-ion battery management in electric vehicles, *Journal of Power Sources*, **226** (2013) 272-288.

[69] B. Diouf, R. Pode, Potential of lithium-ion batteries in renewable energy, *Renewable Energy*, **76** (2015) 375-380.

[70] D.M. Hill, A. Agarwal, B. Gully, A Review of Engineering and Safety Considerations for Hybrid-Power (Lithium-Ion) Systems in Offshore Applications, *Oil and Gas Facilities*, **4** (2015) 68-77.

[71] D. Xu, L. Wang, J. Yang, Research on Li-ion Battery Management System, in: 2010 International Conference on Electrical and Control Engineering, 2010, pp. 4106-4109.

[72] D. Andrea, Battery management systems for large lithium-ion battery packs, 1st ed., Artech House, Norwood, MA, 2010.

[73] N.A. Chaturvedi, R. Klein, J. Christensen, J. Ahmed, A. Kojic, Algorithms for Advanced Battery-Management Systems, *IEEE Control Systems*, **30** (2010) 49-68.

[74] X. Hu, S. Li, H. Peng, A comparative study of equivalent circuit models for Li-ion batteries, *Journal of Power Sources*, **198** (2012) 359-367.

[75] V.R. Subramanian, J.A. Ritter, R.E. White, Approximate Solutions for Galvanostatic Discharge of Spherical Particles I. Constant Diffusion Coefficient, *Journal of The Electrochemical Society*, **148** (2001) E444-E449.

[76] V.R. Subramanian, V.D. Diwakar, D. Tapriyal, Efficient Macro-Micro Scale Coupled Modeling of Batteries, *Journal of The Electrochemical Society*, **152** (2005) A2002-A2008.

[77] V.R. Subramanian, V. Boovaragavan, V.D. Diwakar, Toward Real-Time Simulation of Physics Based Lithium-Ion Battery Models, *Electrochemical and Solid-State Letters*, **10** (2007) A255-A260.

[78] D.D. Domenico, G. Fiengo, A. Stefanopoulou, Lithium-ion battery state of charge estimation with a Kalman Filter based on a electrochemical model, in: 2008 IEEE International Conference on Control Applications, 2008, pp. 702-707.

[79] K.A. Smith, C.D. Rahn, C.-Y. Wang, Model Order Reduction of 1D Diffusion Systems Via Residue Grouping, *Journal of Dynamic Systems, Measurement, and Control*, **130** (2008) 011012-011012-011018.

[80] L. Cai, R.E. White, Reduction of Model Order Based on Proper Orthogonal Decomposition for Lithium-Ion Battery Simulations, *Journal of The Electrochemical Society*, **156** (2009) A154-A161.

[81] V.R. Subramanian, V. Boovaragavan, V. Ramadesigan, M. Arabandi, Mathematical Model Reformulation for Lithium-Ion Battery Simulations: Galvanostatic Boundary Conditions, *Journal of The Electrochemical Society*, **156** (2009) A260-A271.

[82] K.A. Smith, C.D. Rahn, C.Y. Wang, Model-Based Electrochemical Estimation and Constraint Management for Pulse Operation of Lithium Ion Batteries, *IEEE Transactions on Control Systems Technology*, **18** (2010) 654-663.

[83] V. Ramadesigan, V. Boovaragavan, J.C. Pirkle, V.R. Subramanian, Efficient Reformulation of Solid-Phase Diffusion in Physics-Based Lithium-Ion Battery Models, *Journal of The Electrochemical Society*, **157** (2010) A854-A860.

[84] J.C. Forman, S. Bashash, J.L. Stein, H.K. Fathy, Reduction of an Electrochemistry-Based Li-Ion Battery Model via Quasi-Linearization and Padé Approximation, *Journal of The Electrochemical Society*, **158** (2011) A93-A101.

[85] J.L. Lee, A. Chemistruck, G.L. Plett, One-dimensional physics-based reduced-order model of lithium-ion dynamics, *Journal of Power Sources*, **220** (2012) 430-448.

[86] W. Luo, C. Lyu, L. Wang, L. Zhang, An approximate solution for electrolyte concentration distribution in physics-based lithium-ion cell models, *Microelectronics Reliability*, **53** (2013) 797-804.

[87] W. Luo, C. Lyu, L. Wang, L. Zhang, A new extension of physics-based single particle model for higher charge–discharge rates, *Journal of Power Sources*, **241** (2013) 295-310.

[88] J. Marcicki, M. Canova, A.T. Conlisk, G. Rizzoni, Design and parametrization analysis of a reduced-order electrochemical model of graphite/LiFePO4 cells for SOC/SOH estimation, *Journal of Power Sources*, **237** (2013) 310-324.

[89] M. Mastali Majdabadi, S. Farhad, M. Farkhondeh, R.A. Fraser, M. Fowler, Simplified electrochemical multi-particle model for LiFePO4 cathodes in lithium-ion batteries, *Journal of Power Sources*, **275** (2015) 633-643.

[90] C.Y. Wang, W.B. Gu, B.Y. Liaw, Micro-Macroscopic Coupled Modeling of Batteries and Fuel Cells: I. Model Development, *Journal of The Electrochemical Society*, **145** (1998) 3407-3417.

[91] C. Speltino, D.D. Domenico, G. Fiengo, A. Stefanopoulou, Comparison of reduced order lithium-ion battery models for control applications, in: Proceedings of the 48h IEEE Conference on Decision and Control (CDC) held jointly with 2009 28th Chinese Control Conference, 2009, pp. 3276-3281.

[92] V. Ramadesigan, K. Chen, N.A. Burns, V. Boovaragavan, R.D. Braatz, V.R. Subramanian, Parameter Estimation and Capacity Fade Analysis of Lithium-Ion Batteries Using Reformulated Models, *Journal of The Electrochemical Society*, **158** (2011) A1048-A1054.

[93] J.C. Forman, S.J. Moura, J.L. Stein, H.K. Fathy, Genetic identification and fisher identifiability analysis of the Doyle–Fuller–Newman model from experimental cycling of a LiFePO4 cell, *Journal of Power Sources*, **210** (2012) 263-275.

[94] http://www.maplesoft.com/company/casestudies/stories/98868.aspx., in.

[95] T.R. Tanim, C.D. Rahn, Aging formula for lithium ion batteries with solid electrolyte interphase layer growth, *Journal of Power Sources*, **294** (2015) 239-247.

[96] H. Rahimi-Eichi, U. Ojha, F. Baronti, M.Y. Chow, Battery Management System: An Overview of Its Application in the Smart Grid and Electric Vehicles, *IEEE Industrial Electronics Magazine*, **7** (2013) 4-16.

[97] Q. Guo, V.A. Sethuraman, R.E. White, Parameter Estimates for a PEMFC Cathode, *Journal of The Electrochemical Society*, **151** (2004) A983-A993.

[98] L. Zhang, L. Wang, G. Hinds, C. Lyu, J. Zheng, J. Li, Multi-objective optimization of lithium-ion battery model using genetic algorithm approach, *Journal of Power Sources*, **270** (2014) 367-378.

[99] R. Masoudi, T. Uchida, J. McPhee, Parameter estimation of an electrochemistry-based lithium-ion battery model, *Journal of Power Sources*, **291** (2015) 215-224.

[100] M.A. Rahman, S. Anwar, A. Izadian, Electrochemical model parameter identification of a lithium-ion battery using particle swarm optimization method, *Journal of Power Sources*, **307** (2016) 86-97.

[101] J.H. Holland, Adaptation in natural and artificial systems: an introductory analysis with applications to biology, control, and artificial intelligence, U Michigan Press, 1975.

[102] A. Jokar, A.A. Godarzi, M. Saber, M.B. Shafii, Simulation and optimization of a pulsating heat pipe using artificial neural network and genetic algorithm, *Heat and Mass Transfer*, **52** (2016) 2437-2445.

[103] A.A. Godarzi, M. Jalilian, J. Samimi, A. Jokar, M.A. Vesaghi, Design of a PCM storage system for a solar absorption chiller based on exergoeconomic analysis and genetic algorithm, *International Journal of Refrigeration*, **36** (2013) 88-101.

[104] B. Rajabloo, A. Jokar, M. Désilets, M. Lacroix, An Inverse Method for Estimating the Electrochemical Parameters of Lithium-Ion Batteries: II: Implementation, *Journal of The Electrochemical Society*, **164** (2017) A99-A105.

[105] Internal Hydro-Québec Report: Experimental data for the Li-ion batteries in, 2016.

[106] D. Xu, L. Wang, J. Yang, Research on Li-ion Battery Management System, in: Electrical and Control Engineering (ICECE), 2010 International Conference on, 2010, pp. 4106-4109.

[107] Z. Rao, S. Wang, A review of power battery thermal energy management, *Renewable and Sustainable Energy Reviews*, **15** (2011) 4554-4571.

[108] R. Mahamud, C. Park, Reciprocating air flow for Li-ion battery thermal management to improve temperature uniformity, *Journal of Power Sources*, **196** (2011) 5685-5696.

[109] Y. Inui, Y. Kobayashi, Y. Watanabe, Y. Watase, Y. Kitamura, Simulation of temperature distribution in cylindrical and prismatic lithium ion secondary batteries, *Energy Conversion and Management*, **48** (2007) 2103-2109.

[110] M. Muratori, N. Ma, M. Canova, Y. Guezennec, A model order reduction method for the temperature estimation in a cylindrical li-ion battery cell, in: ASME 2010 Dynamic Systems and Control Conference, American Society of Mechanical Engineers, 2010, pp. 633-640.

[111] C. Forgez, D. Vinh Do, G. Friedrich, M. Morcrette, C. Delacourt, Thermal modeling of a cylindrical LiFePO4/graphite lithium-ion battery, *Journal of Power Sources*, **195** (2010) 2961-2968.

[112] X. Zhang, Thermal analysis of a cylindrical lithium-ion battery, *Electrochimica Acta*, **56** (2011) 1246-1255.

[113] D.H. Jeon, S.M. Baek, Thermal modeling of cylindrical lithium ion battery during discharge cycle, *Energy Conversion and Management*, **52** (2011) 2973-2981.

[114] X. Lin, H.E. Perez, J.B. Siegel, A.G. Stefanopoulou, Y. Li, R.D. Anderson, Y. Ding, M.P. Castanier, Online Parameterization of Lumped Thermal Dynamics in Cylindrical Lithium Ion Batteries for Core Temperature Estimation and Health Monitoring, *IEEE Transactions on Control Systems Technology*, **21** (2013) 1745-1755.

[115] Y. Kim, J.B. Siegel, A.G. Stefanopoulou, A computationally efficient thermal model of cylindrical battery cells for the estimation of radially distributed temperatures, in: 2013 American Control Conference, 2013, pp. 698-703.

[116] L.H. Saw, Y. Ye, A.A.O. Tay, Electrochemical–thermal analysis of 18650 Lithium Iron Phosphate cell, *Energy Conversion and Management*, **75** (2013) 162-174.

[117] J.S. Hong, H. Maleki, S. Al Hallaj, L. Redey, J.R. Selman, Electrochemical-Calorimetric Studies of Lithium-Ion Cells, *Journal of The Electrochemical Society*, **145** (1998) 1489-1501.

[118] T.I. Evans, R.E. White, A Thermal Analysis of a Spirally Wound Battery Using a Simple Mathematical Model, *Journal of The Electrochemical Society*, **136** (1989) 2145-2152.

[119] I.V. Thorat, T. Joshi, K. Zaghib, J.N. Harb, D.R. Wheeler, Understanding Rate-Limiting Mechanisms in LiFePO4 Cathodes for Li-Ion Batteries, *Journal of The Electrochemical Society*, **158** (2011) A1185-A1193.

[120] V.V. Viswanathan, D. Choi, D. Wang, W. Xu, S. Towne, R.E. Williford, J.-G. Zhang, J. Liu, Z. Yang, Effect of entropy change of lithium intercalation in cathodes and anodes on Li-ion battery thermal management, *Journal of Power Sources*, **195** (2010) 3720-3729.

[121] J. Crank, P. Nicolson, A practical method for numerical evaluation of solutions of partial differential equations of the heat-conduction type, in: Mathematical Proceedings of the Cambridge Philosophical Society, Cambridge Univ Press, 1947, pp. 50-67.

[122] M. Safari, C. Delacourt, Modeling of a Commercial Graphite/LiFePO4 Cell, *Journal of The Electrochemical Society*, **158** (2011) A562-A571.

[123] E. Prada, D. Di Domenico, Y. Creff, J. Bernard, V. Sauvant-Moynot, F. Huet, Simplified Electrochemical and Thermal Model of LiFePO4-Graphite Li-Ion Batteries for Fast Charge Applications, *Journal of The Electrochemical Society*, **159** (2012) A1508-A1519.

[124] A.S. Andersson, J.O. Thomas, The source of first-cycle capacity loss in LiFePO4, *Journal of Power Sources*, **97–98** (2001) 498-502.

[125] X. Li, F. He, L. Ma, Thermal management of cylindrical batteries investigated using wind tunnel testing and computational fluid dynamics simulation, *Journal of Power Sources*, **238** (2013) 395-402.

[126] R.R. Richardson, D.A. Howey, Sensorless Battery Internal Temperature Estimation Using a Kalman Filter With Impedance Measurement, *IEEE Transactions on Sustainable Energy*, **6** (2015) 1190-1199.

[127] W. van Schalkwijk, B. Scrosati, Advances in lithium-ion batteries, Springer Science & Business Media, 2007.

[128] K. Zaghib, A. Mauger, F. Gendron, C.M. Julien, Surface Effects on the Physical and Electrochemical Properties of Thin LiFePO4 Particles, *Chemistry of Materials*, **20** (2008) 462-469.

[129] B. Scrosati, J. Garche, Lithium batteries: Status, prospects and future, *Journal of Power Sources*, **195** (2010) 2419-2430.

[130] A. Yamada, Y. Kudo, K.-Y. Liu, Phase Diagram of $Li_x(Mn_yFe_{1-y})PO_4$ $(0 \leqslant x, y \leqslant 1)$ *Journal of The Electrochemical Society*, **148** (2001) A1153-A1158.

[131] V. Srinivasan, J. Newman, Discharge Model for the Lithium Iron-Phosphate Electrode, *Journal of The Electrochemical Society*, **151** (2004) A1517-A1529.

[132] S. Dargaville, T.W. Farrell, Predicting Active Material Utilization in LiFePO4 Electrodes Using a Multiscale Mathematical Model, *Journal of The Electrochemical Society*, **157** (2010) A830-A840.

[133] G. Chen, X. Song, T.J. Richardson, Electron Microscopy Study of the LiFePO4 to FePO4 Phase Transition, *Electrochemical and Solid-State Letters*, **9** (2006) A295-A298.

[134] J. Lim, Y. Li, D.H. Alsem, H. So, S.C. Lee, P. Bai, D.A. Cogswell, X. Liu, N. Jin, Y.-s. Yu, N.J. Salmon, D.A. Shapiro, M.Z. Bazant, T. Tyliszczak, W.C. Chueh, Origin and hysteresis of lithium compositional spatiodynamics within battery primary particles, *Science*, **353** (2016) 566-571.

[135] L. Laffont, C. Delacourt, P. Gibot, M.Y. Wu, P. Kooyman, C. Masquelier, J.M. Tarascon, Study of the LiFePO4/FePO4 Two-Phase System by High-Resolution Electron Energy Loss Spectroscopy, *Chemistry of Materials*, **18** (2006) 5520-5529.

[136] C. Delmas, M. Maccario, L. Croguennec, F. Le Cras, F. Weill, Lithium deintercalation in LiFePO4 nanoparticles via a domino-cascade model, *Nat Mater*, **7** (2008) 665-671.

[137] W. Dreyer, J. Jamnik, C. Guhlke, R. Huth, J. Moskon, M. Gaberscek, The thermodynamic origin of hysteresis in insertion batteries, *Nat Mater*, **9** (2010) 448-453.

[138] W. Dreyer, C. Guhlke, M. Herrmann, Hysteresis and phase transition in many-particle storage systems, *Continuum Mechanics and Thermodynamics*, **23** (2011) 211-231.

[139] M. Farkhondeh, M. Pritzker, M. Fowler, M. Safari, C. Delacourt, Mesoscopic modeling of Li insertion in phase-separating electrode materials: application to lithium iron phosphate, *Physical Chemistry Chemical Physics*, **16** (2014) 22555-22565.

[140] M. Farkhondeh, M. Pritzker, M. Fowler, C. Delacourt, Mesoscopic Modeling of a LiFePO4 Electrode: Experimental Validation under Continuous and Intermittent Operating Conditions, *Journal of The Electrochemical Society*, **164** (2017) E3040-E3053.

[141] G.K. Singh, G. Ceder, M.Z. Bazant, Intercalation dynamics in rechargeable battery materials: General theory and phase-transformation waves in LiFePO4, *Electrochimica Acta*, **53** (2008) 7599-7613.

[142] P. Bai, D.A. Cogswell, M.Z. Bazant, Suppression of Phase Separation in LiFePO4 Nanoparticles During Battery Discharge, *Nano Letters*, **11** (2011) 4890-4896.

[143] M.Z. Bazant, Theory of Chemical Kinetics and Charge Transfer based on Nonequilibrium Thermodynamics, *Accounts of Chemical Research*, **46** (2013) 1144-1160.

[144] T.R. Ferguson, M.Z. Bazant, Nonequilibrium Thermodynamics of Porous Electrodes, *Journal of The Electrochemical Society*, **159** (2012) A1967-A1985.

[145] C. Delacourt, M. Safari, Analysis of lithium deinsertion/insertion in LiyFePO4 with a simple mathematical model, *Electrochimica Acta*, **56** (2011) 5222-5229.

[146] A. Maheshwari, M.A. Dumitrescu, M. Destro, M. Santarelli, Inverse parameter determination in the development of an optimized lithium iron phosphate – Graphite battery discharge model, *Journal of Power Sources*, **307** (2016) 160-172.

[147] H. Joachin, T.D. Kaun, K. Zaghib, J. Prakash, Electrochemical and Thermal Studies of Carbon-Coated LiFePO4 Cathode, *Journal of The Electrochemical Society*, **156** (2009) A401-A406.

[148] A. Jokar, B. Rajabloo, M. Désilets, M. Lacroix, K. Zaghib, A Modified Mosaic (MM) model for commercial Li-ion batteries based on LiFePO4/Graphite, *Submitted to Electrochimica Acta*, (2017).

[149] R.T. Marler, J.S. Arora Survey of multi-objective optimization methods for engineering, *Structural and Multidisciplinary Optimization*, **26** (2004) 369-395.

[150] D.K. Karthikeyan, G. Sikha, R.E. White, Thermodynamic model development for lithium intercalation electrodes, *Journal of Power Sources*, **185** (2008) 1398-1407.

[151] A. Jokar, B. Rajabloo, M. Desilets, M. Lacroix, An On-line Electrochemical Parameter Estimation Study of Lithium-Ion Batteries Using Neural Networks, *ECS Transactions*, **75** (2017) 73-87.

[152] R. Beale, T. Jackson, Neural Computing-an introduction, CRC Press, 1990.

[153] A.G. Parlos, K.T. Chong, A.F. Atiya, Application of the recurrent multilayer perceptron in modeling complex process dynamics, *IEEE Transactions on Neural Networks*, **5** (1994) 255-266.

[154] Z. Ullah, B. Burford, S. Dillip, Fast intelligent battery charging: neural-fuzzy approach, *IEEE Aerospace and Electronic Systems Magazine*, **11** (1996) 26-34.

[155] S. Grewal, D. Grant, A novel technique for modelling the state of charge of lithium ion batteries using artificial neural networks, in: In Telecommunications Energy Conference, INTELEC 2001, Twenty-Third International 2001.

[156] A. Affanni, A. Bellini, C. Concari, G. Franceschini, E. Lorenzani, C. Tassoni, EV battery state of charge: neural network based estimation, in: Electric Machines and Drives Conference, 2003. IEMDC'03. IEEE International, 2003, pp. 684-688 vol.682.

[157] K.T. Chau, K.C. Wu, C.C. Chan, A new battery capacity indicator for lithium-ion battery powered electric vehicles using adaptive neuro-fuzzy inference system, *Energy Conversion and Management*, **45** (2004) 1681-1692.

[158] I.H. Li, W.Y. Wang, S.F. Su, Y.S. Lee, A Merged Fuzzy Neural Network and Its Applications in Battery State-of-Charge Estimation, *IEEE Transactions on Energy Conversion*, **22** (2007) 697-708.

[159] T. Parthiban, R. Ravi, N. Kalaiselvi, Exploration of artificial neural network [ANN] to predict the electrochemical characteristics of lithium-ion cells, *Electrochimica Acta*, **53** (2007) 1877-1882.

[160] M. Charkhgard, M. Farrokhi, State-of-Charge Estimation for Lithium-Ion Batteries Using Neural Networks and EKF, *IEEE Transactions on Industrial Electronics*, **57** (2010) 4178-4187.

[161] A. Eddahech, O. Briat, N. Bertrand, J.-Y. Delétage, J.-M. Vinassa, Behavior and state-of-health monitoring of Li-ion batteries using impedance spectroscopy and recurrent neural networks, *International Journal of Electrical Power & Energy Systems*, **42** (2012) 487-494.

[162] H.T. Lin, T.J. Liang, S.M. Chen, Estimation of Battery State of Health Using Probabilistic Neural Network, *IEEE Transactions on Industrial Informatics*, **9** (2013) 679-685.

[163] M. Boroushaki, M.B. Ghofrani, C. Lucas, M.J. Yazdanpanah, Identification and control of a nuclear reactor core (VVER) using recurrent neural networks and fuzzy systems, *IEEE Transactions on Nuclear Science*, **50** (2003) 159-174.